



# Couplages entre métamorphisme, fluides et déformation : étude de cas de l'éclogitisation dans les Arcs de Bergen

Erwan Bras

## ► To cite this version:

Erwan Bras. Couplages entre métamorphisme, fluides et déformation : étude de cas de l'éclogitisation dans les Arcs de Bergen. Sciences de la Terre. Université de Rennes, 2023. Français. NNT : 2023URENB069 . tel-04620340

**HAL Id: tel-04620340**

<https://theses.hal.science/tel-04620340>

Submitted on 21 Jun 2024

**HAL** is a multi-disciplinary open access archive for the deposit and dissemination of scientific research documents, whether they are published or not. The documents may come from teaching and research institutions in France or abroad, or from public or private research centers.

L'archive ouverte pluridisciplinaire **HAL**, est destinée au dépôt et à la diffusion de documents scientifiques de niveau recherche, publiés ou non, émanant des établissements d'enseignement et de recherche français ou étrangers, des laboratoires publics ou privés.

COLLEGE	ECOLOGIE
DOCTORAL	GEOSCIENCES
BRETAGNE	AGRONOMIE ALIMENTATION



# THÈSE DE DOCTORAT DE

L'UNIVERSITÉ DE RENNES

ÉCOLE DOCTORALE N° 600  
*Écologie, Géosciences, Agronomie, Alimentation*  
 Spécialité : *Sciences de la Terre et des Planètes*

Par

**Erwan BRAS**

## Couplages entre métamorphisme, fluides et déformation : étude de cas de l'éclogitisation dans les Arcs de Bergen

Couplings between metamorphism, fluids and deformation : a case study of eclogitisation in the Bergen Arcs

Thèse présentée et soutenue à Rennes, le 15 décembre 2023  
 Unité de recherche : Géosciences Rennes, UMR 6118

### Rapporteurs avant soutenance :

Laetitia LE POURHIET Professeure, Institut des Sciences de la Terre de Paris

Philippe GONCALVES Maître de conférences, Université de Franche-Comté

### Composition du Jury :

Présidente : Laetitia LE POURHIET Professeure, Institut des Sciences de la Terre de Paris

Examinateurs : Lucie TAJČMANOVÁ Professeure, Université de Heidelberg

Benjamin MALVOISIN Chargé de recherche, Institut des Sciences de la Terre de Grenoble

Rapporteurs : Laetitia LE POURHIET Professeure, Institut des Sciences de la Terre de Paris

Philippe GONCALVES Maître de conférences, Université de Franche-Comté

Dir. de thèse : Philippe YAMATO Professeur, Université de Rennes

Co-encadrant : Thibault DURETZ Professeur, Université Goethe de Francfort

### Invité :

Loïc LABROUSSE Professeur, Institut des Sciences de la Terre de Paris



## Remerciements

Je tiens avant toute chose à chaudemment te remercier Pipo, toi qui m'as aidé et supporté durant ces presque quatre années de thèse. Ça a été un plaisir de travailler avec toi, j'espère que c'était réciproque. Un grand merci à toi aussi Thibault, toujours de bon conseil et disponible pour me filer un coup de main malgré ton exil en Allemagne. Qui sait, on aura peut-être encore l'occasion de travailler ensemble ?

Thank you Stefan, for your invaluable advice, and for dedicating so much time to a project that was not yours to start with. Thank you Yury, for helping me when I needed it the most. This thesis would be very different without you two.

Merci à Loïc et Marie pour les coups de main et les discussions au labo, sur le terrain ou autour d'une bière ! And thank you Lisa, we had a great time cleaning dirty rocks under the rain.

Je tiens aussi à remercier les membres de mon CSI, Hugues et Benjamin. Vous avez été d'une grande aide, et avez certainement orienté cette thèse dans une direction bien différente de celle que j'envisageais.

Je veux également remercier ma famille. Mes parents Alain et Christine, sans qui je ne serais pas où j'en suis aujourd'hui, et mon frère Yannick et sa présence sans faille, que ce soit pour discuter, jouer, marcher, grimper, travailler (dans cet ordre).

Qu'auraient été ces années sans les ami.es ? Alors, et j'espère n'oublier personne, merci à Fanny, Félix, Rodolphe, Xavier, Emyrose, Lucas, Lydéric, Maxime, Noémie, Samuel, Margot, Marion, Tristan, Jacques, Thomas, Julie, Lise, Léna, Lucie, Antoine, Elise, Victoria, Nato, Marie, Jim, Solène, Jeanne, Nico. Et merci Melyssa d'être toujours là pour moi, que ce soit pour m'encourager ou m'écouter râler ; merci simplement d'être toi. Un mot encore pour remercier l'infatigable Tommy et son aide précieuse sur MATLAB, et Marcelle pour sa présence toujours réconfortante dans les moments de doute.

Mes remerciements vont enfin aux membres du jury, Laetitia, Philippe, Benjamin, Lucie, pour avoir accepté d'évaluer mon travail de thèse.



**COUPLAGES ENTRE MÉTAMORPHISME, FLUIDES ET DÉFORMATION : ÉTUDE DE CAS DE L'ÉCLOGITISATION DANS LES ARCS DE BERGEN****Couplings between metamorphism, fluids and deformation : a case study of eclogitisation in the Bergen Arcs****Résumé**

L'éclogitisation est un processus emblématique des zones de subduction continentales. Elle fait intervenir aussi bien la transformation de l'assemblage minéralogique, une modification de rhéologie et de perméabilité, une interaction entre fluides et roche, et une déformation tantôt visqueuse, tantôt cassante, susceptible de causer des séismes. L'étude des couplages entre réactions métamorphiques, déformation et fluides est donc cruciale pour comprendre la nature et la rhéologie de la croûte continentale inférieure lorsque celle-ci atteint des conditions de haute pression.

Cette thèse a pour objet l'étude de ces couplages, à travers un cas de terrain précis : l'éclogitisation de la granulite de l'île d'Holsnøy, une partie aujourd'hui exhumée de l'ancienne croûte inférieure de la chaîne de montagnes calédonienne, dans les Arcs de Bergen à l'ouest de la Norvège. L'observation des structures sur le terrain révèle que la déformation et la circulation de fluides sont les moteurs de l'éclogitisation de la croûte inférieure. Cependant, l'évolution temporelle et les conditions de pression des zones éclogitiques sont toujours énigmatiques. Au cours de cette thèse, je me suis donc appliqué à comprendre comment les rétroactions entre transformation métamorphique, transport de fluides et déformation peuvent expliquer l'évolution spatio-temporelle des zones éclogitiques d'Holsnøy. Cette thèse est structurée en trois chapitres principaux, qui correspondent à deux articles scientifiques déjà publiés, et un troisième en préparation.

Dans un premier temps, j'ai réalisé une étude pétrologique détaillée d'une bande de cisaillement éclogistique de Holsnøy, afin de déterminer les changements minéralogiques et texturaux qui transforment la granulite en éclogite au cours des réactions métamorphiques successives. Ces observations révèlent que les premières réactions affaiblissent la granulite, et les dernières réactions restaurent en partie la résistance de la roche. J'ai élaboré un modèle numérique qui illustre que ce mécanisme d'affaiblissement transitoire, associé à la circulation de fluides, contribue à l'élargissement des bandes de cisaillement au cours du temps.

Dans un deuxième temps, j'ai élaboré un modèle numérique pour étudier comment l'apport épisodique de fluides pressurisés peut propager l'éclogitisation dans la granulite, même si elle est imperméable. Je montre qu'il existe une rétroaction positive entre circulation de fluides et éclogitisation : un apport de fluides provoque l'éclogitisation, et cette réaction densifie la roche, ce qui génère de la porosité, favorisant ainsi la circulation de fluides. Un front hydro-réactif peut donc se propager rapidement dans la granulite imperméable et causer son éclogitisation. Le couplage fluides-réaction est donc un processus plausible d'évolution des zones éclogitiques de Holsnøy.

Afin de réunir les résultats des deux premiers articles, j'ai pour finir complété le modèle précédent afin de prendre en compte la déformation ainsi que les effets rhéologiques de l'éclogitisation. Cette étude montre que la déformation dans un milieu rhéologiquement hétérogène peut générer des variations locales de pression de plusieurs kbar. Celles-ci peuvent expliquer la juxtaposition de roches de faciès métamorphiques différents au même niveau crustal. La circulations de fluides peut toutefois affecter ces variations de pression.

**Mots clés :** éclogitisation, bande de cisaillement, interaction fluides-roche, modélisation numérique

### Abstract

Eclogitisation is an emblematic process of continental subduction zones. It involves transformation of the mineralogical assemblage, changes in rheology and permeability, fluid-rock interactions, and deformation that is either viscous or brittle, with the potential to cause earthquakes. The study of the coupling between metamorphic reactions, deformation and fluids is therefore crucial to understand the nature and rheology of the lower continental crust when it reaches high-pressure conditions.

The aim of this thesis is to study these couplings, focusing on a specific field case: the eclogitisation of granulite on Holsnøy Island, a now-exhumed part of the ancient lower crust of the Caledonian mountain range, in the Bergen Arcs in western Norway. Observation of field relations shows that deformation and fluid circulation are the forces that drive eclogitisation of the lower crust. However, the temporal evolution and pressure conditions of eclogitic zones are still enigmatic. During this thesis, I therefore set out to understand how feedbacks between metamorphic transformation, fluid transport and deformation can explain the spatio-temporal evolution of the Holsnøy eclogite zones. This thesis is structured into three main chapters that correspond to two previously published scientific articles, and a third in preparation.

As a first step, I carried out a detailed petrological study of an eclogite shear zone at Holsnøy, in order to determine the mineralogical and textural changes during the successive metamorphic reactions that transform granulite into eclogite. These observations reveal that the first reactions weaken the granulite, and the last ones partially restore the strength of the rock. I developed a numerical model that illustrates that this transient weakening mechanism, associated with fluid circulation, contributes to the widening of the shear zones over time.

Secondly, I developed a numerical model to study how episodic high pressure pulses can propagate eclogitisation into the granulite, even if it is impermeable. I show that there is a positive feedback between fluid circulation and eclogitisation: a fluid influx causes eclogitisation, which increases the rock density, generating porosity and thus promoting fluid flow. A hydro-reactive front can propagate rapidly into the impermeable granulite and cause its eclogitisation. Therefore, fluid-reaction coupling is a plausible process for the evolution of Holsnøy eclogite zones.

In order to bring together the results of the first two articles, I finally extended the previous model to include deformation and the rheological effects of eclogitisation. This study shows that deformation in a rheologically heterogeneous medium can generate local pressure variations of several kbar, which can explain the juxtaposition of rocks with different metamorphic facies at the same crustal level. Fluid circulation, however, may affect these pressure variations.

---

**Keywords:** eclogitisation, shear zone, fluid-rock interaction, numerical modelling

---

## Sommaire

<b>Remerciements</b>	<b>iii</b>
<b>Résumé</b>	<b>v</b>
<b>Sommaire</b>	<b>vii</b>
<b>1 Introduction générale</b>	<b>1</b>
Avant-propos . . . . .	3
1.1 La croûte continentale . . . . .	3
1.1.1 Tectonique des plaques . . . . .	3
1.1.2 Méthodes d'étude de la croûte . . . . .	5
1.1.3 Rhéologie de la croûte . . . . .	6
1.1.4 Structure de la croûte . . . . .	8
1.1.5 Devenir de la croûte inférieure dans les zones de convergence . . . . .	9
1.2 Le métamorphisme . . . . .	10
1.2.1 Chemins pression-température . . . . .	10
1.2.2 Métamorphisme de la croûte inférieure . . . . .	12
1.3 Qu'enregistrent vraiment les roches métamorphiques? . . . . .	13
1.3.1 Variations locales de pression . . . . .	14
1.3.2 Rôle des fluides . . . . .	16
1.3.3 Éclogitisation de la croûte inférieure . . . . .	17
1.4 Les rétroactions déformation - réactions - fluides . . . . .	19
1.4.1 Exemples de rétroactions . . . . .	19
1.4.2 Bandes de cisaillement . . . . .	21
1.5 Holsnøy : un exemple d'éclogitisation de la croûte inférieure . . . . .	23
1.5.1 Contexte géologique . . . . .	23
1.5.2 L'éclogitisation à Holsnøy . . . . .	24

---

1.6 La modélisation numérique . . . . .	28
1.6.1 Principe . . . . .	28
1.6.2 Équations de conservation . . . . .	29
1.6.3 Modèles à deux phases . . . . .	30
1.6.4 Équations constitutives . . . . .	30
1.6.5 Modèles numériques et couplages . . . . .	32
1.7 Problématique et structure de la thèse . . . . .	34
Bibliographie . . . . .	36
<b>2 Article 1 : un affaiblissement transitoire causé par l'éclogitisation</b>	<b>55</b>
Points clés . . . . .	55
2.1 Résumé . . . . .	56
2.2 Article de Bras et al. (2021), <i>Tectonophysics</i> . . . . .	57
2.3 Annexes à l'article de Bras et al. (2021) . . . . .	74
<b>3 Article 2 : un modèle hydro-réactif de l'éclogitisation</b>	<b>79</b>
Points clés . . . . .	79
3.1 Résumé . . . . .	80
3.2 Article de Bras et al. (2023), <i>EPSL</i> . . . . .	81
3.3 Annexes à l'article de Bras et al. (2023) . . . . .	94
<b>4 Article 3 : l'éclogitisation causée par des surpressions locales</b>	<b>97</b>
Points clés . . . . .	98
4.1 Résumé . . . . .	99
4.2 Abstract . . . . .	100
4.3 Introduction . . . . .	100
4.4 Methods . . . . .	104
4.4.1 Hydro-chemical model . . . . .	104
4.4.2 Mechanical model . . . . .	108
4.4.3 Solving procedure . . . . .	111
4.4.4 Model configuration . . . . .	113
4.4.5 Resolution test . . . . .	115
4.5 Results . . . . .	115
4.5.1 Reference model . . . . .	116
4.5.2 Parametric study . . . . .	118
4.6 Discussion . . . . .	120
4.6.1 Deformation-induced eclogitisation . . . . .	120
4.6.2 Competition between strain rate and Darcy flow . . . . .	121

4.6.3 Implications for eclogitisation in Holsnøy . . . . .	122
4.6.4 Comparison with single phase models . . . . .	123
4.6.5 Transient weakening . . . . .	124
4.6.6 Choice of a thermodynamic pressure . . . . .	125
4.6.7 Limitations and perspectives . . . . .	126
4.7 Summary and conclusion . . . . .	127
Appendix . . . . .	129
Supplementary figures . . . . .	130
References . . . . .	131
<b>5 Synthèse, discussions et perspectives</b>	<b>141</b>
5.1 Synthèse des résultats . . . . .	142
5.1.1 Synthèse de l'article 1 . . . . .	142
5.1.2 Synthèse de l'article 2 . . . . .	143
5.1.3 Synthèse de l'article 3 . . . . .	144
5.2 Discussions . . . . .	145
5.2.1 Variations locales de pression . . . . .	145
5.2.2 Vitesse de propagation de l'éclogitisation . . . . .	146
5.2.3 Perméabilité et porosité dans la croûte inférieure . . . . .	147
5.3 L'éclogitisation de la croûte inférieure vue d'Holsnøy . . . . .	149
5.4 Perspectives et travaux futurs . . . . .	149
5.4.1 Amphibolitisation . . . . .	149
5.4.2 Pression d'équilibre métamorphique . . . . .	151
Bibliographie . . . . .	152



# 1

## Introduction générale

### Sommaire du présent chapitre

---

<b>Avant-propos</b>	<b>3</b>
<b>1.1 La croûte continentale</b>	<b>3</b>
1.1.1 Tectonique des plaques . . . . .	3
1.1.2 Méthodes d'étude de la croûte . . . . .	5
1.1.3 Rhéologie de la croûte . . . . .	6
1.1.4 Structure de la croûte . . . . .	8
1.1.5 Devenir de la croûte inférieure dans les zones de convergence	9
<b>1.2 Le métamorphisme</b>	<b>10</b>
1.2.1 Chemins pression-température . . . . .	10
1.2.2 Métamorphisme de la croûte inférieure . . . . .	12
<b>1.3 Qu'enregistrent vraiment les roches métamorphiques ?</b>	<b>13</b>
1.3.1 Variations locales de pression . . . . .	14
1.3.2 Rôle des fluides . . . . .	16
1.3.3 Éclogitisation de la croûte inférieure . . . . .	17
<b>1.4 Les rétroactions déformation - réactions - fluides</b>	<b>19</b>
1.4.1 Exemples de rétroactions . . . . .	19
1.4.2 Bandes de cisaillement . . . . .	21
<b>1.5 Holsnøy : un exemple d'éclogitisation de la croûte inférieure</b>	<b>23</b>
1.5.1 Contexte géologique . . . . .	23
1.5.2 L'éclogitisation à Holsnøy . . . . .	24
<b>1.6 La modélisation numérique</b>	<b>28</b>
1.6.1 Principe . . . . .	28

1.6.2 Équations de conservation . . . . .	29
1.6.3 Modèles à deux phases . . . . .	30
1.6.4 Équations constitutives . . . . .	30
1.6.5 Modèles numériques et couplages . . . . .	32
<b>1.7 Problématique et structure de la thèse</b>	<b>34</b>
<b>Bibliographie</b>	<b>36</b>

---

## Avant-propos

Cette thèse est la synthèse de trois années de recherche qui ont donné lieu à trois articles scientifiques, publiés ou en préparation. Elle est structurée en cinq chapitres : le présent chapitre d'introduction, trois chapitres qui correspondent aux articles publiés ou en préparation, rédigés en anglais, et un chapitre de synthèse et conclusion. L'objectif du présent chapitre est de donner un état de l'art des connaissances actuelles dans les domaines abordés par cette thèse : la rhéologie de la croûte continentale, la croûte inférieure, les processus qui s'y déroulent - métamorphisme, déformation, circulation de fluides, rétroactions - et la modélisation numérique. Le contexte géologique de la zone d'étude de cette thèse, l'île d'Holsnøy en Norvège, est également expliqué en détail.

### 1.1 La croûte continentale

#### 1.1.1 Tectonique des plaques

La Terre est constituée de plusieurs enveloppes solides : noyau, manteau, et croûte terrestre. L'enveloppe la plus superficielle, la croûte, est de deux types distincts : la croûte continentale, épaisse en moyenne de 30 km, et la croûte océanique, épaisse en moyenne de 8 km.

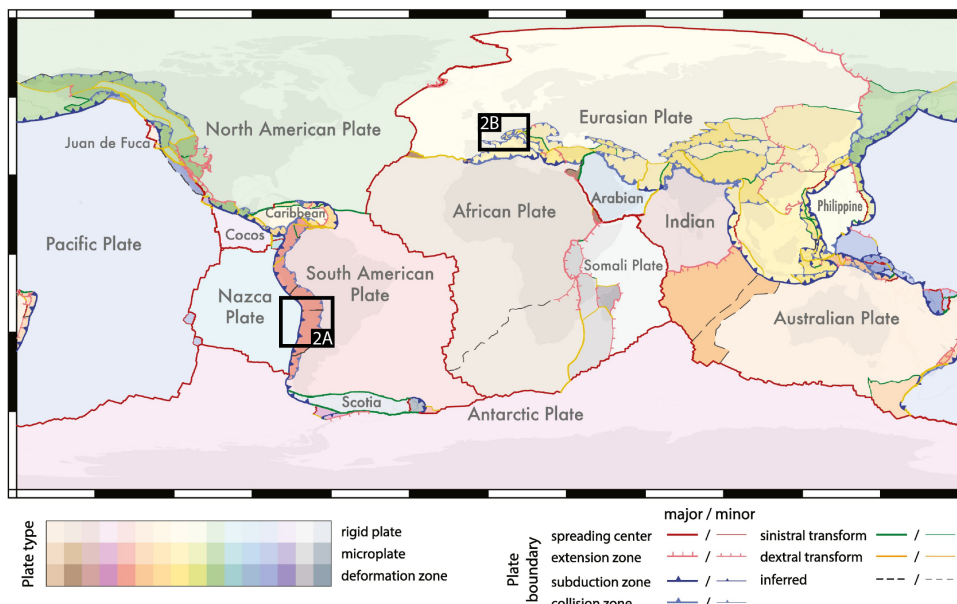


FIGURE 1.1 – Modèle de plaques tectoniques, et nature des limites de plaques, d'après Hasterok et al. (2022). Les limites rouges sont des dorsales océaniques, frontières divergentes qui sont le lieu de production de nouvelle lithosphère océanique. Les limites bleues sont des zones de convergence, soit océan-continent en bleu foncé, soit continent-continent en bleu clair. Les cadres noirs positionnent les zones de convergence de la figure 1.2.

Les croûtes océaniques et continentales et la partie la plus superficielle du manteau forment une enveloppe rigide, la lithosphère. Dans les années 1950 et 1960, la découverte de l'expansion des fonds océaniques (Dietz, 1961 ; Hess, 1962 ; Heezen et Tharp, 1965) a donné naissance à la théorie de la tectonique des plaques (McKenzie et Parker, 1967 ; Isacks et al., 1968 ; Le Pichon, 1968), selon laquelle la lithosphère est découpée en un petit nombre de plaques en mouvement les unes par rapport aux autres (figure 1.1). La tectonique des plaques a démontré que les océans et continents ne sont pas des objets permanents et fixes à la surface de la Terre, donnant une explication physique au concept de dérive des continents formulé au début du vingtième siècle par Alfred Wegener (Wegener, 1912, 1922).

Lorsque deux plaques se rapprochent, la plaque la plus dense plonge sous la plaque la moins dense durant le processus de subduction (figure 1.2). Dans le cas d'une subduction océanique, une portion de lithosphère océanique dense plonge et s'enfonce sous une lithosphère continentale. La subduction de la plaque de Nazca sous la plaque sud-américaine, et la formation de la Cordillère des Andes qui en résulte, est un exemple emblématique de subduction océanique (figure 1.2A). La convergence entre deux lithosphères continentales entraîne une collision et une subduction d'une plaque continentale sous l'autre. Le faible contraste de densité rend difficile la subduction, et cause un fort épaississement de la croûte continentale et la formation d'une chaîne de montagnes (orogenèse). C'est le cas des Alpes, qui résultent de la subduction de la plaque européenne sous la plaque adriatique (figure 1.2B), et de l'Himalaya, issue de la subduction de la plaque indienne sous la plaque eurasienne.

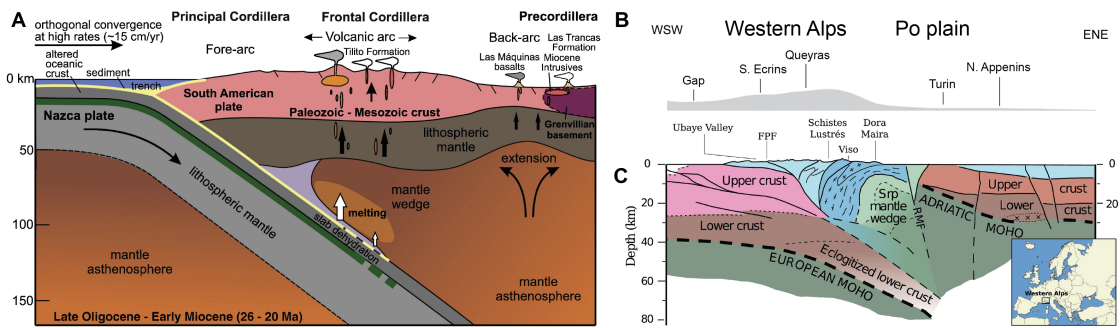


FIGURE 1.2 – Exemples de zones de subduction océanique (A) et continentale (B,C). (A) Reconstitution de la subduction de la lithosphère océanique de la plaque de Nazca sous la lithosphère continentale de la plaque sud-américaine au miocène, d'après Jones et al. (2016). La subduction a occasionné la formation de la Cordillère des Andes, un intense volcanisme ainsi qu'une forte activité sismique. (B) Profil topographique des Alpes, et (C) coupe interprétative correspondante de la subduction continentale alpine, d'après Solarino et al. (2018) et Beaucé et al. (2019). Le Moho, limite entre la croûte et le manteau, atteint localement 70 km, alors qu'il se situe à une profondeur de 30 à 40 km en dehors des zones de collision.

### 1.1.2 Méthodes d'étude de la croûte

L'étude de la croûte continentale et des zones de subduction est essentielle pour comprendre l'évolution des chaînes de montagnes et des continents, ainsi que les risques naturels qui y sont associés, comme les séismes, tsunamis et volcans. Cependant l'origine de ces phénomènes ne se trouve pas à la surface de la Terre, mais à des kilomètres ou dizaines de kilomètres de profondeur dans la croûte. Cette profondeur rend difficile l'observation directe des processus crustaux. De plus, la dynamique de la croûte implique à la fois des processus lents (subduction) et rapides (séismes), ainsi que des processus à l'échelle de la lithosphère comme à l'échelle du minéral (figure 1.3), ce qui complexifie son étude. Avant de détailler les processus à l'œuvre dans la croûte continentale, il convient donc de détailler quels outils permettent de l'étudier.

**Les forages** sont la solution la plus évidente pour étudier directement les roches crustales *in situ*. C'était par exemple l'objectif du forage de Kola en URSS, effectué entre 1970 et 1994 et qui a atteint une profondeur de 12 km (Kozlovsky, 1984), ou du forage KTB en Allemagne (9 km), entre 1987 et 1995 (Emmermann et Lauterjung, 1997). Bien que le forage de Kola soit le forage le plus profond jamais réalisé, il n'a pas pu accomplir son objectif de traverser les 35 km de la croûte continentale jusqu'au manteau, à cause des difficultés techniques dues aux fortes pressions et températures qui régnait au niveau de la tête de forage. Ainsi, même si ces forages permettent des observations *in situ* remarquables, ils restent limités à des lieux précis de la croûte continentale, et seulement dans sa partie la plus superficielle.

**L'étude de roches crustales exhumées** permet de comprendre les processus en cours dans les chaînes de montagnes actuelles. C'est le principe d'actualisme, selon lequel les processus actifs dans le passé s'exercent toujours aujourd'hui. On peut alors étudier des roches de la croûte, et même du manteau, directement sur le terrain. Cependant, dans certains contextes géologiques les roches exhumées sont rares. C'est le cas de la base des croûtes continentales des zones de collision, dont il n'existe que quelques affleurements emblématiques, comme les Monts Musgrave en Australie (Hawemann et al., 2019), le Mont Emilius dans les Alpes (Weber et al., 2022), les îles Lofoten (Campbell et Menegon, 2019) ou la nappe de Lindås (Austrheim, 1987) en Norvège. Cette rareté peut soulever la question de la représentativité de ces roches crustales exhumées, dont les propriétés sont extrapolées à la croûte toute entière.

**Les études expérimentales en laboratoire** permettent de déterminer les propriétés physiques des roches en reproduisant des processus naturels pour en extrapoler les résultats à la nature. On peut ainsi déformer en laboratoire des minéraux afin de déterminer leur rhéologie, et en déduire la résistance de la croûte dans son ensemble. Par exemple, les rhéologies du quartz (Hirth et al., 2001) et du plagioclase (Rybacki et Dresen, 2000) sont utilisées pour inférer les rhéologies de la croûte supérieure et

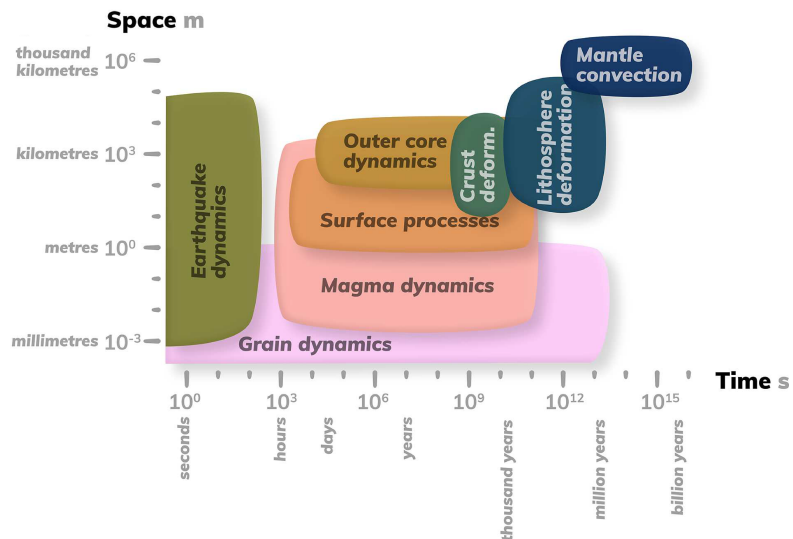


FIGURE 1.3 – Echelles spatiales et temporelles rencontrées en géologie, d’après van Zelst et al. (2022).

inférieure, respectivement. Cependant les expériences ne durent généralement pas plus de quelques semaines, sur des échantillons de quelques centimètres, alors que dans la croûte ces processus peuvent durer des milliers ou millions d’années, à des échelles spatiales bien plus grandes. Ainsi, les expériences doivent appliquer des vitesses de déformation de l’ordre de  $10^{-6}$  -  $10^{-5} \text{ s}^{-1}$  (e.g. Incel et al., 2020), pour extrapoler leurs résultats à la croûte où les vitesses de déformation sont typiquement de l’ordre de  $10^{-14}$  -  $10^{-13} \text{ s}^{-1}$  (Fagereng et Biggs, 2019).

**La modélisation numérique** est une méthode qui peut compenser certaines des lacunes des méthodes citées précédemment. Les modèles numériques sont des programmes informatiques régis par des équations qui décrivent des processus physiques, et utilisent des méthodes numériques pour les résoudre (e.g. Gerya, 2019). Ils permettent de reproduire de manière simplifiée la réalité, afin d’isoler certains processus pour en étudier les causes et les effets. On peut par exemple modéliser l’évolution des zones de subduction, en utilisant des équations de mécanique des fluides, des loi expérimentales décrivant la rhéologie des minéraux, et connaissant les propriétés thermiques des roches (e.g. Duretz et al., 2011). Par nature les modèles sont forcément simplifiés et ne peuvent pas prendre en compte tous les processus, en particulier s’ils se déroulent sur des échelles temporelles et spatiales très différentes.

### 1.1.3 Rhéologie de la croûte

Quand les plaques tectoniques rentrent en collision, les roches crustales se déforment, soit de manière cassante/fragile, soit de manière visqueuse/ductile (e.g. Turcotte et Schubert, 2002). La manière dont les roches se déforment lorsqu’elles sont soumises à des contraintes, ce que l’on nomme rhéologie, est dépendante de plusieurs paramètres,

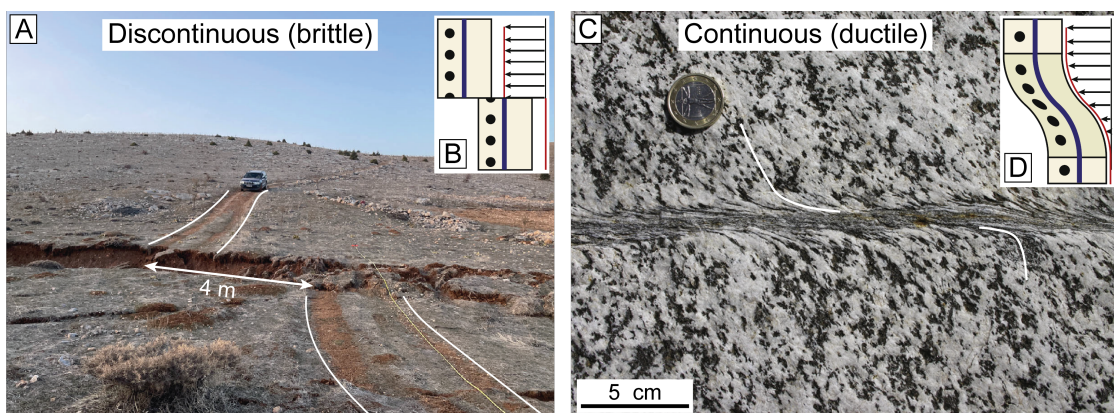


FIGURE 1.4 – Comparaison entre déformation fragile (A, B) et ductile (C, D). (A) Décalage d'une piste en Turquie causé par le séisme de Pazarcık de février 2023, de magnitude 7.8<sup>1</sup>. Le bloc du fond où se trouve la voiture est décalé horizontalement d'environ 4 mètres vers la gauche par rapport au bloc du premier plan. (B) Schéma d'une déformation cassante où le déplacement est discontinu, correspondant à une faille. (C) Bande de cisaillement centimétrique avec une foliation sigmoïdale dans un granitoïde des Alpes autrichiennes. Le décalage de la foliation est continu à travers la bande de cisaillement, et est souligné par les traits blancs. (D) Schéma d'une déformation ductile où le déplacement varie graduellement, correspondant à une bande de cisaillement. (A) modifié d'après une photo de Sinan Akciz, dans Gürer et al. (2023); (C) modifié d'après Pennacchioni et Mancktelow (2018); (B) et (D) modifiés d'après Fossen et Cavalcante (2017).

notamment la nature des minéraux qui les composent, leur état d'hydratation, leur état thermique, et la vitesse à laquelle elles sont déformées.

La déformation cassante, ou fragile, correspond à la rupture d'une roche lorsqu'elle est soumise à des contraintes trop intenses (figure 1.4A, B). Cette rupture se manifeste par des failles, parfois associées à des séismes. Les séismes dévastateurs qui se produisent dans les zones de subduction et de collision, par exemple ceux de Valvidia en 1960 au Chili (magnitude 9.5, Kanamori, 1977), ou de Gorkha en 2015 au Népal (magnitude 7.8<sup>2</sup>), témoignent des intenses contraintes auxquelles les plaques sont soumises. Le comportement cassant des roches est bien décrit par une loi de friction (e.g. Coulomb, 1773; Mohr et al., 1900; Nádai, 1950), selon laquelle plus les roches sont profondément enfouies, plus des contraintes élevées sont nécessaires pour les fracturer.

Les roches sont également des matériaux ductiles, capables de se déformer sans rupture (figure 1.4C, D). Sur des échelles de temps de l'ordre de milliers ou de millions d'années, leur mouvement s'apparente à un écoulement qui est décrit par des lois de fluage (Turcotte et Schubert, 2002). La capacité de la lithosphère à plonger en profondeur au sein des zones de subduction met en évidence le comportement ductile des roches crustales et mantelliques. Le comportement ductile des roches est contrôlé par une

1. USGS, (2023). <https://earthquake.usgs.gov/earthquakes/eventpage/us6000jllz/executive>  
 2. USGS, (2015). <https://earthquake.usgs.gov/earthquakes/eventpage/us20002926/executive>

caractéristique physique issue de la mécanique des fluides, la viscosité. Elle caractérise la résistance qu'un fluide oppose à son écoulement : plus un fluide est visqueux plus la contrainte imposée doit être forte pour le forcer à s'écouler.

#### 1.1.4 Structure de la croûte

La croûte continentale peut être séparée en 2 parties, en se basant sur des différences de vitesse d'ondes sismiques, de densité, et de composition chimique et minéralogique (Hacker et al., 2015). La croûte supérieure, de composition généralement granitique, constitue les 15-20 kilomètres les plus superficiels. La croûte inférieure, de composition le plus souvent granulitique, en forme la partie plus profonde. Cette distinction pétrologique coïncide avec une différence de sismicité : la plupart des séismes mesurés, dont les séismes les plus dévastateurs, se produisent dans la croûte supérieure, alors qu'ils sont plus rares dans la croûte inférieure (Chen et Molnar, 1983 ; Sloan et al., 2011). Il est donc bien établi que la croûte supérieure se déforme de manière fragile, mais la rareté des séismes dans la croûte inférieure est plus difficile à interpréter rhéologiquement.

L'apparente absence de sismicité de la croûte inférieure a conduit Chen et Molnar (1983) à l'interpréter comme une zone de faible résistance mécanique, où la déformation ductile prédomine et empêche la déformation cassante. La capacité de la croûte inférieure à se déformer de manière ductile est également attestée par la présence de grandes bandes de cisaillement dans les roches exhumées de croûtes inférieures anciennes (Bürgmann et Dresen, 2008). Cependant, des observations plus récentes de sismicité dans la croûte inférieure ont remis en cause ce modèle (Maggi et al., 2000a ; Jackson, 2002 ; Priestley et al., 2008). L'activité sismique de la croûte inférieure a été notamment mise en évidence dans le rift Baïkal (Déverchère et al., 2001), l'Himalaya (Hetényi et al., 2007), les Alpes (Singer et al., 2014) ou le rift est-africain (Stevens et al., 2021). Ceci suggère que la croûte inférieure est, au moins dans certains contextes, une zone résistante capable de se déformer de manière fragile.

Bien que la croûte inférieure soit sismiquement active, les séismes y sont systématiquement plus rares que dans la croûte supérieure (Maggi et al., 2000b ; Sloan et al., 2011), voire complètement absents dans certaines régions, par exemple le Zagros (Jackson et al., 2021). Jamtveit et al. (2016, 2019) suggèrent que cette relative rareté s'explique par la grande résistance de la croûte inférieure, qui peut supporter des contraintes élevées de l'ordre du gigapascal sans rupture fragile, plutôt que par sa faiblesse mécanique. Jackson et al. (2004) suggèrent en outre qu'une croûte inférieure résistante est nécessaire pour la survie des racines crustales qui forment le support des chaînes de montagnes.

La rhéologie de la croûte inférieure est toujours sujette à controverse, et varie probablement d'un contexte géologique à l'autre (Bürgmann et Dresen, 2008). Même si nos connaissances sur la croûte inférieure sont parcellaires, son étude demeure primordiale

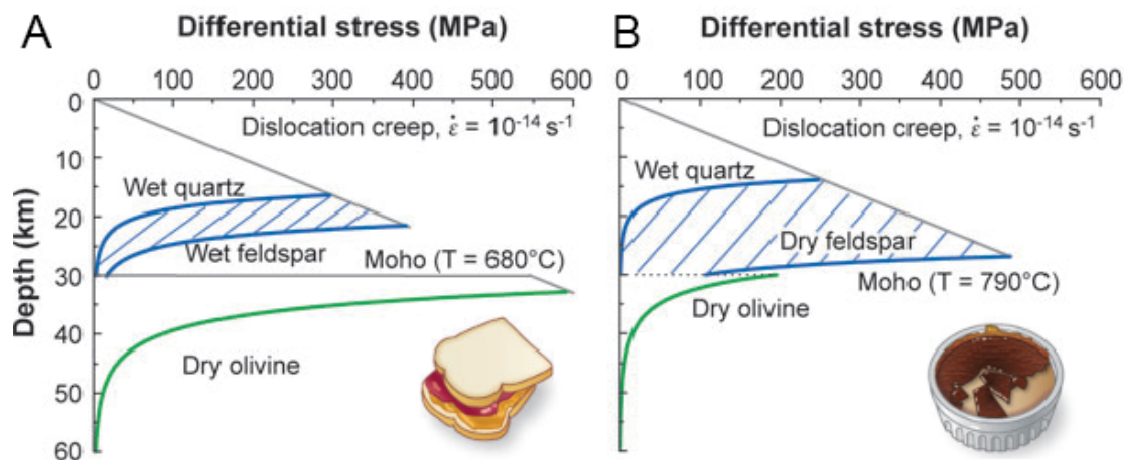


FIGURE 1.5 – Deux modèles de rhéologie de la lithosphère continentale, d'après Bürgmann et Dresen (2008). L'axe des abscisses représente la contrainte déviatorique maximale que peut subir une couche avant de se déformer. Plus cette contrainte est élevée plus la couche est résistante. (A) Modèle "Jelly sandwich" (Chen et Molnar, 1983), où la croûte inférieure, modélisée par le feldspath hydraté, est une couche peu résistante prise en sandwich entre la croûte supérieure et le manteau supérieur résistants. (B) Modèle "Crème brûlée" (Maggi et al., 2000a), où la croûte inférieure et supérieure forment un ensemble résistant surplombant le manteau peu résistant. Ces profils rhéologiques sont établis à partir de lois de fluages de minéraux représentatifs des enveloppes étudiées (quartz, feldspath et olivine), déterminées en laboratoire.

pour mieux comprendre la géodynamique globale, l'évolution des chaînes de montagnes et le potentiel sismique de la croûte continentale. C'est dans ce contexte que s'inscrivent mes travaux de thèse qui se focalisent sur l'étude de la croûte continentale inférieure, et plus spécifiquement sur les processus qui l'affectent dans les zones de convergence continentales.

### 1.1.5 Devenir de la croûte inférieure dans les zones de convergence

Lorsque la théorie de la tectonique des plaques était en train d'être établie, Dewey et Bird (1970) ont proposé une distinction entre deux grands types de zones de convergence : les zones de subduction entre continent et océan et les zones de collision entre deux continents. Ils affirmaient que, contrairement aux zones de subduction, la lithosphère continentale n'est pas entraînée en profondeur dans les zones de collision. Dans la lignée des travaux fondateurs de Dewey et Bird (1970), la capacité de la croûte continentale à subduire à de grandes profondeurs ( $\geq 80$  km) a été longtemps débattue (Molnar et Gray, 1979 ; Schreyer, 1988 ; van den Beukel, 1992 ; Ducea, 2016). La croûte continentale étant moins dense que le manteau dans lequel elle s'enfouit, elle possède une grande flottabilité qui s'oppose à son enfouissement.

Néanmoins la découverte de roches crustales exhumées de ultra-haute pression (e.g. Chopin, 1984 ; Smith, 1984), les observations géophysiques dans les orogènes actuelles

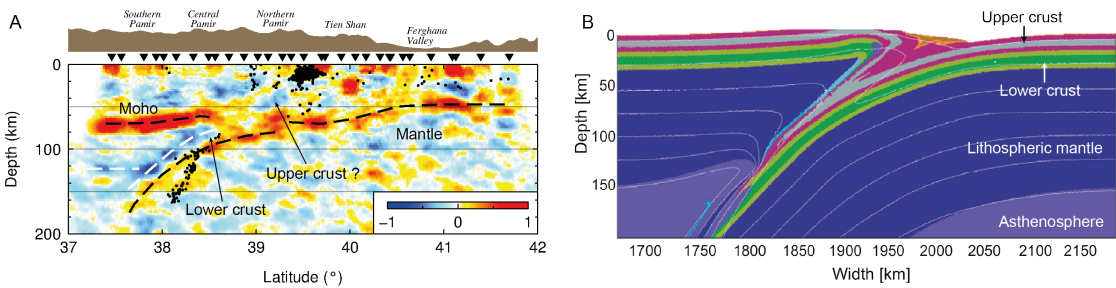


**FIGURE 1.6 – Subduction profonde de la croûte inférieure.** (A) Évidences sismiques (image fonction récepteur) de la subduction de la croûte inférieure eurasienne sous le Pamir, à la frontière entre le Tadjikistan, le Kirghizistan et la Chine. La croûte supérieure et moyenne est incorporée dans le Pamir, alors que la croûte inférieure est subduite. Les points indiquent les séismes de profondeur intermédiaire. Modifié d'après Schneider et al. (2013). (B) Modèle numérique de subduction continentale avec une croûte inférieure résistante, modifié d'après Reuber et al. (2016).

(e.g. Hetényi et al., 2007; Schneider et al., 2013; Zhao et al., 2015) et les modèles numériques (e.g. Li, 2014; Reuber et al., 2016; Porkoláb et al., 2021) montrent que la subduction de la croûte inférieure est possible à de grandes profondeurs (figure 1.6). L'existence d'affleurements de roches crustales enfouies à de grandes profondeurs (e.g. Austrheim, 1987; Hawemann et al., 2019) montre que leur exhumation est elle aussi possible. Cependant les mécanismes à l'origine de l'exhumation restent très controversés (Guillot et al., 2009; Hacker et al., 2013; Burov et al., 2014; Li, 2014; Yamato et Brun, 2017; Zhang et Wang, 2020), et sont fortement dépendant de l'état des contraintes ainsi que des propriétés physiques de la croûte inférieure.

Lors de sa subduction, la croûte inférieure subit des augmentations de température, de pression et est exposée à de fortes déformations et à la circulation de fluides. Ces changements de conditions sont à l'origine de transformations des roches, décrites dans les sections 1.2 et 1.3, qui modifient les propriétés physiques de la croûte. Les propriétés les plus importantes auxquelles je m'intéresse dans cette thèse sont la densité et la viscosité. Ce sont les paramètres principaux des équations de la mécanique, cruciaux pour déterminer l'évolution des zones de subduction et des chaînes montagneuses dans le temps, pour interpréter les mesures géophysiques, et pour comprendre la sismicité dans les zones de convergence.

## 1.2 Le métamorphisme

### 1.2.1 Chemins pression-température

Pendant les orogenèses, les roches de la croûte sont entraînées à de grandes profondeurs lors de leur subduction. Durant leur enfouissement, les roches se transforment

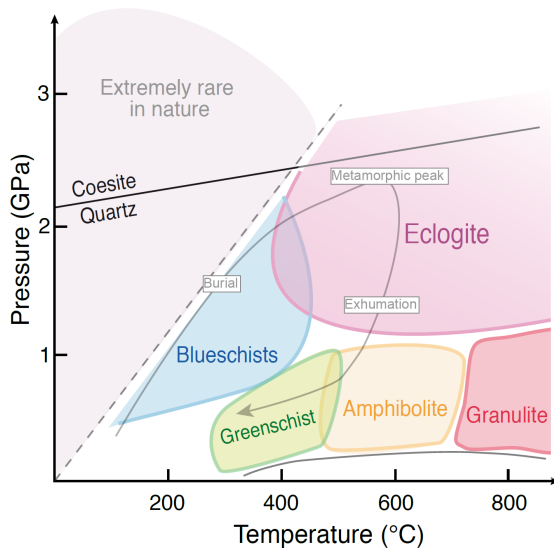


FIGURE 1.7 – Principaux faciès métamorphiques, modifié d'après Yamato et Brun (2017). La flèche grise donne un exemple de chemin  $P$ - $T$  parcouru par une roche métamorphique au cours de son enfouissement jusqu'au faciès des éclogites, et de l'exhumation qui s'en suit.

sous l'effet de l'augmentation de la pression ( $P$ ) et de la température ( $T$ ). Les minéraux stables à des basses pression et température, en général peu denses, sont remplacés par de nouveaux minéraux plus stables aux nouvelles conditions  $P$ - $T$ , de manière à réduire l'énergie libre du système. Ce processus de transformation de l'assemblage minéralogique en réponse à des changements de pression et de température est nommé métamorphisme, et les roches ainsi transformées sont des roches métamorphiques (figure 1.7).

La composition minéralogique d'une roche métamorphique dépend donc des conditions  $P$ - $T$  à laquelle elle est exposée, mais aussi de sa composition chimique : pour deux roches équilibrées aux mêmes conditions  $P$ - $T$  mais de chimie différente, les mêmes minéraux ne seront pas forcément présents, ni dans les mêmes proportions. Si l'on mesure la composition chimique d'une roche à l'affleurement, et que l'on détermine quels minéraux sont présents ou non, on peut alors déterminer quelles sont ses conditions  $P$ - $T$  d'équilibre. Cette détermination utilise des lois de thermodynamique à l'équilibre (Gibbs, 1876) et des bases de données de propriétés thermodynamiques des minéraux (e.g. Holland et Powell, 1998). Les pétrologues utilisent communément des logiciels tels que Thermocalc (Powell et al., 1998), Perple\_X (Connolly, 2005), ou Theriax-Domino (de Capitani et Petrakakis, 2010) pour calculer les champs de stabilité d'assemblages minéralogiques par minimisation d'énergie libre de Gibbs, étant donnée la composition chimique du système.

La composition chimique de certains minéraux est également très dépendante de la pression ou de la température, et est donc un bon indicateur de la pression ou de la température à laquelle ils se sont formés. Par exemple, dans le rutile la proportion de zirconium dépend essentiellement de la température et peu de la pression (Zack

et al., 2004), ce qui permet de l'utiliser comme thermomètre. La proportion de silicium dans la phengite dépend essentiellement de la pression mais peu de la température (Massonne et Schreyer, 1987), ce qui permet de l'utiliser comme baromètre. En outre, la présence d'éléments radioactifs dans certains minéraux permet de dater la formation des minéraux en connaissant la période radioactive de ces éléments, à l'instar du carbone 14 mais pour des dates bien plus anciennes. A titre d'exemple la datation uranium-plomb sur les zircons est la méthode la plus utilisée, grâce à sa fiabilité et à la présence du zircon dans la plupart des roches métamorphiques (Spencer et al., 2016).

L'étude des roches métamorphiques, associée à des techniques de datation, permet de déterminer le chemin  $P-T$  d'une unité métamorphique, c'est à dire son évolution  $P-T$  au cours du temps depuis son enfouissement jusqu'à son exhumation (e.g. Thompson et England, 1984). On peut typiquement déterminer les conditions  $P-T$  maximales qu'une roche métamorphique a atteintes, et dater ce pic métamorphique. Lors de l'exhumation vers la surface, la pression et la température diminuent, et les roches métamorphiques se retrouvent souvent partiellement en réponse à ces nouveaux changements de pression et de température. Ce processus, nommé rétromorphose, peut être lui aussi daté, et ses conditions  $P-T$  estimées.

### 1.2.2 Métamorphisme de la croûte inférieure

Dans cette thèse, je m'intéresse tout particulièrement à la relation entre deux roches métamorphiques, la granulite et l'éclogite (figure 1.8). La **granulite** est une roche métamorphique de basse ou moyenne pression (6-12 kbar), et de haute température (700-900 °C). Elle est le composant principal de la croûte continentale inférieure à des profondeurs supérieures à 20 km (Rudnick et Fountain, 1995 ; Touret et al., 2022). Sa densité est de l'ordre de 2800 à 3000 kg/m<sup>3</sup>, variable selon sa composition chimique : les granulites felsiques, riches en SiO<sub>2</sub>, sont moins denses que les granulites mafiques, pauvres en SiO<sub>2</sub>. Le composant principal de la granulite est le plagioclase, qui peut représenter jusqu'à 90 % du volume de la roche.

L'**éclogite** est une roche métamorphique de haute pression (>15 kbar) typiques des zones de subduction océaniques et continentales. Au sens le plus strict, les éclogites sont les roches qui se forment à haute pression au cours de la subduction de la croûte océanique mafique par déshydratation des roches de faciès schiste bleu (e.g. Peacock, 1990), mais les roches continentales plus felsiques sont elles aussi capables d'enregistrer des pressions de faciès éclogitique. Ainsi, lors des collisions continent-continent, des éclogites continentales se forment suite au métamorphisme haute pression de roches granulitiques de la croûte inférieure (e.g. Austrheim, 1991 ; Monsalve et al., 2008 ; Steltzenpohl et al., 2011). Ces éclogites ont une densité d'environ 3300 à 3400 kg/m<sup>3</sup>, et une composition généralement plus felsique que les éclogites océaniques. L'éclogitisation de

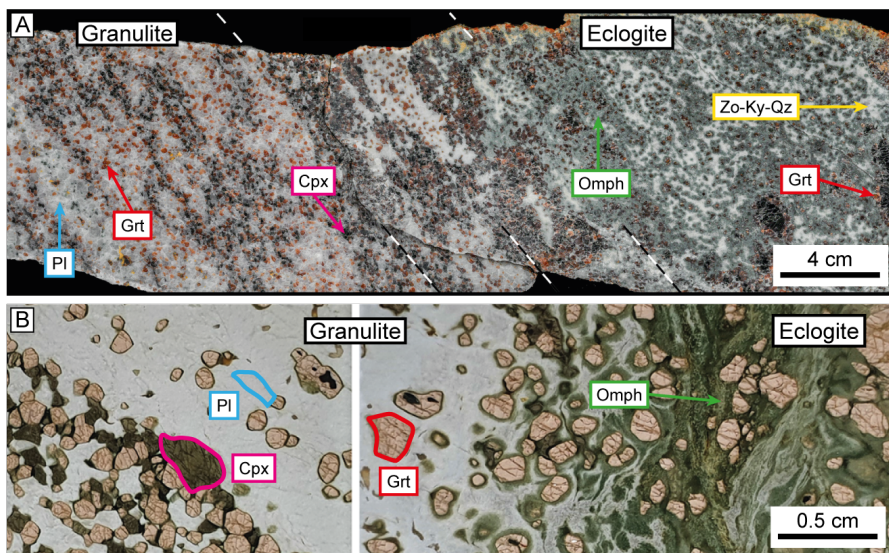


FIGURE 1.8 – Minéralogie de la granulite et de l’éclogite, à Holsnøy, Norvège. Pl = plagioclase (grains blancs), Grt = grenat (rouge), Cpx = clinopyroxène (noir), Omph = Omphacite (vert), Zo-Ky-Qz = assemblage à grains fins de zoisite, disthène et quartz (blanc). (A) Échantillon vu à l’oeil nu, modifié d’après Putnis et al. (2021), et (B) vu au microscope optique, modifié d’après Kaatz et al. (2022).

la granulite se caractérise principalement par le remplacement du plagioclase par des minéraux stables à plus haute pression, tels que l’omphacite, la zoisite, et le disthène. Les éclogites continentales sont essentielles à notre compréhension des processus géodynamiques car elles contiennent des informations sur les conditions maximales atteintes dans la croûte, ainsi que sur son exhumation (Brown, 2023).

### 1.3 Qu'enregistrent vraiment les roches métamorphiques ?

La description qui précède est une vision simplifiée du métamorphisme, où les roches métamorphiques ne sont sensibles qu'à des conditions  $P$ - $T$  déterminées par la profondeur d'enfouissement. Cette vision, séduisante par sa simplicité, repose sur deux hypothèses qui ne sont néanmoins pas toujours valides.

Une première hypothèse simplificatrice est que la pression est lithostatique, c'est-à-dire que la pression  $P$  qui s'exerce en un point de la croûte est uniquement due au poids de la colonne de roche qui le surplombe :

$$P = \rho g z, \quad (1.1)$$

où  $\rho$  est la densité,  $g$  l'accélération de la pesanteur et  $z$  la profondeur. Cette hypothèse permet de directement convertir la pression enregistrée par les roches métamorphiques en profondeur, si l'on connaît la densité des roches. Cependant, l'augmentation de

pression enregistrée par le métamorphisme peut être due à un changement de l'état des contraintes tectoniques, sans nécessiter d'enfouissement (Bauville et Yamato, 2021). Je détaille dans la section 1.3.1 qui suit en quoi les contraintes tectoniques peuvent faire dévier la pression métamorphique de la pression lithostatique.

La deuxième hypothèse simplificatrice est que les roches sont systématiquement à l'équilibre avec les conditions  $P-T$  qu'elles subissent. Ceci ne peut pas être vrai dans un cas général, puisqu'on observe des roches préservant des assemblages de hautes pression et/ou température à la surface de la Terre. De la même manière, des assemblages de relatives basses pression et/ou température peuvent être préservés lors des subductions. Je détaille dans la section 1.3.2 en quoi la présence de fluides est nécessaire aux réactions métamorphiques.

### 1.3.1 Variations locales de pression

Dans les zones de convergence, métamorphisme et déformation vont de pair : la compréhension des roches métamorphiques se fait aussi bien par l'étude de leur composition minéralogique et chimique, que par l'étude des structures présentes (bandes de cisaillement, linéations...), qui sont autant d'indices sur les déformations enregistrées par les roches métamorphiques. Pourtant, on néglige souvent que la déformation peut créer des variations de pression de plusieurs kbar qui sont enregistrées par les assemblages métamorphiques (Moulas et al., 2013; Schmalholz et al., 2014b; Tajčmanová et al., 2014). Il n'est donc pas trivial de convertir la pression en profondeur (Schmalholz et Podladchikov, 2014; Bauville et Yamato, 2021; Tajčmanová et al., 2021).

En effet, la pression est définie comme la somme d'une contribution lithostatique, qui correspond au poids de la colonne de roche qui surplombe un point, et une contribution déviatorique, qui correspond à des contraintes dues à la déformation et à la viscosité des roches (e.g. Mancktelow, 1993; Petrini et Podladchikov, 2000; Gerya, 2015). L'hypothèse que dans la croûte la pression est lithostatique ( $P = \rho g z$ ) presuppose que les contraintes dans la croûte sont isotropes, c'est-à-dire que les contraintes déviatoriques sont nulles (Schmalholz et Podladchikov, 2014; Moulas et al., 2019). Cependant, les modèles géodynamiques montrent que les contraintes peuvent être fortement anisotropiques dans la croûte continentale en collision (figure 1.9, Babeyko et Sobolev, 2008; Schmalholz et Podladchikov, 2013; Gerya, 2015; Reuber et al., 2016). La pression peut alors dévier jusqu'à 10 kbar de la pression lithostatique.

Les études expérimentales (Hirth et Tullis, 1994; Cionoiu et al., 2019; Cionoiu et al., 2022) et de terrain (Pleuger et Podladchikov, 2014; Luisier et al., 2019; Hoiland et al., 2022; Simon et al., 2023) confirment que dans les zones de convergence, les roches métamorphiques peuvent enregistrer des surpressions tectoniques significatives. A titre d'exemple, Luisier et al. (2019) ont récemment montré que dans le Grand Paradis,

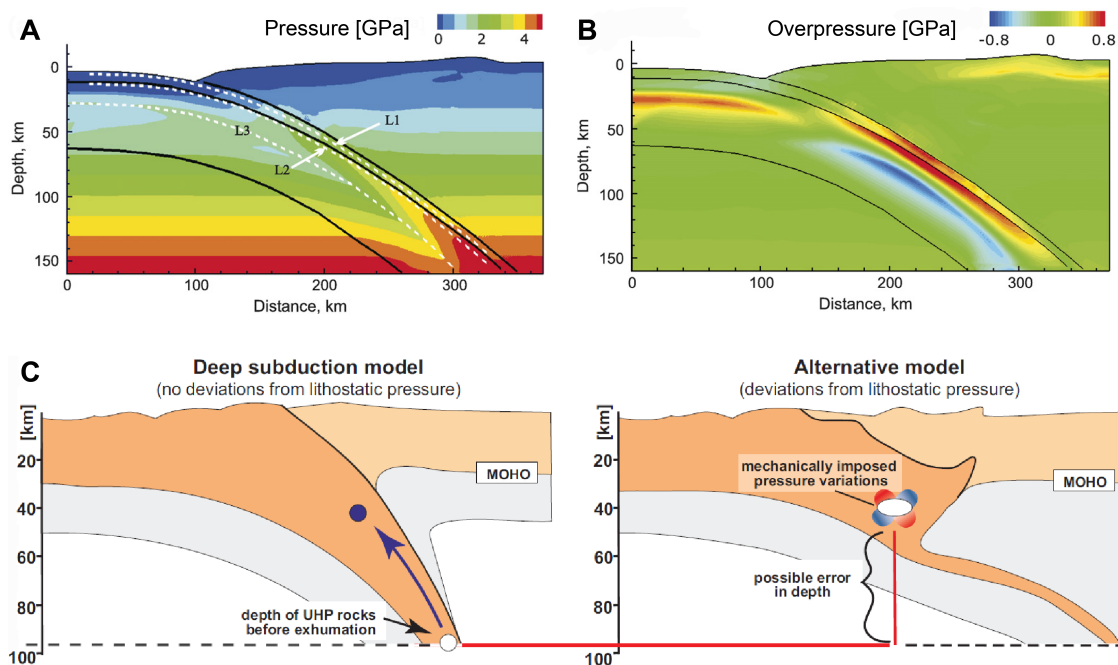


FIGURE 1.9 – Effet de la déformation sur la pression. Modélisation numérique d'une zone de subduction par Babeyko et Sobolev (2008), montrant (A) la distribution de la pression, et (B) les déviations de la pression par rapport à la pression lithostatique. (C) Comparaison entre 2 reconstructions possibles d'une zone de collision prenant en compte ou non les pressions non-lithostatiques, d'après Tajčmanová et al. (2021), modifié d'après Schmalholz et al. (2014a). A gauche, le modèle "Subduction profonde" suppose que les roches métamorphiques enregistrent des pressions lithostatiques, et donc des grandes profondeurs. A droite, le modèle alternatif explique les hautes pressions par les contraintes subies par la croûte.

plusieurs roches interprétées comme s'étant formées à la même profondeur présentent des assemblages métamorphiques équilibrés à des pressions qui diffèrent de 8 kbar. A l'échelle du minéral, Tajčmanová et al. (2014) expliquent que les zonations chimiques observées dans des couronnes de réactions autour de grains de disthène dans des granites du massif de Bohème sont dues à des variations de pression de 8 kbar à l'échelle du grain.

Ces déviations de 8 à 10 kbar dues à l'anisotropie des contraintes peuvent être interprétées à tort par des différences de profondeur de l'ordre de l'épaisseur de la croûte (figure 1.9C, Petrini et Podladchikov, 2000; Tajčmanová et al., 2015). Ces différences peuvent drastiquement changer notre interprétation des chemins  $P-T$  métamorphiques et de l'évolution des zones de convergence (Yamato et Brun, 2017; Bauville et Yamato, 2021). Ainsi, la découverte de coésite, polymorphe de haute pression du quartz, dans des éclogites des Alpes (Chopin, 1984) et des Calédonides (Smith, 1984), est classiquement interprétée comme la preuve d'un enfouissement de la croûte à des pressions lithostatiques supérieures à 28 kbar, soit à des profondeurs supérieures à 100 km. Mais

l'exhumation de roches enfouies à une telle profondeur est difficile à expliquer, et il est plausible que ces pressions extrêmes correspondent à des contraintes non-lithostatiques plutôt qu'à un enfouissement (Yamato et Brun, 2017).

D'autre part, dans un système rhéologiquement hétérogène déformé, les matériaux faibles et résistants peuvent subir des variations de pression de plusieurs kbar (Mancktelow, 1993, 2008). L'équilibre des forces entre la pression et les contraintes déviatoriques nécessite une augmentation de la pression si les contraintes déviatoriques diminuent en raison de la présence d'un matériau faible (Schmalholz et Podladchikov, 2013). Or, dans la croûte inférieure, la granulite est plus résistante que l'éclogite (Jolivet et al., 2005; Raimbourg et al., 2007a; Kaatz et al., 2023). L'éclogitisation génère donc des hétérogénéités rhéologiques qui peuvent être la source de variations de pression de plusieurs kbar (Jamtveit et al., 2018b).

### 1.3.2 Rôle des fluides

Les réactions métamorphiques consistent en un remplacement de certains minéraux par d'autres de manière à minimiser l'énergie libre du système chimique, en réponse à des changements de pression et de température. Mais quels sont les mécanismes qui remplacent un assemblage minéralogique par un autre ?

Même dans un système chimique fermé, un transport de masse local, à l'échelle du grain, doit se produire lors d'une réaction métamorphique (Carmichael, 1969). Bien que ce transport soit possible via une diffusion à l'état solide, le transport via dissolution-précipitation en présence d'une phase fluide libre est significativement plus rapide (Dohmen et Milke, 2010). Il s'agit donc du mécanisme dominant de remplacement des minéraux lors des réactions métamorphiques (Putnis, 2009). Ainsi, si un minéral est localement en déséquilibre avec un fluide, il commence à se dissoudre dans la phase fluide, et les éléments qui le composent sont transportés vers un autre sous-domaine d'équilibre. A l'interface fluide-minéral, un minéral plus stable peut précipiter si le fluide est supersaturé (figure 1.10, Putnis et John, 2010). La dissolution génère de la porosité qui permet la migration des fluides vers l'interface des minéraux en cours de dissolution.

En outre, les fluides réduisent l'énergie d'activation nécessaire aux réactions (e.g., Rubie, 1986; Zertani et al., 2022), et sont nécessaires à la cristallisation de minéraux hydratés tels que le mica ou la zoisite. Ils sont donc fondamentaux pour activer et accélérer les réactions.

Lorsque des roches anhydres sont enfouies en profondeur dans des zones de subduction, elles peuvent alors être préservées dans un état métastable (Rubie, 1998) : elles sont portées à des conditions de pression et température favorables à une réaction métamorphique, voire les excéder, mais l'infiltration de fluides est nécessaire pour dé-

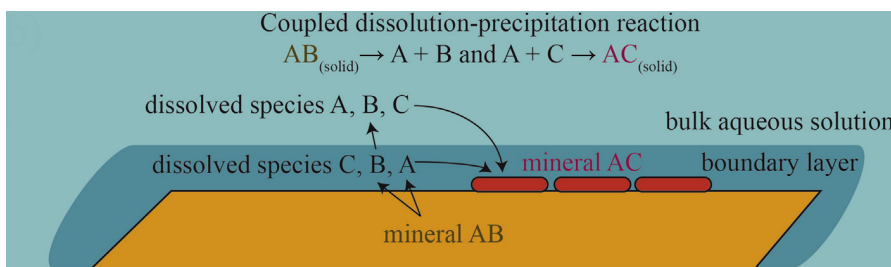


FIGURE 1.10 – Schéma conceptuel de la dissolution-précipitation, d'après Renard et al. (2019). AB est un minéral en train de se dissoudre, et contient un cation A qui peut se lier à l'élément C jusqu'à atteindre la supersaturation du fluide en A+C, permettant la précipitation du minéral AC. La dissolution et la précipitation se produisent dans une couche à l'interface fluide-roche, où l'équilibre thermodynamique est différent du reste du fluide.

clencher la réaction (John et Schenk, 2003). La métastabilité dans le faciès des éclogites est communément suggérée dans les roches de la croûte continentale, par exemple en Norvège dans les Arcs de Bergen (Austrheim, 1987), dans la région des Gneiss de l'Ouest (Wain et al., 2001), dans les Lofoten (Steltenpohl et al., 2004), dans les Alpes autrichiennes (Rogowitz et Huet, 2021), ou encore dans les Monts Dabie en Chine (Shuwen et al., 2002). Dans la croûte inférieure subduite, les assemblages minéralogiques peuvent rester métastables 10 kbar et 150 °C au delà de leur champ de stabilité (Austrheim, 1998 ; Hetényi et al., 2007). La réaction métamorphique se produit dès qu'un fluide est apporté à la roche métastable (e.g. Jackson et al., 2004), et d'autant plus rapidement que l'excès de pression/température est grand.

### 1.3.3 Éclogitisation de la croûte inférieure

Les précédents paragraphes illustrent que l'étude des roches métamorphiques ne se résume pas à déterminer les chemins pression-température des roches métamorphiques, mais plutôt pression-température-fluides-déformation. Ces conditions sont particulièrement difficiles à déterminer dans les croûtes inférieures en subduction, où la rhéologie et l'état d'hydratation des roches sont mal connus. Dans ce contexte, ma thèse s'attache à étudier les processus qui transforment une granulite en éclogite au cours des orogenèses, lorsque la croûte continentale inférieure granulitique est portée à des conditions *P-T* éclogitiques.

Sous l'Himalaya, les mesures géophysiques mettent en évidence des variations de vitesse des ondes sismiques qui suggèrent que la croûte continentale indienne s'éclogitise en profondeur durant la subduction (Schulte-Pelkum et al., 2005 ; Hetényi et al., 2007 ; Monsalve et al., 2008, figure 1.11). Cependant, le calcul de profils de densité révèle que l'éclogitisation de la croûte inférieure se produit à des profondeurs supérieures à celles attendues, et qu'elle est donc retardée cinétiquement. L'éclogitisation est partielle

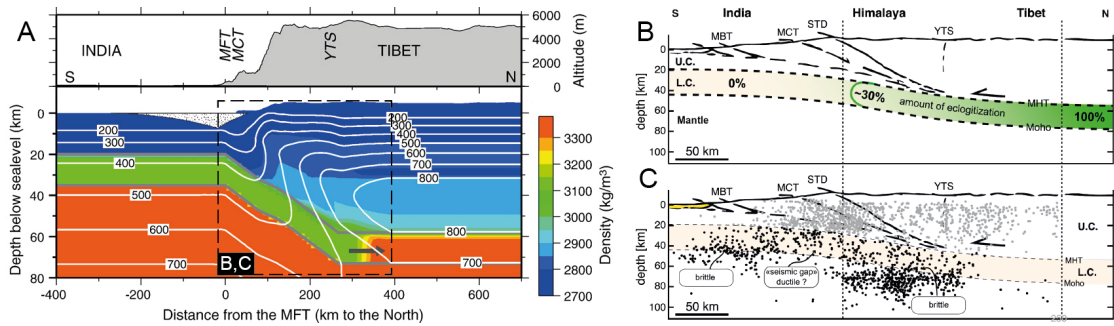


**FIGURE 1.11 – Métastabilité, réactions métamorphiques et déformation dans la croûte inférieure sous l’Himalaya.** (A) Profil topographique (haut), et profil de densité (bas), modifiés d’après Hetényi et al. (2007). On peut identifier la croûte inférieure plongeante par sa densité de 3000-3100 kg/m<sup>3</sup> (en vert), et sa transition rapide vers une densité de 3300 kg/m<sup>3</sup> à l’aplomb de la chaîne. Le cadre pointillé noir montre la position des profils (B) et (C). (B) État métamorphique supposé de la croûte inférieure, déduit des mesures de densité. (C) Re-localisations des séismes de la croûte inférieure indienne, qui coïncident avec l’initiation de l’éclogitisation. (B) et (C) modifiés d’après Yamato et al. (2022).

et diffuse, n’affectant que 30 % de la croûte inférieure indienne en Himalaya (Schulte-Pelkum et al., 2005, figure 1.11B).

La métastabilité de la coûte inférieure, suggérée par les observations géophysiques, est confirmée par des observations de terrain (e.g. Austrheim, 1987; Jackson et al., 2004) et de laboratoire (Shi et al., 2018; Incel et al., 2020). En effet, les granulites de la croûte inférieure sont anhydres et imperméables (e.g. Yardley et Valley, 1997; Yardley, 2009; Jamtveit et al., 2016), ce qui empêche une circulation permanente de fluides permettant de déclencher la réaction métamorphique.

D’autre part, l’initiation de l’éclogitisation de la croûte inférieure métastable coïncide avec des séismes dans l’Himalaya (figure 1.11C), ce qui suggère que les deux processus sont liés (Shi et al., 2018). Cette corrélation s’observe aussi dans les roches exhumées : sur les terrains granulitiques partiellement éclogitisés de Holsnøy ou des Lofoten, en Norvège, l’éclogitisation est parfois associée à des pseudotachylytes, roches de faille issues de la fusion frictionnelle lors d’un séisme (Lund et Austrheim, 2003; Steltenpohl et al., 2006; Menegon et al., 2017; Petley-Ragan et al., 2018). L’éclogitisation partielle et diffuse de la croûte inférieure peut alors s’expliquer si des fluides sont introduits dans la croûte inférieure de manière épisodique, vraisemblablement associés à des séismes (e.g. Jamtveit et al., 2016). L’endommagement des roches causé par la déformation cassante génère de la porosité et de la perméabilité qui permettent aux fluides de s’infilttrer dans les granulites métastables et déclencher leur éclogitisation (figure 1.12, Jamtveit et al., 2018a, 2019). La déformation cassante n’est toutefois pas systématiquement suivie de l’infiltation de fluides (Hawemann et al., 2019; Mancktelow et al., 2022).

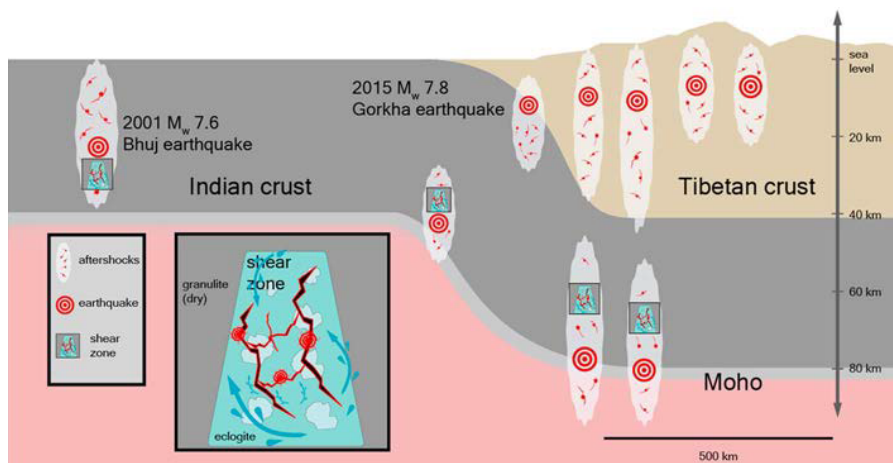


FIGURE 1.12 – Représentation schématique de la relation entre séismes et fluides dans les croûtes indiennes et tibétaines sous l’Himalaya. Chaque séisme majeur est entouré d’une série de répliques (zone gris clair). Pour certains séismes, comme ceux de Bhuj (Copley et al., 2011) et de Gorkha (McNamara et al., 2017), les répliques se propagent jusqu’à la croûte inférieure. Ces répliques créent des chemins d’infiltration de fluides, symbolisés par les flèches bleues dans l’encart. Les fluides permettent l’hydratation et le métamorphisme de la granulite en éclogite et amphibolite. Dans la croûte inférieure la déformation se localise alors dans des bandes de cisaillement éclogitiques et amphibolitiques. Les fluides peuvent provenir de la déshydratation de méta-sédiments de la croûte plongeante ou du manteau sous-jacent. D’après Jamtveit et al. (2019), modifié d’après Jamtveit et al. (2018a).

## 1.4 Les rétroactions déformation - réactions - fluides

### 1.4.1 Exemples de rétroactions

Les précédents paragraphes montrent que l’éclogitisation de la croûte inférieure nécessite infiltration de fluides et déformation. La figure 1.13 illustre schématiquement certaines des rétroactions possibles entre réactions métamorphiques, circulation de fluides, déformation et rhéologie dans les roches crustales ; et la figure 1.14 illustre la complexité de ces rétroactions à travers un exemple de terrain des Alpes (Steffen et al., 2001). La synthèse suivante propose une brève description des couplages schématisés sur la figure 1.13.

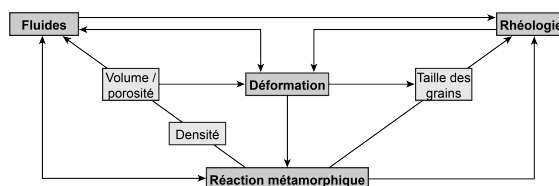


FIGURE 1.13 – Rétroactions possibles entre fluides, déformation et réaction métamorphique.

**Effet des fluides.** La présence de fluides facilite les réactions métamorphiques en catalysant la réaction des roches métastables (e.g. Austrheim, 1987 ; Incel et al., 2020 ; Baïsset,

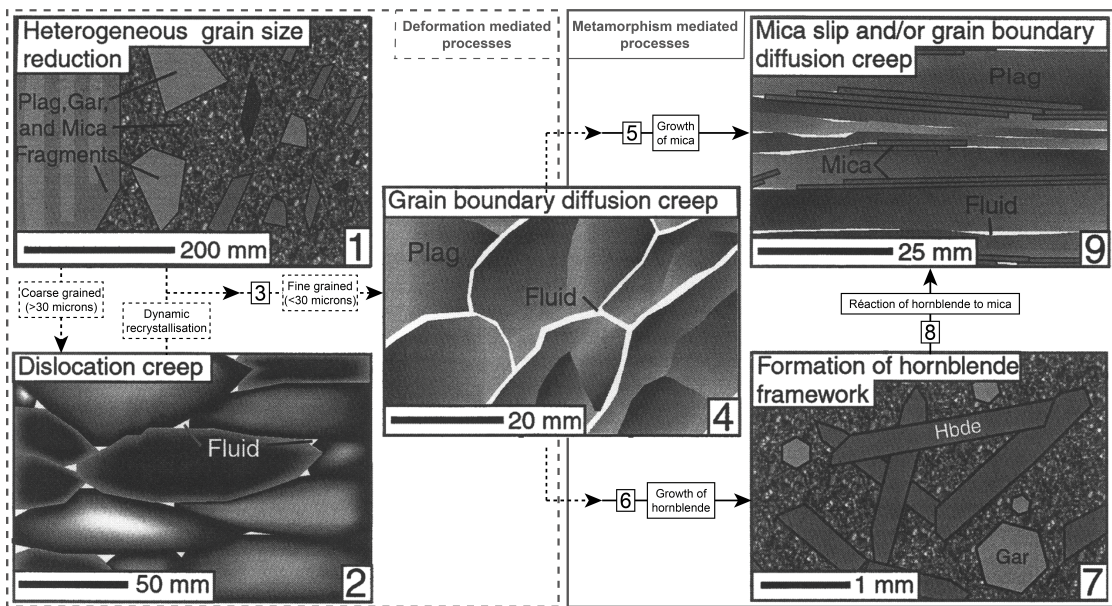


FIGURE 1.14 – Rétroactions fluides-déformation-réaction dans une bande de cisaillement amphotolitique des Alpes, modifié d'après Steffen et al. (2001). A gauche, les processus sont dominés par la déformation (traits pointillés), et à droite par les réactions métamorphiques (traits pleins). (1) au début du cisaillement, la taille des grains est hétérogène. (2) La déformation est accommodée par fluage de dislocations, et l'apport de fluides est limité. (3) La taille des grains est réduite par cataclase et par recristallisation dynamique. (4) La faible taille des grains et l'afflux de fluides causés par la déformation activent un mécanisme de déformation par fluage diffusion aux joints de grains (Tullis et Yund, 1991), qui affaiblit la roche. La présence de fluides interconnectés favorise la cristallisation de micas (5) et de hornblende (6) aux dépens du plagioclase. (7) Les grains millimétriques de hornblende forment une structure rigide qui augmente la résistance de la roche. (8) La hornblende est remplacée par de la biotite, plagioclase et quartz. (9) Le nouvel assemblage dominé par des grains allongés de mica et de plagioclase est fortement déformé.

2023), et en permettant le remplacement des minéraux par dissolution-précipitation (Putnis et Austrheim, 2010). Ils fournissent également un mécanisme de transport d'éléments dissous (e.g. Putnis et Austrheim, 2010) qui induit un changement de la composition chimique thermodynamique et peut induire des réactions métamorphiques (e.g. Koons et al., 1987 ; Goncalves et al., 2012). L'introduction de fluides dans la maille cristalline des minéraux réduit leur viscosité, les rendant plus facilement déformables (e.g. Rybacki et Dresen, 2000 ; Kohlstedt, 2006 ; Baïsset, 2023). De hautes pressions fluides peuvent également diminuer la pression effective et ainsi faciliter la fracturation et les séismes (e.g. Audet et al., 2009 ; Sibson, 2014).

**Effet des réactions métamorphiques.** Les réactions de déshydratation des minéraux hydratés sont une source majeure de fluides dans la croûte (e.g. Peacock, 1990). Les réactions métamorphiques augmentent la densité de la roche si les minéraux néoformés sont plus denses que ceux du protolith, comme lors de la transformation de la granu-

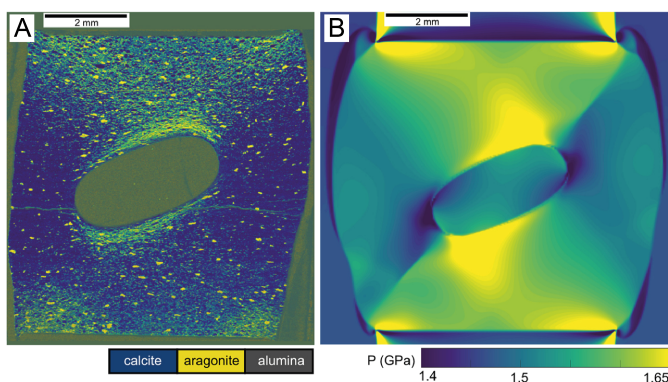


FIGURE 1.15 – Impact de la déformation sur les transitions de phases métamorphiques, modifié d'après Cionoiu et al. (2019). A la fin d'une expérience de compression verticale d'un milieu contenant une inclusion résistante d'alumine, la calcite de départ s'est transformée en son polymorphe de haute pression, l'aragonite (A). (B) Un modèle numérique montre que la distribution des hautes pression est associée à la transformation de calcite en aragonite.

lite en éclogite (e.g. Austrheim, 1987). Une augmentation de densité peut causer une augmentation de la porosité permettant la circulation de fluides (Plümper et al., 2017), ou peut générer des contraintes capables de fracturer la roche (Yamato et al., 2022). Les réactions métamorphiques qui diminuent la densité, par exemple l'amphibolitisation de la granulite (Centrella, 2019), occasionnent une augmentation du volume solide, qui peuvent causer la fracturation (e.g. Jamtveit et al., 2008 ; Malvoisin et al., 2021). Les réactions métamorphiques peuvent remplacer des phases résistantes par d'autres moins résistantes (e.g. Oliot et al., 2010), et diminuer la taille des grains néoformés (e.g. Marti et al., 2018), ce qui affaiblit la roche en activant des mécanismes de déformation par fluage diffusion, sensibles à la taille des grains (e.g. Rutter et Brodie, 1988, figure 1.14).

**Effet de la déformation.** Les déformations cassantes et visqueuses créent des chemins d'infiltration de fluides, sous forme de réseaux de fractures et de bandes de cisaillement, qui apportent des fluides au système (e.g. Fusseis et al., 2009). Les contraintes tectoniques peuvent créer des variations locales de pression de l'ordre de 10 kbar, à l'échelle de la croûte (Gerya, 2015 ; Bauville et Yamato, 2021) ou du grain (Tajčmanová et al., 2014). Les variations de pression peuvent déclencher des réactions métamorphiques, même à l'échelle millimétrique (figure 1.15, Cionoiu et al., 2019). La déformation peut entraîner une recristallisation des minéraux qui réduit la taille des grains (e.g. Rutter, 1995, 1.14), changeant la rhéologie de la roche.

#### 1.4.2 Bandes de cisaillement

Les rétroactions fluides-réaction-déformation dans la croûte inférieure s'expriment au mieux dans les bandes de cisaillement (figure 1.16, Fossen et Cavalcante, 2017 ; Ceccato et al., 2022). Ce sont des objets géologiques de toute première importance car elles localisent une grande partie de la déformation dans la croûte inférieure et le manteau, et sont donc les homologues plus profonds des failles de la croûte supérieure

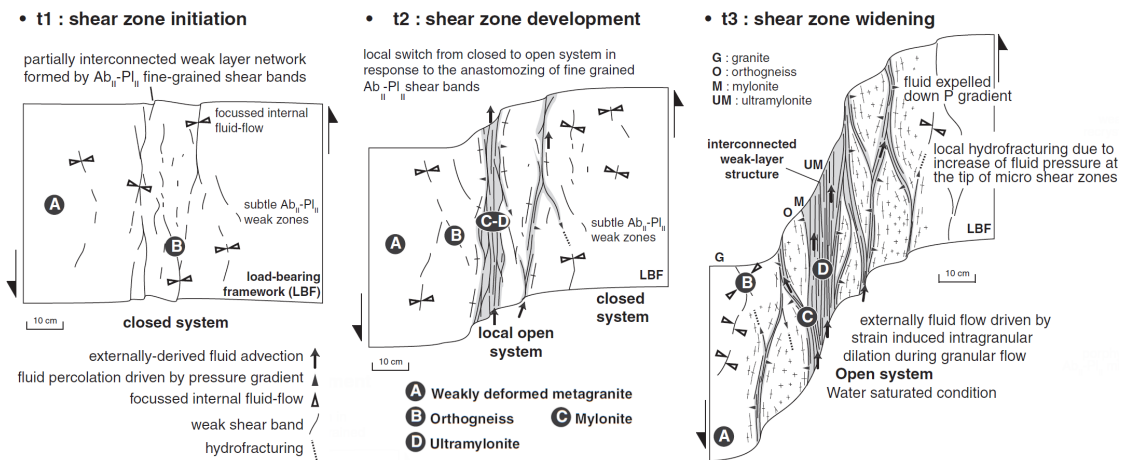


FIGURE 1.16 – Exemple de formation et évolution d'une bande de cisaillement granitique dans le massif du Saint-Gothard, Alpes suisses, modifié d'après Oliot et al. (2014). L'évolution du réseau de bandes de cisaillement est due à la fois à la déformation et aux fluides. Des gradients de pressions causent le transport de fluides vers l'extérieur de la bande de cisaillement. Le transport d'éléments chimiques assisté par les fluides cause le rééquilibrage de l'assemblage granitique en un assemblage métamorphique moins résistant à grains fins, provoquant l'élargissement la bande de cisaillement.

(Bürgmann et Dresen, 2008 ; Fossen et Cavalcante, 2017).

La nucléation des bandes de cisaillement se fait à partir de structures cassantes pré-existantes (veines, failles), dans lesquels l'infiltration de fluides induit une transition entre un régime cassant et un régime ductile (figure 1.16 t1, Mancktelow et Pennacchioni, 2005 ; Pennacchioni et Mancktelow, 2018 ; Leydier et al., 2019). Dans un deuxième temps, le développement de bandes de cisaillement s'accompagne de modifications minéralogiques, qui dans la plupart des cas diminuent la taille des grains, provoquent l'affaiblissement rhéologique et la localisation de la déformation (figure 1.16 t2, Gueydan et al., 2003 ; Oliot et al., 2010 ; Oliot et al., 2014 ; Ceccato et al., 2018). Déformation et réaction métamorphique sont concomitants avec l'infiltration de fluides qui viennent accélérer la cinétique des réactions métamorphiques (Austrheim, 1987 ; Früh-Green, 1994 ; Incel et al., 2020) et faciliter le transport et la redistribution d'éléments chimiques (Goncalves et al., 2012 ; Oliot et al., 2014 ; Moore et al., 2020a ; Weber et al., 2022).

Les bandes de cisaillement s'élargissent progressivement si le contraste de viscosité entre bande de cisaillement et encaissant est diminué au cours du temps (Fossen et Cavalcante, 2017), soit par affaiblissement de l'encaissant (figure 1.16 t3, Oliot et al., 2010 ; Kaatz et al., 2021), soit par durcissement de la bande de cisaillement (Steffen et al., 2001 ; Vitale et Mazzoli, 2008).

Étant donné l'omniprésence des bandes de cisaillement dans la croûte inférieure (Fossen et Cavalcante, 2017), étudier les rétroactions fluides-réaction-déformation qui s'y produisent est primordial pour comprendre la progression des réactions métamor-

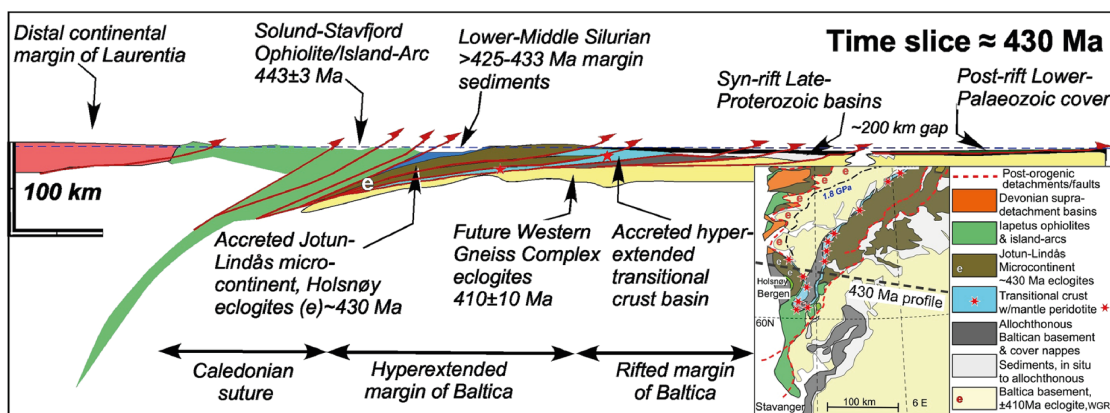


FIGURE 1.17 – Reconstitution d'une coupe géologique E-W du Sud des Calédonides scandinaves il y a 430 Ma, d'après Jamtveit et al. (2018b). Le micro-continent Jotun-Lindås, auquel appartiennent les roches de Holsnøy, est en cours d'enfouissement. Le métamorphisme amphibolitique et éclogitique se produit à cette période. L'encart montre la localisation de la coupe sur la carte géologique du sud-ouest de la Norvège.

phiques, le comportement mécanique, et l'exhumation des roches subduites. Cette thèse s'attache donc en partie à comprendre la formation et l'évolution de bandes de cisaillements éclogitiques dans la croûte inférieure à partir de l'exemple de terrain d'Holsnøy, en Norvège.

## 1.5 Holsnøy : un exemple d'éclogitisation de la croûte inférieure

L'île d'Holsnøy, au sud-ouest de la Norvège, est une fenêtre idéale sur les processus métamorphiques, les interactions fluides-roche et la déformation cassante comme ductile qui se sont produits dans la croûte inférieure aujourd'hui exhumée (Austrheim, 1987, 2013 ; Putnis et al., 2017). La relation entre éclogite et granulite y est exceptionnellement bien préservée, ce qui en fait un analogue idéal de l'état métamorphique de la croûte inférieure enfouie en profondeur lors d'événements orogéniques (Jackson et al., 2004 ; Labrousse et al., 2010). La relation entre éclogite et granulite peut y être étudiée à toutes les échelles, de l'échelle de la carte à l'échelle microscopique.

### 1.5.1 Contexte géologique

L'île d'Holsnøy appartient à la nappe de Lindås, qui est marquée par deux événements métamorphiques distincts : l'orogenèse Grenvillienne (ou Svéconorvégienne) et l'orogenèse Calédonienne (Glodny et al., 2008).

Les anorthosites (plus de 90 % de plagioclase) granulitiques de la nappe de Lindås appartiennent à un ensemble magmatique dont la composition va de l'anorthosite au granite (Kolderup et Kolderup, 1940), cristallisé entre 1240 Ma et 950 Ma (Bingen

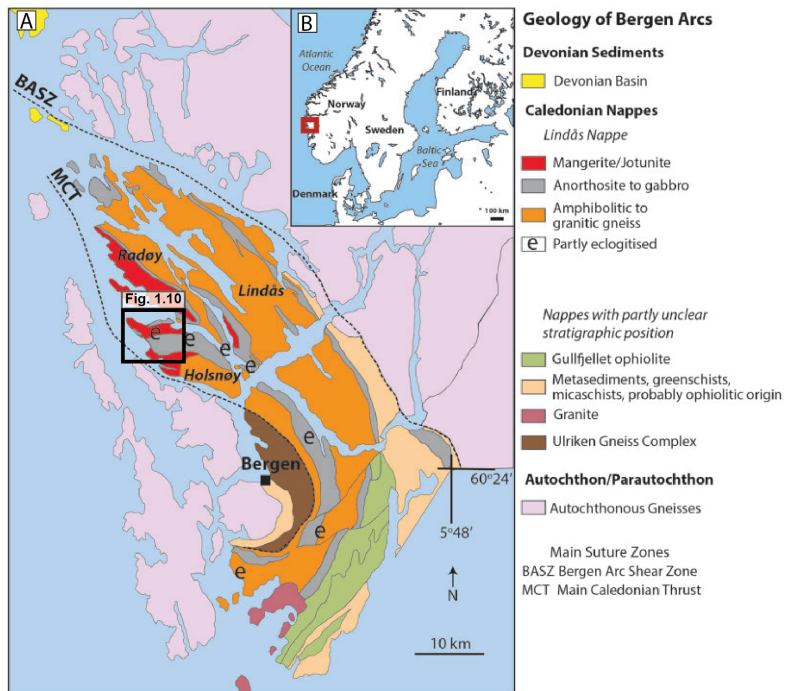


FIGURE 1.18 – Carte géologique des Arcs de Bergen (A), et leur position en Norvège (B), d'après Putnis et al., 2017. Le faciès éclogitique, indiqué par "e", est limité à l'ouest des Arcs de Bergen.

et al., 2001). Ces anorthosites ont été métamorphisées et déformées dans le faciès des granulites ( $P < 10$  kbar,  $T = 800\text{--}900$  °C, Austrheim et Griffin, 1985) entre 910 et 930 Ma, lors de l'orogenèse Grenvillienne/Svéconorvégienne (Cohen et al., 1988 ; Bingen et al., 2001), ce qui a résulté en un assemblage minéralogique anhydre. Ces granulites faisaient alors partie de la croûte inférieure du supercontinent Rodinia.

L'orogenèse Calédonienne, causée par la convergence entre les continents Laurentia et Baltica, a résulté en la formation de la chaîne de montagnes calédonienne entre 400 et 440 Ma (Roberts, 2003 ; Jakob et al., 2017). La collision a notamment entraîné l'empilement d'une série de nappes, les Arcs de Bergen, dont fait partie la nappe de Lindås. La figure 1.17 montre une interprétation de la phase de collision il y a 430 Ma.

Lors de cette collision et de la subduction qui a suivi, les granulites se sont partiellement métamorphisées dans le faciès des amphibolites et des éclogites. Le métamorphisme amphibolitique est observé sur toute la nappe de Lindås, et le métamorphisme éclogitique se concentre essentiellement sur l'île d'Holsnøy (figure 1.18, Boundy et al., 1996 ; Glodny et al., 2008 ; Moore et al., 2020b). A Holsnøy, les métamorphismes amphibolitique et éclogitique sont quasiment contemporains, se produisant tous deux entre 423 et 428 Ma (Jamtveit et al., 2018b, 2019 ; Moore et al., 2020b).

### 1.5.2 L'éclogitisation à Holsnøy

A Holsnøy, la transformation de la granulite en éclogite n'est que partielle, et l'éclogitisation est hétérogène à toutes les échelles, de celle de l'échantillon à celle de la

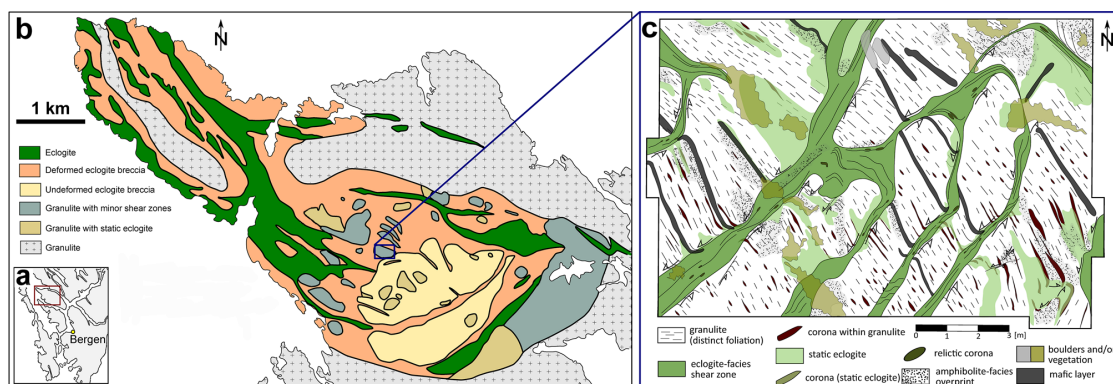


FIGURE 1.19 – Hétérogénéité de l’éclogitisation à Holsnøy, d’après Kaatz et al. (2023). (a) Position de Holsnøy dans les Arcs de Bergen, et (b) carte géologique du nord-ouest d’Holsnøy, montrant l’étendue de l’éclogitisation, d’après Zertani et al. (2020). (c) Carte d’un affleurement montrant un réseau de bandes de cisaillement éclogitiques décimétriques à métriques recoupant la granulite, d’après Kaatz et al. (2021).

carte (figure 1.19). Un apport de fluides est nécessaire pour cristalliser les minéraux éclogitiques hydratés (zoisite, mica), et pour catalyser les réactions métamorphiques (Rubie, 1986; Putnis et John, 2010). La granulite n’a donc été affectée par l’éclogitisation qu’aux endroits affectés par une circulation de fluides, sans quoi elle a été préservée à des conditions  $P-T$  métastables (Austrheim, 1987; Jamtveit et al., 1990). Les éclogites sont équilibrées à des conditions  $P-T$  de 17–22 kbar et 670–760 °C (Austrheim, 1987; Jamtveit et al., 1990; Austrheim, 1998; Kühn et al., 2002; Raimbourg et al., 2007b; Glodny et al., 2008; Bhowany et al., 2018; Zhong et al., 2019).

Les roches de Holsnøy, ainsi que le reste de la nappe de Lindås, ont subi un métamorphisme dans le faciès des amphibolites à des conditions  $P-T$  estimées à 8–14 kbar, 525–730 °C (Austrheim et Griffin, 1985; Austrheim, 1987; Boundy et al., 1996; Kühn et al., 2002; Glodny et al., 2008; Jamtveit et al., 2019; Moore et al., 2020b). Des datations récentes suggèrent que le métamorphisme amphibolitique pourrait avoir eu lieu moins de 5 Ma après les conditions maximales du métamorphisme éclogistique, voire simultanément (Jamtveit et al., 2018b, 2019). Le métamorphisme amphibolitique est similaire au métamorphisme éclogistique, se formant dans des bandes de cisaillement et dans des zones d’altération statiques, les deux faciès métamorphiques pouvant coexister sur le même affleurement (Centrella, 2019).

L’éclogitisation est majoritairement observée dans des bandes de cisaillement éclogitiques qui associent circulation de fluides, réactions métamorphiques, et déformation ductile (Austrheim, 1987; Bjørnerud et al., 2002; Putnis et al., 2017). Ces bandes de cisaillement s’élargissent progressivement au fil du temps et s’anastomosent pour former des réseaux de bandes de cisaillement (Jolivet et al., 2005; Zertani et al., 2019; Kaatz et al., 2021). Ainsi, des bandes de cisaillement de quelques centimètres d’épaisseur

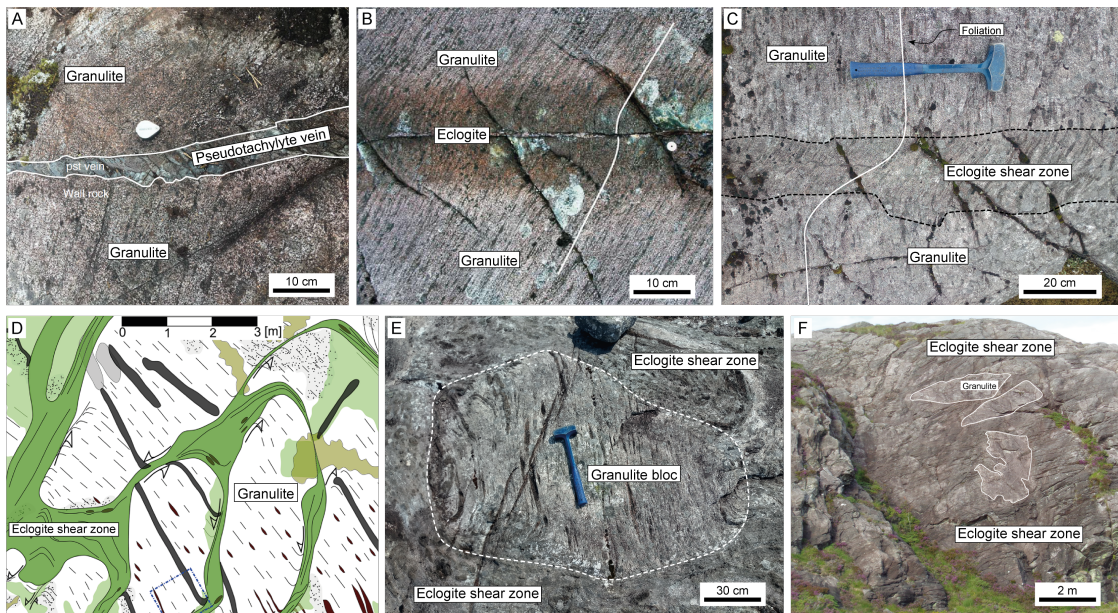


FIGURE 1.20 – Exemples des différents stades d’éclogitisation à Holsnøy. (A) Pseudotachylyte, issue de la fusion frictionnelle causée par la chaleur libérée lors du glissement rapide le long d’un plan de faille pendant un séisme. La pseudotachylyte recoupe la granulite. Modifié d’après Zhong et al. (2021). (B) Halo d’éclogitisation causé par l’infiltration de fluides autour d’une fracture centrale. La foliation granulitique, soulignée par le trait blanc, est légèrement déviée par le halo éclogitique, formant le début d’une bande de cisaillement. Modifié d’après Fossen et Cavalcante (2017). (C) Bande de cisaillement éclogitique décimétrique recoupant et déviant nettement la foliation granulitique, soulignée par le trait blanc. (D) Détail de la carte d’un affleurement présenté sur la figure 1.19, montrant un réseau de bandes de cisaillement éclogitiques décimétriques à métriques recoupant la granulite. Modifié d’après Kaatz et al. (2021). (E) Bloc de granulite isolé par des bandes de cisaillement éclogitiques. (F) Bande de cisaillement majeure englobant des blocs de granulite préservés, encadrés en blanc.

peuvent finir par former des bandes majeures de plus de 100 m de large (Boundy et al., 1992; Raimbourg et al., 2005), dont tous les intermédiaires sont visibles à l’affleurement (figure 1.20). L’histoire de l’éclogitisation et de la déformation à Holsnøy peut être résumée comme suit (e.g. Austrheim, 1987; Boundy et al., 1992; Jolivet et al., 2005; Raimbourg et al., 2005; Jamtveit et al., 2018b; Zertani et al., 2019; Kaatz et al., 2021) :

- (1) Des séismes dans la croûte inférieure en collision propagent des fractures dans la granulite anhydre et rigide. Cet épisode de déformation est associé à la formation de pseudotachylites (roches de faille issues de la fusion frictionnelle lors d’un séisme, figure 1.20A) bordées de zones d’endommagement, témoins de l’activité sismique (Petley-Ragan et al., 2018, 2019). L’intense diminution de taille de grain dans les zones de faille affaiblit mécaniquement la granulite.
- (2) Les fractures permettent l’infiltration de fluides dans la granulite métastable.
- (3) La présence de fluides déclenche l’éclogitisation de la granulite dans les régions hydratées qui entourent les fractures (figure 1.20B). L’éclogitisation et l’hydratation affaiblissent mécaniquement la granulite.
- (4) La déformation se localise

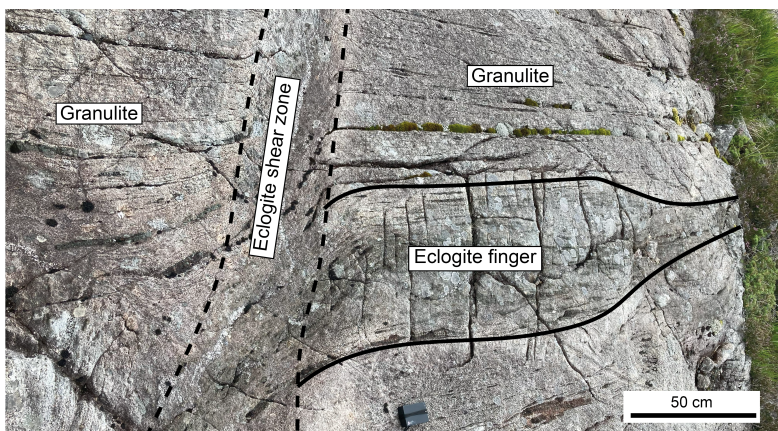


FIGURE 1.21 – Relation entre bande de cisaillement et digitation éclogitique à Holsnøy.

dans les régions affaiblies, formant des bandes de cisaillement éclogitiques (figure 1.20C). Simultanément, un front d'hydratation se propage vers l'extérieur de la bande de cisaillement, élargissant progressivement la région affaiblie. (5) La propagation du front d'hydratation permet l'éclogitisation et donc l'affaiblissement de la granulite hôte qui se met à localiser la déformation. Ainsi les bandes de cisaillement éclogitiques se propagent, s'élargissent et se connectent entre elles (figure 1.20D). (6) Suivant le même processus, un réseau de bandes de cisaillement anastomosées d'échelle métrique se forme, et découpe des blocs de granulite qui survivent à l'éclogitisation (figure 1.20E). (7) Au stade le plus avancé, l'éclogite est organisée en bandes de cisaillement décamétriques à hectométriques, dans lesquelles des blocs de granulite isolés sont orientés aléatoirement, suite à la rotation subie pendant le cisaillement (figure 1.20F).

Alors que l'éclogitisation à Holsnøy est systématiquement associée à la circulation de fluides, ce n'est pas le cas pour la déformation. Une grande partie de l'éclogitisation à Holsnøy ne se fait pas dans des bandes de cisaillement, mais dans des zones d'éclogitisation dites "statiques", associées seulement à l'infiltration de fluides (Jamtveit et al., 2000; Zertani et al., 2019). L'éclogitisation statique se manifeste sous forme de digitations éclogitiques qui se propagent dans la granulite le long de sa foliation, et qui ont le plus souvent pour base des bandes de cisaillement (figure 1.21). Alors que les bandes de cisaillement recoupent la foliation granulitique préexistante, les digitations éclogitiques s'impriment sur la foliation granulitique. Putnis et al. (2021) interprètent ces digitations comme le résultat d'afflux sporadiques (pulses) de fluides qui font épisodiquement progresser l'éclogitisation dans la granulite.

L'évolution de l'éclogitisation et de la déformation présentée précédemment suppose que la granulite anhydre et métastable a subi les mêmes conditions  $P-T$  que l'éclogite, mais que l'absence de fluides comme catalyseur de la réaction a permis sa préservation. Une autre explication plausible (Jamtveit et al., 2018b; Bhowany, 2020; Putnis et al., 2021; Zhong et al., 2021; Moulas et al., 2022) est que l'affaiblissement causé par les

fluides crée des hétérogénéités rhéologiques dans une roche subissant des déformations, ce qui peut entraîner des variations de pression significatives. Cela peut expliquer la coexistence d'éclogite et granulite sans que cette dernière soit métastable à des conditions de pressions du faciès éclogite. Ainsi, l'étude de pseudotachylytes a montré que l'épisode de déformation cassante a pu avoir lieu à des conditions  $P-T$  de 15-16 kbar et 675–700 °C (Bhowany et al., 2018 ; Zhong et al., 2021). La différence entre les pressions enregistrées pendant l'initiation de la déformation (15-16 kbar) et les pressions enregistrées par l'éclogite (17-22 kbar) pourraient alors s'expliquer par des variations locales de pression causées par la déformation (Jamtveit et al., 2018b).

La distinction entre ces deux scénarios est cruciale pour interpréter la profondeur à laquelle s'est produit l'éclogitisation. Le scénario "métastable" suppose que la pression enregistrée par les roches métamorphiques est uniquement due à la pression lithostatique, c'est à dire au poids de la colonne de roche sus-jacente. Ainsi la pression de 21-22 kbar correspondrait à une profondeur d'environ 70 km (Jamtveit et al., 2018b). Dans l'hypothèse "surpression locale" la pression lithostatique serait de l'ordre de 15 kbar, ce qui correspond à une profondeur d'environ 50 km. Cette différence de 20 km changerait drastiquement nos interprétations des chemin  $P-T$  d'enfouissement et d'exhumation de la croûte inférieure en subduction (Jolivet et al., 2005 ; Raimbourg et al., 2007a ; Bhowany et al., 2018 ; Bhowany, 2020).

## 1.6 La modélisation numérique

### 1.6.1 Principe

Les modèles numériques tentent de combler un vide (Gerya, 2019) : l'étude de roches métamorphiques à l'affleurement donne accès à une information spatialement limitée, et les méthodes géophysiques donnent accès à l'état actuel de la croûte, mais pas son évolution temporelle. La modélisation numérique permet de donner une information sur l'évolution spatio-temporelle de la Terre, en utilisant des données pétrologiques et géophysiques. Selon la finalité du modèle numérique, les processus peuvent être modélisés à l'échelle de la Terre toute entière (Coltice et Shephard, 2018) comme à celle du grain (Tajčmanová et al., 2015) ; à l'échelle du jour (Malvoisin et al., 2020) comme à celle du milliard d'années (Rolf et Tackley, 2011).

Les modèles numériques nécessitent de résoudre des **équations de conservation** qui décrivent des processus physiques, telles que les lois du mouvement de Newton, ainsi que des **équations constitutives** qui décrivent comment les matériaux réagissent aux forces extérieures, telles que les lois de fluage. Un principe fondamental de la modélisation numérique est de résoudre autant d'équations qu'il y a d'inconnues à

calculer. Ainsi plus un modèle est complexe et inclut de variables, plus il doit inclure d'équations à résoudre.

### 1.6.2 Équations de conservation

Les modèles thermomécaniques "classiques" (e.g. Duretz et al., 2011; Le Pourhiet et al., 2012; Schmalholz et Podladchikov, 2013) ne considèrent pas plus de 3 équations de conservations (e.g. Gerya, 2019; van Zelst et al., 2022) : la conservation de la masse, la conservation du moment, et la conservation de l'énergie thermique. La résolution de ces équations permet respectivement de calculer l'évolution de la pression, de la vitesse et de la température.

(1) L'équation de continuité, ou conservation de la masse :

$$\frac{\partial \rho}{\partial t} + \nabla \cdot (\rho \vec{v}) = 0, \quad (1.2)$$

où  $\rho$  est la densité,  $t$  est le temps, et  $\vec{v}$  est la vitesse. Le terme  $\frac{\partial \rho}{\partial t}$  représente la variation de masse au cours du temps, et  $\nabla \cdot (\rho \vec{v})$  le flux de masse rentrant ou sortant. Selon cette équation, les variations de masse par expansion ou contraction doivent être compensées par un flux de matériel qui rentre ou sort du système.

(2) L'équation du mouvement, équation de Stokes, ou conservation du moment :

$$\nabla \sigma + \rho g = 0, \quad (1.3)$$

où  $\sigma$  est le tenseur des contraintes totales et  $g$  l'accélération gravitationnelle. Le terme  $\nabla \sigma$  représente les contraintes surfaciques, dues à la viscosité des fluides, et  $\rho g$  une force volumique, en l'occurrence le poids. Issue de la deuxième loi de Newton, cette équation décrit les changements de vitesse d'un milieu quand il est soumis à des forces. A l'échelle géodynamique les termes inertIELS sont négligeables à cause de la grande viscosité des fluides considérés.

(3) L'équation de la chaleur, ou conservation de l'énergie thermique :

$$\rho C_p \left( \frac{\partial T}{\partial t} + \vec{v} \nabla T \right) - \nabla \cdot (k \nabla T) = \rho H + S, \quad (1.4)$$

où  $C_p$  est la capacité thermique,  $T$  la température,  $k$  la conductivité thermique,  $H$  une production de chaleur volumétrique interne, et  $S$  une source de chaleur externe. Le terme  $\rho C_p \frac{\partial T}{\partial t}$  représente les variations d'énergie thermique au cours du temps,  $\rho C_p \vec{v} \nabla T$  le transport de chaleur par advection, et  $\nabla \cdot (k \nabla T)$  la diffusion de la chaleur. Cette équation décrit les variations de chaleur dans un milieu en fonction de son transport par advection et conduction, et de sa production ou consommation.

### 1.6.3 Modèles à deux phases

Les modèles thermomécaniques font l'approximation que le milieu à modéliser n'est composé que d'une phase solide. Ces modèles peuvent être étendus pour inclure à la fois une phase solide et une phase fluide, par exemple de l'eau ou du magma. La phase fluide est stockée dans la porosité de la roche, et la phase solide constitue le reste du milieu. Il faut alors résoudre les équations de conservation de la masse, du moment et de l'énergie pour chacune des 2 phases (e.g. McKenzie, 1984; Bercovici et al., 2001).

Dans les modèles à deux phases, les propriétés de l'ensemble fluide-solide peuvent être définies comme une moyenne des propriétés des deux phases, pondérées par la porosité (e.g. Keller et al., 2013) :

$$\bar{a} = (1 - \phi)a_s + \phi a_f, \quad (1.5)$$

où  $a$  est une propriété de valeur  $a_s$  dans la phase solide et  $a_f$  dans la phase fluide, et  $\phi$  la porosité.

### 1.6.4 Équations constitutives

Les équations de conservation nécessitent des hypothèses sur la façon dont les matériaux réagissent aux forces et conditions extérieures. Ces relations sont appelées équations constitutives et décrivent les propriétés des matériaux, et leur dépendance aux variables qui apparaissent dans les équations de conservation, telles que la température et la pression (van Zelst et al., 2022). Le choix des équations constitutives est une source de grande variabilité des résultats des modèles numériques. Des équations constitutives peuvent être par exemple :

(1) La rhéologie, qui détermine la relation entre les contraintes et la vitesse de déformation, et décrit ainsi comment les matériaux se déforment lorsqu'ils sont exposés à des contraintes. Dans la croûte, la déformation des roches est une combinaison de comportement visqueux (écoulement d'un fluide), fragile (rupture cassante d'un solide) et élastique (déformation réversible d'un solide) (e.g. Gerya, 2019). Des lois rhéologiques décrivent alors ces modes de déformation, et déterminent lequel est actif à des conditions de pression, température et vitesse de déformation données. Pour des fluides newtoniens, la rhéologie visqueuse est décrite par :

$$\tau = 2\eta\dot{\epsilon}, \quad (1.6)$$

où  $\tau$  est la contrainte déviatorique (en Pa),  $\eta$  est la viscosité (en Pa s) et  $\dot{\epsilon}$  est la vitesse de déformation (en  $s^{-1}$ ). La viscosité est une propriété d'un matériau ductile qui décrit la résistance qu'il oppose à son écoulement.

La rhéologie fragile est classiquement décrite par la loi de Drucker-Prager, ou loi de friction :

$$\tau_y = C \cos(\alpha) + P \sin(\alpha), \quad (1.7)$$

où  $\tau_y$  est la contrainte cisaillante de rupture (en Pa),  $P$  la pression (en Pa),  $C$  la cohésion du matériau (en Pa) et  $\alpha$  l'angle de friction du matériau.

La rhéologie élastique est classiquement décrite par la loi de Hooke, où la déformation élastique est proportionnelle aux contraintes appliquées :

$$\sigma = E \varepsilon, \quad (1.8)$$

où  $\sigma$  est la contrainte (en Pa),  $E$  un module d'élasticité caractéristique du matériau (en Pa), et  $\varepsilon$  est la variation de longueur relative (adimensionnée). Pour un matériau isotrope, la loi de Hooke peut s'écrire comme une combinaison d'une contribution déviatorique et une contribution volumétrique :

$$\tau = 2G\varepsilon', \quad (1.9)$$

$$P = 3K\bar{\varepsilon}, \quad (1.10)$$

où  $\tau$  est la contrainte cisaillante (en Pa),  $P$  la pression (en Pa),  $G$  le module de cisaillement (en Pa),  $K$  le module d'incompressibilité (en Pa),  $\varepsilon'$  la déformation élastique cisaillante (adimensionnée),  $\bar{\varepsilon}$  la déformation élastique volumétrique (adimensionnée).  $G$  et  $K$  sont des propriétés des solides qui décrivent leur rigidité vis à vis, respectivement, d'une déformation cisaillante et d'une déformation volumétrique. La déformation élastique est réversible : si la contrainte appliquée à un matériau élastique disparaît, le matériau retrouve sa forme d'origine.

(2) Des équations d'état décrivant la relation entre les propriétés d'un matériau, comme sa densité, et sa température, pression et composition chimique. Des logiciels tels que Perple\_X (Connolly, 2005) ou Theriaak-Domino (de Capitani et Petrakakis, 2010) utilisent ces équations d'état pour calculer les propriétés des matériaux à une température, pression et composition chimique donnée, à l'aide de bases de données des propriétés thermodynamiques des minéraux (Holland et Powell, 1998; Holland et Powell, 2011). Ces propriétés peuvent ensuite être intégrées dans les équations de conservation des modèles numériques (e.g. Gerya et al., 2004; Nakagawa et al., 2009; Malvoisin et al., 2015).

(3) La loi de Darcy (Darcy, 1856), qui peut être généralisée pour décrire la conservation du moment d'un fluide compressible peu visqueux se déplaçant à travers le milieu

poreux visqueux, dans les modèles à deux phases (e.g. Connolly et Podladchikov, 1998) :

$$\phi(\vec{v}_f - \vec{v}_s) = \frac{k_\phi}{\eta_f}(\nabla P_f + \rho_f g), \quad (1.11)$$

où  $\phi$  est la porosité (adimensionnée),  $\vec{v}_f$  et  $\vec{v}_s$  sont les vitesses du fluide et du solide (en m/s),  $k_\phi$  est la perméabilité du milieu poreux (en  $\text{m}^2$ ),  $\eta_f$  est la viscosité du fluide (en Pa s),  $P_f$  la pression fluide (en Pa),  $\rho_f$  la densité du fluide (en  $\text{kg/m}^3$ ) et  $g$  l'accélération de la pesanteur (en  $\text{m/s}^2$ ).  $\eta_f$  et  $\rho_f$  sont des propriétés du fluide, et  $k_\phi$  est une fonction de la porosité et des propriétés du milieu solide.

### 1.6.5 Modèles numériques et couplages

L'état de l'art qui a précédé a montré que l'éclogitisation de la croûte inférieure est un phénomène complexe qui implique des rétroactions entre déformation, transport de fluides et réactions métamorphiques. Pour modéliser ces phénomènes, il faut donc prendre en compte à la fois (1) l'évolution de la pression et le transport de masse causés par la déformation, (2) l'évolution de la pression fluide et le transport de masse causés par la circulation des fluides, et (3) l'évolution des propriétés physiques des roches, comme la densité et la viscosité, en fonction des réactions métamorphiques.

Même si le comportement de la croûte est largement étudié par des modèles mécaniques et thermomécaniques, (e.g. Bird, 1978 ; Beaumont et al., 1996 ; Burg et Gerya, 2005 ; Duretz et al., 2011 ; Le Pourhiet et al., 2017), les modèles mécaniques prenant en compte les réactions métamorphiques sont plus rares (e.g. Gerya et al., 2004 ; Yamato et al., 2007 ; Larvet et al., 2022). Afin de prendre en compte l'interaction fluides-roche, le milieu modélisé est constitué d'une phase solide et d'une phase fluide indépendantes, chacune possédant ses propres propriétés, comme la densité, la viscosité ou la vitesse (e.g. McKenzie, 1984 ; Bercovici et al., 2001). Ces modèles à 2 phases ont été largement utilisés et développés pour étudier le comportement des magmas (e.g. McKenzie, 1984 ; Šrámek et al., 2007 ; Li et al., 2023), des ondes de porosité (e.g. Connolly et Podladchikov, 1998 ; Connolly et Podladchikov, 2013 ; Räss et al., 2019) ou de la lithosphère des zones de subduction (e.g. Dymkova et Gerya, 2013 ; Wang et al., 2019).

Il est commun en modélisation géodynamique d'utiliser l'approximation de Boussinesq (Boussinesq, 1897), suivant laquelle les variations de densité sont suffisamment petites pour pouvoir considérer que les roches sont des fluides incompressibles. L'équation de continuité (1.2) se simplifie alors pour devenir :

$$\nabla \cdot \vec{v} = 0. \quad (1.12)$$

Hetényi et al. (2011) ont mis en évidence que la plupart des modèles mécaniques qui

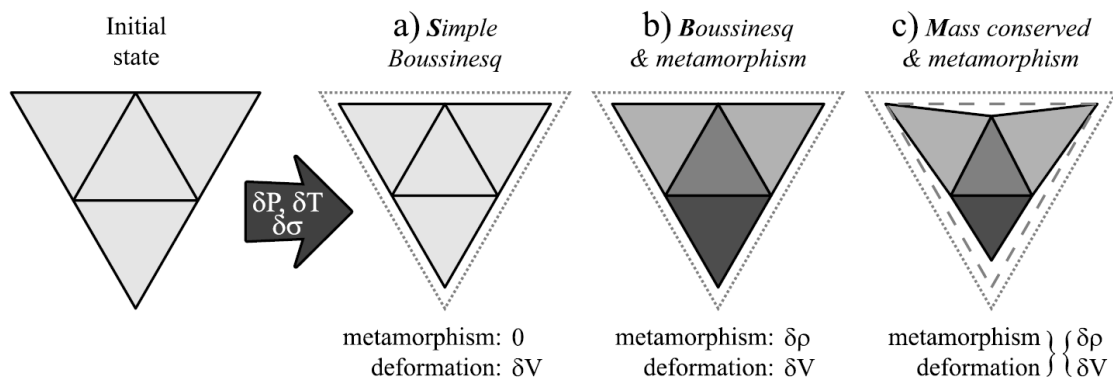


FIGURE 1.22 – Représentation schématique de différentes implémentations de la conservation de la masse et du métamorphisme dans les modèles numériques, Hetényi et al. (2011). La densité et le volume évoluent suivant la déformation et la variation de pression et température. (a) Le modèle le plus simple suit l’approximation de Boussinesq et ne prend pas en compte le métamorphisme ni n’inclut de variation de densité, même quand la déformation affecte le volume. (b) Dans un modèle qui suit l’approximation de Boussinesq et considère des réactions métamorphiques, les réactions font varier la densité mais pas le volume. Dans (a) et (b) la masse n’est pas conservée car volume et densité varient indépendamment. (c) Respectant la conservation de la masse, les variations de densité sont liées aux variations de volume.

ne prennent en compte ni les fluides ni les réactions métamorphiques utilisent cette approximation, alors que les variations de densité et de volume peuvent avoir des conséquences importantes sur le comportement mécaniques des roches (Schmeling et al., 2012; Keller et al., 2013; Yarushina et Podladchikov, 2015).

Dans la majorité des modèles qui prennent en compte les variations métamorphiques (e.g. Kaus et al., 2005; Yamato et al., 2007; Larvet et al., 2022), la densité change en fonction de la pression et de la température, mais le changement de volume associé est négligé, ce qui crée ou supprime artificiellement de la masse (figure 1.22b, Hetényi, 2014). Ces approximations (pas de variation de densité et pas de variation de volume) peuvent être une source d’erreurs significatives et la compressibilité devrait être prise en compte dans les modèles qui prennent en compte les réactions métamorphiques (figure 1.22, Hetényi et al., 2011; Hetényi, 2014). Dans les modèles qui incluent une phase fluide, prendre en compte les variations de densité et de volume induites par les réactions est essentiel et permet de modéliser la canalisation de fluides à grande échelle dans les zones de subduction (Plümper et al., 2017) ou bien l’évolution de fronts de réactions dans la croûte profonde peu perméable (Beinlich et al., 2020).

Récemment, Malvoisin et al. (2015) ont présenté un modèle à 2 phases qui permet de prendre en compte la conservation de la masse (équation 1.2), la déformation d’un solide compressible (équation 1.3), le transport d’un fluide compressible (équation 1.11), et les changements de propriétés du solide par réactions métamorphiques. Cette approche a permis le développement de modèles d’ondes de porosité réactives dans la croûte

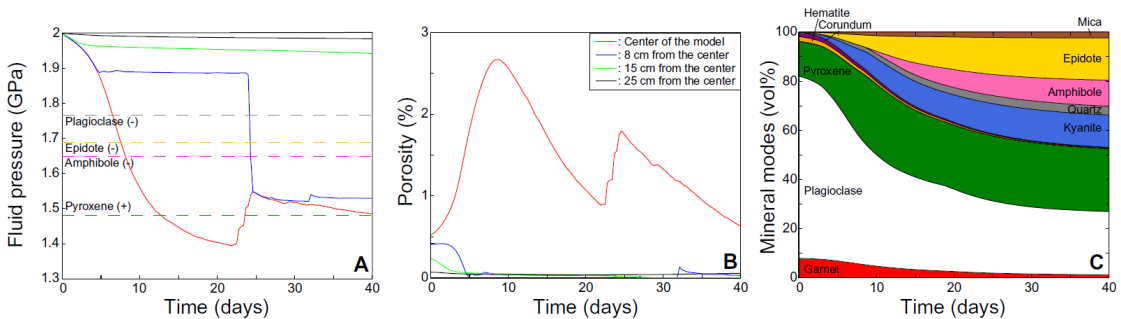


FIGURE 1.23 – Résultats d'un modèle numérique d'éclogitisation de la croûte inférieure, couplant réaction métamorphique, déformation et circulation de fluides, d'après Malvoisin et al., 2020. (A) Évolution au cours du temps de la pression fluide au centre du modèle, (ligne rouge), à 8 cm du centre (bleu), 15 cm (vert) et 25 cm (noir). Les lignes pointillées montrent les champs de stabilités des minéraux présents. (B) Évolution de la porosité en différents points du modèle. (C) Évolution des proportions minérales au coeur du modèle au cours du temps.

inférieure (Omlin et al., 2017), de déformation d'un milieu réactif rhéologiquement hétérogène (Schmalholz et al., 2020), de densification auto-entretenue de la croûte inférieure (figure 1.23, Malvoisin et al., 2020) ou de migration de matériel fondu dans le manteau (Bessat et al., 2022). Les modèles à 2 phases réactifs sont donc un outil puissant pour étudier les couplages entre déformation, transport des fluides et réaction métamorphique. Un des objectifs de cette thèse est de développer un tel modèle pour étudier l'éclogitisation de la croûte inférieure.

## 1.7 Problématique et structure de la thèse

L'état de l'art qui précède montre qu'il subsiste des lacunes dans nos connaissances de la croûte inférieure. Nos lacunes tiennent pour une part à la difficulté d'étudier cette couche profonde : l'observation directe par forage est impossible, les roches exhumées sont rares, les observations géophysiques peu précises. Ainsi, la rhéologie, la composition, la densité, l'état d'hydratation et même l'épaisseur de la croûte inférieure sont encore mal connus (Hacker et al., 2015).

Nos lacunes tiennent d'autre part à la complexité des interactions entre déformation cassante et ductile, réactions métamorphiques et fluides qui ont lieu dans la croûte inférieure en subduction. Ces interactions mal comprises qui peuvent agir à l'échelle du minéral déterminent la rhéologie, la densité et la composition de la croûte inférieure subduite. Ainsi, dans les zones de subduction on ne sait toujours pas si la croûte inférieure est rigide ou ductile, anhydre ou hydratée, dense ou non, éclogitisée ou granulitique, subduite à des profondeurs de 100 km ou 50 km.

J'ai présenté deux approches complémentaires permettant de répondre à ces questions : l'étude des roches crustales inférieures exhumées de Holsnøy, et la modélisation

numérique. L'objet de cette thèse est de combiner ces deux approches, afin d'améliorer notre compréhension de la rhéologie et des processus métamorphiques qui se déroulent au sein de la croûte inférieure dans les zones de convergence, en s'appuyant sur l'exemple de la réaction d'éclogitisation de la granulite. Les questions auxquelles je tente de répondre dans cette thèse sont les suivantes :

1. Par quels processus la granulite se transforme-t-elle en éclogite ?
2. Comment les bandes de cisaillement éclogitiques se propagent-elles dans la granulite ?
3. La déformation peut-elle propager l'éclogitisation de la croûte inférieure ?
4. Comment les fluides sont-ils transportés dans la croûte inférieure imperméable ?

Chacun des 3 articles écrits au cours de cette thèse apporte des éléments de réponse à ces questions. Si les applications de ces articles, et donc de cette thèse, peuvent sembler limitées à ce contexte, les méthodes développées et les implications des travaux peuvent s'appliquer à d'autres réactions et d'autres contextes géologiques.

Le premier article (Bras et al., 2021) porte sur les processus de transformation de la granulite en éclogite, et sur l'implication rhéologique d'une telle transformation. Je montre dans cette étude, en m'appuyant sur des observations pétrologiques, de terrain, et sur un modèle numérique, que l'éclogitisation assistée par des fluides affaiblit la granulite de manière transitoire.

Le deuxième article (Bras et al., 2023) étudie comment se propage la réaction d'éclogitisation à l'aide d'un modèle numérique. Je montre dans cette étude que même si la granulite n'a pas de porosité, et est donc imperméable, la propagation d'un front de haute pression fluide qui transforme la granulite en éclogite est possible, du moment que la transformation s'accompagne d'une augmentation de densité.

Le troisième article, en préparation, est une extension du précédent article qui prend en compte la mécanique et explore les conséquences de la déformation sur l'éclogitisation. Je montre que la déformation peut générer des variations locales de pression suffisantes pour éclogitiser la granulite.

## Bibliographie du présent chapitre

- Audet, P., Bostock, M. G., Christensen, N. I. & Peacock, S. M. (2009). Seismic evidence for overpressured subducted oceanic crust and megathrust fault sealing. *Nature*, 457(7225), 76-78. <https://doi.org/10.1038/nature07650>
- Austrheim, H. (1991). Eclogite formation and dynamics of crustal roots under continental collision zones. *Terra Nova*, 3(5), 492-499. <https://doi.org/10.1111/j.1365-3121.1991.tb00184.x>
- Austrheim, H. (1987). Eclogitization of lower crustal granulites by fluid migration through shear zones. *Earth and Planetary Science Letters*, 81(2-3), 221-232. [https://doi.org/10.1016/0012-821X\(87\)90158-0](https://doi.org/10.1016/0012-821X(87)90158-0)
- Austrheim, H. (2013). Fluid and deformation induced metamorphic processes around Moho beneath continent collision zones : Examples from the exposed root zone of the Caledonian mountain belt, W-Norway. *Tectonophysics*, 609, 620-635. <https://doi.org/10.1016/j.tecto.2013.08.030>
- Austrheim, H. (1998). Influence of fluid and deformation on metamorphism of the deep crust and consequences for the geodynamics of collision zones. In B. R. Hacker & J. G. Liou (Éd.), *When Continents Collide : Geodynamics and Geochemistry of Ultrahigh-Pressure Rocks* (p. 297-323). Springer Netherlands. [https://doi.org/10.1007/978-94-015-9050-1\\_12](https://doi.org/10.1007/978-94-015-9050-1_12)
- Austrheim, H. & Griffin, W. L. (1985). Shear deformation and eclogite formation within granulite-facies anorthosites of the Bergen Arcs, western Norway. *Chemical Geology*, 50(1-3), 267-281. [https://doi.org/10.1016/0009-2541\(85\)90124-X](https://doi.org/10.1016/0009-2541(85)90124-X)
- Babeyko, A. & Sobolev, S. V. (2008). High-resolution numerical modeling of stress distribution in visco-elasto-plastic subducting slabs. *Lithos*, 103(1-2), 205-216. <https://doi.org/10.1016/j.lithos.2007.09.015>
- Baïsset, M. (2023). *Déformation et transformations du plagioclase sous contrainte : implications pour la rhéologie de la croûte continentale inférieure à haute pression* (thèse de doct.). Sorbonne université.
- Bauville, A. & Yamato, P. (2021). Pressure-to-depth conversion models for metamorphic rocks : derivation and applications. *Geochemistry, Geophysics, Geosystems*, 22(1), e2020GC009280. <https://doi.org/10.1029/2020GC009280>
- Beaucé, E., Frank, W. B., Paul, A., Campillo, M. & van Der Hilst, R. D. (2019). Systematic detection of clustered seismicity beneath the Southwestern Alps. *Journal of Geophysical Research : Solid Earth*, 124(11), 11531-11548. <https://doi.org/10.1029/2019JB018110>
- Beaumont, C., Ellis, S., Hamilton, J. & Fullsack, P. (1996). Mechanical model for subduction-collision tectonics of Alpine-type compressional orogens. *Geology*, 24(8), 675-678. [https://doi.org/10.1130/0091-7613\(1996\)024<0675:MMFSCT>2.3.CO;2](https://doi.org/10.1130/0091-7613(1996)024<0675:MMFSCT>2.3.CO;2)
- Beinlich, A., John, T., Vrijmoed, J. C., Tominaga, M., Magna, T. & Podladchikov, Y. Y. (2020). Instantaneous rock transformations in the deep crust driven by reactive fluid flow. *Nature Geoscience*, 13(4), 307-311. <https://doi.org/10.1038/s41561-020-0554-9>
- Bercovici, D., Ricard, Y. & Schubert, G. (2001). A two-phase model for compaction and damage : 1. General theory. *Journal of Geophysical Research : Solid Earth*, 106(B5), 8887-8906. <https://doi.org/10.1029/2000JB900430>

- Bessat, A., Pilet, S., Podladchikov, Y. Y. & Schmalholz, S. M. (2022). Melt migration and chemical differentiation by reactive porosity waves. *Geochemistry, Geophysics, Geosystems*, 23(2), e2021GC009963. <https://doi.org/10.1029/2021GC009963>
- Bhowany, K. (2020). *Constraints on the fluid enhanced eclogitisation of granulite domains in the Bergen Arcs, Norway* (thèse de doct.).
- Bhowany, K., Hand, M., Clark, C., Kelsey, D. E., Reddy, S. M., Pearce, M. A., Tucker, N. M. & Morrissey, L. J. (2018). Phase equilibria modelling constraints on P-T conditions during fluid catalysed conversion of granulite to eclogite in the Bergen Arcs, Norway. *Journal of Metamorphic Geology*, 36(3), 315-342. <https://doi.org/10.1111/jmg.12294>
- Bingen, B., Davis, W. J. & Austrheim, H. (2001). Zircon U-Pb geochronology in the Bergen arc eclogites and their Proterozoic protoliths, and implications for the pre-Scandian evolution of the Caledonides in western Norway. *Geological Society of America Bulletin*, 113(5), 640-649. [https://doi.org/10.1130/0016-7606\(2001\)113<0640:ZUPGIT>2.0.CO;2](https://doi.org/10.1130/0016-7606(2001)113<0640:ZUPGIT>2.0.CO;2)
- Bird, P. (1978). Finite element modeling of lithosphere deformation : the Zagros collision orogeny. *Tectonophysics*, 50(2-3), 307-336. [https://doi.org/10.1016/0040-1951\(78\)90140-3](https://doi.org/10.1016/0040-1951(78)90140-3)
- Bjørnerud, M., Austrheim, H. & Lund, M. (2002). Processes leading to eclogitization (densification) of subducted and tectonically buried crust. *Journal of Geophysical Research : Solid Earth*, 107(B10), ETG-14. <https://doi.org/10.1029/2001JB000527>
- Boundy, T. M., Essene, E. J., Hall, C. M., Austrheim, H. & Halliday, A. (1996). Rapid exhumation of lower crust during continent-continent collision and late extension : Evidence from  $^{40}\text{Ar}/^{39}\text{Ar}$  incremental heating of hornblendes and muscovites, Caledonian orogen, western Norway. *Geological Society of America Bulletin*, 108(11), 1425-1437. [https://doi.org/10.1130/0016-7606\(1996\)108<1425:REOLCD>2.3.CO;2](https://doi.org/10.1130/0016-7606(1996)108<1425:REOLCD>2.3.CO;2)
- Boundy, T., Fountain, D. & Austrheim, H. (1992). Structural development and petrofabrics of eclogite facies shear zones, Bergen Arcs, western Norway : implications for deep crustal deformational processes. *Journal of Metamorphic Geology*, 10(2), 127-146. <https://doi.org/10.1111/j.1525-1314.1992.tb00075.x>
- Boussinesq, J. (1897). *Théorie de l'écoulement tourbillonnant et tumultueux des liquides dans les lits rectilignes à grande section...* (T. 1). Gauthier-Villars.
- Bras, E., Yamato, P., Schmalholz, S. M., Duretz, T. & Podladchikov, Y. Y. (2023). Eclogitisation of dry and impermeable granulite by fluid flow with reaction-induced porosity : Insights from hydro-chemical modelling. *Earth and Planetary Science Letters*, 617, 118256. <https://doi.org/10.1016/j.epsl.2023.118256>
- Bras, E., Baïsset, M., Yamato, P. & Labrousse, L. (2021). Transient weakening during the granulite to eclogite transformation within hydrous shear zones (Holsnøy, Norway). *Tectonophysics*, 819, 229026. <https://doi.org/10.1016/j.tecto.2021.229026>
- Brown, M. (2023). Some thoughts about eclogites and related rocks. *European Journal of Mineralogy*, 35(4), 523-547. <https://doi.org/10.5194/ejm-35-523-2023>
- Burg, J.-P. & Gerya, T. (2005). The role of viscous heating in Barrovian metamorphism of collisional orogens : thermomechanical models and application to the Lepontine

- Dome in the Central Alps. *Journal of Metamorphic Geology*, 23(2), 75-95. <https://doi.org/10.1111/j.1525-1314.2005.00563.x>
- Bürgmann, R. & Dresen, G. (2008). Rheology of the lower crust and upper mantle : Evidence from rock mechanics, geodesy, and field observations. *Annu. Rev. Earth Planet. Sci.*, 36, 531-567. <https://doi.org/10.1146/annurev.earth.36.031207.124326>
- Burov, E., Francois, T., Agard, P., Le Pourhiet, L., Meyer, B., Tirel, C., Lebedev, S., Yamato, P. & Brun, J.-P. (2014). Rheological and geodynamic controls on the mechanisms of subduction and HP/UHP exhumation of crustal rocks during continental collision : Insights from numerical models. *Tectonophysics*, 631, 212-250. <https://doi.org/10.1016/j.tecto.2014.04.033>
- Campbell, L. & Menegon, L. (2019). Transient high strain rate during localized viscous creep in the dry lower continental crust (Lofoten, Norway). *Journal of Geophysical Research : Solid Earth*, 124(10), 10240-10260. <https://doi.org/10.1029/2019JB018052>
- Carmichael, D. M. (1969). On the mechanism of prograde metamorphic reactions in quartz-bearing pelitic rocks. *Contributions to Mineralogy and Petrology*, 20, 244-267. <https://doi.org/10.1007/BF00377479>
- Ceccato, A., Menegon, L., Pennacchioni, G. & Morales, L. F. G. (2018). Myrmekite and strain weakening in granitoid mylonites. *Solid Earth*, 9(6), 1399-1419. <https://doi.org/10.5194/se-9-1399-2018>
- Ceccato, A., Goncalves, P. & Menegon, L. (2022). On the petrology and microstructures of small-scale ductile shear zones in granitoid rocks : An overview. *Journal of Structural Geology*, 161, 104667. <https://doi.org/10.1016/j.jsg.2022.104667>
- Centrella, S. (2019). The granulite-to eclogite-and amphibolite-facies transition : a volume and mass transfer study in the Lindås Nappe, Bergen Arcs, west Norway. *Geological Society, London, Special Publications*, 478(1), 241-264. <https://doi.org/10.1144/SP478.9>
- Chen, W.-P. & Molnar, P. (1983). Focal depths of intracontinental and intraplate earthquakes and their implications for the thermal and mechanical properties of the lithosphere. *Journal of Geophysical Research : Solid Earth*, 88(B5), 4183-4214. <https://doi.org/10.1029/JB088iB05p04183>
- Chopin, C. (1984). Coesite and pure pyrope in high-grade blueschists of the Western Alps : a first record and some consequences. *Contributions to Mineralogy and Petrology*, 86, 107-118. <https://doi.org/10.1007/BF00381838>
- Cionoiu, S., Moulas, E., Stünitz, H. & Tajčmanová, L. (2022). Locally Resolved Stress-State in Samples During Experimental Deformation : Insights Into the Effect of Stress on Mineral Reactions. *Journal of Geophysical Research : Solid Earth*, 127(8), e2022JB024814. <https://doi.org/10.1029/2022JB024814>
- Cionoiu, S., Moulas, E. & Tajčmanová, L. (2019). Impact of interseismic deformation on phase transformations and rock properties in subduction zones. *Scientific Reports*, 9(1), 19561. <https://doi.org/10.1038/s41598-019-56130-6>
- Cohen, A., O'nions, R., Siegenthaler, R. & Griffin, W. (1988). Chronology of the pressure-temperature history recorded by a granulite terrain. *Contributions to Mineralogy and Petrology*, 98, 303-311. <https://doi.org/10.1007/BF00375181>

- Coltice, N. & Shephard, G. E. (2018). Tectonic predictions with mantle convection models. *Geophysical Journal International*, 213(1), 16-29. <https://doi.org/10.1093/gji/ggx531>
- Connolly, J. A. D. & Podladchikov, Y. Y. (2013). A Hydromechanical Model for Lower Crustal Fluid Flow. *Metasomatism and the Chemical Transformation of Rock : The Role of Fluids in Terrestrial and Extraterrestrial Processes*, 599-658. [https://doi.org/10.1007/978-3-642-28394-9\\_14](https://doi.org/10.1007/978-3-642-28394-9_14)
- Connolly, J. & Podladchikov, Y. Y. (1998). Compaction-driven fluid flow in viscoelastic rock. *Geodinamica Acta*, 11(2-3), 55-84. <https://doi.org/10.1080/09853111.1998.11105311>
- Connolly, J. A. (2005). Computation of phase equilibria by linear programming : a tool for geodynamic modeling and its application to subduction zone decarbonation. *Earth and Planetary Science Letters*, 236(1-2), 524-541. <https://doi.org/10.1016/j.epsl.2005.04.033>
- Copley, A., Avouac, J.-P., Hollingsworth, J. & Leprince, S. (2011). The 2001 Mw 7.6 Bhuj earthquake, low fault friction, and the crustal support of plate driving forces in India. *Journal of Geophysical Research : Solid Earth*, 116(B8). <https://doi.org/10.1029/2010JB008137>
- Coulomb, C. A. (1773). Essai sur une application des règles de maximis et minimis à quelques problèmes de statique relatifs à l'architecture. *Mem. Div. Sav. Acad.*
- Darcy, H. (1856). *Les fontaines publiques de la ville de Dijon : exposition et application des principes à suivre et des formules à employer dans les questions de distribution d'eau* (T. 1). Victor dalmont.
- de Capitani, C. & Petrakakis, K. (2010). The computation of equilibrium assemblage diagrams with Theriax/Domino software. *American mineralogist*, 95(7), 1006-1016. <https://doi.org/10.2138/am.2010.3354>
- Déverchère, J., Petit, C., Gileva, N., Radziminovitch, N., Melnikova, V. & San'Kov, V. (2001). Depth distribution of earthquakes in the Baikal rift system and its implications for the rheology of the lithosphere. *Geophysical Journal International*, 146(3), 714-730. <https://doi.org/10.1046/j.0956-540x.2001.1484.484.x>
- Dewey, J. F. & Bird, J. M. (1970). Mountain belts and the new global tectonics. *Journal of geophysical Research*, 75(14), 2625-2647. <https://doi.org/10.1029/JB075i014p02625>
- Dietz, R. S. (1961). Continent and ocean basin evolution by spreading of the sea floor. *Nature*, 190(4779), 854-857.
- Dohmen, R. & Milke, R. (2010). Diffusion in polycrystalline materials : grain boundaries, mathematical models, and experimental data. *Reviews in Mineralogy and Geochemistry*, 72(1), 921-970. <https://doi.org/10.2138/rmg.2010.72.21>
- Ducea, M. N. (2016). RESEARCH FOCUS : Understanding continental subduction : A work in progress. *Geology*, 44(3), 239-240. <https://doi.org/10.1130/focus032016.1>
- Duretz, T., Gerya, T. V. & May, D. A. (2011). Numerical modelling of spontaneous slab breakoff and subsequent topographic response. *Tectonophysics*, 502(1-2), 244-256. <https://doi.org/10.1016/j.tecto.2010.05.024>

- Dymkova, D. & Gerya, T. (2013). Porous fluid flow enables oceanic subduction initiation on Earth. *Geophysical Research Letters*, 40(21), 5671-5676. <https://doi.org/10.1002/2013GL057798>
- Emmermann, R. & Lauterjung, J. (1997). The German continental deep drilling program KTB : overview and major results. *Journal of Geophysical Research : Solid Earth*, 102(B8), 18179-18201. <https://doi.org/10.1029/96JB03945>
- Fagereng, Å. & Biggs, J. (2019). New perspectives on 'geological strain rates' calculated from both naturally deformed and actively deforming rocks. *Journal of Structural Geology*, 125, 100-110. <https://doi.org/10.1016/j.jsg.2018.10.004>
- Fossen, H. & Cavalcante, G. C. G. (2017). Shear zones—A review. *Earth-Science Reviews*, 171, 434-455. <https://doi.org/10.1016/j.earscirev.2017.05.002>
- Früh-Green, G. L. (1994). Interdependence of deformation, fluid infiltration and reaction progress recorded in eclogitic metagranitoids (Sesia Zone, Western Alps). *Journal of Metamorphic Geology*, 12(3), 327-343. <https://doi.org/10.1111/j.1525-1314.1994.tb00026.x>
- Fusseis, F., Regenauer-Lieb, K., Liu, J., Hough, R. M. & De Carlo, F. (2009). Creep cavitation can establish a dynamic granular fluid pump in ductile shear zones. *Nature*, 459(7249), 974-977. <https://doi.org/10.1038/nature08051>
- Gerya, T. (2019). *Introduction to numerical geodynamic modelling*. Cambridge University Press. <https://doi.org/10.1017/9781316534243>
- Gerya, T. (2015). Tectonic overpressure and underpressure in lithospheric tectonics and metamorphism. *Journal of Metamorphic Geology*, 33(8), 785-800. <https://doi.org/10.1111/jmg.12144>
- Gerya, T. V., Perchuk, L. L., Maresch, W. V. & Willner, A. P. (2004). Inherent gravitational instability of hot continental crust : Implications for doming and diapirism in granulite facies terrains. *Special Papers-Geological Society of America*, 97-116. <https://doi.org/10.1130/0-8137-2380-9.97>
- Gibbs, J. W. (1876). On the equilibrium of heterogeneous substances. *Transactions of Connecticut Academy of Arts and Sciences*, 108-248.
- Glodny, J., Kühn, A. & Austrheim, H. (2008). Geochronology of fluid-induced eclogite and amphibolite facies metamorphic reactions in a subduction–collision system, Bergen Arcs, Norway. *Contributions to Mineralogy and Petrology*, 156, 27-48. <https://doi.org/10.1007/s00410-007-0272-y>
- Goncalves, P., Oliot, E., Marquer, D. & Connolly, J. (2012). Role of chemical processes on shear zone formation : an example from the Grimsel metagranodiorite (Aar massif, Central Alps). *Journal of Metamorphic Geology*, 30(7), 703-722. <https://doi.org/10.1111/j.1525-1314.2012.00991.x>
- Gueydan, F., Leroy, Y. M., Jolivet, L. & Agard, P. (2003). Analysis of continental mid-crustal strain localization induced by microfracturing and reaction-softening. *Journal of Geophysical Research : Solid Earth*, 108(B2). <https://doi.org/10.1029/2001JB000611>
- Guillot, S., Hattori, K., Agard, P., Schwartz, S. & Vidal, O. (2009). Exhumation processes in oceanic and continental subduction contexts : a review. *Subduction zone geodynamics*, 175-205. [https://doi.org/10.1007/978-3-540-87974-9\\_10](https://doi.org/10.1007/978-3-540-87974-9_10)
- Gürer, D., Hubbard, J. & Bohon, W. (2023). Science on social media. *Communications Earth & Environment*, 4(1), 148. <https://doi.org/10.1038/s43247-023-00810-9>

- Hacker, B. R., Kelemen, P. B. & Behn, M. D. (2015). Continental lower crust. *Annual Review of Earth and Planetary Sciences*, 43, 167-205. <https://doi.org/10.1146/annurev-earth-050212-124117>
- Hacker, B. R., Gerya, T. V. & Gilotti, J. A. (2013). Formation and exhumation of ultrahigh-pressure terranes. *Elements*, 9(4), 289-293. <https://doi.org/10.2113/gselements.9.4.289>
- Hasterok, D., Halpin, J. A., Collins, A. S., Hand, M., Kreemer, C., Gard, M. G. & Glorie, S. (2022). New maps of global geological provinces and tectonic plates. *Earth-Science Reviews*, 231, 104069. <https://doi.org/10.1016/j.earscirev.2022.104069>
- Hawemann, F., Mancktelow, N. S., Pennacchioni, G., Wex, S. & Camacho, A. (2019). Weak and slow, strong and fast : How shear zones evolve in a dry continental crust (Musgrave Ranges, Central Australia). *Journal of Geophysical Research : Solid Earth*, 124(1), 219-240. <https://doi.org/10.1029/2018JB016559>
- Heezen, B. & Tharp, M. (1965). Tectonic fabric of the Atlantic and Indian Oceans and continental drift. *Philosophical transactions of the Royal Society of London. Series A, Mathematical and Physical Sciences*, 258(1088), 90-106. <https://doi.org/10.1098/rsta.1965.0024>
- Hess, H. H. (1962). History of ocean basins. <https://doi.org/10.1130/Petrologic.1962.599>
- Hetényi, G. (2014). To conserve or not to conserve (mass in numerical models). *Terra Nova*, 26(5), 372-376. <https://doi.org/10.1111/ter.12109>
- Hetényi, G., Cattin, R., Brunet, F., Bollinger, L., Vergne, J., Nábělek, J. L. & Diament, M. (2007). Density distribution of the India plate beneath the Tibetan plateau : Geophysical and petrological constraints on the kinetics of lower-crustal eclogitization. *Earth and Planetary Science Letters*, 264(1-2), 226-244. <https://doi.org/10.1016/j.epsl.2007.09.036>
- Hetényi, G., Godard, V., Cattin, R. & Connolly, J. A. (2011). Incorporating metamorphism in geodynamic models : the mass conservation problem. *Geophysical Journal International*, 186(1), 6-10. <https://doi.org/10.1111/j.1365-246X.2011.05052.x>
- Hirth, G. & Tullis, J. (1994). The brittle-plastic transition in experimentally deformed quartz aggregates. *Journal of Geophysical Research : Solid Earth*, 99(B6), 11731-11747. <https://doi.org/10.1029/93JB02873>
- Hirth, G., Teyssier, C. & Dunlap, J. W. (2001). An evaluation of quartzite flow laws based on comparisons between experimentally and naturally deformed rocks. *International Journal of Earth Sciences*, 90, 77-87. <https://doi.org/10.1007/s005310000152>
- Hoiland, C., Hourigan, J. & Miller, E. (2022). Evidence for large departures from lithostatic pressure during Late Cretaceous metamorphism in the northern Snake Range metamorphic core complex, Nevada. *Tectonic Evolution of the Sevier-Laramide Hinterland, Thrust Belt, and Foreland, and Postorogenic Slab Rollback (180–20 Ma)*. Geological Society of America. [https://doi.org/10.1130/2021.2555\(07\)](https://doi.org/10.1130/2021.2555(07))
- Holland, T. & Powell, R. (2011). An improved and extended internally consistent thermodynamic dataset for phases of petrological interest, involving a new equation of state for solids. *Journal of metamorphic Geology*, 29(3), 333-383. <https://doi.org/10.1111/j.1525-1314.2010.00923.x>

- Holland, T. & Powell, R. (1998). An internally consistent thermodynamic data set for phases of petrological interest. *Journal of metamorphic Geology*, 16(3), 309-343. <https://doi.org/10.1111/j.1525-1314.1998.00140.x>
- Incel, S., Renner, J. & Jamtveit, B. (2020). Evolution of brittle structures in plagioclase-rich rocks at high-pressure and high-temperature conditions—Linking laboratory results to field observations. *Geochemistry, Geophysics, Geosystems*, 21(8), e2020GC009028. <https://doi.org/10.1029/2020GC009028>
- Isacks, B., Oliver, J. & Sykes, L. R. (1968). Seismology and the new global tectonics. *Journal of geophysical research*, 73(18), 5855-5899. <https://doi.org/10.1029/JB073i018p05855>
- Jackson, J. (2002). Strength of the continental lithosphere : time to abandon the jelly sandwich ? *GSA today*, 12, 4-10. [https://doi.org/10.1130/1052-5173\(2002\)012<0004:SOTCLT>2.0.CO;2](https://doi.org/10.1130/1052-5173(2002)012<0004:SOTCLT>2.0.CO;2)
- Jackson, J., McKenzie, D. & Priestley, K. (2021). Relations between earthquake distributions, geological history, tectonics and rheology on the continents. *Philosophical Transactions of the Royal Society A*, 379(2193), 20190412. <https://doi.org/10.1098/rsta.2019.0412>
- Jackson, J. A., Austrheim, H., McKenzie, D. & Priestley, K. (2004). Metastability, mechanical strength, and the support of mountain belts. *Geology*, 32(7), 625-628. <https://doi.org/10.1130/G20397.1>
- Jakob, J., Alsaif, M., Corfu, F. & Andersen, T. B. (2017). Age and origin of thin discontinuous gneiss sheets in the distal domain of the magma-poor hyperextended pre-Caledonian margin of Baltica, southern Norway. *Journal of the Geological Society*, 174(3), 557-571. <https://doi.org/10.1144/jgs2016-049>
- Jamtveit, B., Austrheim, H. & Malthe-Sørenssen, A. (2000). Accelerated hydration of the Earth's deep crust induced by stress perturbations. *Nature*, 408(6808), 75-78. <https://doi.org/10.1038/35040537>
- Jamtveit, B., Austrheim, H. & Putnis, A. (2016). Disequilibrium metamorphism of stressed lithosphere. *Earth-Science Reviews*, 154, 1-13. <https://doi.org/10.1016/j.earscirev.2015.12.002>
- Jamtveit, B., Ben-Zion, Y., Renard, F. & Austrheim, H. (2018a). Earthquake-induced transformation of the lower crust. *Nature*, 556(7702), 487-491. <https://doi.org/10.1038/s41586-018-0045-y>
- Jamtveit, B., Petley-Ragan, A., Incel, S., Dunkel, K. G., Aupart, C., Austrheim, H., Corfu, F., Menegon, L. & Renard, F. (2019). The effects of earthquakes and fluids on the metamorphism of the lower continental crust. *Journal of Geophysical Research : Solid Earth*, 124(8), 7725-7755. <https://doi.org/10.1029/2018JB016461>
- Jamtveit, B., Bucher-Nurminen, K. & Austrheim, H. (1990). Fluid controlled eclogitization of granulites in deep crustal shear zones, Bergen arcs, Western Norway. *Contributions to Mineralogy and Petrology*, 104, 184-193. <https://doi.org/10.1007/BF00306442>
- Jamtveit, B., Moulas, E., Andersen, T. B., Austrheim, H., Corfu, F., Petley-Ragan, A. & Schmalholz, S. M. (2018b). High pressure metamorphism caused by fluid induced weakening of deep continental crust. *Scientific Reports*, 8(1), 17011. <https://doi.org/10.1038/s41598-018-35200-1>

- Jamtveit, B., Malthe-Sørenssen, A. & Kostenko, O. (2008). Reaction enhanced permeability during retrogressive metamorphism. *Earth and Planetary Science Letters*, 267(3-4), 620-627. <https://doi.org/10.1016/j.epsl.2007.12.016>
- John, T. & Schenk, V. (2003). Partial eclogitisation of gabbroic rocks in a late Precambrian subduction zone (Zambia) : prograde metamorphism triggered by fluid infiltration. *Contributions to Mineralogy and Petrology*, 146, 174-191. <https://doi.org/10.1007/s00410-003-0492-8>
- Jolivet, L., Raimbourg, H., Labrousse, L., Avigad, D., Leroy, Y., Austrheim, H. & Andersen, T. B. (2005). Softening triggered by eclogitization, the first step toward exhumation during continental subduction. *Earth and Planetary Science Letters*, 237(3-4), 532-547. <https://doi.org/10.1016/j.epsl.2005.06.047>
- Jones, R. E., Kirstein, L. A., Kasemann, S. A., Litvak, V. D., Poma, S., Alonso, R. N., Hinton, R. et al. (2016). The role of changing geodynamics in the progressive contamination of Late Cretaceous to Late Miocene arc magmas in the southern Central Andes. *Lithos*, 262, 169-191. <https://doi.org/10.1016/j.lithos.2016.07.002>
- Kaatz, L., Reynes, J., Hermann, J. & John, T. (2022). How fluid infiltrates dry crustal rocks during progressive eclogitization and shear zone formation : insights from H<sub>2</sub>O contents in nominally anhydrous minerals. *Contributions to Mineralogy and Petrology*, 177(7), 72. <https://doi.org/10.1007/s00410-022-01938-1>
- Kaatz, L., Schmalholz, S. & John, T. (2023). Numerical simulations reproduce field observations showing transient weakening during shear zone formation by diffusional hydrogen influx and H<sub>2</sub>O inflow. *Geochemistry, Geophysics, Geosystems*, 24(5), e2022GC010830. <https://doi.org/10.1029/2022GC010830>
- Kaatz, L., Zertani, S., Moulas, E., John, T., Labrousse, L., Schmalholz, S. M. & Andersen, T. B. (2021). Widening of hydrous shear zones during incipient eclogitization of metastable dry and rigid lower crust—Holsnøy, western Norway. *Tectonics*, 40(3), e2020TC006572. <https://doi.org/10.1029/2020TC006572>
- Kanamori, H. (1977). The energy release in great earthquakes. *Journal of geophysical research*, 82(20), 2981-2987. <https://doi.org/10.1029/JB082i020p02981>
- Kaus, B. J., Connolly, J. A., Podladchikov, Y. Y. & Schmalholz, S. M. (2005). Effect of mineral phase transitions on sedimentary basin subsidence and uplift. *Earth and Planetary Science Letters*, 233(1-2), 213-228. <https://doi.org/10.1016/j.epsl.2005.01.032>
- Keller, T., May, D. A. & Kaus, B. J. (2013). Numerical modelling of magma dynamics coupled to tectonic deformation of lithosphere and crust. *Geophysical Journal International*, 195(3), 1406-1442. <https://doi.org/10.1093/gji/ggt306>
- Kohlstedt, D. L. (2006). The role of water in high-temperature rock deformation. *Reviews in mineralogy and geochemistry*, 62(1), 377-396. <https://doi.org/10.2138/rmg.2006.62.16>
- Kolderup, C. F. & Kolderup, N.-H. (1940). *Geology of the Bergen arc system*. Grieg.
- Koons, P., Rubie, D. & Fruch-Green, G. (1987). The effects of disequilibrium and deformation on the mineralogical evolution of quartz diorite during metamorphism in the eclogite facies. *Journal of Petrology*, 28(4), 679-700. <https://doi.org/10.1093/petrology/28.4.679>
- Kozlovsky, Y. A. (1984). The world's deepest well. *Scientific American*, 251(6), 98-105.

- Kühn, A., Glodny, J., Austrheim, H. & Råheim, A. (2002). The Caledonian tectono-metamorphic evolution of the Lindås Nappe : Constraints from U-Pb, Sm-Nd and Rb-Sr ages of granitoid dykes. *Norwegian Journal of Geology/Norsk Geologisk Forening*, 82(1).
- Labrousse, L., Hetényi, G., Raimbourg, H., Jolivet, L. & Andersen, T. B. (2010). Initiation of crustal-scale thrusts triggered by metamorphic reactions at depth : Insights from a comparison between the Himalayas and Scandinavian Caledonides. *Tectonics*, 29(5), TC5002. <https://doi.org/10.1029/2009TC002602>
- Larvet, T., Le Pourhiet, L. & Agard, P. (2022). Cimmerian block detachment from Gondwana : a slab pull origin ? *Earth and Planetary Science Letters*, 596, 117790. <https://doi.org/10.1016/j.epsl.2022.117790>
- Le Pichon, X. (1968). Sea-floor spreading and continental drift. *Journal of geophysical research*, 73(12), 3661-3697. <https://doi.org/10.1029/JB073i012p03661>
- Le Pourhiet, L., May, D. A., Huille, L., Watremez, L. & Leroy, S. (2017). A genetic link between transform and hyper-extended margins. *Earth and Planetary Science Letters*, 465, 184-192. <https://doi.org/10.1016/j.epsl.2017.02.043>
- Le Pourhiet, L., Huet, B., May, D. A., Labrousse, L. & Jolivet, L. (2012). Kinematic interpretation of the 3D shapes of metamorphic core complexes. *Geochemistry, Geophysics, Geosystems*, 13(9). <https://doi.org/doi.org/10.1029/2012GC004271>
- Leydier, T., Goncalves, P., Lanari, P. & Oliot, E. (2019). On the petrology of brittle precursors of shear zones—An expression of concomitant brittle deformation and fluid–rock interactions in the ‘ductile’continental crust ? *Journal of metamorphic geology*, 37(8), 1129-1149. <https://doi.org/10.1111/jmg.12504>
- Li, Y., Pusok, A. E., Davis, T., May, D. A. & Katz, R. F. (2023). Continuum approximation of dyking with a theory for poro-viscoelastic-viscoplastic deformation. *Geophysical Journal International*, 234(3), 2007-2031. <https://doi.org/10.1093/gji/ggad173>
- Li, Z. (2014). A review on the numerical geodynamic modeling of continental subduction, collision and exhumation. *Science China Earth Sciences*, 57, 47-69. <https://doi.org/10.1007/s11430-013-4696-0>
- Luisier, C., Baumgartner, L., Schmalholz, S. M., Siron, G. & Vennemann, T. (2019). Metamorphic pressure variation in a coherent Alpine nappe challenges lithostatic pressure paradigm. *Nature communications*, 10(1), 4734. <https://doi.org/10.1038/s41467-019-12727-z>
- Lund, M. G. & Austrheim, H. (2003). High-pressure metamorphism and deep-crustal seismicity : evidence from contemporaneous formation of pseudotachylites and eclogite facies coronas. *Tectonophysics*, 372(1-2), 59-83. [https://doi.org/10.1016/S0040-1951\(03\)00232-4](https://doi.org/10.1016/S0040-1951(03)00232-4)
- Maggi, A., Jackson, J., Mckenzie, D. & Priestley, K. (2000a). Earthquake focal depths, effective elastic thickness, and the strength of the continental lithosphere. *Geology*, 28(6), 495-498. [https://doi.org/10.1130/0091-7613\(2000\)28<495:EFDEET>2.0.CO;2](https://doi.org/10.1130/0091-7613(2000)28<495:EFDEET>2.0.CO;2)
- Maggi, A., Jackson, J., Priestley, K. & Baker, C. (2000b). A re-assessment of focal depth distributions in southern Iran, the Tien Shan and northern India : Do earthquakes really occur in the continental mantle ? *Geophysical Journal International*, 143(3), 629-661. <https://doi.org/10.1046/j.1365-246X.2000.00254.x>

- Malvoisin, B., Podladchikov, Y. Y. & Myasnikov, A. V. (2021). Achieving complete reaction while the solid volume increases : A numerical model applied to serpentinisation. *Earth and Planetary Science Letters*, 563, 116859. <https://doi.org/10.1016/j.epsl.2021.116859>
- Malvoisin, B., Podladchikov, Y. Y. & Vrijmoed, J. C. (2015). Coupling changes in densities and porosity to fluid pressure variations in reactive porous fluid flow : Local thermodynamic equilibrium. *Geochemistry, Geophysics, Geosystems*, 16(12), 4362-4387. <https://doi.org/10.1002/2015GC006019>
- Malvoisin, B., Austreheim, H., Hetényi, G., Reynes, J., Hermann, J., Baumgartner, L. P. & Podladchikov, Y. Y. (2020). Sustainable densification of the deep crust. *Geology*, 48(7), 673-677. <https://doi.org/10.1130/G47201.1>
- Mancktelow, N. S. (1993). Tectonic overpressure in competent mafic layers and the development of isolated eclogites. *Journal of metamorphic Geology*, 11(6), 801-812. <https://doi.org/10.1111/j.1525-1314.1993.tb00190.x>
- Mancktelow, N. S. (2008). Tectonic pressure : Theoretical concepts and modelled examples. *Lithos*, 103(1-2), 149-177. <https://doi.org/10.1016/j.lithos.2007.09.013>
- Mancktelow, N. S. & Pennacchioni, G. (2005). The control of precursor brittle fracture and fluid–rock interaction on the development of single and paired ductile shear zones. *Journal of structural Geology*, 27(4), 645-661. <https://doi.org/10.1016/j.jsg.2004.12.001>
- Mancktelow, N. S., Camacho, A. & Pennacchioni, G. (2022). Time-Lapse Record of an Earthquake in the Dry Felsic Lower Continental Crust Preserved in a Pseudotachylite-Bearing Fault. *Journal of Geophysical Research : Solid Earth*, 127(4), e2021JB022878. <https://doi.org/10.1029/2021JB022878>
- Marti, S., Stünitz, H., Heilbronner, R., Plümper, O. & Kilian, R. (2018). Syn-kinematic hydration reactions, grain size reduction, and dissolution–precipitation creep in experimentally deformed plagioclase–pyroxene mixtures. *Solid Earth*, 9(4), 985-1009. <https://doi.org/10.5194/se-9-985-2018>
- Massonne, H. -J. & Schreyer, W. (1987). Phengite geobarometry based on the limiting assemblage with K-feldspar, phlogopite, and quartz. *Contributions to mineralogy and petrology*, 96, 212-224. <https://doi.org/10.1007/BF00375235>
- McKenzie, D. (1984). The generation and compaction of partially molten rock. *Journal of petrology*, 25(3), 713-765. <https://doi.org/10.1093/petrology/25.3.713>
- McKenzie, D. P. & Parker, R. L. (1967). The North Pacific : an example of tectonics on a sphere. *Nature*, 216(5122), 1276-1280. <https://doi.org/10.1038/2161276a0>
- McNamara, D. E., Yeck, W. L., Barnhart, W. D., Schulte-Pelkum, V., Bergman, E., Adhikari, L., Dixit, A., Hough, S., Benz, H. M. & Earle, P. S. (2017). Source modeling of the 2015 Mw 7.8 Nepal (Gorkha) earthquake sequence : Implications for geodynamics and earthquake hazards. *Tectonophysics*, 714, 21-30. <https://doi.org/10.1016/j.tecto.2016.08.004>
- Menegon, L., Pennacchioni, G., Malaspina, N., Harris, K. & Wood, E. (2017). Earthquakes as precursors of ductile shear zones in the dry and strong lower crust. *Geochemistry, Geophysics, Geosystems*, 18(12), 4356-4374. <https://doi.org/10.1002/2017GC007189>

- Mohr, O. et al. (1900). Welche Umstände bedingen die Elastizitätsgrenze und den Bruch eines Materials. *Zeitschrift des Vereins Deutscher Ingenieure*, 46(1524-1530), 1572-1577.
- Molnar, P. & Gray, D. (1979). Subduction of continental lithosphere : Some constraints and uncertainties. *Geology*, 7(1), 58-62. [https://doi.org/10.1130/0091-7613\(1979\)7<58:SOCLSC>2.0.CO;2](https://doi.org/10.1130/0091-7613(1979)7<58:SOCLSC>2.0.CO;2)
- Monsalve, G., Sheehan, A., Rowe, C. & Rajaure, S. (2008). Seismic structure of the crust and the upper mantle beneath the Himalayas : Evidence for eclogitization of lower crustal rocks in the Indian Plate. *Journal of Geophysical Research : Solid Earth*, 113(B8).
- Moore, J., Beinlich, A., Piazolo, S., Austrheim, H. & Putnis, A. (2020a). Metamorphic differentiation via enhanced dissolution along high permeability zones. *Journal of Petrology*, 61(10), egaa096. <https://doi.org/10.1093/petrology/egaa096>
- Moore, J., Beinlich, A., Porter, J. K., Talavera, C., Berndt, J., Piazolo, S., Austrheim, H. & Putnis, A. (2020b). Microstructurally controlled trace element (Zr, U-Pb) concentrations in metamorphic rutile : an example from the amphibolites of the Bergen Arcs. *Journal of Metamorphic Geology*, 38(1), 103-127. <https://doi.org/10.1111/jmg.12514>
- Moulas, E., Podladchikov, Y. Y., Aranovich, L. Y. & Kostopoulos, D. (2013). The problem of depth in geology : When pressure does not translate into depth. *Petrology*, 21, 527-538. <https://doi.org/10.1134/S0869591113060052>
- Moulas, E., Kaus, B. & Jamtveit, B. (2022). Dynamic pressure variations in the lower crust caused by localized fluid-induced weakening. *Communications Earth & Environment*, 3(1), 157. <https://doi.org/10.1038/s43247-022-00478-7>
- Moulas, E., Schmalholz, S. M., Podladchikov, Y., Tajčmanová, L., Kostopoulos, D. & Baumgartner, L. (2019). Relation between mean stress, thermodynamic, and lithostatic pressure. *Journal of metamorphic geology*, 37(1), 1-14. <https://doi.org/10.1111/jmg.12446>
- Nádai, A. (1950). Theory of flow and fracture of solids.
- Nakagawa, T., Tackley, P. J., Deschamps, F. & Connolly, J. A. (2009). Incorporating self-consistently calculated mineral physics into thermochemical mantle convection simulations in a 3-D spherical shell and its influence on seismic anomalies in Earth's mantle. *Geochemistry, Geophysics, Geosystems*, 10(3). <https://doi.org/10.1029/2008GC002280>
- Oliot, E., Goncalves, P. & Marquer, D. (2010). Role of plagioclase and reaction softening in a metagranite shear zone at mid-crustal conditions (Gotthard Massif, Swiss Central Alps). *Journal of Metamorphic Geology*, 28(8), 849-871. <https://doi.org/10.1111/j.1525-1314.2010.00897.x>
- Oliot, E., Goncalves, P., Schulmann, K., Marquer, D. & Lexa, O. (2014). Mid-crustal shear zone formation in granitic rocks : Constraints from quantitative textural and crystallographic preferred orientations analyses. *Tectonophysics*, 612, 63-80. <https://doi.org/10.1016/j.tecto.2013.11.032>
- Omlin, S., Malvoisin, B. & Podladchikov, Y. Y. (2017). Pore fluid extraction by reactive solitary waves in 3-D. *Geophysical Research Letters*, 44(18), 9267-9275. <https://doi.org/10.1002/2017GL074293>

- Peacock, S. A. (1990). Fluid processes in subduction zones. *Science*, 248(4953), 329-337. <https://doi.org/DOI:10.1126/science.248.4953.329>
- Pennacchioni, G. & Mancktelow, N. (2018). Small-scale ductile shear zones : neither extending, nor thickening, nor narrowing. *Earth-Science Reviews*, 184, 1-12. <https://doi.org/10.1016/j.earscirev.2018.06.004>
- Petley-Ragan, A., Ben-Zion, Y., Austrheim, H., Ildefonse, B., Renard, F. & Jamtveit, B. (2019). Dynamic earthquake rupture in the lower crust. *Science Advances*, 5(7), eaaw0913. <https://doi.org/DOI:10.1126/sciadv.aaw0913>
- Petley-Ragan, A., Dunkel, K. G., Austrheim, H., Ildefonse, B. & Jamtveit, B. (2018). Micro-structural records of earthquakes in the lower crust and associated fluid-driven metamorphism in plagioclase-rich granulites. *Journal of Geophysical Research : Solid Earth*, 123(5), 3729-3746. <https://doi.org/10.1029/2017JB015348>
- Petrini & Podladchikov. (2000). Lithospheric pressure-depth relationship in compressive regions of thickened crust. *Journal of metamorphic Geology*, 18(1), 67-77. <https://doi.org/10.1046/j.1525-1314.2000.00240.x>
- Pleuger, J. & Podladchikov, Y. Y. (2014). A purely structural restoration of the NFP20-East cross section and potential tectonic overpressure in the Adula nappe (central Alps). *Tectonics*, 33(5), 656-685. <https://doi.org/10.1002/2013TC003409>
- Plümper, O., John, T., Podladchikov, Y. Y., Vrijmoed, J. C. & Scambelluri, M. (2017). Fluid escape from subduction zones controlled by channel-forming reactive porosity. *Nature Geoscience*, 10(2), 150-156. <https://doi.org/10.1038/ngeo2865>
- Porkoláb, K., Duretz, T., Yamato, P., Auzemery, A. & Willingshofer, E. (2021). Extrusion of subducted crust explains the emplacement of far-travelled ophiolites. *Nature Communications*, 12(1), 1499. <https://doi.org/10.1038/s41467-021-21866-1>
- Powell, R., Holland, T. & Worley, B. (1998). Calculating phase diagrams involving solid solutions via non-linear equations, with examples using THERMOCALC. *Journal of metamorphic Geology*, 16(4), 577-588. <https://doi.org/10.1111/j.1525-1314.1998.00157.x>
- Priestley, K., Jackson, J. & McKenzie, D. (2008). Lithospheric structure and deep earthquakes beneath India, the Himalaya and southern Tibet. *Geophysical Journal International*, 172(1), 345-362. <https://doi.org/10.1111/j.1365-246X.2007.03636.x>
- Putnis, A. (2009). Mineral replacement reactions. *Reviews in mineralogy and geochemistry*, 70(1), 87-124. <https://doi.org/10.2138/rmg.2009.70.3>
- Putnis, A. & Austrheim, H. (2010). Fluid-induced processes : metasomatism and metamorphism. *Geofluids*, 10(1-2), 254-269. <https://doi.org/10.1111/j.1468-8123.2010.00285.x>
- Putnis, A. & John, T. (2010). Replacement processes in the Earth's crust. *Elements*, 6(3), 159-164. <https://doi.org/10.2113/gselements.6.3.159>
- Putnis, A., Jamtveit, B. & Austrheim, H. (2017). Metamorphic processes and seismicity : the Bergen Arcs as a natural laboratory. *Journal of Petrology*, 58(10), 1871-1898. <https://doi.org/10.1093/petrology/egx076>
- Putnis, A., Moore, J., Prent, A. M., Beinlich, A. & Austrheim, H. (2021). Preservation of granulite in a partially eclogitized terrane : Metastable phenomena or local pressure variations? *Lithos*, 400, 106413. <https://doi.org/10.1016/j.lithos.2021.106413>

- Raimbourg, H., Jolivet, L. & Leroy, Y. (2007a). Consequences of progressive eclogitization on crustal exhumation, a mechanical study. *Geophysical Journal International*, 168(1), 379-401. <https://doi.org/10.1111/j.1365-246X.2006.03130.x>
- Raimbourg, H., Goffé, B. & Jolivet, L. (2007b). Garnet reequilibration and growth in the eclogite facies and geodynamical evolution near peak metamorphic conditions. *Contributions to Mineralogy and Petrology*, 153, 1-28. <https://doi.org/10.1007/s00410-006-0130-3>
- Raimbourg, H., Jolivet, L., Labrousse, L., Leroy, Y. & Avigad, D. (2005). Kinematics of syneclogite deformation in the Bergen Arcs, Norway : implications for exhumation mechanisms. *Geological Society, London, Special Publications*, 243(1), 175-192. <https://doi.org/10.1144/GSL.SP.2005.243.01.13>
- Räss, L., Duretz, T. & Podladchikov, Y. (2019). Resolving hydromechanical coupling in two and three dimensions : spontaneous channelling of porous fluids owing to decompression weakening. *Geophysical Journal International*, 218(3), 1591-1616. <https://doi.org/10.1093/gji/ggz239>
- Renard, F., Røyne, A. & Putnis, C. V. (2019). Timescales of interface-coupled dissolution-precipitation reactions on carbonates. *Geoscience Frontiers*, 10(1), 17-27. <https://doi.org/10.1016/j.gsf.2018.02.013>
- Reuber, G., Kaus, B. J., Schmalholz, S. M. & White, R. W. (2016). Nonlithostatic pressure during subduction and collision and the formation of (ultra) high-pressure rocks. *Geology*, 44(5), 343-346. <https://doi.org/10.1130/G37595.1>
- Roberts, D. (2003). The Scandinavian Caledonides : event chronology, palaeogeographic settings and likely modern analogues. *Tectonophysics*, 365(1-4), 283-299. [https://doi.org/10.1016/S0040-1951\(03\)00026-X](https://doi.org/10.1016/S0040-1951(03)00026-X)
- Rogowitz, A. & Huet, B. (2021). Evolution of fluid pathways during eclogitization and their impact on formation and deformation of eclogite : A microstructural and petrological investigation at the type locality (Koralpe, Eastern Alps, Austria). *Tectonophysics*, 819, 229079. <https://doi.org/10.1016/j.tecto.2021.229079>
- Rolf, T. & Tackley, P. (2011). Focussing of stress by continents in 3D spherical mantle convection with self-consistent plate tectonics. *Geophysical Research Letters*, 38(18). <https://doi.org/10.1029/2011GL048677>
- Rubie, D. C. (1986). The catalysis of mineral reactions by water and restrictions on the presence of aqueous fluid during metamorphism. *Mineralogical Magazine*, 50(357), 399-415. <https://doi.org/doi:10.1180/minmag.1986.050.357.05>
- Rubie, D. C. (1998). Disequilibrium during metamorphism : the role of nucleation kinetics. *Geological Society, London, Special Publications*, 138(1), 199-214. <https://doi.org/10.1144/GSL.SP.1996.138.01.12>
- Rudnick, R. L. & Fountain, D. M. (1995). Nature and composition of the continental crust : a lower crustal perspective. *Reviews of geophysics*, 33(3), 267-309. <https://doi.org/10.1029/95RG01302>
- Rutter, E. & Brodie, K. (1988). The role of tectonic grain size reduction in the rheological stratification of the lithosphere. *Geologische Rundschau*, 77, 295-307. <https://doi.org/10.1007/BF01848691>
- Rutter, E. H. (1995). Experimental study of the influence of stress, temperature, and strain on the dynamic recrystallization of Carrara marble. *Journal of Geophysical*

- Research : Solid Earth*, 100(B12), 24651-24663. <https://doi.org/10.1029/95JB02500>
- Rybacki, E. & Dresen, G. (2000). Dislocation and diffusion creep of synthetic anorthite aggregates. *Journal of Geophysical Research : Solid Earth*, 105(B11), 26017-26036. <https://doi.org/10.1029/2000JB900223>
- Schmalholz, S. M. & Podladchikov, Y. (2014). Metamorphism under stress : The problem of relating minerals to depth. *Geology*, 42(8), 733-734. <https://doi.org/10.1130/focus0822014.1>
- Schmalholz, S. M. & Podladchikov, Y. Y. (2013). Tectonic overpressure in weak crustal-scale shear zones and implications for the exhumation of high-pressure rocks. *Geophysical Research Letters*, 40(10), 1984-1988. <https://doi.org/10.1002/grl.50417>
- Schmalholz, S. M., Moulas, E., Plümper, O., Myasnikov, A. V. & Podladchikov, Y. Y. (2020). 2D Hydro-Mechanical-Chemical Modeling of (De)hydration Reactions in Deforming Heterogeneous Rock : The Periclase-Brucite Model Reaction. *Geochemistry, Geophysics, Geosystems*, 21(11), e2020GC009351. <https://doi.org/10.1029/2020GC009351>
- Schmalholz, S. M., Duretz, T., Schenker, F. L. & Podladchikov, Y. Y. (2014a). Kinematics and dynamics of tectonic nappes : 2-D numerical modelling and implications for high and ultra-high pressure tectonism in the Western Alps. *Tectonophysics*, 631, 160-175. <https://doi.org/10.1016/j.tecto.2014.05.018>
- Schmalholz, S. M., Medvedev, S., Lechmann, S. M. & Podladchikov, Y. (2014b). Relationship between tectonic overpressure, deviatoric stress, driving force, isostasy and gravitational potential energy. *Geophysical Journal International*, 197(2), 680-696. <https://doi.org/10.1093/gji/ggu040>
- Schmeling, H., Kruse, J. P. & Richard, G. (2012). Effective shear and bulk viscosity of partially molten rock based on elastic moduli theory of a fluid filled poroelastic medium. *Geophysical Journal International*, 190(3), 1571-1578. <https://doi.org/10.1111/j.1365-246X.2012.05596.x>
- Schneider, F., Yuan, X., Schurr, B., Mechle, J., Sippl, C., Haberland, C., Minaev, V., Oimahmadov, I., Gadoev, M., Radjabov, N. et al. (2013). Seismic imaging of subducting continental lower crust beneath the Pamir. *Earth and Planetary Science Letters*, 375, 101-112. <https://doi.org/10.1016/j.epsl.2013.05.015>
- Schreyer, W. (1988). Subduction of continental crust to mantle depths : Petrological evidence. *Episodes Journal of International Geoscience*, 11(2), 97-104. <https://doi.org/10.18814/epiiugs/1988/v11i2/005>
- Schulte-Pelkum, V., Monsalve, G., Sheehan, A., Pandey, M., Sapkota, S., Bilham, R. & Wu, F. (2005). Imaging the Indian subcontinent beneath the Himalaya. *Nature*, 435(7046), 1222-1225. <https://doi.org/10.1038/nature03678>
- Shi, F., Wang, Y., Yu, T., Zhu, L., Zhang, J., Wen, J., Gasc, J., Incel, S., Schubnel, A., Li, Z., Chen, T., Liu, W., Prakapenka, V. & Jin, Z. (2018). Lower-crustal earthquakes in southern Tibet are linked to eclogitization of dry metastable granulite. *Nature communications*, 9(1), 1-13. <https://doi.org/10.1038/s41467-018-05964-1>
- Shuwen, D., Oberhänsli, R., Schmid, R., Xiaochun, L., Jiafu, T. & Huaimin, X. (2002). Occurrence of metastable rocks in deeply subducted continental crust from

- the Dabie Mountains, central China. *Episodes Journal of International Geoscience*, 25(2), 84-89. <https://doi.org/10.18814/epiugs/2002/v25i2/003>
- Sibson, R. H. (2014). Earthquake rupturing in fluid-overpressured crust : how common ? *Pure and Applied Geophysics*, 171, 2867-2885. <https://doi.org/10.1007/s00024-014-0838-3>
- Simon, M., Pitra, P., Yamato, P. & Poujol, M. (2023). Isothermal compression of an eclogite from the Western Gneiss Region (Norway). *Journal of Metamorphic Geology*, 41(1), 181-203. <https://doi.org/10.1111/jmg.12692>
- Singer, J., Diehl, T., Husen, S., Kissling, E. & Duretz, T. (2014). Alpine lithosphere slab rollback causing lower crustal seismicity in northern foreland. *Earth and Planetary Science Letters*, 397, 42-56. <https://doi.org/10.1016/j.epsl.2014.04.002>
- Sloan, R., Jackson, J., McKenzie, D. & Priestley, K. (2011). Earthquake depth distributions in central Asia, and their relations with lithosphere thickness, shortening and extension. *Geophysical Journal International*, 185(1), 1-29. <https://doi.org/10.1111/j.1365-246X.2010.04882.x>
- Smith, D. C. (1984). Coesite in clinopyroxene in the Caledonides and its implications for geodynamics. *Nature*, 310(5979), 641-644. <https://doi.org/10.1038/310641a0>
- Solarino, S., Malusà, M. G., Eva, E., Guillot, S., Paul, A., Schwartz, S., Zhao, L., Aubert, C., Dumont, T., Pondrelli, S. et al. (2018). Mantle wedge exhumation beneath the Dora-Maira (U) HP dome unravelled by local earthquake tomography (Western Alps). *Lithos*, 296, 623-636. <https://doi.org/10.1016/j.lithos.2017.11.035>
- Spencer, C. J., Kirkland, C. L. & Taylor, R. J. (2016). Strategies towards statistically robust interpretations of in situ U-Pb zircon geochronology. *Geoscience Frontiers*, 7(4), 581-589. <https://doi.org/10.1016/j.gsf.2015.11.006>
- Šrámek, O., Ricard, Y. & Bercovici, D. (2007). Simultaneous melting and compaction in deformable two-phase media. *Geophysical Journal International*, 168(3), 964-982. <https://doi.org/10.1111/j.1365-246X.2006.03269.x>
- Steffen, K., Selverstone, J. & Brearley, A. (2001). Episodic weakening and strengthening during synmetamorphic deformation in a deep-crustal shear zone in the Alps. *Geological Society, London, Special Publications*, 186(1), 141-156. <https://doi.org/10.1144/GSL.SP.2001.186.01.09>
- Steltenpohl, M. G., Kassos, G., Andresen, A., Rehnström, E. F. & Hames, W. E. (2011). Eclogitization and exhumation of Caledonian continental basement in Lofoten, North Norway. *Geosphere*, 7(1), 202-218. <https://doi.org/10.1130/GES00573.1>
- Steltenpohl, M. G., Kassos, G. & Andresen, A. (2006). Retrograded eclogite-facies pseudidotachylites as deep-crustal paleoseismic faults within continental basement of Lofoten, north Norway. *Geosphere*, 2(1), 61-72. <https://doi.org/10.1130/GES00035.1>
- Steltenpohl, M. G., Hames, W. E. & Andresen, A. (2004). The Silurian to Permian history of a metamorphic core complex in Lofoten, northern Scandinavian Caledonides. *Tectonics*, 23(1). <https://doi.org/10.1029/2003TC001522>
- Stevens, V., Sloan, R., Chindandali, P., Wedmore, L. N., Salomon, G. & Muir, R. (2021). The entire crust can be seismogenic : Evidence from southern Malawi. *Tectonics*, 40(6), e2020TC006654. <https://doi.org/10.1029/2020TC006654>
- Tajčmanová, L., Podladchikov, Y., Powell, R., Moulas, E., Vrijmoed, J. & Connolly, J. (2014). Grain-scale pressure variations and chemical equilibrium in high-grade

- metamorphic rocks. *Journal of Metamorphic Geology*, 32(2), 195-207. <https://doi.org/10.1111/jmg.12066>
- Tajčmanová, L., Vrijmoed, J. & Moulas, E. (2015). Grain-scale pressure variations in metamorphic rocks : implications for the interpretation of petrographic observations. *Lithos*, 216, 338-351. <https://doi.org/10.1016/j.lithos.2015.01.006>
- Tajčmanová, L., Manzotti, P. & Alvaro, M. (2021). Under pressure : high-pressure metamorphism in the Alps. *Elements : An International Magazine of Mineralogy, Geochemistry, and Petrology*, 17(1), 17-22. <https://doi.org/10.2138/gselements.17.1.17>
- Thompson, A. B. & England, P. C. (1984). Pressure—temperature—time paths of regional metamorphism II. Their inference and interpretation using mineral assemblages in metamorphic rocks. *Journal of Petrology*, 25(4), 929-955. <https://doi.org/10.1093/petrology/25.4.929>
- Touret, J. L., Santosh, M. & Huizenga, J. M. (2022). Composition and evolution of the continental crust : Retrospect and prospect. *Geoscience Frontiers*, 101428. <https://doi.org/10.1016/j.gsf.2022.101428>
- Tullis, J. & Yund, R. A. (1991). Diffusion creep in feldspar aggregates : experimental evidence. *Journal of Structural Geology*, 13(9), 987-1000. [https://doi.org/10.1016/0191-8141\(91\)90051-J](https://doi.org/10.1016/0191-8141(91)90051-J)
- Turcotte, D. L. & Schubert, G. (2002). *Geodynamics*. Cambridge university press. <https://doi.org/10.1017/CBO9780511843877>
- van den Beukel, J. (1992). Some thermomechanical aspects of the subduction of continental lithosphere. *Tectonics*, 11(2), 316-329. <https://doi.org/10.1029/91TC01039>
- van Zelst, I., Crameri, F., Pusok, A. E., Glerum, A., Dannberg, J. & Thieulot, C. (2022). 101 geodynamic modelling : how to design, interpret, and communicate numerical studies of the solid Earth. *Solid Earth*, 13(3). <https://doi.org/10.5194/se-13-583-2022>
- Vitale, S. & Mazzoli, S. (2008). Heterogeneous shear zone evolution : the role of shear strain hardening/softening. *Journal of Structural Geology*, 30(11), 1383-1395. <https://doi.org/10.1016/j.jsg.2008.07.006>
- Wain, A., Waters, D. & Austrheim, H. (2001). Metastability of granulites and processes of eclogitisation in the UHP region of western Norway. *Journal of Metamorphic Geology*, 19(5), 609-625. <https://doi.org/10.1046/j.0263-4929.2001.00333.x>
- Wang, H., Huismans, R. S. & Rondenay, S. (2019). Water migration in the subduction mantle wedge : A two-phase flow approach. *Journal of Geophysical Research : Solid Earth*, 124(8), 9208-9225. <https://doi.org/10.1029/2018JB017097>
- Weber, S., Hauke, M., Martinez, R. E., Redler, C., Münker, C. & Froitzheim, N. (2022). Fluid-driven transformation of blueschist to vein eclogite during the Early Eocene in a subducted sliver of continental crust (Monte Emilius, Italian Western Alps). *Journal of Metamorphic Geology*, 40(3), 553-584. <https://doi.org/10.1111/jmg.12638>
- Wegener, A. (1912). Die entstehung der kontinente. *Geologische Rundschau*, 3(4), 276-292. <https://doi.org/doi.org/10.1007/BF02202896>
- Wegener, A. (1922). *Die entstehung der kontinente und ozeane* (T. 66). F. Vieweg & sohn akt.-ges.
- Yamato, P., Agard, P., Burov, E., Le Pourhiet, L., Jolivet, L. & Tiberi, C. (2007). Burial and exhumation in a subduction wedge : Mutual constraints from thermomechanical

- modeling and natural P-T-t data (Schistes Lustrés, western Alps). *Journal of Geophysical Research : Solid Earth*, 112(B7). <https://doi.org/10.1029/2006JB004441>
- Yamato, P. & Brun, J.-P. (2017). Metamorphic record of catastrophic pressure drops in subduction zones. *Nature Geoscience*, 10(1), 46-50. <https://doi.org/10.1038/ngeo2852>
- Yamato, P., Duretz, T., Baïsset, M. & Luisier, C. (2022). Reaction-induced volume change triggers brittle failure at eclogite facies conditions. *Earth and Planetary Science Letters*, 584, 117520. <https://doi.org/10.1016/j.epsl.2022.117520>
- Yardley, B. W. (2009). The role of water in the evolution of the continental crust. *Journal of the Geological Society*, 166(4), 585-600. <https://doi.org/10.1144/0016-76492008-10>
- Yardley, B. W. & Valley, J. W. (1997). The petrologic case for a dry lower crust. *Journal of Geophysical Research : Solid Earth*, 102(B6), 12173-12185. <https://doi.org/10.1029/97JB00508>
- Yarushina, V. M. & Podladchikov, Y. Y. (2015). (De) compaction of porous viscoelasto-plastic media : Model formulation. *Journal of Geophysical Research : Solid Earth*, 120(6), 4146-4170. <https://doi.org/10.1002/2014JB011258>
- Zack, T., Moraes, R. d. & Kronz, A. (2004). Temperature dependence of Zr in rutile : empirical calibration of a rutile thermometer. *Contributions to Mineralogy and Petrology*, 148, 471-488. <https://doi.org/10.1007/s00410-004-0617-8>
- Zertani, S., Labrousse, L., John, T., Andersen, T. B. & Tilmann, F. (2019). The interplay of Eclogitization and deformation during deep burial of the lower continental crust—A case study from the Bergen Arcs (Western Norway). *Tectonics*, 38(3), 898-915. <https://doi.org/10.1029/2018TC005297>
- Zertani, S., Vrijmoed, J. C., Tilmann, F., John, T., Andersen, T. B. & Labrousse, L. (2020). P wave anisotropy caused by partial eclogitization of descending crust demonstrated by modeling effective petrophysical properties. *Geochemistry, Geophysics, Geosystems*, 21(6), e2019GC008906. <https://doi.org/10.1029/2019GC008906>
- Zertani, S., John, T., Brachmann, C., Vrijmoed, J. C. & Plümper, O. (2022). Reactive fluid flow guided by grain-scale equilibrium reactions during eclogitization of dry crustal rocks. *Contributions to Mineralogy and Petrology*, 177(6), 61. <https://doi.org/10.1007/s00410-022-01928-3>
- Zhang, L. & Wang, Y. (2020). The exhumation of high-and ultrahigh-pressure metamorphic terranes in subduction zone : Questions and discussions. *Science China Earth Sciences*, 63, 1884-1903. <https://doi.org/10.1007/s11430-020-9579-3>
- Zhao, L., Paul, A., Guillot, S., Solarino, S., Malusà, M. G., Zheng, T., Aubert, C., Salimbeni, S., Dumont, T., Schwartz, S. et al. (2015). First seismic evidence for continental subduction beneath the Western Alps. *Geology*, 43(9), 815-818. <https://doi.org/10.1130/G36833.1>
- Zhong, X., Petley-Ragan, A. J., Incel, S. H., Dabrowski, M., Andersen, N. H. & Jamtveit, B. (2021). Lower crustal earthquake associated with highly pressurized frictional melts. *Nature Geoscience*, 14(7), 519-525. <https://doi.org/10.1038/s41561-021-00760-x>
- Zhong, X., Andersen, N. H., Dabrowski, M. & Jamtveit, B. (2019). Zircon and quartz inclusions in garnet used for complementary Raman thermobarometry : appli-

cation to the Holsnøy eclogite, Bergen Arcs, Western Norway. *Contributions to Mineralogy and Petrology*, 174, 1-17. <https://doi.org/10.1007/s00410-019-1584-4>



# 2

## Transient weakening during the granulite to eclogite transformation within hydrous shear zones (Holsnøy, Norway)

### Sommaire du présent chapitre

---

<b>Points clés</b>	<b>55</b>
<b>2.1 Résumé</b>	<b>56</b>
<b>2.2 Article de Bras et al. (2021), <i>Tectonophysics</i></b>	<b>57</b>
<b>2.3 Annexes à l'article de Bras et al. (2021)</b>	<b>74</b>

---

### Points clés

- Je fais une description pétrologique détaillée des réactions successives qui transforment la granulite en éclogite.
- Au cours de cette transformation, la roche traverse un stade transitoire où sa viscosité est minimale.
- La circulation de fluides provoque la réaction métamorphique et donc l'élargissement des bande de cisaillement.
- L'affaiblissement transitoire contribue à l'élargissement des bandes de cisaillement.

## 2.1 Résumé

Ce chapitre se focalise sur l'impact de l'éclogitisation, assistée par les fluides, sur la viscosité de la granulite en cours de réaction. Cette étude met en oeuvre à la fois des observations de terrain, une étude pétrologique détaillée et un modèle numérique.

À Holsnøy, dans les Calédonides scandinaves, des anorthosites granulitiques sont partiellement éclogitisées dans des bandes de cisaillement, qui s'élargissent au fil du temps en conséquence de l'afflux de fluides et de la déformation. Mes observations de terrain montrent que les bandes de cisaillement ne sont pas homogènes entre leur cœur et leur bordure. La bordure des bandes de cisaillement semble subir plus de déformation que leur cœur, ce qui laisse penser que la bordure est la partie rhéologiquement la moins résistante des bandes de cisaillement.

Pour vérifier cette hypothèse, j'ai étudié en détail la pétrologie de deux bandes de cisaillement d'échelle métrique de cette région. A 50 centimètres des bandes de cisaillement, la granulite (initialement plagioclase + grenat + deux pyroxènes) est déjà transformée en un assemblage à albite + zoisite + grenat + clinopyroxène. La bordure des bandes de cisaillement consiste en un assemblage hétérogène à grains fins d'omphacite + zoisite + disthène + grenat + phengite ± albite ± quartz. Le cœur des bandes de cisaillement est une éclogite homogène à omphacite + zoisite + grenat + zoisite + phengite ± quartz. Étant donné que les bandes de cisaillement se sont élargies au fil du temps, cette évolution latérale du bord vers le cœur des bandes de cisaillement reflète une évolution temporelle de l'assemblage minéralogique du début à la fin de l'éclogitisation. L'assemblage de la bordure représente donc un assemblage transitoire, dont les observations de terrain et pétrologiques suggèrent qu'il est mécaniquement plus faible que la granulite initiale et que l'éclogite finale.

Afin de confirmer et de quantifier l'affaiblissement transitoire en cours d'éclogitisation, j'ai développé un modèle numérique en une dimension d'une bande de cisaillement soumise à l'afflux de fluides et à la déformation. Je montre que l'affaiblissement transitoire permet d'expliquer nos observations de terrain et nos observations pétrologiques. En conclusion, l'évolution des bandes de cisaillement associe fluides, déformation et réaction, en étant contrôlée à la fois par la circulation de fluides et par l'affaiblissement transitoire en cours de réaction.

L'article est publié dans : Bras, E., Baïsset, M., Yamato, P., & Labrousse, L. (2021). Transient weakening during the granulite to eclogite transformation within hydrous shear zones (Holsnøy, Norway). *Tectonophysics*, 819, 229026. <https://doi.org/10.1016/j.tecto.2021.229026>.



Contents lists available at ScienceDirect

# Tectonophysics

journal homepage: [www.elsevier.com/locate/tecto](http://www.elsevier.com/locate/tecto)

## Transient weakening during the granulite to eclogite transformation within hydrous shear zones (Holsnøy, Norway)

Erwan Bras <sup>a,\*</sup>, Marie Baïsset <sup>b</sup>, Philippe Yamato <sup>a,c</sup>, Loic Labrousse <sup>b</sup><sup>a</sup> Univ Rennes, CNRS, Géosciences Rennes - UMR 6118, F-35000 Rennes, France<sup>b</sup> Sorbonne Université, CNRS-INSU, Institut des Sciences de la Terre Paris, ISTEPP UMR 7193, F-75005 Paris, France<sup>c</sup> Institut Universitaire de France, Paris, France

## ARTICLE INFO

**Keywords:**  
Eclogitization  
Metamorphic reactions  
Shear zone widening  
Transient weakening

## ABSTRACT

In Holsnøy (Bergen Arcs, Norway), metastable granulite facies anorthosite rocks are partially eclogitised within hydrous shear zones, that have been interpreted as widening over time with fluid influx and strain. We here present a detailed petrological description of two different metre-scale shear zones from this area. Within a few tens of centimetres of each shear zone, the granulite protolith (initially plagioclase + garnet + two pyroxenes) is transformed into an albite + zoisite + garnet + clinopyroxene assemblage. The outer edge of the shear zones consists in a fine-grained heterogeneous assemblage of omphacite + zoisite + kyanite + phengite ± albite ± quartz. The core of the shear zones is an homogeneous eclogite assemblage of coarser omphacite + kyanite + garnet + zoisite + phengite ± quartz. As the shear zones widened over time, this lateral evolution from the edge to the core of the shear zones reflects the temporal evolution of the granulite from the beginning to the end of the eclogitisation reaction. The outer omphacite + zoisite + kyanite + garnet + phengite ± albite ± quartz assemblage therefore represents a transient eclogite facies assemblage. Field and petrological observations suggest that this transient assemblage is mechanically weaker than both the starting strong granulite and the final eclogite. We here investigate the impact of transient weakening during syn-tectonic metamorphism using a one-dimensional numerical model of a fluid-fluxed, reacting shear zone. We show that transient weakening is required to explain our field and petrological observations. Furthermore, although the widening of the shear zones was primarily controlled by fluid infiltration, we show that strain hardening during the end of the eclogitisation reactions sequence had a noticeable widening effect on the shear zones.

## 1. Introduction

Shear zones are geological features of key importance for understanding the mechanical behaviour of the deep crust (e.g. Fossen and Cavalcante, 2017; Hawemann et al., 2019). The formation and evolution of a deep crustal shear zone is a complex process involving interplay between deformation, metamorphic reaction, fluid and element transport (e.g. Früh-Green, 1994; Austrheim, 1998, 2013; Jamtveit et al., 2016). At large scales metamorphic transformations constitute a first order control on the rheological behaviour throughout the crust. For example, eclogitisation of nominally dry metastable granulite has been invoked as a cause for earthquakes in the deep Tibetan crust (Shi et al., 2018). As these large scale processes have only been imaged through geophysical investigations in active orogens (e.g. in the Himalaya, Hetényi et al., 2007), direct petrological and structural observations of

exhumed crustal rocks from ancient orogens are crucial in understanding the role of metamorphic reactions on the rheology of the deep crust (e.g. Austrheim, 1990; Jackson et al., 2004; Labrousse et al., 2010).

The island of Holsnøy (Bergen Arcs, Norway) constitutes a natural laboratory for investigating the interplay between eclogitisation, fluid transport and deformation of subducted crust (e.g. Austrheim, 1987, 2013; Putnis et al., 2017; Jamtveit et al., 2019; Zertani et al., 2019). Holsnøy's rocks are mostly granulite-facies anorthosites in which eclogite-facies deformation is mainly localised in crosscutting hydrous eclogite shear zones (e.g. Austrheim and Griffin, 1985; Boundy et al., 1992). Field measurements show a positive correlation between the width  $W$  of shear zones and the total displacement  $D$  they accommodated (Boundy et al., 1992; Raimbourg et al., 2005). This positive correlation has been observed in others geological contexts (see Fig. 18 of the review paper of Fossen and Cavalcante, 2017), and can either be

\* Corresponding author.

E-mail address: [erwan.bras@univ-rennes1.fr](mailto:erwan.bras@univ-rennes1.fr) (E. Bras).

caused by progressive widening of the shear zones, or can be inherited from the precursor structure they exploited (e.g. Mancktelow and Pennacchioni, 2005; Pennacchioni, 2005). As an example, a set of shear zones from the Neves area (Tauern window, Italy, Pennacchioni and Mancktelow, 2018) show a tendency toward increasing  $D$  with increasing  $W$ , but without widening beyond the original extent of the precursor structure. Instead, the shear zone width, length and strain gradients are inherited from the overprinted structure that acted as a nucleation site.

However, in Holsnøy several arguments indicate that the  $D$ - $W$  correlation is rather due to the widening of the eclogite shear zones: (1) Between major shear zones ( $>100$  m wide) and the granulite host-rock, Jolivet et al. (2005) and Zertani et al. (2019) observed a transitional zone, formed by networks of smaller and narrower shear zones delimiting metre-scale granulite blocks. This progressive transition suggests that the small shear zones are an intermediate state of development of larger and wider shear zones, implying that they widen over time. (2) Major eclogite shear zones enclose rotated and scattered metre-scale granulite boudins, within which the orientation of the granulitic foliation varies (Boundy et al., 1992; Jolivet et al., 2005). These boudins are the same size as the blocks delimited by minor shear zones in the outer zone of the major shear zones, and can be considered as their later evolution at larger finite strain. (3) Using a scale-independent numerical model, Kaatz et al. (2021) also showed that Holsnøy shear zones widen over time, owing to synchronous fluid infiltration and deformation. (4) Deformation experiments by Incel et al. (2020) showed that fluid influx and subsequent metamorphic reactions in plagioclase-rich rocks result in the widening of shear zones at eclogite facies conditions.

Such widening can occur if the viscosity contrast between the shear zone and the host rock decreases over time. Viscosity contrasts can be reduced either by mechanical weakening of the host rock (e.g. Oliot et al., 2010; Goncalves et al., 2012), or by strengthening of the shear zone itself (e.g. Steffen et al., 2001; Vitale and Mazzoli, 2008). In Holsnøy, the widening of the shear zones is inferred to occur by weakening of the granulite host-rock, due to its eclogitisation promoted by fluid infiltration (e.g. Austrheim, 1987; Kaatz et al., 2021). As eclogite facies deformation was localised within eclogite shear zones, eclogite is considered to be a mechanically weaker rock than granulite (e.g. Austrheim, 1991; Bjørnerud et al., 2002; Jolivet et al., 2005; Raimbourg et al., 2005), and the widening is considered to be only caused by weakening of the host rock (Kaatz et al., 2021). However this does not take into account the kinetics of the metamorphic reactions responsible for eclogitisation, and the potential complex change in strength during the granulite to eclogite transition. As an example, the relationship between deformation and metamorphic reactions has been studied in eclogite facies shear zones in the Sesia Zone (Koops et al., 1987; Rubie, 1998), and in an amphibolite facies shear zone in the Tauern window (Steffen et al., 2001). In both cases the authors showed that transient weakening can be a prominent process operating during the evolution of the shear zones: rocks weaken during the first stage of metamorphic reaction, and thus localise deformation within a shear zone. During a later stage of reaction, the strength of the rocks is restored. The first weakening stage of the reacting rock can be caused by several mechanisms (Fossen and Cavalcante, 2017):

1. Reaction softening, i.e. the replacement of mechanically strong phases by weaker phases such as mica (e.g. Rubie, 1990; Gueydan et al., 2003; Oliot et al., 2010)
2. Hydrolytic softening, i.e. introduction of water into the crystal lattice of nominally anhydrous minerals, reducing the intercrystalline rock strength and promoting a switch in deformation mechanism (e.g. Tullis and Yund, 1980; Stünitz and Tullis, 2001; Chen et al., 2006; Kohlstedt, 2006).
3. A reduction in grain size (e.g. Rutter and Brodie, 1988b; Handy, 1989; Klaper, 1990).

4. The development of a foliation that increases connectivity between weak phases (Handy, 1990, 1994).

A later "re-hardening" stage of the reacting rock can be caused either by the replacement of weaker phases by stronger ones (Steffen et al., 2001), or by an increase in grain size (Koops et al., 1987). Additionally, the literature abounds with description of transient weakening processes such as transformation plasticity, dissolution precipitation creep or grain boundary sliding that enhance the deformability of transforming rocks (e.g. Poirier, 1982; Brodie and Rutter, 1985, 1987; Rutter and Brodie, 1988a, 1995; Marti et al., 2018; Stünitz et al., 2020), regardless of the rheological properties of the reaction products. Enhanced deformability is no longer active at the completion of the reaction, the rock behaviour being then governed by the properties of the reaction products.

However, transient weakening during the granulite to eclogite transition has yet to be explored in Holsnøy shear zones. In order to constrain the rheological evolution of the granulite during deformation at eclogite facies in Holsnøy, a detailed petrological study of a shear zone extending from the unaltered granulite protolith to the transformed eclogite is required. Matthey et al. (1994) studied the transformation of granulite to eclogite across a metre-scale shear zone in Holsnøy. They however focused on the composition of the fluids infiltrating the shear zones, and did not explore the rheological impact of the metamorphic reactions. In this contribution, we present a detailed petrological study of two eclogite shear zones, extending from the granulite host-rock to the eclogite core. We describe in detail the mineralogical and textural changes associated with progressive eclogitisation. Based on these and field observations, we argue that the granulite to eclogite transformation induces transient weakening of the reacting rock. We then establish the role of transient weakening using a one-dimensional numerical model of a hydrous, reacting shear zone. We show that the geometry and petrological pattern of metric-scale eclogite shear zones is not controlled by the rheology of eclogite, but rather by the rheology of the transient assemblage. We also investigate values for fluid diffusivity and reaction rates by comparing the numerical results to our field data.

## 2. Geological setting

Holsnøy Island, in southwestern Norway, belongs to the Lindås nappe (Fig. 1), a part of the Bergen Arcs thrust sheets that formed during the Scandian collisional phase of the Caledonian orogeny (Roberts, 2003). The outcrops studied here are located on northwestern Holsnøy, and are composed of anorthositic granulites that are partially eclogitised. The granulite facies event occurred at 930 Ma during the Grenvillian orogeny (Bingen et al., 2001), during which the rocks equilibrated at temperature ( $T$ ) and pressure ( $P$ ) conditions of 800–850 °C and  $< 10$  kbar (Austrheim and Griffin, 1985).

The anorthositic granulite was part of the Jotun-Lindås microcontinent, along the hyper-extended margin of Baltica, and was subducted during collision between Baltica and Laurentia (Andersen et al., 1991; Jakob et al., 2017). Bhowany et al. (2018) determined peak  $P$ - $T$  conditions for eclogite facies metamorphism in Holsnøy at 670–690 °C, 21–22 kbar. The eclogite facies event has been dated at 435–420 Ma (Glodny et al., 2008; Jamtveit et al., 2019). Despite residing at eclogite facies conditions during several Ma (Glodny et al., 2008), the granulite remained partly untransformed. As hydrous minerals (zoisite, phengite) are part of the eclogite paragenesis, and as fluid is a catalyst for metamorphic reactions (Rubie, 1986; Putnis and Austrheim, 2010), the availability of fluid has been inferred as the limiting factor for eclogitisation of the metastable granulite (Austrheim, 1987; Jamtveit et al., 1990).

The widely accepted scenario invoked to explain the formation of Holsnøy eclogite shear zones (Austrheim, 1987; Boundy et al., 1992; Raimbourg et al., 2005; Jamtveit et al., 2018; Zertani et al., 2019; Kaatz et al., 2021) can be summarised as follow: (1) Lower-crustal earthquakes

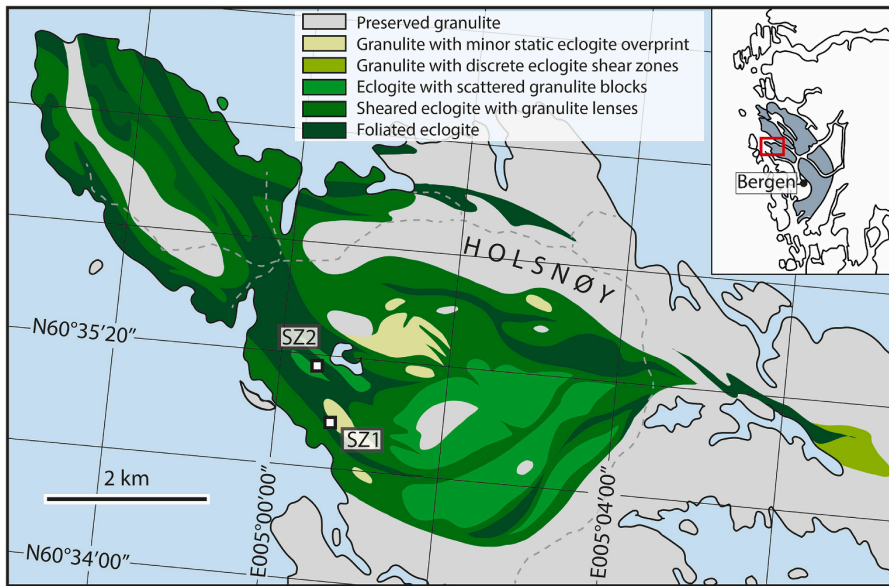


**Fig. 1.** Geological map of northern Holsnøy island, in south-western Norway, modified from Austrheim (2013) and Zertani et al. (2019). Inset shows the position of Holsnøy in the Lindås Nappe (blue). Black squares indicate the location of the shear zones studied in this work. Shear zone SZ1: 60°34'57"N, 5°00'43.56"E. Shear zone SZ2: 60°35'20.1"N, 5°00'27.8"E. (For interpretation of the references to colour in this figure legend, the reader is referred to the web version of this article.)

propagated fractures in the brittle granulite. (2) Those fractures acted as a pathway for fluid infiltration into the granulite. (3) The presence of fluids triggered eclogitisation of the granulite located in undeformed hydration halos surrounding the initial fractures, typically a few tens of centimetres wide. The eclogitisation weakened the granulite located within the hydration halos. (4) Once the eclogitised halos were sufficiently weakened, they started to deform in a ductile manner, so that they were the precursor structures of small-scale eclogite shear zones that localised deformation. (5) The shear zones widened owing to diffusion of the fluid along a pressure gradient orthogonal to the shear direction. (6) Multiple shear zones coalesced into shear zone networks, then into major 100-m wide eclogite shear zones that enclose preserved granulite blocks.

Large areas of Holsnøy also show a partial "static" eclogite facies overprint of the granulite, which was associated with fluid infiltration but no deformation (Zertani et al., 2019).

### 3. Analytical methods

Two 1 m-wide shear zones, located on Fig. 1, were sampled from their margin to their core. Photographs and interpretative sketches of the shear zones along with sample locations are shown in Fig. 2. Since the outcrops are horizontal with almost no topography, eclogite lineations could not be measured accurately. However regional lineation measurements by Boundy et al. (1992), Raimbourg et al. (2005) and Kaatz et al. (2021) show that shear zones regionally have a lineation dip between 10 and 30° toward the East. The outcrop surface is therefore close to the shear zone XZ plane, with X parallel to the movement direction and Z orthogonal to the shear plane.

Thin sections were analysed with scanning electron microscopy (SEM) to obtain  $2.25 \times 1.69$  mm EDS (Energy-dispersive spectroscopy) chemical element maps of representative areas (e.g. coronas, matrix). Quantitative mineral compositions were measured using electron probe micro-analysis (EPMA). Analyses were performed at ISTeP (Sorbonne Université, Paris) using a ZEISS Supra 55 VP Scanning Electron Microscope (spatial resolution 2.2  $\mu\text{m}$ ), and at the CAMECA SX-100 Electron Microprobe (spatial resolution 2  $\mu\text{m}$ ).

Grain sizes were quantitatively estimated from EDS maps and photomicrographs using a watershed segmentation algorithm written in MATLAB. EDS maps were processed with MATLAB to compute mineral phase maps (presented in supplementary material A), using a nearest neighbour algorithm: for each map, control points of known mineralogy were identified, using EPMA analyses. The euclidean distance of each pixel to each of the control points was calculated in a  $n$ -dimensional space, where  $n$  is the number of chemical elements mapped with EDS. Each pixel was then assigned the mineralogy of the nearest control point. If the distance between a pixel and the closest control point was greater than a preset threshold, the pixel was not indexed. Mineral proportions were then calculated by pixel counting on the phases maps. The proportions of the investigated areas (e.g. coronas, matrix) were estimated in thin sections and hand samples, allowing to calculate the mineral proportions at the sample scale. Compared to other quantitative techniques such as X-ray powder diffraction (XRPD), using EDS maps to quantify the minerals proportions allows to remove the effects of amphibolitisation on the proportions of the eclogite facies minerals. Additionally, as the rocks have a large scale chemical heterogeneity, large volumes of rock would be needed to calculate representative compositions with XRPD. But since we study local equilibria, these volumes may not be representative of the studied domains.

Hereafter, we use the following mineral abbreviations from Kretz (1983): Ab = albite; Alm = almandine; An = anorthite; Cpx = clinopyroxene; di = diopside; grs = grossular; grt = garnet; hd = hedenbergite; jd = jadeite; kfs = K-feldspar; Ky = kyanite; Omp = omphacite; Pl = plagioclase; Prp = pyrope; Qtz = quartz; Zo = zoisite. We also use Amp for amphibole, Ca-ts for Ca-tschermakite and Ph for phengite.

## 4. Results

### 4.1. Petrological description

All samples exhibit weak amphibolite-facies retrogression, as shown by amphibole/clinopyroxene - plagioclase symplectites around garnet and omphacite. As retrograde minerals are not the focus of this work, the following section only deals with minerals formed during prograde to peak eclogite metamorphism.

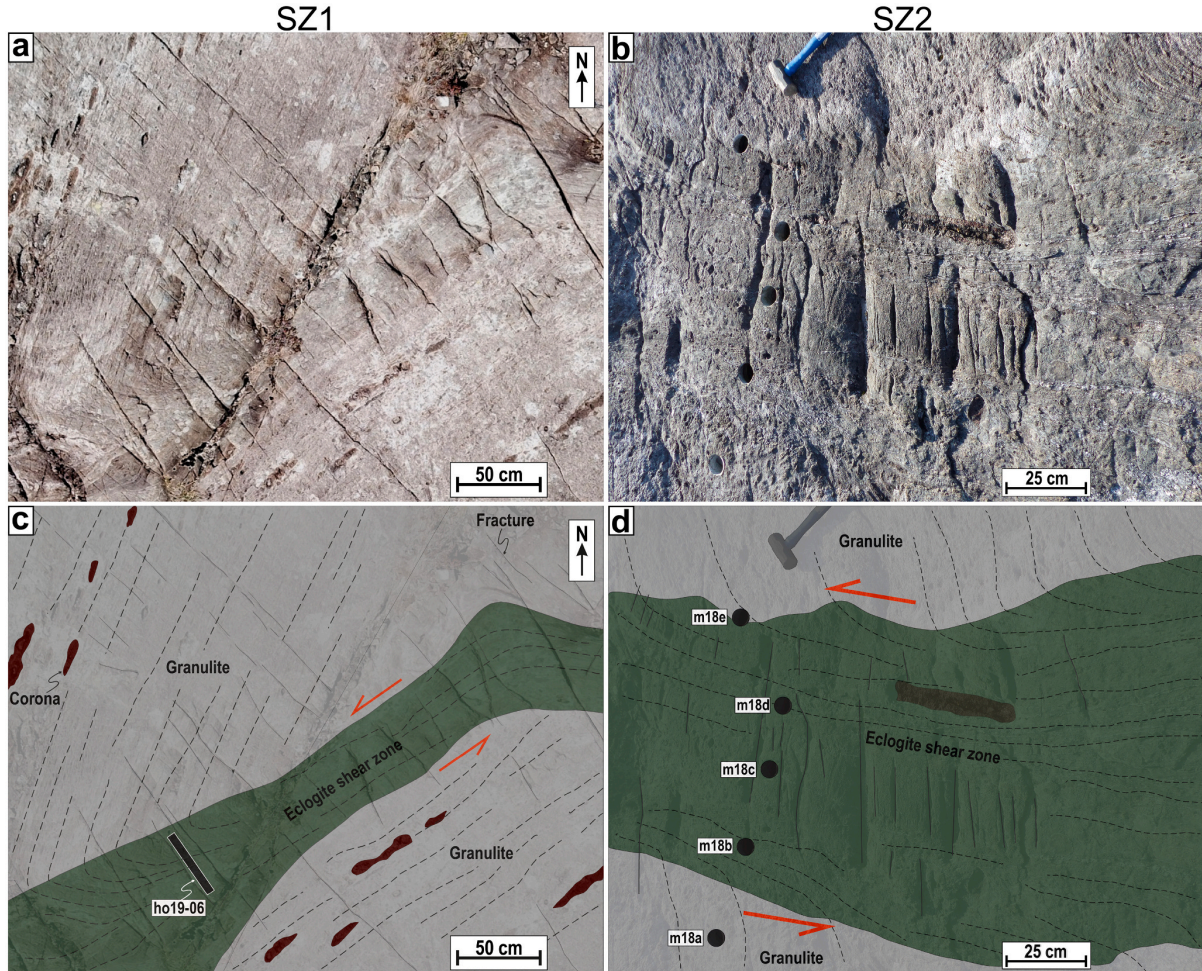


**Fig. 2.** Photographs and interpretative sketches of shear zones SZ1 (a, c) and SZ2 (b, d), showing the location of the samples. SZ1: petrological domains D2, D3 and D4 were sampled in the transect ho19-06. D0 was sampled in the granulite outside the photograph. SZ2: domains D1 (drill cores m18a and m18e), D3 (m18b and m18d) and D4 (m18c) were sampled. See section 4.1 for a description of the domains. Notice how the foliation is more pronounced in the edge of the shear zone than in the core.

Mineralogical assemblages vary from the margins to the core of the shear zones, and the pattern is similar for both shear zones. From the granulite host-rock to the core of an eclogite shear zone, we identified five petrologically distinct domains:

Domain D0 corresponds to the granulite protolith unaffected by eclogite facies deformation and fluid infiltration. D0 is located at least 0.5 m away from the outer edge of the shear zone (Matthey et al., 1994), and was sampled in SZ1. The unaltered granulite is composed of millimetre-sized grains of plagioclase, garnet, clinopyroxene and minor orthopyroxene and amphibole (Fig. 3d-f). Elongated elliptical pyroxene clusters surrounded by garnets form coronitic structures that mark the granulite foliation and lineation. Coronas account for around 30% of the granulite volume, the rest being composed of a matrix of plagioclase and isolated garnets between the plagioclase grains.

Domain D1 is located within 0.5 m of the margin of the shear zone and was sampled in SZ2 (Fig. 2, samples m18a and m18e). The texture is similar to that of D0, with coronas embedded in matrix that contains isolated garnets (Fig. 3d and e). Although the coarse plagioclase grains of D0 are pseudomorphed in D1 by a new matrix of fine-grained (<50  $\mu\text{m}$ ) Ab+Zo + Ky + Ph + Qtz (Fig. 3f), the grain boundaries of former plagioclase grains can still be identified in this new matrix (Fig. 3d).

Clinopyroxenes in the coronas show exsolution lamellae of garnet

and rutile (Fig. 3e). Reaction rims around garnets (Fig. 3e and f) are composed of a very fine-grained Omp + Zo + Ab+Ky + Ph aggregate. Similar reaction rims are found at the matrix/corona interface.

Domain D2 is located at the edge of the shear zone and was sampled in SZ1. The coronas/matrix structure resembles that of D1, but shows a manifest eclogite facies foliation imprint. Reaction rims around garnet grains and around coronas are wider (Fig. 3g and h), and the structure of former D0 plagioclase grains is no longer visible. The composition of the matrix is similar to that of D1, but grains are coarser, up to 100  $\mu\text{m}$  (Fig. 3f). Omphacite replaced clinopyroxene in the coronas, which are now mostly composed of Omp + Grt + Ph.

Domain D3 was sampled in both SZ1 and SZ2 (Fig. 2, samples m18b and m18d in SZ2). The coronas/matrix structure is less distinct than in D1 and D2, and the foliation marked by Zo + Ky + Ph + Qtz layers and Omp + Ky layers is clearly defined (Fig. 3j). The Omp + Ky layers mostly develop around coronas and isolated garnets in the matrix (Fig. 3k and l). The grain size in the matrix is less than 100  $\mu\text{m}$ .

Domain D4 is located at the core of the shear zone, and was sampled in both SZ1 and SZ2 (sample m18c in SZ2). The entire domain is very homogeneous, with no coronas/matrix structure and a poorly defined foliation (Fig. 3m and n). The mineral assemblage is a typical Omp + Ky + Zo + Grt + Ph  $\pm$  Qtz eclogite, with most of the grains coarser than 200

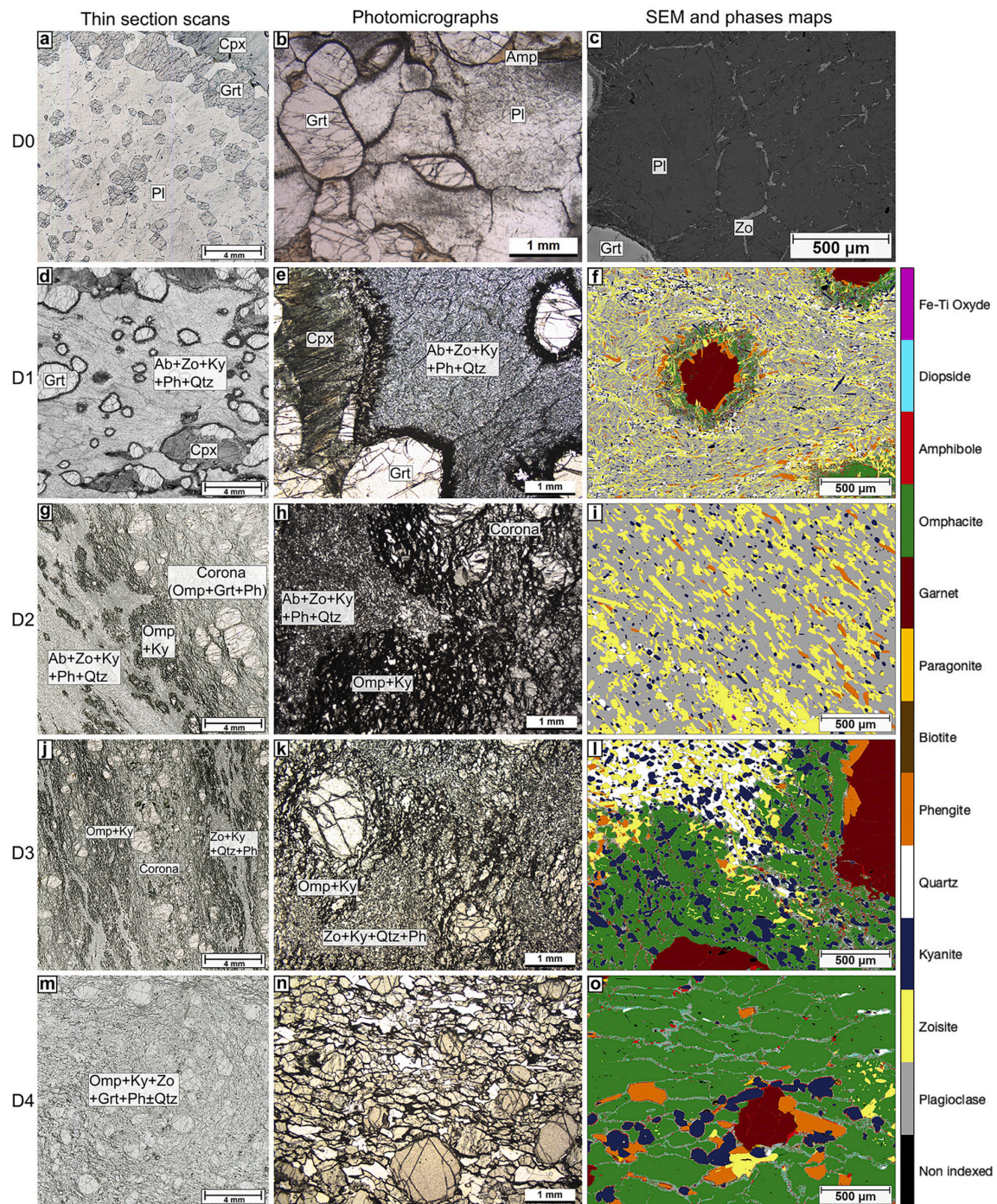


**Fig. 3.** Fig. 3: Petrological features of the domains D0 (a, b, c), D1 (d, e, f), D2 (g, h, i), D3 (j, k, l) and D4 (m, n, o). Most samples are weakly retrogressed in the amphibolite facies. (a, b, c) Detail of a thin section (a), photomicrograph (b) and SEM image (c) showing a typical granulite texture of coarse clinopyroxenes and garnets in a plagioclase matrix. The plagioclase is locally clouded by zoisite needles. (d) Typical granulite texture of coarse clinopyroxenes and garnets in a  $\text{Ab} + \text{Zo} + \text{Ky} + \text{Ph} + \text{Qtz}$  matrix. (e) Photomicrograph showing exsolution lamellae of garnet in clinopyroxene in a corona (left) and reaction rims between garnet/clinopyroxene and the  $\text{Ab} + \text{Zo} + \text{Ky} + \text{Ph} + \text{Qtz}$  matrix. The structure of former coarse plagioclase grains is still visible in the matrix. (f) Phase map derived from EDS element maps. The matrix is made up of Ab, Zo and minor  $\text{Ky} \pm \text{Ph} \pm \text{Qtz}$ . The reaction rim comprises Omp + Zo + Ab + Ky + Ph. (g, h) Contact between a corona (Omp + Grt + Ph) and the matrix ( $\text{Ab} + \text{Zo} + \text{Ky} + \text{Ph} + \text{Qtz}$ ), with an Omp + Ky assemblage at the corona/matrix boundary. The foliation is more pronounced than in D1. (i) Phase map of the matrix showing the foliation. (j) The foliation is well defined by Omp + Ky and Zo + Ky + Qtz + Ph beds. The coronas are more elongated than in D2. (k, l) Reaction rim of Omp + Ky at the garnet/matrix boundary. (m, n, o) Homogeneous Omp + Ky + Zo + Grt + Ph ± Qtz eclogite assemblage.

$\mu\text{m}$  (Fig. 3o).

#### 4.2. Mineral compositions

The compositions of the minerals are different in SZ1 and SZ2, and are therefore reported separately in Table 1 and Table 2, respectively. Within each shear zone, the composition of plagioclase, phengite and zoisite only show some minor variations between D2, D3 and D4, and was averaged over these 3 domains (Tables 1 and 2).

The composition of phengite and plagioclase in D1 is different from that of D2, D3 and D4. In particular, the proportion of the anorthite end-member  $X_{An}$  in plagioclase is higher in D1 (Table 2:  $X_{An} = 0.15$  in D1,  $X_{An} = 0.12$  in D3/D4).

All garnets from D1 to D4 show compositional zoning (see an example in supplementary material B), with a core enriched in pyrope end-member  $X_{Pp}$  and a rim enriched in almandine end-member  $X_{Alm}$ . For example in SZ1 (Table 1),  $X_{Alm} = 0.27$  and  $X_{Pp} = 0.53$  in the core; and  $X_{Alm} = 0.43$  and  $X_{Pp} = 0.33$  in the rim. Although the width of the Fe-rich rims increases from D1 to D4, the compositions of cores and rims are similar within each shear zone and were averaged across all domains in Tables 1 and 2.

The composition of omphacite varies (1) across the shear zones, between the petrological domains D2, D3 and D4, and (2) between the coronas and the matrix of a given domain. In particular, in both shear zones the jadeite end-member proportion  $X_{Jd}$  in matrix omphacites decreases from the edge (D2) to the core (D4): in SZ1 matrix the jadeite end-member decreases from D2 ( $X_{Jd} = 0.54$ ) to D4 ( $X_{Jd} = 0.50$ ); and in SZ2 matrix the jadeite end-member decreases from D3 ( $X_{Jd} = 0.59$ ) to D4 ( $X_{Jd} = 0.54$ ).

#### 4.3. Mineral proportions

Mineral proportions in D0, D1, D2, D3 and D4 were estimated following the method presented in section 3. As they were calculated using small scale EDS maps, the mineral proportions shown in Fig. 4 are semi-quantitative. However, they have been chosen to be as representative as possible of the whole studied domain and estimations have been performed on several EDS maps giving comparable results. Although mineral proportions in SZ1 and SZ2 are different, a similar trend is observed: the proportion of omphacite and kyanite increases from D1 to D4 whereas the proportion of zoisite, garnet and plagioclase decreases from D1 to D4.

### 5. Synthesis on shear zone evolution in Holsnøy

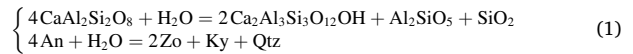
#### 5.1. Succession of metamorphic reactions

Based on our textural and compositional analysis, it is manifest that the eclogite facies imprint increases from the unaltered granulite outside the shear zone (D0) to the eclogite core (D4). We can describe the eclogitisation process across a shear zone as the sequence of mineral reactions (1) to (5), all occurring at around 700 °C, 21 kbar (Bhowany et al., 2018).

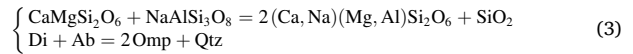
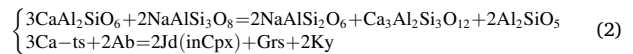
We calculated the bulk composition of each domain using EPMA mineral compositions (Tables 1 and 2), mineral proportions (Fig. 4) and mineral densities at eclogite facies conditions (700 °C and 2 GPa) from the Abers and Hacker (2016) database. The results, presented in supplementary material C, suggest that, other than the introduction of volatile elements, the formation of metric-scale eclogite shear zones can be considered as essentially isochemical. We therefore balance the reactions considering  $\text{H}_2\text{O}$  as the only mobile species.

The reactions are presented in chronological order, from stages D0 to D4. Relative solid volume change and total volume change have been computed for each of the reactions, based on the Abers and Hacker (2016) database, with 1100 kg/m<sup>3</sup> used for the water density (Brodholt and Wood, 1993).

**From D0 to D1.** In the matrix, the anorthitic component of the granulitic plagioclase ( $\text{An}_{40}$ ) reacts to form zoisite, due to the hydration of the granulite:



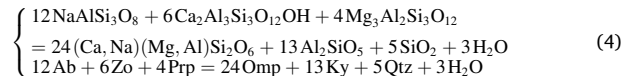
This reaction has been described by numerous authors (e.g. Jamtveit et al., 1990; Matthey et al., 1994). The change in solid volume associated with this reaction is -14%, and the change in total volume is -18%. This reaction leaves the albitic component of plagioclase untransformed, forming the  $\text{Ab} + \text{Zo} + \text{Ky} + \text{Ph} + \text{Qtz}$  matrix of D1. Phengite was not included in the reactions but is also a product of plagioclase destabilisation (K-feldspar end-member). Albite only reacts at the coronas/matrix interface to form omphacite, following the reactions:



A reaction similar to reaction (2) has been described by Raimbourg (2005), and a reaction similar to reaction (3) has been described by Matthey et al. (1994) and Schneider et al. (2007). The changes in volume associated with reactions (2) and (3) are respectively -13% and -10%. The exsolution lamellae of garnet in clinopyroxene observed on Fig. 3e are interpreted as the product of reaction (2).

**From D1 to D2.** Reaction (1) leaves the remaining plagioclase with an average  $\text{Ab}_{86}$  composition in D2 (Table 1). As in D2, D3 and D4 the composition of plagioclase is the same (average  $\text{Ab}_{86}$ ), reaction (1) is considered as complete in D2. Reaction (3) continues until all the former millimetric grains of clinopyroxene react to form small omphacite grains.

The albitic plagioclase and zoisite in the matrix react with garnets (isolated grains or in the coronas) following the reaction:



Similar reactions have been described by Matthey et al. (1994) and Schneider et al. (2007). The change in solid volume associated with this reaction is -10%, and the change in total volume is -8%. The contribution of garnet to the reaction is manifest from the reaction rims around isolated garnets and coronas (Fig. 3g to 3l). The zoning of garnet is also consistent with this reaction: as pyrope preferentially contributes to reaction (4), the garnet rims are enriched in almandine (see supplementary material B). Reaction (4) can be observed in Fig. 3h, where the mineral composition of the corona ( $\text{Omp} + \text{Grt}$ ) is noticeably different from the composition of the corona/matrix interface ( $\text{Omp} + \text{Ky}$ ). The  $\text{Omp} + \text{Ky}$  assemblage is the product of reaction (4). Reactions (2), (3), (4) are balanced without including the minor remaining anorthitic component of plagioclase, although it is also consumed by the reactions as a Ca-bearing reactant.

**From D2 to D3:** Reaction (4) proceeds until all the plagioclase is consumed. The product of this reaction is evidenced in Fig. 3h and i, where a rim of  $\text{Omp} + \text{Ky}$  separates the garnets from a matrix composed mostly of  $\text{Zo} + \text{Ky} \pm \text{Qtz}$  and very little plagioclase.

**Table 1**

Representative EPMA data of minerals in SZ1 (average of representative analyses), given with one sigma standard deviation. Omphacite is normalised to 6 oxygens (O), mica to 11 O, plagioclase to 8 O, garnet to 12 O, zoisite to 12.5 O.

Averaged over	Cpx			Omphacite				Plagioclase		Phengite		Grt		Grt core		Grt rim		Zoisite		Averaged over
	D0	D2 cor	D2 mat	D3 cor	D3 mat	D4	D0	D2-D4	D2-D4	D0	D2-D4	D0	D2-D4	D2-D4	D2-D4	D2-D4	D2-D4	D2-D4		
SiO <sub>2</sub>	46.42 ± 1.32	54.09 ± 1.49	55.27 ± 0.27	55.15 ± 0.42	55.59 ± 0.36	55.52 ± 0.24	58.27 ± 0.45	65.78 ± 0.92	49.48 ± 0.65	41.33 ± 0.48	40.9 ± 0.23	39.54 ± 0.23	39.29 ± 0.3	SiO <sub>2</sub>						
TiO <sub>2</sub>	2.13 ± 1.76	0.23 ± 0.05	0.09 ± 0.03	0.20 ± 0.07	0.10 ± 0.06	0.08 ± 0.05	0.03 ± 0.03	0.01 ± 0.02	0.33 ± 0.11	0.18 ± 0.03	0.08 ± 0.06	0.06 ± 0.04	0.04 ± 0.04	TiO <sub>2</sub>						
Al <sub>2</sub> O <sub>3</sub>	13.66 ± 0.4	12.72 ± 0.39	14.21 ± 0.16	12.49 ± 0.59	13.95 ± 0.4	13.46 ± 0.33	27.64 ± 0.4	22.03 ± 0.57	31.97 ± 0.33	23.76 ± 0.35	23.17 ± 0.15	22.41 ± 0.2	32.64 ± 0.58	Al <sub>2</sub> O <sub>3</sub>						
Cr <sub>2</sub> O <sub>3</sub>	0.01 ± 0.02	4.09 ± 1.21	3.99 ± 0.16	3.38 ± 0.23	3.90 ± 0.17	3.66 ± 0.16	0.02 ± 0.02	0.08 ± 0.06	49.48 ± 0.65	0.02 ± 0.03	13.41 ± 0.98	20.71 ± 1.35	1.23 ± 0.54	Cr <sub>2</sub> O <sub>3</sub>						
FeO	5.17 ± 0.32	0.00 ± 0.03	0.00 ± 0.04	0.01 ± 0.02	0.02 ± 0.02	0.02 ± 0.02	0.03 ± 0.04	0.02 ± 0.03	0.01 ± 0.02	14.10 ± 0.49	0.04 ± 0.04	0.02 ± 0.03	0.02 ± 0.02	FeO						
MgO	10.53 ± 0.27	8.49 ± 0.07	6.81 ± 0.16	8.58 ± 0.46	7.03 ± 0.41	7.66 ± 0.24	0.00 ± 0.01	0.00 ± 0.01	2.31 ± 0.14	15.42 ± 0.2	15.02 ± 0.55	8.85 ± 1.04	0.02 ± 0.03	MgO						
MnO	0.02 ± 0.04	0.04 ± 0.06	0.02 ± 0.03	0.03 ± 0.03	0.05 ± 0.04	0.03 ± 0.03	0.01 ± 0.02	0.02 ± 0.01	0.02 ± 0.02	0.22 ± 0.07	0.19 ± 0.04	0.50 ± 0.14	0.02 ± 0.03	MnO						
CaO	20.97 ± 0.88	13.75 ± 0.36	11.61 ± 0.22	14.05 ± 0.81	12.03 ± 0.64	12.62 ± 0.22	8.62 ± 0.25	2.87 ± 0.74	0.03 ± 0.03	7.43 ± 0.22	7.68 ± 0.07	8.56 ± 1.23	23.90 ± 0.38	CaO						
Na <sub>2</sub> O	2.35 ± 0.12	6.43 ± 0.25	7.62 ± 0.14	6.53 ± 0.44	7.58 ± 0.33	7.28 ± 0.14	6.64 ± 0.17	10.17 ± 0.48	0.92 ± 0.36	0.03 ± 0.03	0.02 ± 0.01	0.02 ± 0.02	0.03 ± 0.02	Na <sub>2</sub> O						
K <sub>2</sub> O	0.02 ± 0.04	0.01 ± 0.01	0.00 ± 0.01	0.01 ± 0.01	0.01 ± 0.02	0.01 ± 0.02	0.25 ± 0.12	0.08 ± 0.07	8.96 ± 0.6	0.03 ± 0.03	0.01 ± 0.01	0.00 ± 0.01	0.01 ± 0.01	K <sub>2</sub> O						
Total	101.28	99.83	99.61	100.43	100.24	100.34	101.52	101.06	95.48	102.52	100.51	100.67	97.20	Total						
Si	1.69	1.93	1.96	1.95	1.96	1.96	2.57	2.87	3.25	2.96	2.97	2.98	3.01	Si						
Al	0.59	0.54	0.59	0.52	0.58	0.56	1.44	1.13	2.48	2.01	1.98	1.99	2.95	Al						
Mg	0.57	0.45	0.36	0.45	0.37	0.40			0.23	1.65	1.62	0.99		Mg						
Fe	0.16	0.12	0.12	0.10	0.12	0.11			0.08	0.84	0.81	1.31	0.08	Fe						
Ca	0.82	0.53	0.44	0.53	0.45	0.48	0.41	0.13		0.57	0.60	0.69	1.96	Ca						
Na	0.17	0.44	0.52	0.45	0.52	0.50	0.57	0.86	0.12		0.00	0.00		Na						
K							0.01	0.00	0.75					K						
End-members	Ca-Ts = 0	0.09	0.04	0.06	0.04	0.05	Ab = 0.57	0.86		Alm = 0.27	0.27	0.43		End-members						
	Di = 0.63	0.39	0.32	0.41	0.33	0.36	An = 0.41	0.13		Grs = 0.18	0.20	0.23								
	Hd = 0.17	0.11	0.10	0.09	0.10	0.10	Kfs = 0.01	0.00		Prp = 0.54	0.53	0.33								
N	10	4	9	26	9	10	4	9	15	10	5	10	27	N						

Cor = coronas. Mat = matrix, including the matrix and the omp + ky assemblages at the matrix/corona or matrix/garnet boundary. All Fe is counted as Fe<sup>2+</sup>. N = number of averaged analyses.

**Table 2**

Representative EPMA data of minerals in SZ2 (average of representative analyses), given with one sigma standard deviation. Structural formulas and abbreviations as in [Table 1](#).

Averaged over	Cpx	Omphacite			Plagioclase		Phengite		Grt core	Grt rim	Zoisite	Averaged over
	D1	D3 cor	D3 mat	D4	D1	D3 + D4	D1	D3 + D4	All	All	All	
SiO <sub>2</sub>	49.64 ± 1.77	55.74 ± 0.32	55.79 ± 0.51	55.09 ± 0.27	64.74 ± 0.72	65.64 ± 0.59	47.76 ± 0.3	47.49 ± 0.65	40.71 ± 0.14	39.00 ± 0.42	39.15 ± 0.31	SiO <sub>2</sub>
TiO <sub>2</sub>	0.89 ± 0.26	0.14 ± 0.04	0.14 ± 0.04	0.16 ± 0.04	0.01 ± 0.01	0.02 ± 0.02	0.46 ± 0.01	0.52 ± 0.13	0.17 ± 0.07	0.17 ± 0.07	0.05 ± 0.06	TiO <sub>2</sub>
Al <sub>2</sub> O <sub>3</sub>	10.28 ± 1.96	14.80 ± 0.2	15.25 ± 0.77	14.19 ± 0.09	22.3 ± 0.28	21.57 ± 0.32	31.36 ± 0.41	32.81 ± 0.67	22.94 ± 0.2	22.06 ± 0.27	32.90 ± 0.32	Al <sub>2</sub> O <sub>3</sub>
Cr <sub>2</sub> O <sub>3</sub>	0.03 ± 0.03	0.03	0.04	0.02	0.01	0.03	0.03	0.04	0.03	0.03	0.01	Cr <sub>2</sub> O <sub>3</sub>
FeO	3.49 ± 0.23	4.37 ± 0.29	4.25 ± 0.2	4.14 ± 0.18	0.01 ± 0.01	0.15 ± 0.13	1.65 ± 0.12	1.45 ± 0.21	15.20 ± 0.36	22.47 ± 0.36	1.12 ± 1.19	FeO
MgO	12.13 ± 0.78	6.20 ± 0.22	5.92 ± 0.49	6.76 ± 0.14	0.00 ± 0.00	0.08 ± 0.21	2.34 ± 0.12	1.77 ± 0.23	13.38 ± 0.49	7.54 ± 0.9	0.03 ± 0.03	MgO
MnO	0.01 ± 0.01	0.06 ± 0.02	0.07 ± 0.05	0.04	0.01 ± 0.02	0.02 ± 0.02	0.02 ± 0.03	0.01 ± 0.02	0.27 ± 0.06	0.69 ± 0.13	0.03 ± 0.13	MnO
CaO	20.35 ± 1.31	10.89 ± 0.41	10.41 ± 0.64	11.52 ± 0.12	3.05 ± 0.44	2.44 ± 0.58	0.34 ± 0.03	1.82 ± 0.03	7.92 ± 0.02	8.29 ± 0.35	23.88 ± 0.42	CaO
Na <sub>2</sub> O	2.24 ± 0.63	8.16 ± 0.28	8.37 ± 0.4	7.61 ± 0.13	9.65 ± 0.24	10.32 ± 0.3	10.32 ± 0.13	1.82 ± 0.3	0.01 ± 0.01	0.05 ± 0.02	0.04 ± 0.01	Na <sub>2</sub> O
K <sub>2</sub> O	0.03 ± 0.01	0.01 ± 0.01	0.00 ± 0.01	0.00	0.32 ± 0.01	0.10 ± 0.01	10.61 ± 0.10	8.53 ± 0.13	0.00 ± 0.01	0.00 ± 0.01	0.00 ± 0.01	K <sub>2</sub> O
Total	99.08	100.40	100.24	0.49	100.10	100.35	94.60	94.44	100.64	100.30	97.20	Total
Si	1.82	1.96	1.96	1.96	2.85	2.88	3.23	3.19	2.99	2.99	3.00	Si
Al	0.44	0.61	0.63	0.59	1.16	1.12	2.50	2.59	1.99	1.99	2.97	Al
Mg	0.66	0.33	0.31	0.36			0.24	0.18	1.47	0.86		Mg
Fe	0.11	0.13	0.13	0.12			0.09	0.08	0.93	1.44	0.07	Fe
Ca	0.80	0.41	0.39	0.44	0.14	0.12			0.62	0.68	1.96	Ca
Na	0.16	0.56	0.57	0.52	0.82	0.88	0.05	0.24				Na
K					0.02	0.01	0.91	0.73				K
End-members	Ca-Ts = 0.22	0.04	0.04	0.05	Ab = 0.83	0.88			Alm = 0.31	0.48		End-members
	Di = 0.61	0.28	0.27	0.31	An = 0.15	0.12			Grs = 0.20	0.22		
	Hd = 0.1	0.11	0.11	0.11	Kfs = 0.02	0.01			Prp = 0.48	0.28		
N	7	8	10	12	3	11	7	11	8	7	4	N

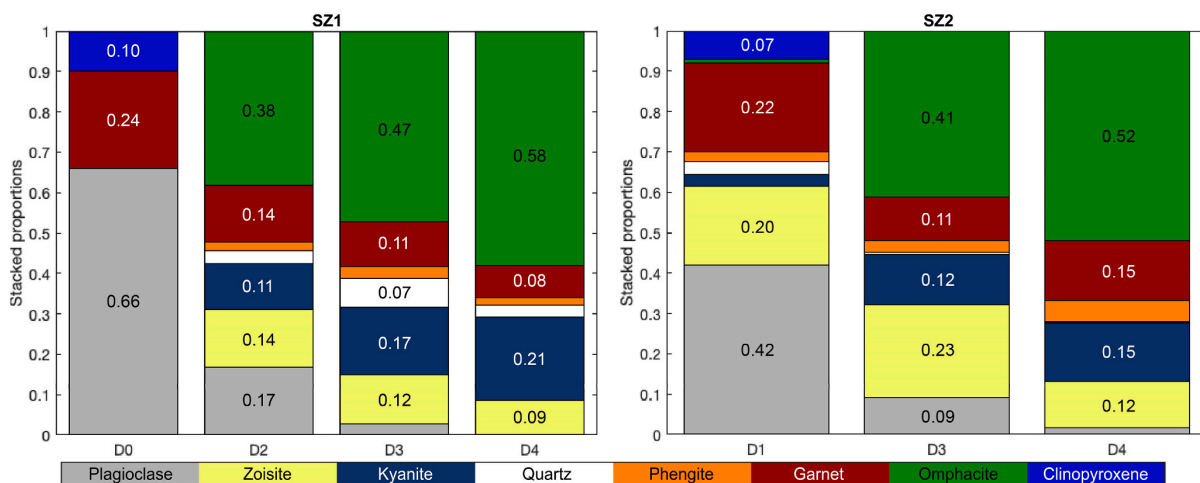
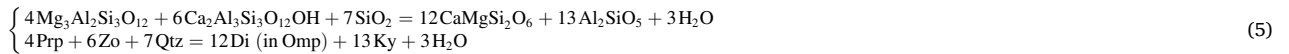


**Fig. 4.** Estimated volumetric proportions of peak minerals in SZ1 and SZ2. Minor phases and retrograde minerals are not included. Proportions below 5% are not labelled.

**From D3 to D4:** The proportion of omphacite and kyanite increases, at the expense of zoisite and quartz. Additionally the jadeite content of omphacite in the matrix decreases. This can be explained by the following reaction taking place in the matrix:

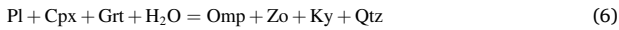


The change in solid volume associated with this reaction is  $-4\%$ , and the change in total volume is  $-1\%$ . Compared to the earliest reactions in the sequence, reaction (5) causes the smallest decrease in volume.

## 5.2. Shear zones evolution and rheological implications

As Holsnøy shear zones widen over time (e.g. Jolivet et al., 2005; Kaatz et al., 2021), the spatial evolution from D0 to D4 described by the sequence of reactions (1) to (5) can be interpreted as a proxy for the temporal evolution of the granulite, from unreacted to fully eclogitised. We use this interpretation as a working hypothesis in the following section. Using this hypothesis, a schematic diagram illustrating the spatial and temporal evolution of a metre-scale shear zone is presented in Fig. 5. The transformation of granulite into eclogite can be subdivided into two successive stages, occurring at the same eclogite facies conditions, that both have a prominent effect on the strength of the transforming rock:

(i) Destabilisation of the metastable granulite assemblage (D0) into a transient assemblage (D3), following reactions (1) to (4). They can synthetically be combined as:



During this first stage, the grain size decreases, weak phases (phenocryst, quartz) replace strong phases (plagioclase, garnet), fluid content increases and solid volume strongly decreases. These changes have a pronounced weakening effect on the rock (e.g. Poirier, 1982; Klaper, 1990; Jamtveit et al., 2019).

(ii) Destabilisation of the transient assemblage (D3) into eclogite (D4), following reaction (5). During this second stage, the grain size increases, the fluid content decreases and the solid rock volume shrinking is minor ( $-4\%$  to be compared to  $-14\%$  for reaction 1). These changes have an overall strengthening effect on the rock. This suggests

that fully-reacted eclogite in the core of the shear zone (D4) is stronger than the rock still undergoing reaction (6) on the edge of the shear zone.

The strength contrast within a shear zone can also be distinguished at the outcrop scale. This is best seen on Fig. 2b, where the eclogite facies foliation at the edge of the shear zone (D2-D3) is more pronounced than in the central part (D4). This suggests that instantaneous shear is higher at the edge than in the core, and therefore that the edge is weaker than the core. It is inferred that the completion of the reactions sequence hardened the core of the shear zones with growth of strong and coarser minerals, moving the deformation toward the peripheral, transiently transformed domains that contain weaker phases. The preservation of the granulite-facies coronas in the shear zone edges and their dismantling in the core of the shear zones also implies a decreasing strength contrast between the coronas and the matrix toward the shear zone cores.

These observations show that eclogitisation does not simply gradually weaken the rock from the granulite initial strength down to the eclogite end-product strength, but rather constitutes a two-stage evolution. First, the granulite (D0) transforms into a "reacting granulite" (D3), weaker than the granulite and the final eclogite, that localises the deformation. Second, the reacting granulite transforms into final eclogite (D4). This second stage partially restores the strength of the rock to reach the final steady-state strength of the eclogite. In order to test this hypothesis, we built a one-dimensional numerical model that aims at reproducing the geometry and petrology of the shear zones from Holsnøy. We also use this model to constrain the fluid diffusivity and the metamorphic reaction rate in the shear zone.

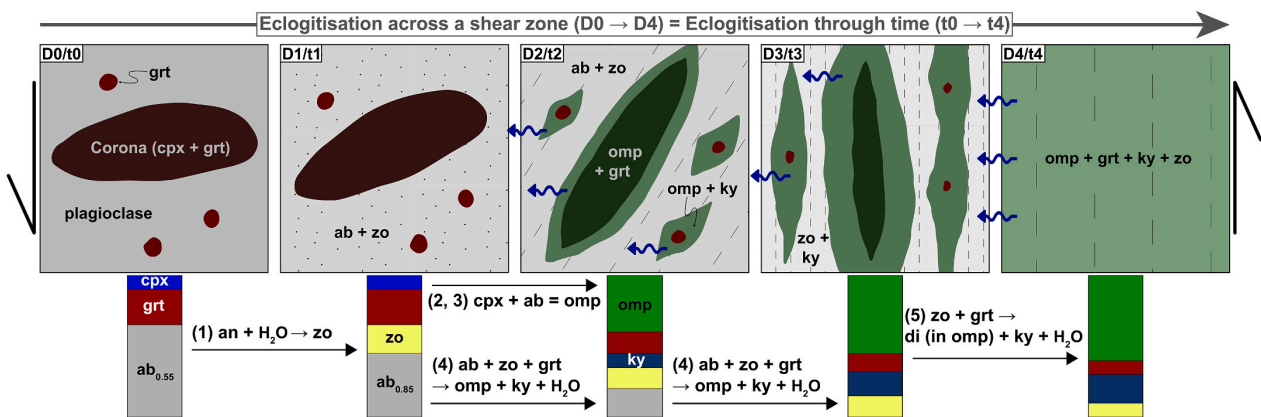


**Fig. 5.** Schematic diagram illustrating the spatial and temporal evolution of a metre-scale eclogite shear zone. From left to right, the sequence of diagrams shows both the spatial evolution of eclogitisation from the border to the core of a shear zone as observed in the field (D0 to D4), as well as the inferred temporal evolution of granulite from the start (t0) to the end of the eclogitisation (t4). Dots and dashes indicate the foliation, denser dashes indicating a well pronounced foliation. Blue arrows indicate fluid transport due to dehydration reactions and fluid transport from the centre of the shear zone. Stacked graphs illustrate the changes in mineral abundance due to the metamorphic reactions. The reactions are those described in section 5.1, simplified to only show major minerals. Mineral proportions are qualitative. (For interpretation of the references to colour in this figure legend, the reader is referred to the web version of this article.)

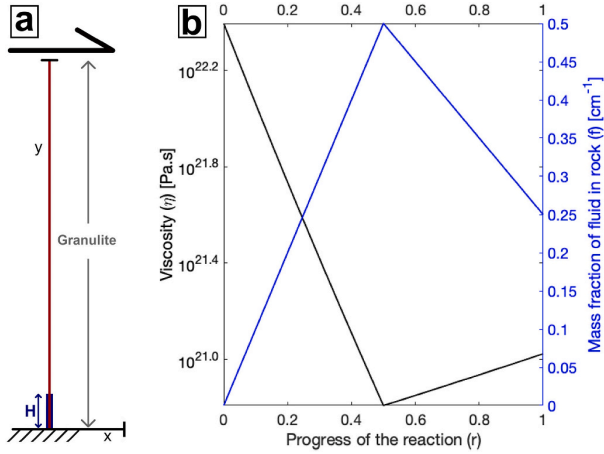


**Fig. 6.** Numerical model setup. (a) Initial state of the model. A finite amount of fluid is injected in a narrow band of width  $H = 5$  cm, which mimics the initial pulse of fluid through a fracture. Simple shear deformation is applied at the top boundary. (b) Changes in viscosity and constitutive fluid content in rock as the reaction progresses from unreacted granulite ( $r = 0$ ) to eclogite ( $r = 1$ ). The evolution of viscosity follows the MPG model of Huet et al. (2014), and the evolution of fluid content follows eq. (6).

## 6. One dimension numerical model of an eclogite shear zone

### 6.1. Model description and equations

The time evolution of a hydrous reacting shear zone was modelled in one dimension (1D) using MATLAB. As boundary conditions and geometry are symmetric, only the half-width of a shear zone, from core to

edge, was modelled.

The initial setup is summarised in Fig. 6a. Initially the entire 1D space consists of metastable granulite, which does not transform into eclogite because of the lack of fluid. At the onset of deformation, simple shear is applied on the model by imposing a horizontal velocity at the top. Simultaneously, a finite amount of fluid is injected at the lower boundary, simulating a pulse of fluid through a fracture.

Fluid propagation in the granulite is modelled with a diffusion equation, as in Kaatz et al. (2021). As the fluid propagates outwards, the eclogitisation reaction starts in the granulite. The evolution of the rock strength reproduces the two-stages rheological evolution deduced from our petrological observations (Fig. 6b). First, the granulite transforms into a reacting granulite which is weaker than the initial granulite. Second, the reacting granulite transforms into eclogite, which is stronger than the reacting granulite.

The fluid is not only a catalyst for the metamorphic reaction, but also a reactant and product of the metamorphic reactions occurring in a shear zone (see reactions in section 5.1, and Fig. 5). Therefore, as the reaction progresses, the rock consumes or releases free fluid available for diffusion in the shear zone (Fig. 6b). The final state of one simulation is shown on Fig. 7.

For simplification, only viscous deformation is accounted for in this model, and volume changes associated with the reactions are not considered. The equations are discretised over the 1D space using finite differences. The values of the parameters are described in section 6.2 and Table 3.

The propagation of free fluid  $F$  is modelled with a diffusion equation:

$$\frac{\partial F}{\partial t} = D \frac{\partial^2 F}{\partial y^2}, \quad (7)$$

where  $D$  is the constant of fluid diffusivity,  $t$  is the time and  $y$  is the 1D spatial coordinate.

As fluid acts as a catalyst, the eclogitisation reaction is modelled with

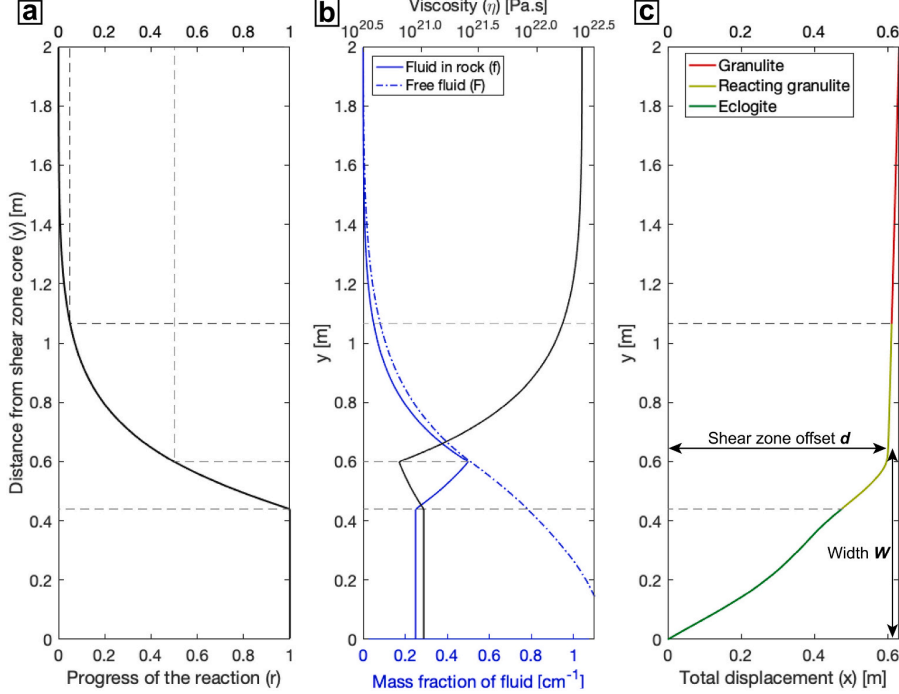


**Fig. 7.** Final state of a modelled shear zone after  $t = 0.5$  Ma, using  $D/\dot{\varepsilon} = 1$ ,  $\alpha_r/\dot{\varepsilon} = 10$ , and other parameters as in Table 3. (a) Progress of the metamorphic reaction along the vertical profile. (b) Fluid content and viscosity. (c) Geometry and petrology of the shear zone. Granulite is defined by  $r < 0.05$ , reacting granulite by  $0.05 \leq r < 1$ , and eclogite by  $r = 1$ .

**Table 3**

Parameters used in the numerical model.

Parameter	Symbol	Unit	Value		
Duration	$t$	Ma	0.5		
Background strain rate	$\dot{\epsilon}$	$s^{-1}$	$10^{-14}$		
Temperature	$T$	°C	700		
Initial fluid pulse	$F_0$	—	50		
Reaction threshold	$r_t$	—	0.5		
Rheological parameters:	Symbol	Unit	Granulite	Reacting granulite	Eclogite
Pre-exponential factor	$A$	$\text{Pa}^{-n} \cdot s^{-1}$	$5.01 \times 10^{-1}$	$6.31 \times 10^{-36}$	$7.94 \times 10^{-18}$
Exponent	$n$	—	3	4	3.4
Activation energy	$Q$	$\text{kJ.mol}^{-1}$	648	135	480
Viscosity at $\dot{\epsilon} = 10^{-14}$	$\eta$	$\text{Pa.s}$	$2.47 \times 10^{22}$	$6.46 \times 10^{20}$	$1.06 \times 10^{21}$
Concentration of fluid in rock	$f$	$\text{cm}^{-1}$	0	0.5	0.25

a linear law involving the constant of reaction rate  $\alpha_r$  and the amount of free fluid  $F$ :

$$\begin{cases} \frac{\partial r}{\partial t} = \alpha_r \times F & \text{if } F < 1, \\ \frac{\partial r}{\partial t} = \alpha_r & \text{if } F > 1, \end{cases} \quad (8)$$

where  $r$  is the progress of the granulite to eclogite reaction:  $r = 0$  corresponds to unaltered granulite, and  $r = 1$  to fully reacted eclogite. When  $F < 1$ , the amount of fluid controls the rate of eclogitisation. When  $F > 1$ , fluid saturation is reached, i.e. adding more fluid does not increase the reaction rate.

As the reaction progresses, the reacting rock consumes or releases free fluid (Fig. 6b). The exchange of fluid is modelled with a 2-steps linear law:

$$\begin{cases} \frac{\partial F}{\partial r} = \frac{f_e - f_g}{r_t} & \text{if } r < r_t, \\ \frac{\partial F}{\partial r} = \frac{f_e - f_r}{r_t} & \text{if } r > r_t, \end{cases} \quad (9)$$

where  $f_g$ ,  $f_r$  and  $f_e$  are the amounts of constitutive fluid in the granulite, reacting granulite and eclogite, respectively.  $r_t$  is the threshold at which the reaction switches from a weakening behaviour to a strengthening behaviour.  $r < r_t$  corresponds to the weakening stage of the reaction, and  $r > r_t$  to the strengthening stage. The solutions of equations involving fluid (eqs. 7, 8 and 9) are solved through convergence of Picard iterations.

The rheology of end-member lithologies (eq. 10) is computed using a viscous rheological model following the dislocation creep eq. (11):

$$\sigma = 2\eta\dot{\epsilon}, \quad (10)$$

$$\eta = \frac{\dot{\epsilon}^{(1-n)/n}}{2 \left[ A \times \exp \left( \frac{-Q}{RT} \right) \right]^{1/n}}, \quad (11)$$

where  $\sigma$  is the stress,  $\dot{\epsilon}$  the strain rate,  $A$  the pre-exponential factor,  $n$  the stress exponent,  $Q$  the activation energy,  $T$  the temperature, and  $R$  the universal gas constant.  $A$ ,  $n$  and  $Q$  are dislocation creep constants of a given end-member lithology (granulite, reacting granulite or eclogite).

The strength of the reacting rock is calculated from the strength of end-member lithologies using the minimised power geometric (MPG) model of Huet et al. (2014) (Fig. 6b). Calculations of intermediate strengths using the Reuss lower bound (weighted harmonic mean of the end-member viscosities, Reuss, 1929) or the Voigt upper bound (weighted arithmetic mean, Voigt, 1928) do not yield widely different results and lead to the same conclusions than the MPG model (see supplementary material D).

The Stokes equation, simplified for 1D simple shear with no inertial forces, is solved to calculate the velocity in the  $x$  direction  $V_x$ :

$$\frac{\partial}{\partial y} \left( \eta \times \frac{\partial V_x}{\partial y} \right) = 0. \quad (12)$$

As the viscosity is nonlinear ( $n \neq 1$  in eq. 11), eq. 12 is solved through convergence of Picard iterations.

## 6.2. Model parameters

This section details how the parameters used in the model are determined. Their values are summarised in Table 3.

**Background strain rate** ( $\dot{\epsilon}$ ). We use a strain rate of  $\dot{\epsilon} = 10^{-14} \text{ s}^{-1}$ , consistent with the estimate of  $\dot{\epsilon} = 10^{-14 \pm 1} \text{ s}^{-1}$  by Fagereng and Biggs (2019) for crustal strain rate.

**Duration of the model** ( $t$ ). The half-width (from core to border) of both SZ1 and SZ2 is about 0.6 m. It was impossible to measure the offset of the shear zones on the field, however Boundy et al. (1992) and Kaatz et al. (2021) reported that the offset of minor shear zones (< 1 m wide) is approximately equal to their width. The offset of SZ1 and SZ2 is therefore considered to be around 0.6 m.

In this model, the shear zone offset  $d$  depends only on the strain rate and on the model duration:

$$d = 2\dot{\epsilon}Lt, \quad (13)$$

where  $L$  is the length of the model. Using  $L = 2 \text{ m}$ , an offset of 0.6 m and a strain rate of  $10^{-14} \text{ s}^{-1}$ , this yields  $t \approx 0.5 \text{ Ma}$ .

**Fluid concentration in rock** ( $f_g$ ,  $f_r$ ,  $f_e$ ). Using the proportions of hydrated phases (zoisite, phengite) given in Fig. 4, we calculated that the mass fraction of fluid is around  $f_g = 0 \text{ wt\%}$  in the granulite,  $f_r = 0.5 \text{ wt\%}$  in the reacting granulite and  $f_e = 0.25 \text{ wt\%}$  in the eclogite. As the mass fraction is dimensionless and the model is one-dimensional, the unit of fluid concentration is  $\text{cm}^{-1}$ .

**Amount of fluid in initial pulse** ( $F_0$ ). This parameter is poorly constrained. However, the total amount of fluid must be somewhat limited, otherwise it would propagate after the deformation is achieved. For this reason we set the initial amount of fluid to be equal to the maximum theoretical amount of fluid contained in the rock:  $F_0 = f_r \times L = 0.5 \times 200 = 100$ . This amount is dimensionless.

**Temperature** ( $T$ ). We used a constant temperature of  $T = 700 \text{ }^{\circ}\text{C}$ , close to that determined by Bhowany et al. (2018) for the peak eclogite facies metamorphism in Holsnøy (670–690 °C).

**End-member rheology** ( $n$ ,  $A$ ,  $Q$ ,  $\eta$ ). We used experimentally determined rheologies to model the rheology of granulite, reacting granulite and eclogite. We used the creep parameters of dry anorthite determined by Rybacki and Dresen (2000) to model the rheology of granulite, and creep parameters of omphacite determined by Zhang et al. (2006) to model the rheology of eclogite. Our previous observations suggest that the reacting granulite is the weakest phase. For this reason it was modelled by quartz, which is weaker than both anorthite and omphacite. We used the creep parameters of quartz determined by Hirth et al.

(2001). At  $T = 700$  °C and  $\dot{\varepsilon} = 10^{-14}$  s<sup>-1</sup>, the strength ratios are  $\eta_t/\eta_g \approx 1/38$  and  $\eta_e/\eta_g \approx 1/23$ , which compares to previous estimates for the same contexts (Labrousse et al., 2010).

**Reaction threshold ( $r_t$ ).** Tests performed using different  $r_t$  values show that model results are not widely different if  $r_t$  varies from 0.1 to 0.9 (see supplementary material E). As the kinetics of reaction is poorly constrained we chose a median value of  $r_t = 0.5$ .

### 6.3. Role of diffusivity and reaction rate

In a first parametric study we determine realistic values of fluid diffusivity  $D$  and metamorphic reaction rate  $\alpha_r$ , using the end-member rheologies chosen in section 6.2. In order to assess the validity of a model, we compare the petrology and geometry of the modelled shear zones to those observed on the field. Key constraints are:

1. the half width of the shear zone,  $W \approx 0.6$  m on the field (Fig. 2). As the width of a single shear zone can significantly vary on the field, we consider that the width of a modelled shear zone must be  $W = 0.6 \pm 0.4$ .
2. the petrology of the shear zone. The core of the shear zone is eclogite (D4) while the edge is reacting granulite (D2-D3). We implement this constraint in the model by monitoring the width of the eclogite core ( $W_e$ ), relative to the width of the entire shear zone ( $W$ ). As both the eclogite and the reacting granulite must coexist in the shear zone, we consider that  $W_e/W$  must be between 0.1 (10% of the shear zone is fully reacted eclogite) and 0.9.
3. the petrology outside the shear zone. On the field, D1 is within 0.5 m of the edge of the shear zone and has already started the metamorphic reaction, therefore the host-rock within a few tens of centimetres of the modelled shear zone must be reacting granulite.

On the figures, granulite is defined by  $r < 0.05$ , reacting granulite by  $0.05 \leq r < 1$ , and eclogite by  $r = 1$ .

There is a trade-off between the duration,  $t$ , and values of  $D$ ,  $\alpha_r$  and  $\dot{\varepsilon}$ . For instance the model yields the same results if  $t$  is multiplied by 10, and  $D$ ,  $\alpha_r$  and  $\dot{\varepsilon}$  are all divided by 10. For this reason we can normalise  $D$  and  $\alpha_r$  to  $\dot{\varepsilon}$ . This allows us to study the role of diffusivity and reaction rate independently of  $\dot{\varepsilon}$ . In order to investigate the role of  $D$  and  $\alpha_r$ , we ran the model for a range of diffusivity values between  $10^{-3} \times \dot{\varepsilon}$  and  $10^3 \times \dot{\varepsilon}$ , and a range of reaction rate values between  $10^{-1} \times \dot{\varepsilon}$  and  $10^4 \times \dot{\varepsilon}$ . The results of this parametric study are shown in Fig. 8.

Different  $D - \alpha_r$  combinations produce shear zones with widely varying geometry and petrology. A slow diffusivity and a fast reaction rate produce a shear zone where all the fluid remains in a narrow zone

which reacts quickly. The final shear zone is very narrow, and has fully reacted (Fig. 8, model 1). A fast diffusivity and a slow reaction rate produce a zone that widens rapidly and consumes all the fluid in the reacting granulite, such that there is no more fluid left to catalyse the reaction. The shear zone is therefore wide but its core has not transformed into eclogite (Fig. 8, model 3). A very slow reaction rate and/or a very fast diffusivity do not result in the formation of a shear zone because the granulite is not weakened enough to localise deformation (Fig. 8, model 4). Only a small range of  $D$  and  $\alpha_r$  values ( $D/\dot{\varepsilon} = 10^{-2} - 10^1$ ,  $\alpha_r/\dot{\varepsilon} = 10^1 - 10^2$ ) results in shear zone geometry and petrology similar to those observed in the field (Fig. 8, model 2): (1) the width is  $\approx 0.6$  m; (2) the shear zone consists of an eclogite core and a reacting edge; and (3) the granulite started to react within 50 cm of the edge of the shear zone.

### 6.4. Role of viscosity changes

The strength of the different end-member lithologies, and especially of reacting granulite, is not well constrained. For this reason we conducted a second parametric study in order to constrain the relative strengths of granulite, reacting granulite and eclogite. We used the parameters in Table 3 and realistic values of  $D$  and  $\alpha_r$  determined in section 6.3:  $D/\dot{\varepsilon} = 1$ ,  $\alpha_r/\dot{\varepsilon} = 10$ . We set the strength of granulite to  $\eta_g = 1$ , and tested a range of reacting granulite strength ( $\eta_t$ ) and of eclogite strength ( $\eta_e$ ), relative to that of granulite. The results of this parametric study are shown in Fig. 9.

For  $\eta_t > \eta_e$  ("transient strengthening", Fig. 9, model 5), the shear zone is entirely composed of eclogite. Reacting granulite is only present outside the shear zone, but not on the edge of the shear zone. This model does not reproduce the observed petrology, which shows that the transient rheology can not be stronger than the end-product eclogite.

For  $\eta_t < \eta_e$  (Transient weakening, Fig. 9, models 6 and 7), the geometry and petrology of the shear zones are realistic and similar to that of model 2 (Fig. 8). The models are realistic even if the final eclogite is stronger than granulite (model 7), as long as transient weakening occurs during the reaction.

Our numerical simulations reproduce realistic shear zones patterns only in a narrow parametric space:  $D/\dot{\varepsilon} = 10^{-2} - 10^1$ ,  $\alpha_r/\dot{\varepsilon} = 10^1 - 10^2$ ,  $\eta_t/\eta_g < 1$ ,  $\eta_e/\eta_g < 1$ . Out of this  $D - \alpha_r - \eta_t - \eta_e$  space, modelled shear zones are too localised or too diffuse, or their petrological pattern does not match that observed on the field.

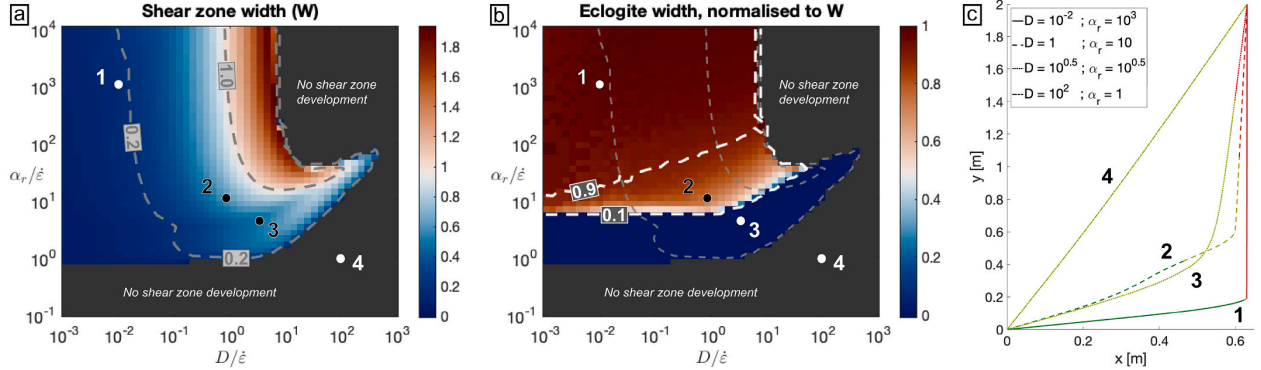


**Fig. 8.** Role of  $D$  and  $\alpha_r$  on (a) the width of the shear zone and (b) the width of the eclogite shear zone core, normalised to the shear zone width. 0.1 means 10% of the width of the shear zone fully reacted to eclogite, i.e. reached  $r = 1$ . Contour lines delimit realistic models, with shear zone width between 0.2 and 1 m and normalised eclogite width between 0.1 and 0.9. (c) Shear zone profile of 4 models localised on (a) and (b).

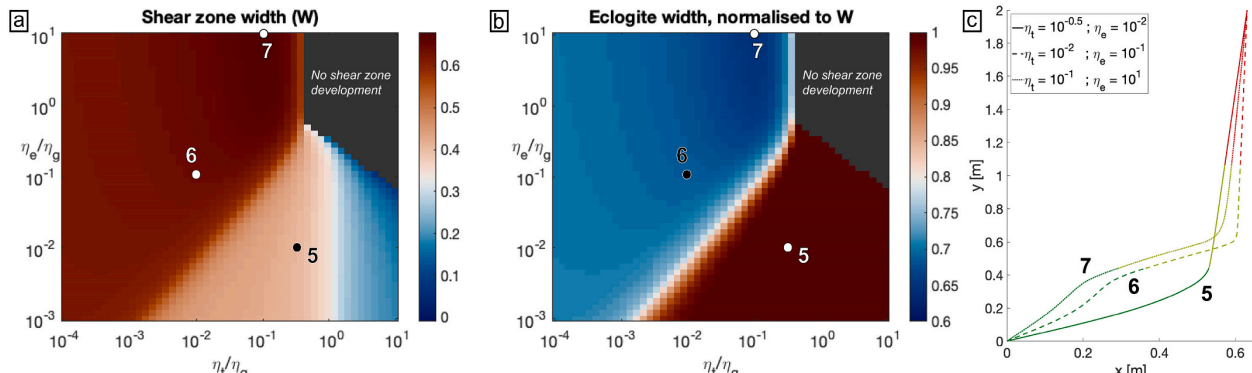


**Fig. 9.** Role of reacting granulite and eclogite strength, relative to granulite strength, on (a) the width of the shear zone and (b) the width of the fully transformed shear zone core, normalised to the shear zone width. In (a), the red domain ( $W \approx 0.65$  m) corresponds to a domain where transient weakening occurs:  $\eta_t < \eta_g$  and  $\eta_t < \eta_e$ . The orange domain ( $W \approx 0.40$  m) corresponds to a domain of gradual weakening:  $\eta_g > \eta_t > \eta_e$ . The blue domain ( $W \approx 0.20$  m) corresponds to a domain of "transient strengthening":  $\eta_t > \eta_g$  and  $\eta_t > \eta_e$ . (For interpretation of the references to colour in this figure legend, the reader is referred to the web version of this article.)

## 7. Discussion

### 7.1. Chemical equilibrium

An important field observation is that the granulite is chemically heterogeneous at the cm-, and even dm-scale, as inferred from the coronas/matrix texture. We have shown that this heterogeneity is well preserved in the shear zone and only disappears in the core of the shear zone (D4), where the metamorphic reactions sequence (1) to (5) is complete. Similarly, there is a compositional heterogeneity of omphacite in the shear zone that only disappears in the core (Tables 1 and 2). In particular, in D2 and D3 the omphacites of the coronas and the omphacites of the matrix have a different composition. For example in D2,  $X_{jd} = 0.42$  in the coronas and  $X_{jd} = 0.54$  in the matrix (Table 1). In D4 the composition of omphacite is the same in the coronas and in matrix. These changes in omphacite composition can be caused by changes in the equilibrium bulk composition, but we showed that minor shear zones in Holsnøy are essentially isochemical. It is therefore likely that the composition of omphacite is controlled by local chemical equilibrium in distinct petrological domains of varying scale, at constant eclogite facies  $P$ - $T$  conditions. In D2 and D3, the omphacites are in equilibrium with different local chemical compositions (matrix vs corona). Likewise, the transient eclogite assemblage in D1-D3 is a result of a local chemical equilibrium. Metamorphic reactions, deformation and fluid assisted chemical diffusion progressively equilibrated the reacting rock at larger scale, until the eclogite became texturally and chemically homogeneous in the core of the shear zone. If the transformation of granulite into eclogite happened instantaneously, with a large scale (over tens of centimetres) equilibrium composition, then the entire shear zone would always be composed of "true" eclogite as observed in the core: Omp + Ky + Grt + Zo + Ph + Qtz. However, because of spatial disequilibrium and reactions kinetics, the margin of the shear zones, which started reacting the latest, consist of a transient transforming assemblage. Observations of such equilibration in shear zones were also made by Koons et al. (1987) in the Sesia zone (Alps), by Mørk (1985) in Flemsøy (Western Norway), or by Goncalves et al. (2012) in the Aar massif (Alps).

### 7.2. Causes of transient weakening

In this work we showed that transient weakening must have occurred in the Holsnøy shear zones, but the mechanisms causing the change in rheology are poorly understood. Dislocation creep probably dominates the deformation mechanisms in omphacite (Boudy et al., 1992; Godard

and van Roermund, 1995; Bascou et al., 2001, 2002) and kyanite (Beane and Field, 2007); however transient mechanisms activated during a metamorphic reaction can enhance deformation of the transforming rock (Brodie and Rutter, 1985; Rubie, 1990; Rutter and Brodie, 1995). We therefore propose the following interpretation for the evolution of rheology during the eclogitisation of granulite:

(1) During the first stage of eclogitisation (D0 to D3, i.e. reactions 1 to 4), most of the original coarse ( $>1$  mm in diameter) granulite facies minerals (plagioclase, pyroxene) are replaced by small eclogite facies minerals (omphacite, zoisite, kyanite), as illustrated on Figs. 4 and 5. The intense mineral replacement, grain size reduction and volume reduction are inferred to activate transient deformation mechanisms that weaken the transforming rock: diffusion creep during dissolution of granulite minerals and precipitation of eclogite minerals (e.g. Stünitz and Tullis, 2001; Marti et al., 2018; Stünitz et al., 2020), grain boundary migration in dynamically recrystallised small plagioclase grains (Klapfer, 1990), transformation plasticity during volume reduction (Poirier, 1982). The volume reduction also yields an increased porosity which can weaken the solid framework and change the fluid pressure field, promote fluid influx and further promote the reaction (Kaatz et al., 2021). The fine-grained matrix forms interconnected weak layers that accommodate most of the strain (Klapfer, 1990; Handy, 1990, 1994).

(2) Contrary to the first stage, the second stage of eclogitisation is not marked by intense mineral replacement but rather by a textural and chemical equilibration induced by reaction (5) (compare D3 and D4 panels on Fig. 5). We therefore expect the weakening induced by the previous transient processes to be limited during this reaction stage. On the contrary, the textural and chemical equilibration increases the grain size and obliterates the interconnected weak layers structure, which hardens the reacted eclogite.

It is out of the scope of this study to determine the deformation mechanisms at work in the shear zones, and for this reason the rheology of the rocks is only modelled by dislocation creep in our numerical model. Taking into account transient deformation mechanisms as described above, such as diffusion creep during the metamorphic reaction (e.g. Stünitz et al., 2020), would amplify the importance of transient weakening on the evolution of the shear zones.

In the shear zones studied in this work, only the core of the shear zone, which started the reaction the earliest and underwent more strain and fluid infiltration, could complete the hardening stage of eclogitisation. The edge, which started the reaction later, only underwent the weakening stage of eclogitisation.

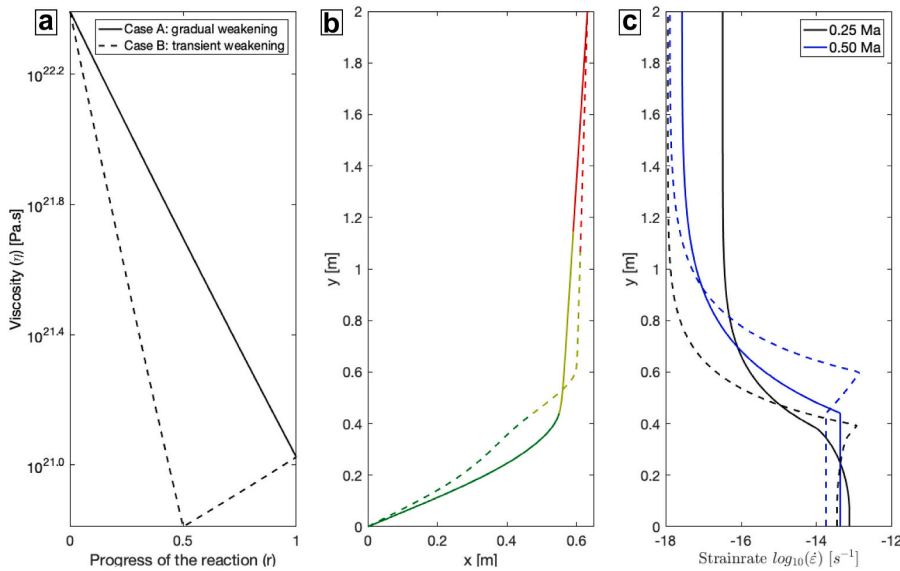


**Fig. 10.** Role of transient weakening on shear zone width. Both cases use the parameters and rheology described in Table 3. (a): changes in viscosity as the reaction progresses from granulite ( $r = 0$ ) to eclogite ( $r = 1$ ). Starting granulite strength and ending eclogite strength are the same in both cases. (b): shear zone geometry. In case A the shear zone is 44 cm wide, and in case B, 62 cm wide. (c): strain rate in the shear zone at two different time steps (middle and end of the simulation) for cases A and B. Without transient weakening the strain rate is localised in the core of the shear zone, whereas it is localised on the edge of the shear zone in the case of transient weakening.

### 7.3. End-members rheologies

The numerical models show that the transient weakening of the granulite undergoing the metamorphic reaction is necessary to explain the geometry and petrology of the shear zones observed in the field. However our model does not constrain the relative strengths of granulite and eclogite: as long as the transforming rock goes through a weak transient stage, the model yields realistic results, regardless of the rheology of the protolith and of the final transformed assemblage.

### 7.4. Role of eclogite hardening on shear zones widening

The acknowledged interpretation of the evolution of Holsnøy shear zones is that only fluid infiltration is responsible for shear zone widening (e.g. Austrheim, 1987; Kaatz et al., 2021). Fig. 10 shows a comparison between this classical scenario (case A) and transient weakening associated with a fluid infiltration scenario (case B). Both cases use the same parameters, although the evolution of rock strength is different (Fig. 10a). In case A the rock strength gradually decreases from granulite strength at  $r = 0$  to eclogite strength at  $r = 1$ . In case B the strength evolution follows the two stages described in the previous models. In case A the shear zone is 44 cm wide while in case B it is 62 cm wide. This substantial width increase (+18 cm, i.e. +40%) is due to the hardening stage: progression of the reaction in the core pushes strain localisation outwards from the shear zone (Fig. 10c) and hence promotes shear zone widening. The strain partition in the shear zone is similar to that of paired shear zones (Mancktelow and Pennacchioni, 2005), with a hardened central part and the margins undergoing most of the strain. However, our model shows that since the shear zones are continuously expanding and transforming due to fluid infiltration, they do not evolve into paired shear zones but rather into shear zones with a sigmoid-shape foliation, as observed on the field. No change in reaction kinetics induced by strain or strain rate has been accounted for in our model, but such feedback mechanisms would amplify the process presented here (e.g. Snow and Yund, 1987; Yund and Tullis, 1991). Therefore, although shear zone widening is mostly controlled by fluid diffusion that weakens the rock, the hardening of the eclogite at the end of the metamorphic reaction also plays an important role in the widening of the shear zone.

### 7.5. Fluid supply in the shear zones

The fluid supply can be modelled by a continuous influx or an instantaneous pulse of fluid (Kaatz et al., 2021). In Holsnøy, fluid infiltration was induced by earthquakes in brittle granulite. This argues in favour of infiltration by instantaneous fluid pulses following earthquakes (as in Malvoisin et al., 2020) and for this reason we used this hypothesis in the model.

For the sake of completeness, we tested a scenario where the fluid continuously infiltrates the granulite, as in the model of Kaatz et al. (2021). Assuming that the total amount of fluid injected into the shear zone is the same in both scenarios, we used a continuous influx of fluid of  $Q = F_0/t = 6.4 \times 10^{-12} \text{ s}^{-1}$ . The results of this model (shown in supplementary material F) show similar results to our scenario that uses pulsed fluid. The only difference is that the continuous influx model allows for lower fluid diffusivity, in agreement with the value determined by Kaatz et al. (2021). Therefore, although the regime of fluid infiltration in Holsnøy is poorly understood, it has little implications on the conclusions presented here.

### 7.6. Fluid diffusivity and reaction rate

Constraining the parametric study with field observations, we found  $D/\dot{\epsilon} = 10^{-2} - 10^1$  and  $\alpha_r/\dot{\epsilon} = 10^1 - 10^2$  as realistic diffusivity and reaction rate values, respectively (Fig. 8). With a strain rate of  $\dot{\epsilon} = 10^{-14} \text{ s}^{-1}$  used in the model, this yields  $D = 10^{-16} - 10^{-13} \text{ m}^2 \cdot \text{s}^{-1}$ , and  $\alpha_r = 10^{-13} - 10^{-12} \text{ s}^{-1}$ . Another commonly used value of strain rate in Holsnøy is  $\dot{\epsilon} = 10^{-13} \text{ s}^{-1}$  (Labrousse et al., 2010; Kaatz et al., 2021). Using this value yields  $D = 10^{-15} - 10^{-12} \text{ m}^2 \cdot \text{s}^{-1}$ , and  $\alpha_r = 10^{-12} - 10^{-11} \text{ s}^{-1}$ . We therefore consider that reasonable values for Holsnøy shear zones are  $D = 10^{-14 \pm 2} \text{ m}^2 \cdot \text{s}^{-1}$  and  $\alpha_r = 10^{-12 \pm 1} \text{ s}^{-1}$ .

Our reaction rate is higher than those compiled by Baxter (2003) in natural rocks undergoing regional metamorphism ( $6 \times 10^{-16} - 6 \times 10^{-14} \text{ s}^{-1}$ ). It is close to the upper bound of reaction rate determined by Cruz-Uribe et al. (2014) in mafic rocks, using Nb diffusion in rutile and titanite ( $4 \times 10^{-16} - 2 \times 10^{-13} \text{ s}^{-1}$ ). The difference in reaction rate magnitudes is likely due to the disequilibrium condition of granulite: as granulite is metastable at eclogite facies  $P$ - $T$  conditions, any source of energy brought to the system, like a fluid pulse, can instantaneously lead to a fast reaction (Rubie, 1998).

Diffusion coefficients of hydrogen can be used to estimate the diffusivity of water, as in Malvoisin et al. (2020). Diffusivity of hydrogen in granulite and eclogite minerals (clinopyroxene, garnet, feldspar, zoisite) at 650–700 °C is between  $10^{-15}$  and  $10^{-11} \text{ m}^2 \cdot \text{s}^{-1}$  (Ingrin and Blanchard, 2006; Farver, 2010). The value we deduced from our numerical model is close to these experimentally determined values and shows that modelling the fluid flow by a diffusion process is reasonable. With a numerical model of Holsnøy eclogite shear zones, Kaatz et al. (2021) determined a value of  $D = 10^{-16 \pm 1}$ , which is in agreement with our work.

### 7.7. Model limitations

In reality, the fluid flow is likely to be controlled by fluid pressure and porosity, following Darcy's law (e.g. Connolly and Podladchikov, 1998). The fluid pressure varies when metamorphic reactions consume or release free fluid. The transformation of granulite into eclogite also induces a significant increase in rock density (Austrheim, 1987; Centrella, 2019, this work), which decreases the rock volume, thus increasing the porosity and enhancing the fluid flow. These couplings between metamorphic reactions, fluid flow and pressure variations are complex, and only few numerical models allow an in-depth study of these processes (Malvoisin et al., 2015; Omlin et al., 2017; Schmalholz et al., 2020). Implementing all these couplings in our 1D model is out of the scope of this work. However, our model accurately replicates field and petrological observations, with parameters in good agreement with those found in the literature. Therefore, even if our 1D numerical model cannot be used as a perfectly quantitative tool, we argue that it provides a sensible insight of the processes at work in the shear zones. A more complex model, with an approach similar to that of Malvoisin et al. (2015) and Schmalholz et al. (2020), would allow to refine the findings of our study.

## 8. Conclusion

In Holsnøy, field observations suggest that the instantaneous shear is higher on the edge of the eclogite shear zones than in the core. This is consistent with the rheological evolution across a shear zone: away from the shear zone, the granulite is dry and is composed of millimetre-sized grains of strong phases (plagioclase, garnet). In the edge of the shear zone, the foliation is marked by interconnected weak layers of denser and smaller grains, and strong layer inherited from the granulite coronas. In the core of the shear zone, the weak phases are less abundant, the foliation is less pronounced and the grains are larger than in the edge of the shear zone. This suggest that the edge of a shear zone is mechanically weaker than its core. As the shear zones widen over time, this spatial evolution is interpreted as a temporal evolution from the unreacted granulite to the fully reacted eclogite. This suggests that transient weakening occurs in the shear zones of Holsnøy, during the granulite to eclogite metamorphic reaction. The weakening is likely to be caused by a combination of grain size reduction and volume decrease. Textural heterogeneities inherited from the protolith are still present in the transforming rock. Textural and chemical equilibration at the cm- and dm-scale is only reached at the end of the reaction, and triggers the hardening of the eclogite.

Pairing petrological and field investigations with numerical modelling confirms the occurrence of transient weakening. We showed that the widening of the shear zones is not only caused by fluid infiltration, but also by shear zone hardening. We highlight the importance of both the reaction rate and the diffusivity on the evolution of eclogite shear zones.

## Declaration of Competing Interest

The authors have no conflict of interest to declare.

## Acknowledgements

This work has been financially supported by the INSU SYSTER program (AO Tellus). P.Y. thanks the Institut Universitaire de France for financial support. The authors thank Håkon Austrheim and Torgeir Andersen for their help on the field and for insightful discussions, Thibault Duretz for his help with numerical modelling, and Omar Bouddouma and Nicolas Rividi for their assistance on SEM and EPMA analyses. We thank Tim Johnson and an anonymous reviewer for very helpful comments that have improved and clarified the paper. The MATLAB numerical code is available on request to E.B.

## Appendix A. Supplementary data

Supplementary data to this article can be found online at <https://doi.org/10.1016/j.tecto.2021.229026>.

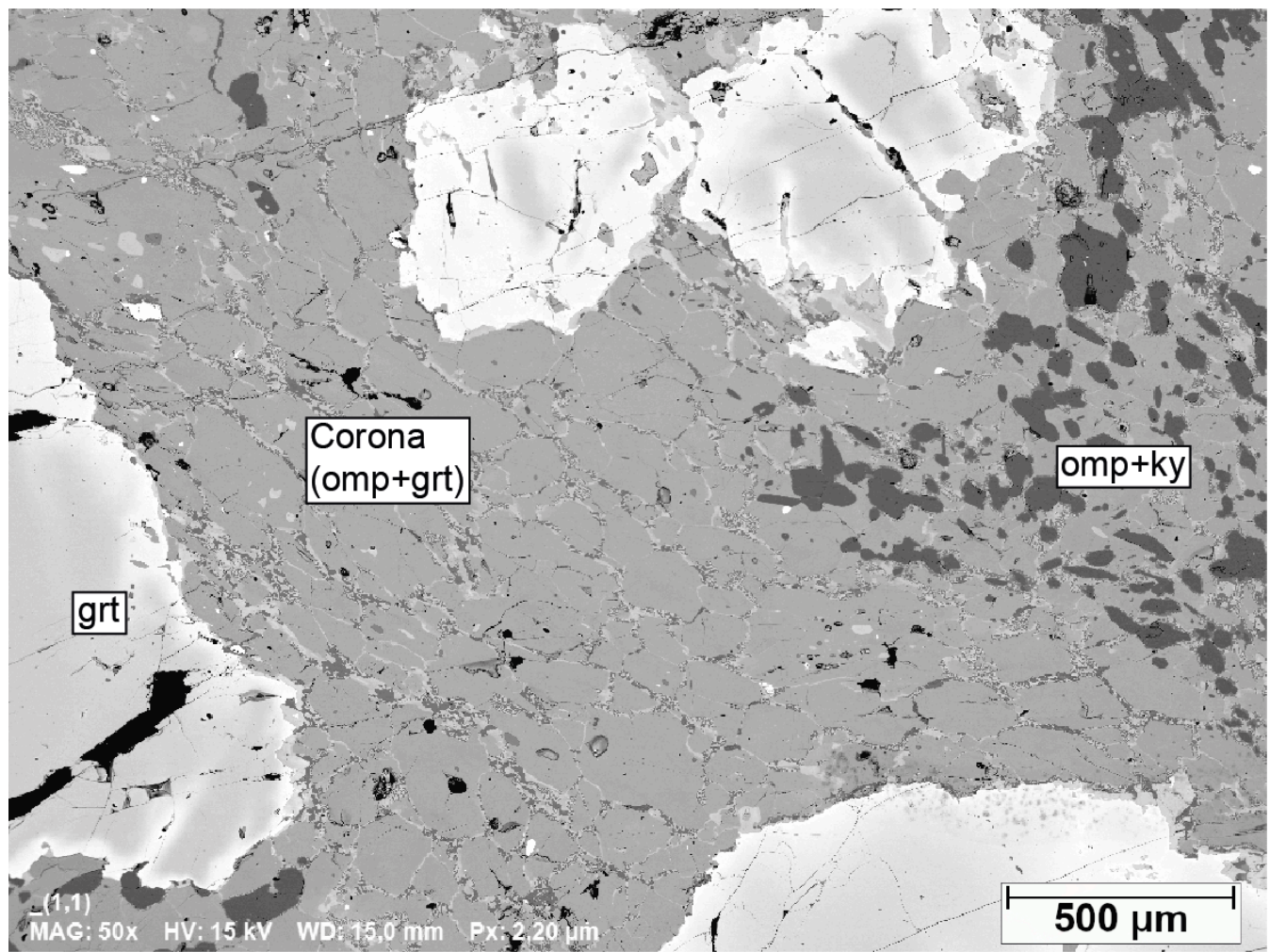
## References

- Abers, G.A., Hacker, B.R., 2016. A matlab toolbox and excel workbook for calculating the densities, seismic wave speeds, and major element composition of minerals and rocks at pressure and temperature. *Geochim. Geophys. Geosyst.* 17, 616–624. <https://doi.org/10.1002/2015GC006171>.
- Andersen, T.B., Jamtveit, B., Dewey, J.F., Swensson, E., 1991. Subduction and eduction of continental crust: Major mechanisms during continent-continent collision and orogenic extensional collapse, a model based on the south norwegian caledonides. *Terra Nova* 3, 303–310. <https://doi.org/10.1111/j.1365-3121.1991.tb00148.x>.
- Austrheim, H., 1987. Eclogitization of lower crustal granulites by fluid migration through shear zones. *Earth Planet. Sci. Lett.* 81, 221–232. [https://doi.org/10.1016/0012-821X\(87\)90158-0](https://doi.org/10.1016/0012-821X(87)90158-0).
- Austrheim, H., 1990. The granulite-eclogite facies transition: a comparison of experimental work and a natural occurrence in the Bergen arcs, western Norway. *Lithos* 25, 163–169. [https://doi.org/10.1016/0024-4937\(90\)90012-P](https://doi.org/10.1016/0024-4937(90)90012-P).
- Austrheim, H., 1991. Eclogite formation and dynamics of crustal roots under continental collision zones. *Terra Nova* 3, 492–499. <https://doi.org/10.1111/j.1365-3121.1991.tb00184.x>.
- Austrheim, H., 1998. Influence of fluid and deformation on metamorphism of the deep crust and consequences for the geodynamics of collision zones. In: Hacker, B.R., Liou, J.G. (Eds.), *When Continents Collide: Geodynamics and Geochemistry of Ultrahigh-Pressure Rocks*. Springer Netherlands, Dordrecht, pp. 297–323. [https://doi.org/10.1007/978-94-015-9050-1\\_12](https://doi.org/10.1007/978-94-015-9050-1_12).
- Austrheim, H., 2013. Fluid and deformation induced metamorphic processes around moho beneath continent collision zones: examples from the exposed root zone of the caledonian mountain belt, w-Norway. *Tectonophysics* 609, 620–635. <https://doi.org/10.1016/j.tecto.2013.08.030>.
- Austrheim, H., Griffin, W.L., 1985. Shear deformation and eclogite formation within granulite-facies anorthosites of the Bergen arcs, western Norway. *Chem. Geol.* 50, 267–281. [https://doi.org/10.1016/0009-2541\(85\)90124-X](https://doi.org/10.1016/0009-2541(85)90124-X).
- Bascou, J., Barruel, G., Vauchez, A., Mainprice, D., Egydio-Silva, M., 2001. Ebsd-measured lattice-preferred orientations and seismic properties of eclogites. *Tectonophysics* 342, 61–80. [https://doi.org/10.1016/S0040-1951\(01\)00156-1](https://doi.org/10.1016/S0040-1951(01)00156-1).
- Bascou, J., Tommasi, A., Mainprice, D., 2002. Plastic deformation and development of clinopyroxene lattice preferred orientations in eclogites. *J. Struct. Geol.* 24, 1357–1368. [https://doi.org/10.1016/S0191-8141\(01\)00137-7](https://doi.org/10.1016/S0191-8141(01)00137-7).
- Baxter, E.F., 2003. Natural constraints on metamorphic reaction rates. *Geol. Soc. Lond., Spec. Publ.* 220, 183–202. <https://doi.org/10.1144/GSL.SP.2003.220.01.11>.
- Beane, R., Field, C., 2007. Kyanite deformation in whiteschist of the ultrahigh-pressure metamorphic kokchetav massif, Kazakhstan. *J. Metamorph. Geol.* 25, 117–128. <https://doi.org/10.1111/j.1525-1314.2007.00692.x>.
- Bhowany, K., Hand, M., Clark, C., Kelsey, D.E., Reddy, S.M., Pearce, M.A., Tucker, N.M., Morrissey, L.J., 2018. Phase equilibria modelling constraints on p-t conditions during fluid catalysed conversion of granulite to eclogite in the Bergen arcs, Norway. *J. Metamorph. Geol.* 36, 315–342. <https://doi.org/10.1111/jmg.12294>.
- Bingen, B., Davis, W.J., Austrheim, H., 2001. Zircon u-pb geochronology in the Bergen arc eclogites and their proterozoic protoliths, and implications for the pre-scandian evolution of the caledonites in western Norway. *Geol. Soc. Am. Bull.* 113, 640–649. [https://doi.org/10.1130/0016-7606\(2001\)113<0640:ZUPGT>2.0.CO;2](https://doi.org/10.1130/0016-7606(2001)113<0640:ZUPGT>2.0.CO;2).
- Bjørnerud, M.G., Austrheim, H., Lund, M.G., 2002. Processes leading to eclogitization (densification) of subducted and tectonically buried crust. *J. Geophys. Res. Solid Earth* 107. <https://doi.org/10.1029/2001JB000527>. ETG-14.
- Boundy, T.M., Fountain, D.M., Austrheim, H., 1992. Structural development and petrofabrics of eclogite facies shear zones, Bergen arcs, western Norway: implications for deep crustal deformational processes. *J. Metamorph. Geol.* 10, 127–146. <https://doi.org/10.1111/j.1525-1314.1992.tb00075.x>.
- Brodholt, J., Wood, B., 1993. Simulations of the structure and thermodynamic properties of water at high pressures and temperatures. *J. Geophys. Res. Solid Earth* 98, 519–536. <https://doi.org/10.1029/92JB01407>.
- Brodie, K.H., Rutter, E.H., 1985. On the relationship between deformation and metamorphism, with special reference to the behavior of basic rocks. In: Thompson, A.B., Rubie, D.C. (Eds.), *Metamorphic Reactions: Kinetics, Textures, and*

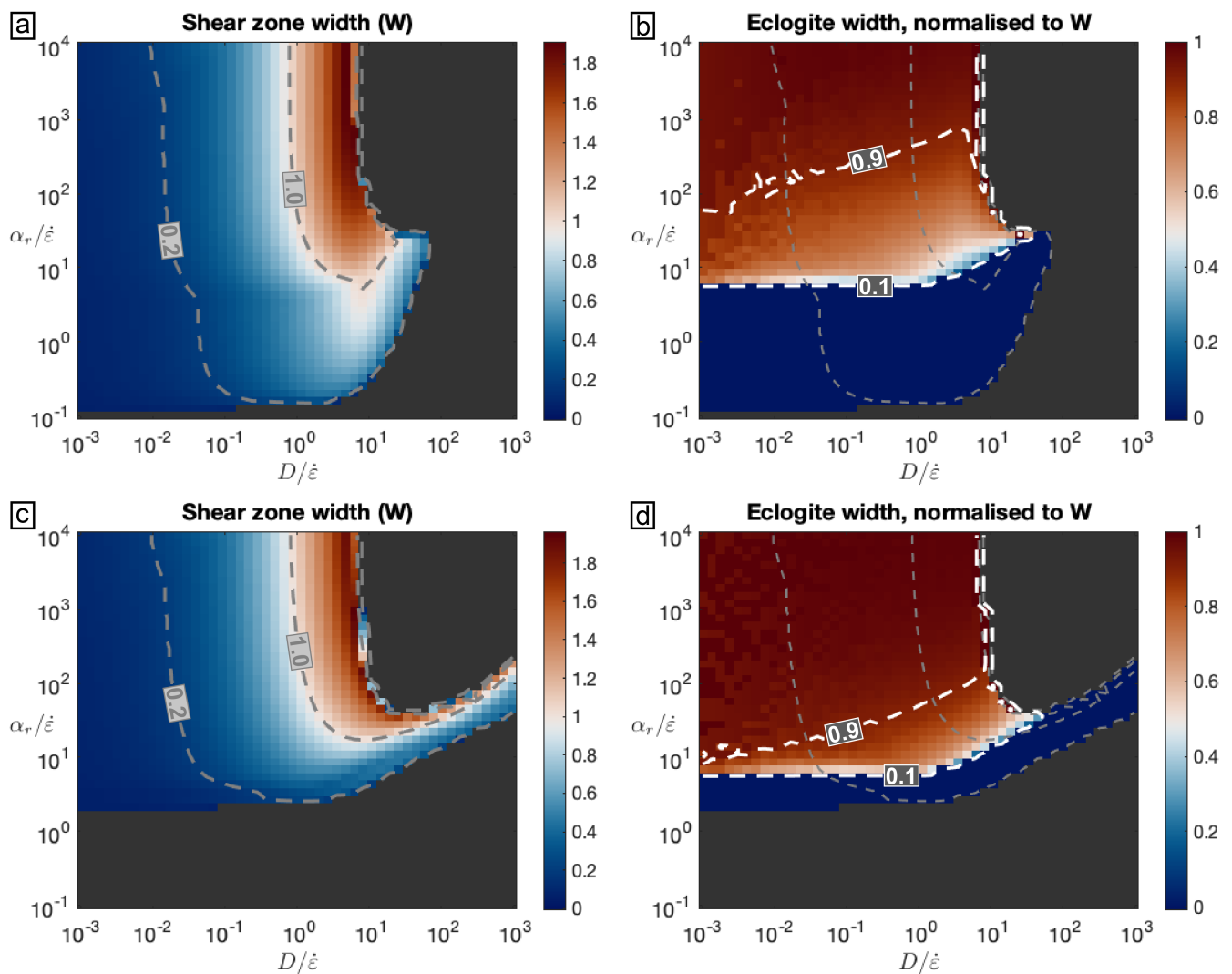
- Deformation. Springer New York, New York, NY, pp. 138–179. [https://doi.org/10.1007/978-1-4612-5066-1\\_6](https://doi.org/10.1007/978-1-4612-5066-1_6).
- Brodie, K.H., Rutter, E.H., 1987. The role of transiently fine-grained reaction products in syntectonic metamorphism: natural and experimental examples. *Can. J. Earth Sci.* 24, 556–564. <https://doi.org/10.1139/e87-054>.
- Centrella, S., 2019. The granulite-to eclogite-and amphibolite-facies transition: a volume and mass transfer study in the lindås nappe, Bergen arcs, West Norway. *Geol. Soc. Lond., Spec. Publ.* 478, 241–264. <https://doi.org/10.1144/SP478.9>.
- Chen, S., Hiraga, T., Kohlstedt, D.L., 2006. Water weakening of clinopyroxene in the dislocation creep regime. *J. Geophys. Res. Solid Earth* 111. <https://doi.org/10.1029/2005JB003885>.
- Connolly, J.A.D., Podladchikov, Y.Y., 1998. Compaction-driven fluid flow in viscoelastic rock. *Geodin. Acta* 11, 55–84. [https://doi.org/10.1016/S0985-3111\(98\)80006-5](https://doi.org/10.1016/S0985-3111(98)80006-5).
- Cruz-Uribe, A.M., Feineman, M.D., Zack, T., Barth, M., 2014. Metamorphic reaction rates at 650–800 °C from diffusion of niobium in rutile. *Geochim. Cosmochim. Acta* 130, 63–77. <https://doi.org/10.1016/j.gca.2013.12.015>.
- Fagereng, Å., Biggs, J., 2019. New perspectives on ‘geological strain rates’ calculated from both naturally deformed and actively deforming rocks. *J. Struct. Geol.* 125, 100–110. <https://doi.org/10.1016/j.jsg.2018.10.004>.
- Farver, J.R., 2010. Oxygen and hydrogen diffusion in minerals. *Rev. Mineral. Geochem.* 72, 447–507. <https://doi.org/10.2138/rmg.2010.72.10>.
- Fossen, H., Cavalante, G.C.G., 2017. Shear zones—a review. *Earth Sci. Rev.* 171, 434–455. <https://doi.org/10.1016/j.earscirev.2017.05.002>.
- Früh-Green, G.L., 1994. Interdependence of deformation, fluid infiltration and reaction progress recorded in eclogitic metagranitoids (sesia zone, western alps). *J. Metamorph. Geol.* 12, 327–343. <https://doi.org/10.1111/j.1525-1314.1994.tb0026x>.
- Glodny, J., Kühn, A., Austrheim, H., 2008. Geochronology of fluid-induced eclogite and amphibolite facies metamorphic reactions in a subduction-collision system, Bergen arcs, Norway. *Contrib. Mineral. Petro.* 156, 27–48. <https://doi.org/10.1007/s00410-007-0272-y>.
- Godard, G., van Roermund, H.L., 1995. Deformation-induced clinopyroxene fabrics from eclogites. *J. Struct. Geol.* 17, 1425–1443. [https://doi.org/10.1016/0191-8141\(95\)00038-F](https://doi.org/10.1016/0191-8141(95)00038-F).
- Goncalves, P., Oliot, E., Marquer, D., Connolly, J., 2012. Role of chemical processes on shear zone formation: an example from the grimsel metagranodiorite (aar massif, central alps). *J. Metamorph. Geol.* 30, 703–722. <https://doi.org/10.1111/j.1525-1314.2012.00991.x>.
- Gueydan, F., Leroy, Y.M., Jolivet, L., Agard, P., 2003. Analysis of continental midcrustal strain localization induced by microfracturing and reaction-softening. *J. Geophys. Res. Solid Earth* 108. <https://doi.org/10.1029/2001JB000611>.
- Handy, M.R., 1989. Deformation regimes and the rheological evolution of fault zones in the lithosphere: the effects of pressure, temperature, grainsize and time. *Tectonophysics* 163, 119–152. [https://doi.org/10.1016/0040-1951\(89\)90122-4](https://doi.org/10.1016/0040-1951(89)90122-4).
- Handy, M.R., 1990. The solid-state flow of polymineralic rocks. *J. Geophys. Res. Solid Earth* 95, 8647–8661. <https://doi.org/10.1029/JB095iB06p08647>.
- Handy, M.R., 1994. Flow laws for rocks containing two non-linear viscous phases: a phenomenological approach. *J. Struct. Geol.* 16, 287–301. [https://doi.org/10.1016/0191-8141\(94\)90035-3](https://doi.org/10.1016/0191-8141(94)90035-3).
- Hawemann, F., Mancktelow, N.S., Pennacchioni, G., Wex, S., Camacho, A., 2019. Weak and slow, strong and fast: how shear zones evolve in a dry continental crust (musgrave ranges, Central Australia). *J. Geophys. Res. Solid Earth* 124, 219–240. <https://doi.org/10.1029/2018JB016559>.
- Hetényi, G., Cattin, R., Brunet, F., Bollinger, L., Vergne, J., Nábělek, J.L., Diament, M., 2007. Density distribution of the India plate beneath the tibetan plateau: Geophysical and petrological constraints on the kinetics of lower-crustal eclogitization. *Earth Planet. Sci. Lett.* 264, 226–244. <https://doi.org/10.1016/j.epsl.2007.09.036>.
- Hirth, G., Teysier, C., Dunlap, J.W., 2001. An evaluation of quartzite flow laws based on comparisons between experimentally and naturally deformed rocks. *Int. J. Earth Sci.* 90, 71–87. <https://doi.org/10.1007/s005310000152>.
- Huet, B., Yamato, P., Grasemann, B., 2014. The minimized power geometric model: an analytical mixing model for calculating polyphe rock viscosities consistent with experimental data. *J. Geophys. Res. Solid Earth* 119, 3897–3924. <https://doi.org/10.1002/2013JB010453>.
- Incel, S., Renner, J., Jamtveit, B., 2020. Evolution of brittle structures in plagioclase-rich rocks at high-pressure and high-temperature conditions—linking laboratory results to field observations. *Geochem. Geophys. Geosyst.* 21 <https://doi.org/10.1029/2020GC009028> e2020GC009028.
- Ingrin, J., Blanchard, M., 2006. Diffusion of hydrogen in minerals. *Rev. Mineral. Geochem.* 62, 291–320. <https://doi.org/10.2138/rmg.2006.62.13>.
- Jackson, J.A., Austrheim, H., McKenzie, D., Priestley, K., 2004. Metastability, mechanical strength, and the support of mountain belts. *Geology* 32, 625–628. <https://doi.org/10.1130/G20397.1>.
- Jakob, J., Alsaif, M., Corfu, F., Andersen, T.B., 2017. Age and origin of thin discontinuous gneiss sheets in the distal domain of the magma-poor hyperextended pre-caledonian margin of baltica, southern Norway. *J. Geol. Soc.* 174, 557–571. <https://doi.org/10.1144/jgs2016-049>.
- Jamtveit, B., Bucher-Nurminen, K., Austrheim, H., 1990. Fluid controlled eclogitization of granulites in deep crustal shear zones, Bergen arcs, western Norway. *Contrib. Mineral. Petro.* 104, 184–193. <https://doi.org/10.1007/BF00306442>.
- Jamtveit, B., Austrheim, H., Putnis, A., 2016. Disequilibrium metamorphism of stressed lithosphere. *Earth Sci. Rev.* 154, 1–13. <https://doi.org/10.1016/j.earscirev.2015.12.002>.
- Jamtveit, B., Ben-Zion, Y., Renard, F., Austrheim, H., 2018. Earthquake-induced transformation of the lower crust. *Nature* 556, 487–491. <https://doi.org/10.1038/s41586-018-0045-y>.
- Jamtveit, B., Petley-Ragan, A., Incel, S., Dunkel, K.G., Aupart, C., Austrheim, H., Corfu, F., Menegon, L., Renard, F., 2019. The effects of earthquakes and fluids on the metamorphism of the lower continental crust. *J. Geophys. Res. Solid Earth* 124, 7725–7755. <https://doi.org/10.1029/2018JB016461>.
- Jolivet, L., Raimbourg, H., Labrousse, L., Avigad, D., Leroy, Y., Austrheim, H., Andersen, T.B., 2005. Softening triggered by eclogitization, the first step toward exhumation during continental subduction. *Earth Planet. Sci. Lett.* 237, 532–547. <https://doi.org/10.1016/j.epsl.2005.06.047>.
- Kaatz, L., Zertani, S., Moulas, E., John, T., Labrousse, L., Schmalholz, S.M., Andersen, T.B., 2021. Widening of hydrous shear zones during incipient eclogitization of metastable dry and rigid lower crust – holsnøy, western Norway. *Tectonics*. <https://doi.org/10.1029/2020TC006572> e2020TC006572.
- Klapfer, E.M., 1990. Reaction-enhanced formation of eclogite-facies shear zones in granulite-facies anorthosites. *Geol. Soc. Lond., Spec. Publ.* 54, 167–173. <https://doi.org/10.1144/GSL.SP.1990.054.01.16>.
- Kohlstedt, D.L., 2006. The role of water in high-temperature rock deformation. *Rev. Mineral. Geochem.* 62, 377–396. <https://doi.org/10.2138/rmg.2006.62.16>.
- Koops, P.O., Rubie, D.C., Früh-Green, G., 1987. The effects of disequilibrium and deformation on the mineralogical evolution of quartz diorite during metamorphism in the eclogite facies. *J. Petro.* 28, 679–700. <https://doi.org/10.1093/petrology/28.4.679>.
- Kretz, R., 1983. Symbols for rock-forming minerals. *Am. Mineral.* 68, 277–279.
- Labrousse, L., Hetényi, G., Raimbourg, H., Jolivet, L., Andersen, T.B., 2010. Initiation of crustal-scale thrusts triggered by metamorphic reactions at depth: Insights from a comparison between the himalayas and scandinavian caledonides. *Tectonics* 29, TC5002. <https://doi.org/10.1029/2009TC002602>.
- Malvoisin, B., Podladchikov, Y.Y., Vrijmoed, J.C., 2015. Coupling changes in densities and porosity to fluid pressure variations in reactive porous fluid flow: local thermodynamic equilibrium. *Geochim. Geophys. Geosyst.* 16, 4362–4387. <https://doi.org/10.1002/2015GC006019>.
- Malvoisin, B., Austrheim, H., Hetényi, G., Reynes, J., Hermann, J., Baumgartner, L.P., Podladchikov, Y.Y., 2020. Sustainable densification of the deep crust. *Geology* 48, 673–677. <https://doi.org/10.1130/G47201.1>.
- Mancktelow, N.S., Pennacchioni, G., 2005. The control of precursor brittle fracture and fluid–rock interaction on the development of single and paired ductile shear zones. *J. Struct. Geol.* 27, 645–661. <https://doi.org/10.1016/j.jsg.2004.12.001>.
- Marti, S., Stünitz, H., Heilbronner, R., Plümper, O., Kilian, R., 2018. Syn-kinematic hydration reactions, grain size reduction, and dissolution–precipitation creep in experimentally deformed plagioclase–pyroxene mixtures. *Solid Earth* 9, 985–1009. <https://doi.org/10.5194/se-9-985-2018>.
- Mattey, D., Jackson, D.H., Harris, N.B.W., Kelley, S., 1994. Isotopic constraints on fluid infiltration from an eclogite facies shear zone, holsnøy, Norway. *J. Metamorph. Geol.* 12, 311–325. <https://doi.org/10.1111/j.1525-1314.1994.tb00025.x>.
- Mørk, M.B.E., 1985. A gabbro to eclogite transition on flemsey, sunnmøre, western Norway. *Chem. Geol.* 50, 283–310. [https://doi.org/10.1016/0009-2541\(85\)90125-1](https://doi.org/10.1016/0009-2541(85)90125-1).
- Oliot, E., Goncalves, P., Marquer, D., 2010. Role of plagioclase and reaction softening in a metagranite shear zone at mid-crustal conditions (gothard massif, swiss central alps). *J. Metamorph. Geol.* 28, 849–871. <https://doi.org/10.1111/j.1525-1314.2010.00897.x>.
- Omlin, S., Malvoisin, B., Podladchikov, Y.Y., 2017. Pore fluid extraction by reactive solitary waves in 3-d. *Geophys. Res. Lett.* 44, 9267–9275. <https://doi.org/10.1002/2017GL074293>.
- Pennacchioni, G., 2005. Control of the geometry of precursor brittle structures on the type of ductile shear zone in the adamello tonalites, southern alps (Italy). *J. Struct. Geol.* 27, 627–644. <https://doi.org/10.1016/j.jsg.2004.11.008>.
- Pennacchioni, G., Mancktelow, N., 2018. Small-scale ductile shear zones: neither extending, nor thickening, nor narrowing. *Earth Sci. Rev.* 184, 1–12. <https://doi.org/10.1016/j.earscirev.2018.06.004>.
- Poirier, J.P., 1982. On transformation plasticity. *J. Geophys. Res. Solid Earth* 87, 6791–6797. <https://doi.org/10.1029/JB087iB08p06791>.
- Putnis, A., Austrheim, H., 2010. Fluid-induced processes: metasomatism and metamorphism. *Geofluids* 10, 254–269. <https://doi.org/10.1111/j.1468-8123.2010.00285.x>.
- Putnis, A., Jamtveit, B., Austrheim, H., 2017. Metamorphic processes and seismicity: the Bergen arcs as a natural laboratory. *J. Petro.* 58, 1871–1898. <https://doi.org/10.1093/petrology/egw076>.
- Raimbourg, H., 2005. Mécanismes d’éclogitisation et conséquences pour l’exhumation des roches métamorphiques de haute pression: l’exemple de l’Arc de Bergen, Norvège. Ph.D. thesis, Paris, p. 6.
- Raimbourg, H., Jolivet, L., Labrousse, L., Leroy, Y., Avigad, D., 2005. Kinematics of syneclogite deformation in the bergen arcs, Norway: implications for exhumation mechanisms. *Geol. Soc. Lond., Spec. Publ.* 243, 175–192. <https://doi.org/10.1144/GSL.SP.2005.243.01.13>.
- Reuss, A., 1929. Berechnung der fließgrenze von mischkrystallen auf grund der plastizitätsbedingung für einkristalle. *Z. Angew. Math. Mech.* 9, 49–58.
- Roberts, D., 2003. The scandinavian caledonides: event chronology, palaeogeographic settings and likely modern analogues. *Tectonophysics* 365, 283–299. [https://doi.org/10.1016/S0040-1951\(03\)00026-X](https://doi.org/10.1016/S0040-1951(03)00026-X).
- Rubie, D.C., 1986. The catalysis of mineral reactions by water and restrictions on the presence of aqueous fluid during metamorphism. *Mineral. Mag.* 50, 399–415. <https://doi.org/10.1180/minmag.1986.050.357.05>.

- Rubie, D.C., 1990. Mechanisms of Reaction-Enhanced Deformability in Minerals and Rocks. Springer Netherlands, Dordrecht, pp. 262–295. [https://doi.org/10.1007/978-94-011-6827-4\\_11](https://doi.org/10.1007/978-94-011-6827-4_11).
- Rubie, D.C., 1998. Disequilibrium during metamorphism: the role of nucleation kinetics. Geol. Soc. Lond., Spec. Publ. 138, 199–214. <https://doi.org/10.1144/GSL.SP.1996.138.01.12>.
- Rutter, E.H., Brodie, K.H., 1988a. Experimental “syntectonic” dehydration of serpentinite under conditions of controlled pore water pressure. J. Geophys. Res. Solid Earth 93, 4907–4932. <https://doi.org/10.1029/JB093iB05p04907>.
- Rutter, E.H., Brodie, K.H., 1988b. The role of tectonic grain size reduction in the rheological stratification of the lithosphere. Geol. Rundsch. 77, 295–307. <https://doi.org/10.1007/BF01848691>.
- Rutter, E.H., Brodie, K.H., 1995. Mechanistic interactions between deformation and metamorphism. Geol. J. 30, 227–240. <https://doi.org/10.1002/gj.3350300304>.
- Rybacki, E., Dresen, G., 2000. Dislocation and diffusion creep of synthetic anorthite aggregates. J. Geophys. Res. Solid Earth 105, 26017–26036. <https://doi.org/10.1029/2000JB900223>.
- Schmalholz, S.M., Moulas, E., Plümper, O., Myasnikov, A.V., Podladchikov, Y.Y., 2020. 2d hydro-mechanical-chemical modeling of (de)hydration reactions in deforming heterogeneous rock: The periclase-brucite model reaction. Geochem. Geophys. Geosyst. 21 <https://doi.org/10.1029/2020GC009351> e2020GC009351.
- Schneider, J., Bosch, D., Monié, P., Bruguier, O., 2007. Micro-scale element migration during eclogitisation in the Bergen arcs (Norway): a case study on the role of fluids and deformation. Lithos 96, 325–352. <https://doi.org/10.1016/j.lithos.2006.10.001>.
- Shi, F., Wang, Y., Yu, T., Zhu, L., Zhang, J., Wen, J., Gasc, J., Incel, S., Schubnel, A., Li, Z., Chen, T., Liu, W., Prakapenka, V., Jin, Z., 2018. Lower-crustal earthquakes in southern Tibet are linked to eclogitization of dry metastable granulite. Nat. Commun. 9, 1–13. <https://doi.org/10.1038/s41467-018-05964-1>.
- Snow, E., Yund, R.A., 1987. The effect of ductile deformation on the kinetics and mechanisms of the aragonite-calcite transformation. J. Metamorph. Geol. 5, 141–153. <https://doi.org/10.1111/j.1525-1314.1987.tb00376.x>.
- Steffen, K., Selverstone, J., Brearley, A., 2001. Episodic weakening and strengthening during synmetamorphic deformation in a deep-crustal shear zone in the alps. Geol. Soc. Lond., Spec. Publ. 186, 141–156. <https://doi.org/10.1144/GSL.SP.2001.186.01.09>.
- Stünitz, H., Tullis, J., 2001. Weakening and strain localization produced by syn-deformational reaction of plagioclase. Int. J. Earth Sci. 90, 136–148. <https://doi.org/10.1007/s005310000148>.
- Stünitz, H., Neufeld, K., Heilbronner, R., Finstad, A.K., Konopásek, J., Mackenzie, J.R., 2020. Transformation weakening: Diffusion creep in eclogites as a result of interaction of mineral reactions and deformation. J. Struct. Geol. 139, 104129. <https://doi.org/10.1016/j.jsg.2020.104129>.
- Tullis, J., Yund, R.A., 1980. Hydrolytic weakening of experimentally deformed westerly granite and hale albite rock. J. Struct. Geol. 2, 439–451. [https://doi.org/10.1016/0191-8141\(80\)90005-X](https://doi.org/10.1016/0191-8141(80)90005-X).
- Vitale, S., Mazzoli, S., 2008. Heterogeneous shear zone evolution: the role of shear strain hardening/softening. J. Struct. Geol. 30, 1383–1395. <https://doi.org/10.1016/j.jsg.2008.07.006>.
- Voigt, W., 1928. Lehrbuch der kristallphysik. Teubner, Leipzig, Germany.
- Yund, R.A., Tullis, J., 1991. Compositional changes of minerals associated with dynamic recrystallization. Contrib. Mineral. Petrol. 108, 346–355. <https://doi.org/10.1007/BF00285942>.
- Zertani, S., Labrousse, L., John, T., Andersen, T.B., Tilmann, F., 2019. The interplay of eclogitization and deformation during deep burial of the lower continental crust—a case study from the Bergen arcs (western Norway). Tectonics 38, 898–915. <https://doi.org/10.1029/2018TC005297>.
- Zhang, J., Green II, H.W., Bozhilov, K.N., 2006. Rheology of omphacite at high temperature and pressure and significance of its lattice preferred orientations. Earth Planet. Sci. Lett. 246, 432–443. <https://doi.org/10.1016/j.epsl.2006.04.006>.

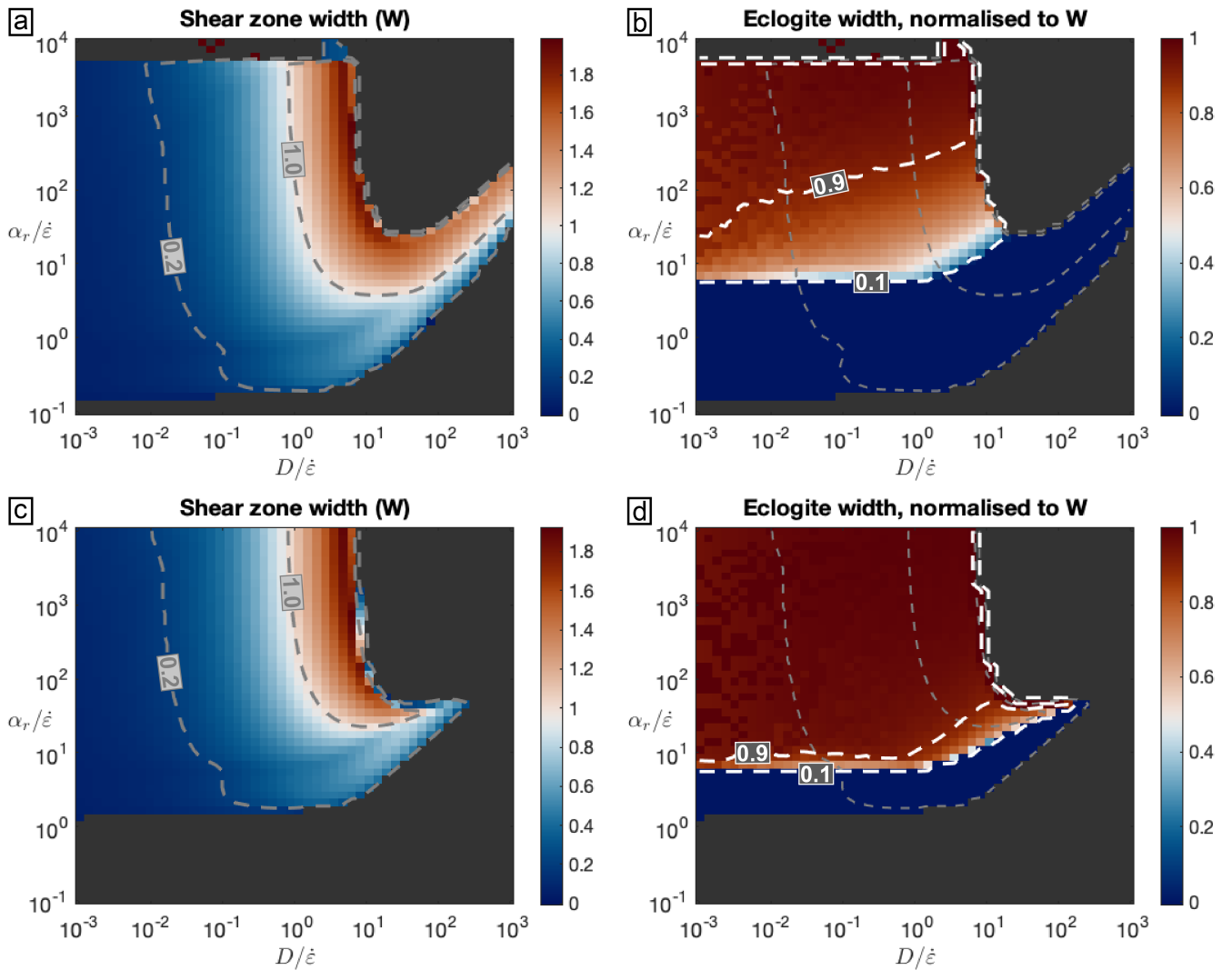
*Supplementary material A: Backscattered electrons image of the edge of a corona in domain D3 of SZ1, showing various extents of garnet zoning. The dark core is rich in pyrope (Mg bearing end-member) whereas the light rim is rich in almandine (Fe bearing end-member).*



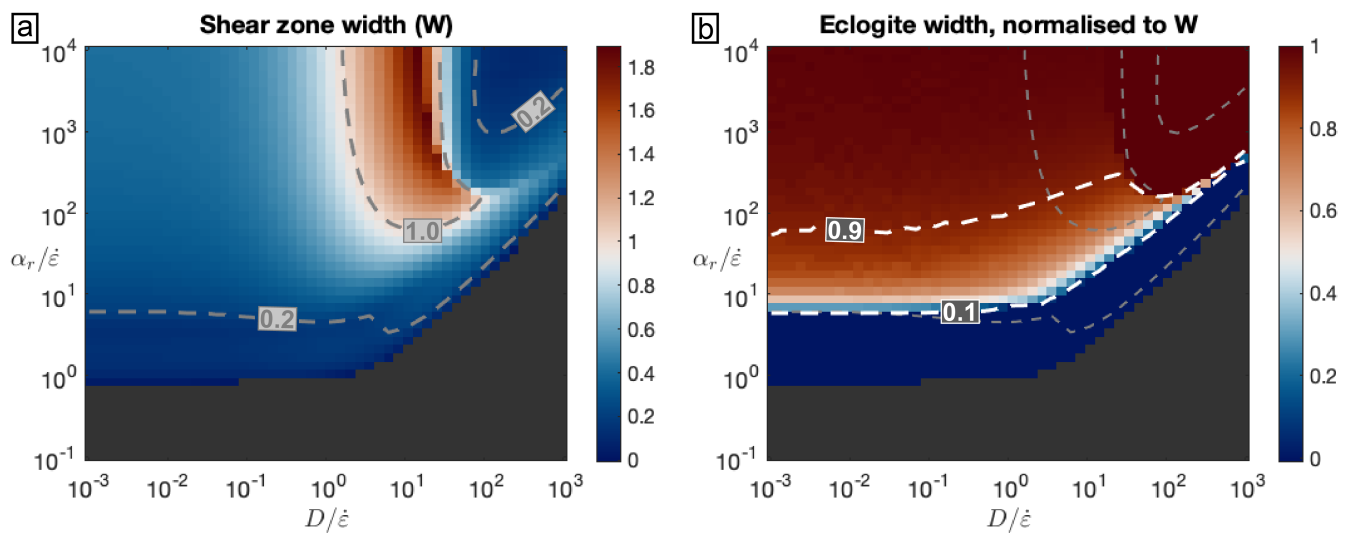
*Supplementary material B: (a, b) Role of diffusivity  $D$  and reaction rate  $\alpha_r$  (relative to  $\dot{\varepsilon}$ ) on (a) the width of the shear zone (in metres) and (b) the width of the fully transformed shear zone core, normalised to the shear zone width, using Reuss lower bound (weighted harmonic mean of the end-member viscosities) to calculate the viscosity. (c, d) Idem using Voigt upper bound (weighted arithmetic mean of the end-member viscosities). Contour lines delimit realistic models, with shear zone width between 0.2 and 1.2 m, and normalised eclogite width between 0.1 and 0.9.*



*Supplementary material C: (a, b) Role of diffusivity  $D$  and reaction rate  $\alpha_r$  (relative to  $\dot{\varepsilon}$ ) on (a) the width of the shear zone (in metres) and (b) the width of the fully transformed shear zone core, normalised to the shear zone width, using a reaction threshold of  $r_t = 0.1$ . (c, d) Idem using  $r_t = 0.9$ . Contour lines delimit realistic models, with shear zone width between 0.2 and 1.2 m, and normalised eclogite width between 0.1 and 0.9.*



*Supplementary material D: Role of diffusivity  $D$  and reaction rate  $\alpha_r$  (relative to  $\dot{\varepsilon}$ ) on (a) the width of the shear zone (in metres) and (b) the width of the fully transformed shear zone core, normalised to the shear zone width, using a continuous input of fluid in the core of the shear zone.*





# 3

## Eclogitisation of dry and impermeable granulite by fluid flow with reaction-induced porosity : Insights from hydro-chemical modelling

### Sommaire du présent chapitre

---

<b>Points clés</b>	<b>79</b>
<b>3.1 Résumé</b>	<b>80</b>
<b>3.2 Article de Bras et al. (2023), <i>EPSL</i></b>	<b>81</b>
<b>3.3 Annexes à l'article de Bras et al. (2023)</b>	<b>94</b>

---

### Points clés

- En présence d'un pulse de fluides, l'éclogitisation peut se propager à une vitesse de l'ordre de 10 centimètres par an dans la granulite.
- L'éclogite est préservée après la fin du pulse de fluides.
- Un front de réaction de haute pression peut se propager dans une roche imperméable si la réaction métamorphique induit une densification.
- Ce processus peut être approximé par un loi de diffusion pour n'importe quelle réaction.

### 3.1 Résumé

Si le chapitre précédent considère bien l'effet des fluides sur la réaction métamorphique, il ne présente pas l'effet inverse : l'impact de la réaction sur la circulation des fluides. Le présent chapitre explore donc comment la rétroaction entre circulation de fluides et réaction permet la propagation de la réaction, à l'aide d'un modèle numérique.

A Holsnøy, l'éclogitisation se produit à haute pression pendant l'hydratation de la granulite, mais les processus physiques contrôlant l'hydratation de la granulite sèche et imperméable restent mal compris. Je présente donc un nouveau modèle hydro-réactif dans lequel une roche poreuse subit des réactions métamorphiques en réponse à des variations de pression fluide.

Une augmentation de pression fluide entraîne une augmentation de la densité de la roche, due à sa compressibilité et à l'éclogitisation qui densifie la roche. La densification génère de la porosité et augmente donc la perméabilité. Je montre qu'un pulse de pression fluide peut entraîner l'éclogitisation de la granulite, ce qui génère de la perméabilité. La perméabilité associée aux gradients de pression fluide conduit à l'écoulement des fluides et à la propagation du front de réaction par flux de Darcy dans la granulite initialement imperméable et non poreuse.

Ce modèle suggère que même si la propagation de l'éclogitisation ne dure que tant qu'un pulse de fluide est présent, la région éclogitique de haute pression est préservée en l'absence de pulse. En présence d'un pulse de fluides, le front d'éclogitisation se propage sur des dizaines de centimètres dans la granulite en l'espace de quelques semaines à quelques mois. Je généralise ces observations en montrant que la propagation d'un front réactif de haute pression est un processus diffusif qui est possible tant que la réaction entraîne une densification.

L'article est publié dans : Bras, E., Yamato, P., Schmalholz, S. M., Duretz, T., & Podladchikov, Y. Y. (2023). Eclogitisation of dry and impermeable granulite by fluid flow with reaction-induced porosity : Insights from hydro-chemical modelling. *Earth and Planetary Science Letters*, 617, 118256. <https://doi.org/10.1016/j.epsl.2023.118256>.



Contents lists available at ScienceDirect

## Earth and Planetary Science Letters

journal homepage: [www.elsevier.com/locate/epsl](http://www.elsevier.com/locate/epsl)

## Eclogitisation of dry and impermeable granulite by fluid flow with reaction-induced porosity: Insights from hydro-chemical modelling



Erwan Bras <sup>a,\*</sup>, Philippe Yamato <sup>a,b</sup>, Stefan M. Schmalholz <sup>c</sup>, Thibault Duretz <sup>d</sup>, Yury Y. Podladchikov <sup>c,e</sup>

<sup>a</sup> Univ. Rennes, CNRS, Géosciences Rennes UMR 6118, 35000 Rennes, France

<sup>b</sup> Institut Universitaire de France, 75005 Paris, France

<sup>c</sup> Institute of Earth Sciences, University of Lausanne, 1015 Lausanne, Switzerland

<sup>d</sup> Institut für Geowissenschaften, Goethe-Universität Frankfurt, Frankfurt, Germany

<sup>e</sup> Faculty of Mechanics and Mathematics, Lomonosov Moscow State University, Moscow, Russia

## ARTICLE INFO

## Article history:

Received 16 March 2023

Received in revised form 25 May 2023

Accepted 30 May 2023

Available online xxxx

Editor: A. Webb

Dataset link: [10.5281/zenodo.7966767](https://doi.org/10.5281/zenodo.7966767)

## Keywords:

eclogitization  
hydration front  
reaction-induced porosity  
hydro-chemical modelling

## ABSTRACT

Eclogitisation is a major metamorphic process of continental subduction zones, where transformation of dry lower crustal rocks into eclogites seems to correlate with seismogenic events. Eclogitisation can occur at high pressure during hydration of granulite, but the physical processes controlling the hydration of dry, impermeable granulite remain poorly understood. Here, we present a new fully coupled hydro-chemical model of a non-deforming porous rock which undergoes metamorphic reactions in response to fluid pressure variations. Conservation equations for total and solid mass are solved, and fluid and solid densities are calculated with look-up tables computed from models relying on equilibrium thermodynamics. Our model shows that a fluid pressure pulse generates a pressure gradient that causes densification when the pressure required for eclogitisation is reached. The reaction generates porosity and subsequent porous fluid flow into the initially non-porous impermeable granulite. This process lasts as long as the pressure pulse is maintained, but high pressure within eclogite can persist for a longer time. The hydration front propagates tens of centimetres into the granulite in the order of weeks to months. We show that propagation of a hydration-reaction front is effectively a diffusive process, with diffusivity in the order of  $10^{-9} \text{ m}^2 \cdot \text{s}^{-1}$  for eclogitisation as in Holsnøy, Norway. Reactive hydration of impermeable granulite is possible because its solid density is smaller than that of eclogite. We discuss the application of our model for eclogitisation and also for other reactions for which hydration of impermeable rock is possible.

© 2023 Elsevier B.V. All rights reserved.

### 1. Introduction

The physical properties of the continental crust, such as density, viscosity and permeability, critically affect fluid migration, orogenic cycles and seismicity, and are primarily controlled by the metamorphic state of the lower crust (Austrheim, 1998; Jackson et al., 2004). Eclogitisation of dry and mechanically strong crustal rocks involves a large increase in solid density, transient rheological weakening, and fluid flow (e.g. Austrheim, 1987; Bras et al., 2021; Kaatz et al., 2023), which play a major role for the stress state of the crust, seismicity and long-term lithosphere dynamics (Labrousse et al., 2010; Jamtveit et al., 2018a; Yamato et al., 2019; Moulas et al., 2022). For example, the strong feedbacks between

metamorphism, deformation, and fluid transport in the lower crust (John and Schenk, 2006; Austrheim, 2013; Jamtveit et al., 2019) are crucial for determining the physical mechanisms that initiate earthquakes (Miller, 2013; Menegon et al., 2021). Hence, studying eclogitisation of dry crustal rocks is crucial for our understanding of the properties and dynamics of the deep crust (Jamtveit et al., 2019).

The interplay between metamorphism, deformation, and fluid flow can be inferred through geophysical investigations in active orogens (e.g. in the Himalaya, Hetényi et al., 2007), high pressure laboratory rock deformation experiments (Incel et al., 2017; Shi et al., 2018) and mathematical modelling based on the concepts of continuum mechanics and thermodynamics (Malvoisin et al., 2020; Schmalholz et al., 2020; Moulas et al., 2022; Yamato et al., 2022). However, investigating this interplay with direct petrological and structural observations from exhumed crustal rocks in the field is essential to understand how metamorphic reactions control the

\* Corresponding author.

E-mail address: [erwan.bras@univ-rennes.fr](mailto:erwan.bras@univ-rennes.fr) (E. Bras).

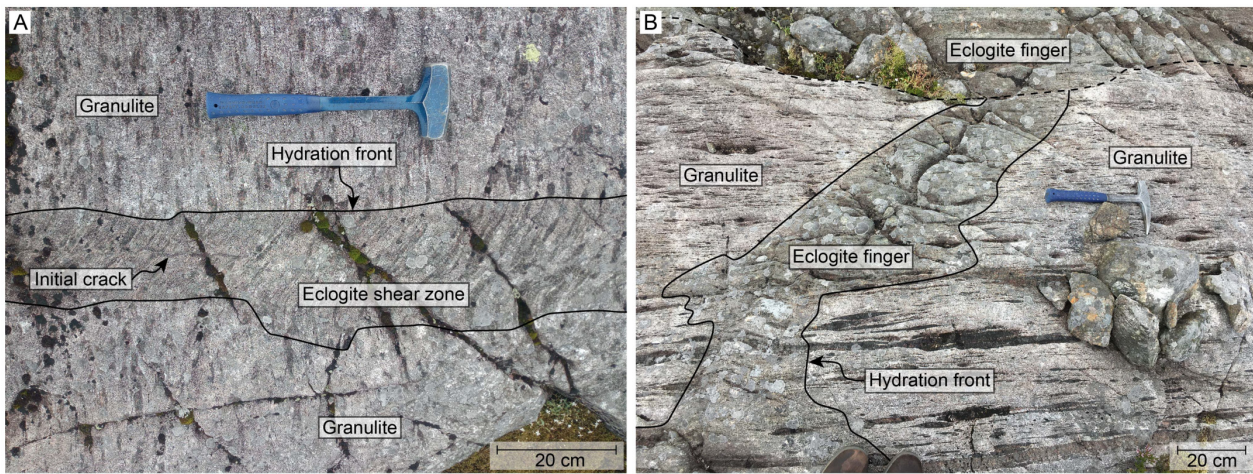


**Fig. 1.** Photographs from Holsnøy (western Norway), showing a halo of eclogitisation overprinting the granulite. (A) Eclogite shear zone (eclogitisation associated with deformation); 60°35'11"N, 5°07'34"E. The shear zone develops around a narrow central crack. (B) Eclogite finger (no deformation); 60°35'27"N, 5°00'44"E.

properties of the deep crust (Jackson et al., 2004; Labrousse et al., 2010; Baïsset et al., 2023).

The island of Holsnøy, in southwestern Norway, constitutes an ideal natural laboratory for investigating the interplay between metamorphism, deformation and fluid flow in the lower crust (Austrheim, 1987, 2013; Putnis et al., 2017). A large part of the island is made of anorthositic granulites, which were formed at ca. 930 Ma during the Grenvillian orogeny (Bingen et al., 2001). During the Caledonian orogeny, the granulites were subducted during convergence and collision between Baltica and Laurentia (Andersen et al., 1991). The high-pressure event occurring during the collision stage caused the partial eclogitisation of the granulitic lower crust, associated with fluid infiltration and shear deformation, and was presumably initiated by fracturing associated with earthquakes (Austrheim, 1987). Peak pressure ( $P$ ) and temperature ( $T$ ) conditions in Holsnøy were 670–690 °C and 21–22 kbar (Bhowany et al., 2018). The relation between eclogite and granulite is exceptionally well preserved, making Holsnøy an ideal analogue for the metamorphic state of the lower crust being deeply buried during orogenic events (Jackson et al., 2004; Labrousse et al., 2010).

In Holsnøy, eclogitisation is spatially heterogeneous at the outcrop scale and is localised in eclogite shear zones crosscutting the granulite protolith, and in eclogite fingers overprinting the granulite without associated deformation (Zertani et al., 2019; Kaatz et al., 2021; Putnis et al., 2021). Our study concerns both eclogite shear zones and eclogite fingers (see examples in Fig. 1), which will both be referred to as “eclogitisation zones” in the rest of this study.

Several authors (e.g. Austrheim, 1987; Zertani et al., 2022; Kaatz et al., 2022) argued that eclogite and granulite coexist in close spatial proximity in eclogitisation zones because granulite is metastable: granulite experienced eclogite facies  $P-T$  conditions, but remained largely untransformed because it lacked fluids to trigger eclogitisation. Only regions infiltrated by fluids transformed into eclogite. However, recent studies suggested that the coexistence of granulite and eclogite due to local pressure variations may be a more consistent interpretation of the field data (Putnis et al., 2021 and references therein). Here, we do not aim to demonstrate which interpretation is more feasible, because our study is compatible with both interpretations.

Several studies suggest that eclogitisation zones widen over time (Jamtveit et al., 2000; Jolivet et al., 2005; Bras et al., 2021; Kaatz et al., 2021), but existing numerical models do not explain

this widening with consistent physics, coupling metamorphic reaction and fluid flow. For example, Jamtveit et al. (2000) explain the development of static eclogitisation zones with a model coupling solid state diffusion and generation of a network of fractures in an elastic model, without porous fluid flow. Bras et al. (2021) and Kaatz et al. (2021, 2023) model the widening of eclogitisation zones with a diffusion equation which mimics the effects of porous fluid flow and/or solid state diffusion of hydrogen and oxygen. Moulas et al. (2022) present a purely mechanical model for metamorphism of the lower crust, without any hydro-chemical aspect, to study the long-term (order of millions of years) impact of such metamorphism on crustal dynamics. Malvoisin et al. (2020) consider porous fluid flow with a fully coupled hydro-chemical-mechanical model and show that hydration of dry granulite can occur in the order of weeks. However, they focus on the influence of the reaction on the generation of seismicity but not on the mechanism of widening of eclogitisation zones. Therefore, although several models already describe the eclogitisation of granulite, it is still not clear how to predict the evolution of eclogitisation zones based on theoretical models which couple reactions and porous fluid flow.

Here, we investigate the time evolution of eclogitisation driven by porous fluid flow following Darcy's law. We apply a simple but physically consistent one dimensional (1D) hydro-chemical (HC) model involving metamorphic reactions, based on the concepts of continuum mechanics and local equilibrium thermodynamics, similar to models presented by Malvoisin et al. (2015), Plümper et al. (2017), and Schmalholz et al. (2020). Pressure variations modify the rock density by solid compressibility and by replacement of low-density granulite-facies minerals with high density eclogite-facies minerals. Density changes that decrease the rock volume generate porosity, and hence permeability if it is dependent on porosity. Permeability associated with fluid pressure gradients leads to fluid flow and reaction front propagation. Our aims are to (1) quantify the widening of the eclogitisation zones and (2) explain the mechanism of hydration of a zero-porosity, and thus impermeable, granulite by porous fluid flow.

From a technical point of view, modelling fluid flow into a zero-porosity region is indeed challenging. The zero porosity limit is typically met in studies involving two-phase flow (e.g. Scott and Stevenson, 1986). Although the set of governing two-phase equations reduce to single-phase equations in the zero porosity limit (e.g. Katz et al., 2007), accounting for transient variations of the relative proportion of porous and non-porous domains in a sin-

**Table 1**

Model variables, and parameters used in the reference model. The equations determining the value of the model unknowns are indicated.

Symbol	Meaning	Unit	Value
$P$	Pressure	Pa	Eq. (12)
$\phi$	Porosity	-	Eq. (9), (13)
$\rho_T$	Total mass per unit volume	$\text{kg} \cdot \text{m}^{-3}$	Eq. (1), (14)
$\rho_s$	Solid density	$\text{kg} \cdot \text{m}^{-3}$	Eq. (11a)
$\rho_f$	Fluid density	$\text{kg} \cdot \text{m}^{-3}$	Eq. (11b)
$X_{\text{H}_2\text{O}}$	$\text{H}_2\text{O}$ mass fraction	-	Eq. (11c)
$X_s$	$1 - X_{\text{H}_2\text{O}}$	-	-
$v_f$	Fluid velocity	$\text{m} \cdot \text{s}^{-1}$	-
$\beta$	Solid compressibility	$\text{Pa}^{-1}$	-
$T$	Temperature	$^{\circ}\text{C}$	700
$P_{\text{bg}}$	Background pressure	kbar	15
$\Delta P_f$	Pulse fluid pressure	kbar	10
$P_r$	Reaction pressure	kbar	19.4
$\Delta P_r$	$P_r - P_{\text{bg}}$	kbar	4.4
$w_0$	Width of initial crack	m	0.01
$t_p$	Duration of fluid pulse	days	50
$\rho_T^s$	Total solid mass per unit volume	$\text{kg} \cdot \text{m}^{-3}$	2685
$k_0$	Permeability coefficient	$\text{m}^2$	$10^{-19}$
$\eta_f$	Fluid viscosity	$\text{Pa} \cdot \text{s}$	$10^{-3}$
$n$	Porosity exponent	-	3

gle simulation can be challenging. Several studies get around this problem by having a minimal background porosity in the dry phases (e.g. Räss et al., 2019; Schmalholz et al., 2020), which allows to apply two-phase flow equations to the whole domain. Other authors have addressed this problem by including a specific treatment of these equations (e.g. Arbogast et al., 2017). In this paper we also address this issue in the context of the hydration of a zero-porosity region.

With our model, we show that fluid flow induced hydration and subsequent eclogitisation of a dry and impermeable rock is possible. We explain the physical mechanisms by which the eclogitisation zones can widen into an initially zero-porosity region, and provide a numerical tool allowing to simulate this process.

## 2. Methods

We consider a 1D hydro-chemical (HC) model, similar to that of Plümper et al. (2017), where a non-deforming porous rock undergoes metamorphic reactions in response to fluid pressure variations. The model is based on local thermodynamic equilibrium and mass conservation. Metamorphic reactions lead to changes in rock density and exchange of  $\text{H}_2\text{O}$  between the fluid and the solid, hence modifying the porosity of the system. Since we use a porosity-dependant, Carman-Kozeny type permeability (Costa, 2006), changes in porosity also modify the permeability. Reaction-induced permeability leads to fluid flow controlled by fluid pressure gradients.

### 2.1. Governing system of equations

In our model, the volatile species, assumed here to be pure  $\text{H}_2\text{O}$ , are either structurally bound to the solid, having a particular solid mass fraction  $X_{\text{H}_2\text{O}}$ , or constitute the fluid filling the porosity. We assume that dissolution of solid species, such as Si, Al, Na and Ca, in the fluid is negligible. Following Malvoisin et al. (2015); Plümper et al. (2017); Schmalholz et al. (2020), solving this system requires (1) conservation of total mass per unit volume of the system ( $\rho_T$ , i.e. sum of fluid mass and solid mass) and (2) conservation of the mass per unit volume of solid species ( $\rho_T^s$ ). All variables used in this study are listed in Table 1.

#### 2.1.1. Conservation of total mass

We consider a porous medium, with porosity  $\phi$ , which consists of a solid phase with density  $\rho_s$  and a fluid phase with density  $\rho_f$  stored in the pores. Per unit volume, the total mass  $\rho_T$  of the porous medium is:

$$\rho_T = \rho_f \phi + \rho_s (1 - \phi). \quad (1)$$

In a general case, the one-dimensional conservation equation of a given quantity A, expressing the variation of quantity A (per unit volume) over time, is:

$$\frac{\partial A}{\partial t} = -\frac{\partial q_A}{\partial x}. \quad (2)$$

In absence of diffusive flux, the flux of A ( $q_A$ ) is purely advective and can be expressed as:

$$q_A = A v_A, \quad (3)$$

which is simply the amount of A multiplied by the velocity of A. Using equations (1) and (3), the advective flux of total mass  $\rho_T$  can be written as:

$$q_{\rho_T} = \rho_f \phi v_f + \rho_s (1 - \phi) v_s, \quad (4)$$

where  $v_f$  and  $v_s$  are respectively the velocities of the fluid and the solid. Using equations (2) and (4), the conservation of total mass  $\rho_T$  is then:

$$\frac{\partial \rho_T}{\partial t} = -\frac{\partial}{\partial x} (\rho_f \phi v_f + \rho_s (1 - \phi) v_s). \quad (5)$$

In the absence of solid deformation ( $v_s = 0$ ), the conservation equation of total mass simplifies to:

$$\frac{\partial \rho_T}{\partial t} = -\frac{\partial}{\partial x} (\rho_f \phi v_f). \quad (6)$$

The force balance for the fluid in the absence of gravity and solid velocity can be expressed using Darcy's law:

$$\phi v_f = -\frac{k_0 \phi^3}{\eta_f} \left( \frac{\partial P_f}{\partial x} \right), \quad (7)$$

where  $k_0$  is the permeability coefficient in a porosity-dependant Carman-Kozeny type permeability expression,  $\eta_f$  is the fluid viscosity, and  $P_f$  is the fluid pressure. Substituting equation (7) into equation (6) yields the total mass conservation equation:

$$\frac{\partial \rho_T}{\partial t} = \frac{\partial}{\partial x} \left[ \rho_f \frac{k_0 \phi^3}{\eta_f} \left( \frac{\partial P_f}{\partial x} \right) \right]. \quad (8)$$

#### 2.1.2. Total solid mass

We assume that solid components, such as Si, Al, Na and Ca, never enter the fluid phase, whereas the volatile component  $\text{H}_2\text{O}$  can be part of the solid phase in the form of hydrous minerals.  $X_{\text{H}_2\text{O}}$  is the mass fraction of volatile components structurally bound in the solid. The total solid mass (without structurally bound  $\text{H}_2\text{O}$ ) of the system per unit volume,  $\rho_T^s$ , is:

$$\rho_T^s = \rho_s (1 - \phi) (1 - X_{\text{H}_2\text{O}}). \quad (9)$$

Solid components remain in the solid, so in the absence of solid velocity there is never any advective flux of solid mass (equation (3)), and thus there is no time evolution of  $\rho_T^s$ :

$$\frac{\partial \rho_T^s}{\partial t} = 0. \quad (10)$$

Hence, equation (9) can be used to express the solid mass conservation equation if  $\rho_T^s$  is a known, constant parameter of the model.

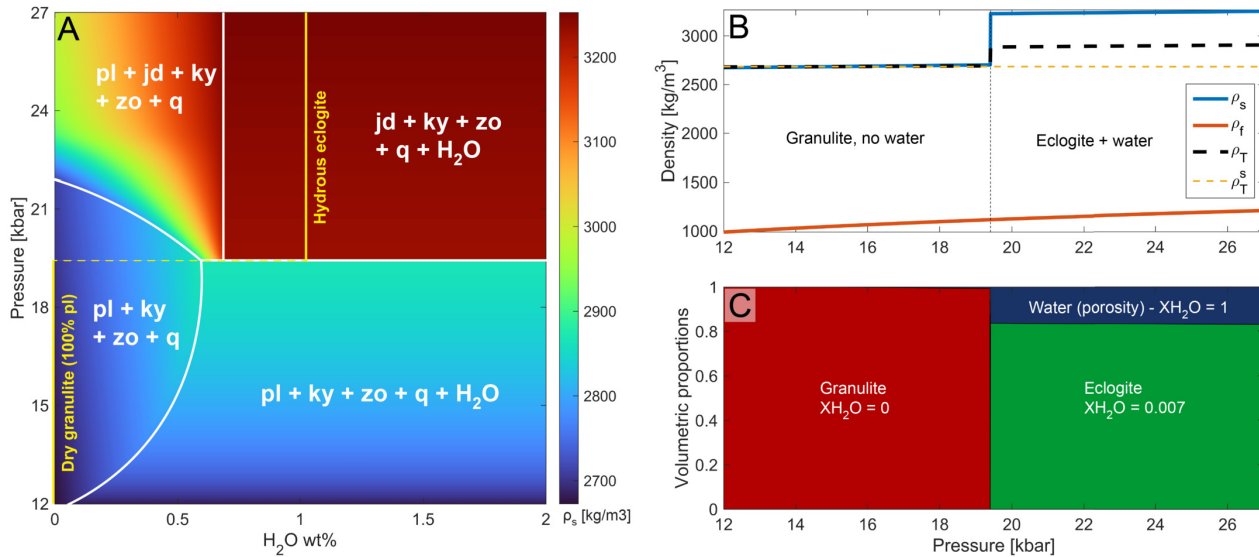


**Fig. 2.** Thermodynamic data used in the model. (A) Perple\_X pseudosection used to mimic the stable mineralogical assemblages resulting from destabilisation of anorthosite, as a function of water content and pressure. The yellow line shows the H<sub>2</sub>O wt% conditions at which we retrieve solid density data: dry conditions for granulite at low pressure, and 1 wt% (saturated in H<sub>2</sub>O) for eclogite at high pressure. Abbreviations after Holland and Powell (1998): pl: plagioclase, ky: kyanite, zo: zoisite, q: quartz, jd: jadeite. (B) Corresponding 1D look-up tables for solid ( $\rho_s$ ) and fluid ( $\rho_f$ ) density as a function of pressure, and total density ( $\rho_T$ ) look-up table calculated from equation (12). The total solid mass ( $\rho_T^s$ ) is a constant value of 2685 kg · m<sup>-3</sup>. (C) Phase composition of the system. At 15 kbar, granulite has zero porosity.

## 2.2. Precomputed thermodynamic data

### 2.2.1. Thermodynamic model

The equations described above require prior knowledge of the densities of fluid, eclogite and granulite at any pressure, as well as the amount of fluid structurally bound to the solid  $X_{\text{H}_2\text{O}}$ . We compute these values by minimisation of Gibbs free-energy using the software Perple\_X (Connolly, 2005), with the internally consistent thermodynamic data set of Holland and Powell (1998).

To study the eclogitisation of granulite in Holsnøy, we consider the model chemical system Na<sub>2</sub>O-CaO-SiO<sub>2</sub>-Al<sub>2</sub>O<sub>3</sub>-H<sub>2</sub>O. We do not consider FeO and MgO because the main reactions of granulite to eclogite are destabilisation of the anorthite and albite components of plagioclase (e.g. Bras et al., 2021): with increasing pressure and in the presence of water, anorthite transforms into zoisite, kyanite and quartz, and albite transforms into jadeite and quartz. Our modelled granulite is therefore composed of only plagioclase, and our modelled eclogite of jadeite, zoisite, kyanite, quartz. We use a system composition of 57.64 wt% SiO<sub>2</sub>, 26.92 wt% Al<sub>2</sub>O<sub>3</sub>, 8.76 wt% CaO and 6.68 wt% Na<sub>2</sub>O, without FeO or MgO, corresponding to a representative composition of plagioclase in Holsnøy granulite (Bras et al., 2021). We use the solid solution for plagioclase of Newton et al. (1980) (Pl(h) in Perple\_X). We use a constant bulk composition and variable water content, as there is no major variation of composition between granulite and eclogite, besides the introduction of water (Centrella, 2019; Bras et al., 2021). Rock properties are computed at a constant temperature of 700 °C, consistent with temperature estimates in both granulite and eclogite by Bhowany et al. (2018).

The aim of the thermodynamic calculation is to compute bulk rock densities as a function of pressure in order to use them in our model, and not to predict mineral assemblages. We can therefore simplify the thermodynamic database by only including minerals that are present in substantial proportions in Holsnøy granulites and eclogites. This simplification produces the pseudosection displayed in Fig. 2A. With this simplified set-up, dry granulite is modelled with pure plagioclase and no water at low pressure,

and hydrous eclogite is modelled with the products of plagioclase destabilisation (jadeite + kyanite + zoisite + quartz) and water at high pressure (Fig. 2A, yellow line). Due to the aforementioned simplifications the modelled data is not identical to field data, but has the same general behaviour: a jump in density and amount of fluid stored in minerals between granulite and eclogite.

When solid-fluid interactions are considered, it is the fluid pressure that determines which phases are stable in a local equilibrium domain, rather than the mean stress (e.g. Dahmen, 1992). Indeed, Llana-Fúnez et al. (2012) experimentally demonstrated that metamorphic reactions are controlled by fluid pressure rather than by confining pressure. Fluid pressure is therefore an appropriate macroscopic proxy of the pressure that rocks are in equilibrium with, but in the absence of porosity there is no fluid pressure. Hence, throughout this study we use the general term "pressure" ( $P$ ) to designate both fluid pressure in porous rocks and mean stress in rocks without porosity.

### 2.2.2. Look-up tables

The solid density  $\rho_s$ , fluid density  $\rho_f$ , and the amount of fluid structurally bound in the solid  $X_{\text{H}_2\text{O}}$  at each pressure are precomputed with the thermodynamic model described above, for use as look-up tables during simulations:

$$\rho_s = \rho_s(P), \quad (11a)$$

$$\rho_f = \rho_f(P), \quad (11b)$$

$$X_{\text{H}_2\text{O}} = X_{\text{H}_2\text{O}}(P). \quad (11c)$$

Additionally, an inverse look-up table can be computed using these data. At any given pressure, the values of  $\rho_s$ ,  $\rho_f$  and  $X_{\text{H}_2\text{O}}$  are thermodynamically constrained (equation (11)). Since the value of  $\rho_T^s$  is a known parameter of the model,  $\phi$  can be computed at any pressure as well, using equation (9).  $\phi$ ,  $\rho_s$  and  $\rho_f$  can then be used to compute  $\rho_T$  with equation (1), ending up with a total mass look-up table ( $\rho_T = \rho_T(P)$ , Fig. 2B).  $\rho_T$  must monotonously increase with pressure, which is a consequence of thermodynamic

stability (e.g. Landau and Lifshitz, 1980). Hence, for every given pressure there is a uniquely corresponding  $\rho_T$ . This uniqueness makes the inverse statement true: for every given  $\rho_T$  there is one uniquely corresponding pressure. We therefore have an inverse look-up table of the form:

$$P = P(\rho_T). \quad (12)$$

This inverse look-up table approach allows our model to account for both porous and non-porous regions. There is thus no need to assume an artificially low porosity in the non-porous domain.

### 2.3. Solving procedure

All partial differential equations are approximated with a finite-difference discretisation (e.g. Gerya, 2019). Our HC model consists of a closed system of 6 unknowns ( $\rho_s$ ,  $\rho_f$ ,  $X_{H_2O}$ ,  $\rho_T$ ,  $\phi$ ,  $P$ ) and 6 equations (8), (9), (11a), (11b), (11c), (12). We use a pseudo-transient method (e.g. Räss et al., 2022) to iteratively solve these 6 equations until a converged solution is found, proceeding as follows:

1. Use the forward look-up tables (equation (11)) to compute  $\rho_s$ ,  $\rho_f$  and  $X_{H_2O}$  as a function of  $P$ ,
2. Rearrange equation (9) to solve for  $\phi$  as a function of  $\rho_s$  and  $X_{H_2O}$ :

$$\phi = 1 - \frac{\rho_T^s}{\rho_s(1 - X_{H_2O})}, \quad (13)$$

3. Explicitly solve equation (8) to compute  $\rho_T$  as a function of  $\phi$ ,  $P$  and  $\rho_f$ :
4. Use the inverse look-up table (equation (12)) to compute  $P$  as a function of  $\rho_T$ .

In practice, at each time step we iterate this set of equations until the difference in calculated pressure from one iteration to another is smaller than a chosen convergence tolerance.

### 2.4. Model configuration

The parameters of our reference model are chosen to be close to natural values reported in the literature. Unless stated otherwise, all simulations displayed in this study use the parameters described below and shown in Table 1.

#### 2.4.1. Starting conditions

A common explanation of the development of eclogitisation zones (e.g. Austrheim, 1987; Zertani et al., 2019; Kaatz et al., 2021) can be summarised as follows: (1) Lower crustal earthquakes cause stress pulses and propagate fractures in the brittle granulite, which act as a pathway for fluids. (2) Fluid availability triggers eclogitisation. (3) Infiltration of fluid into the granulite further promotes eclogitisation. Our model reproduces this configuration (Fig. 3): when the simulation starts, the entire domain is made up of granulite, with pressure set at  $P_{bg} = 15$  kbar, close to the pressure of seismic faulting reported by Bhowany et al. (2018). In the centre of the domain a pulse of high fluid pressure is applied to a narrow band ( $w_0 = 1$  cm), mimicking the initial crack that allows for fluid flow into the granulite host-rock. Introducing the shorthand notation  $\Delta P_r = P_r - P_{bg}$ , with  $P_r$  the reaction pressure, that expresses the increase in pressure needed for the granulite to cross the reaction, it is clear that the pressure pulse must be greater than  $\Delta P_r$

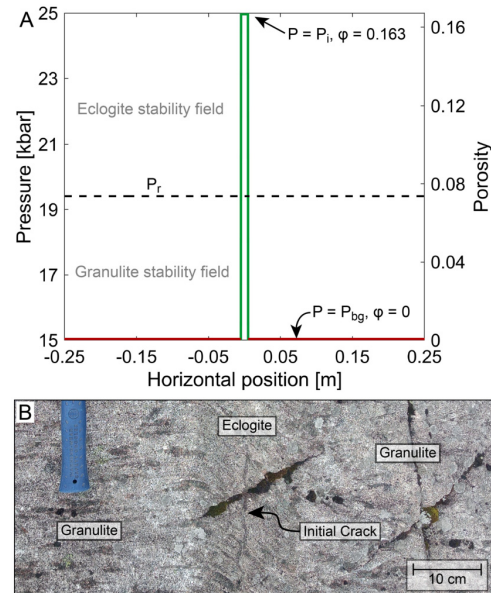


**Fig. 3.** Model configuration. (A) Initial profiles of pressure and porosity. All the domain is made up of granulite with no porosity initially placed at 15 kbar ( $P_{bg}$ , red line), except the central narrow crack that is submitted to a high fluid pressure pulse. This initial pressure  $P_i$ , higher than the reaction pressure  $P_r$  (dotted line), is enough to trigger eclogitisation and generate porosity (green line). (B) Detail of the shear zone from photograph 1A (top view) with features comparable to our configuration: a central narrow crack cutting through the granulite, from which the eclogitisation front propagates.

to trigger eclogitisation. The pressure of the fluid pulse is set at  $\Delta P_f = 10$  kbar, consistent with estimates of possible overpressure in Holsnøy (Centrella, 2019; Jamtveit et al., 2018b; Moulas et al., 2022), and fluid pressure pulses in other geological contexts (e.g. Vrijmoed et al., 2009; Viate et al., 2018). A study of the effect of  $\Delta P_f$  is presented in the result section. To assert the robustness of our approach, the initial pressure perturbation is applied as a step function:  $P = 25$  kbar in the central crack and 15 kbar in the background.

#### 2.4.2. Pressure pulse duration

Episodic high fluid pressure pulses in eclogite-facies rocks have been linked to dehydration reactions (Taetz et al., 2018; Hoover et al., 2022). Indeed, dehydration of adjacent units of the subducting plate can cause accumulation of pore fluids, resulting in periodic fluid pressure pulses that may cause brittle failure (Audet et al., 2009; Broadwell et al., 2019). Viate et al. (2018) showed that metamorphic rocks can record such fluid overpressure events.

The scenario we model is consistent with these observations. A fluid pressure pulse is applied in the central crack during a period  $t_p = 50$  days, that can be interpreted as a single short pulse, or a series of very short-lived pressure pulses. This is consistent with the study of Malvoisin et al. (2020), who conclude that eclogitisation of dry granulite promotes further earthquake generation, which can self-sustain the presence of high pressure pulses. It is also in agreement with the study of Putnis (2021) who argue that the transition in texture and composition from an untransformed granulite to an eclogite finger suggest a series of fluid pulses that advance the eclogitisation front into the granulite. Sporadic fluid pressure pulses can also be related to seismic aftershocks (Jamtveit et al., 2018a).

During the 50 days of the fluid pulse event, the model is an open system and the pressure in the initial crack is always  $P_{bg} + \Delta P_f = 25$  kbar. This period is thereafter referred to as the open

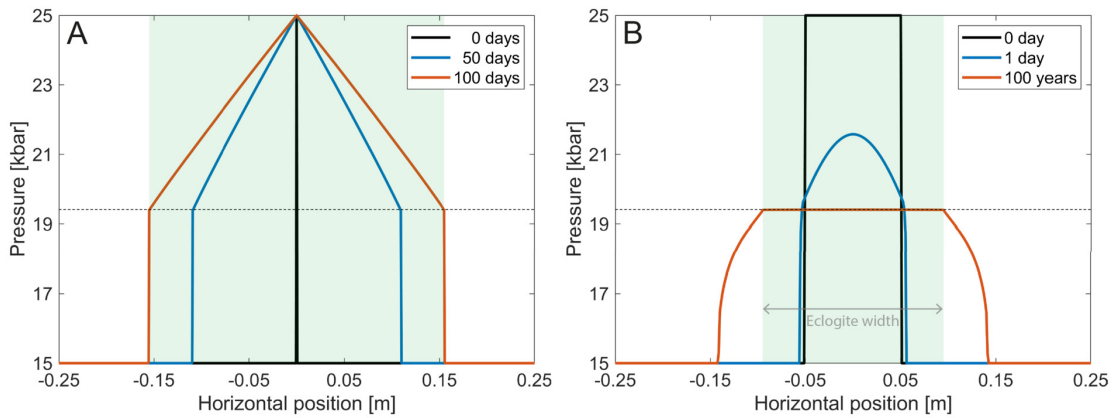


**Fig. 4.** Introductory examples to the hydro-chemical model. Light green areas represent the eclogite width after 100 years. A: Open system. In the centre of the domain, the pressure is always fixed at 25 kbar as a boundary condition. This corresponds to a fluid pulse that is continuously supplied by the central crack. B: Closed system. There is no fluid supply except the initial step-like pressure profile that decays rapidly, and then slowly diffuses into the granulite. Notice the difference in time scales between A and B.

system period. After the first 50 days, the system closes and the pressure is free to drop in the initial crack. This period is referred to as the closed system period and lasts another 50 days, after which the simulation ends. Kaatz et al. (2021) likewise considered both open and closed systems, but in terms of amount of available fluid instead of fluid pressure.

#### 2.4.3. Total solid mass

To assert the robustness of our approach, we set the background granulite porosity to 0 by using equation (9): given that  $X_{\text{H}_2\text{O}} = 0$  in granulite, we set  $\rho_T^s = \rho_s$  to ensure that  $\phi = 0$ . In other words, the solid mass per unit volume  $\rho_T^s$  must be equal to the density of granulite at 15 kbar, i.e.  $2685 \text{ kg} \cdot \text{m}^{-3}$  (Fig. 2B). In the central crack, where the total pressure is higher than the reaction pressure, the granulite of density  $2685 \text{ kg} \cdot \text{m}^{-3}$  is replaced by eclogite, with a density of  $3228 \text{ kg} \cdot \text{m}^{-3}$ . As the total solid mass is conserved (equation (9)), the porosity in the eclogite increases from 0 to 16% (Fig. 2C).

#### 2.4.4. Permeability and fluid viscosity

In a Carman-Kozeny type relationship, the permeability is equal to  $k_0\phi^3$ , where  $k_0$  is a permeability coefficient and  $\phi$  the porosity. In our model, eclogite porosity is around 0.16 (Fig. 2C). Using a permeability coefficient  $k_0 = 10^{-19} \text{ m}^2$  yields an eclogite permeability of  $4 \times 10^{-22} \text{ m}^2$ , consistent with estimates of crustal permeability by Shmonov et al. (2003) or Mindaleva et al. (2020). Granulite permeability is 0 because its porosity is 0. We use a dynamic fluid viscosity  $\eta_f = 10^{-3} \text{ Pa} \cdot \text{s}$ , consistent with Audébat and Keppler (2004); Hack and Thompson (2011).

#### 2.5. Validation of the model: resolution test

Resolution tests in both space and time were performed and are presented in supplementary figures S1 and S2. The results of tests for spatial resolution (S1) show convergence with increasing resolution, indicating that the employed finite differences discretisation is appropriate for HC modelling. We use 400 numerical grid points for the discretisation in space. One simulation can be computed in a few minutes on a standard laptop. Changing the time resolution (Courant–Friedrichs–Lowy condition, CFL) does not affect the predicted eclogite width (S2A) and has very little effects on the modelled pressure (S2B).

### 3. Results

#### 3.1. Introductory examples

Fig. 4 illustrates the behaviour of the two end-member cases described previously: open system with a fluid pulse continuous in time, and closed system with an instantaneous fluid pulse only during the first numerical time step. The separate study of these two cases is useful to understand the following HC models that include both behaviours.

##### 3.1.1. Open system

Fig. 4A shows the behaviour of an open system. The high pressure perturbation in the centre of the domain is maintained, mimicking a continuous fluid supply, or a succession of fluid pressure pulses very close in time. This results in a continuous influx of mass into the system, since  $\rho_T = \rho_T(P)$  (Fig. 2B). The rest of the configuration is identical to that presented in Fig. 3, except that the pressure perturbation is applied at only one numerical grid point. The continuous high pressure perturbation creates a pressure gradient between the crack and the granulite, leading to a fast hydration due to high Darcy flow. The eclogitisation zone expands rapidly from the crack, and is around 30 cm wide after 100 days.

##### 3.1.2. Closed system

Fig. 4B shows the behaviour of a closed system. Here, there is no additional supply of fluid pressure after the initial pressure perturbation, so the total mass present in the system is conserved. In a few days, the pressure profile evolves from the initial pressure perturbation to a plateau at the reaction pressure  $P_r$ . Afterwards, this plateau widens, although much more slowly than in the open system case, and persists long after the initial pressure perturbation has decayed.

#### 3.2. Reference model

The time evolution of our reference model is presented in Fig. 5, with a total simulation time of 100 days. The system is open during the first half of the simulation, with a behaviour similar to Fig. 4A, and is closed during the second half, with a behaviour similar to Fig. 4B. Granulite instantaneously transforms into eclogite when the pressure leaves the granulite stability field. Because of the densification reaction, the eclogitisation zone is characterised by a high reaction-induced porosity. The eclogitisation zone

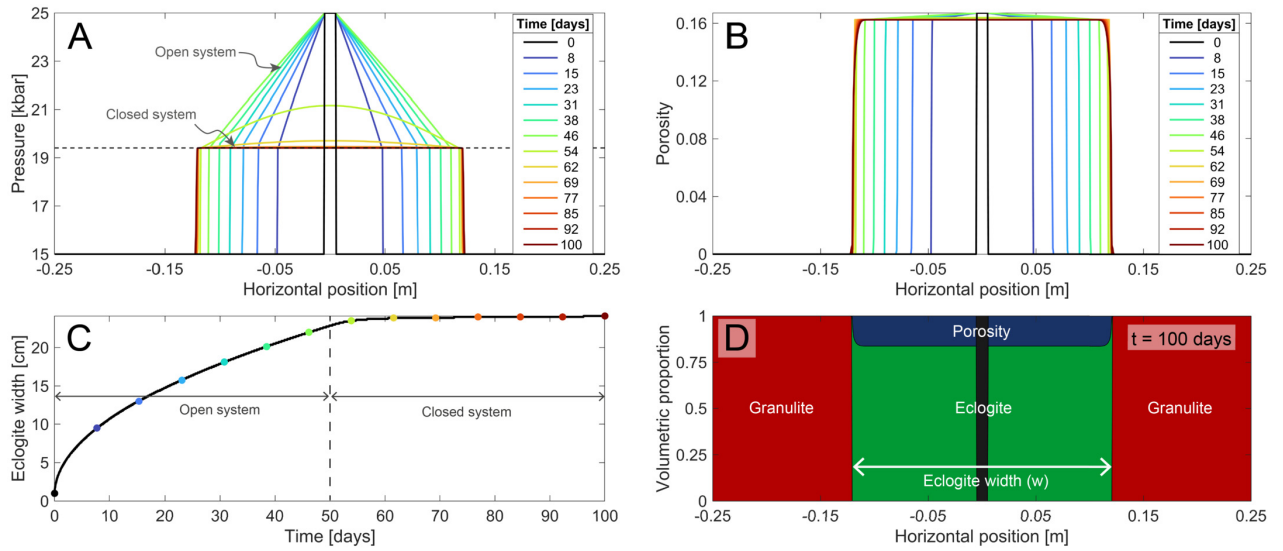


**Fig. 5.** Result of a simulation after 100 days. The fluid pulse lasts 50 days with a behaviour similar to the model of Fig. 4A, and then the fluid supply ends, rapidly shifting to the behaviour shown in Fig. 4B. (A) Evolution of the pressure and (B) evolution of the porosity with time. (C) Evolution of the width of the eclogitisation zone over time. The colour dots correspond to profiles in A and B. (D) Phase composition at the end of the simulation (100 days). The narrow black region shows the region where the fluid pulse is applied, of width  $w_0 = 1$  cm. It is already eclogitised at the start of the simulation.

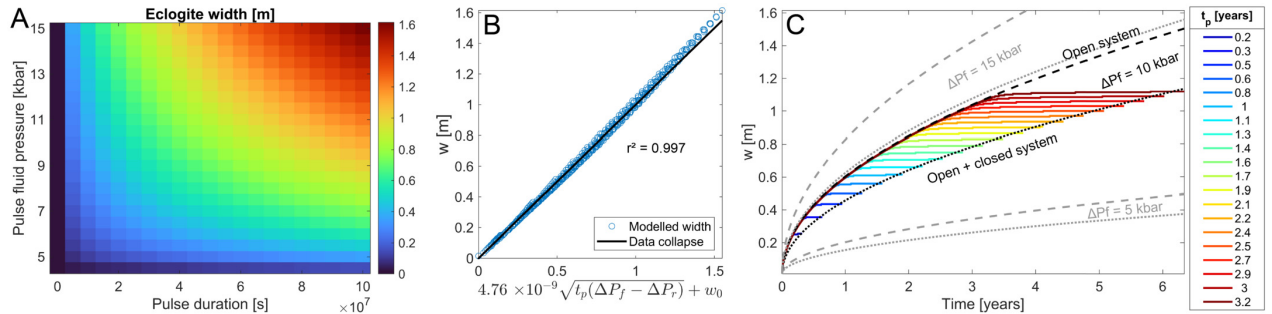


**Fig. 6.** Parametric study. (A) Eclogitisation zone width  $w$  as a function of the duration of the fluid pulse  $t_p$  and of the fluid pressure of the pulse  $\Delta P_f$ . The duration of the simulation is  $2 \times t_p$  for all simulations. (B) Data collapse for the eclogite width at the end of the simulation (open + closed system). See text for details and explanation of the parameters. (C) Time evolution of the eclogite width  $w$  for different  $t_p$  and  $\Delta P_f$ . The colour lines show the modelled time evolution for 6B and equation (15) with  $\alpha = 4.76 \times 10^{-9}$ , for the indicated  $\Delta P_f$ . The dashed lines show the eclogite width time evolution predicted by equation (15) with  $\alpha = 4.47 \times 10^{-9}$ . The predictive lines align closely to the modelled colour lines. Colour lines for the other  $\Delta P_f$  are not plotted to reduce cluttering on the diagram, but they would align with the dotted and dashed lines in a similar fashion.

spreads rapidly during the open system phase, from its initial width of 1 cm to 23 cm in 50 days (Fig. 5C). During the closed system stage the eclogite width increases only slightly, from 23 to 26 cm. Most of the widening occurs while the system is open, i.e. when a fluid pressure perturbation is active. At the end of the simulation the system is composed of a central eclogite region with  $P = 19.4$  kbar and  $\phi = 0.16$ , with a sharp transition to the granulite region with  $P = 15$  kbar and  $\phi = 0$ .

### 3.3. Parametric study

Simulations with varying duration of the pulse ( $t_p$ ) and varying magnitude of the fluid pressure pulse ( $\Delta P_f$ ) were performed in order to determine how they affect the width of the eclogitisation zone (Fig. 6). Each simulation lasts for twice the duration of the fluid pulse: if  $t_p = 50$  days, the simulation stops after 100 days. This allows us to compare the width of the eclogitisation zones in the same closed-system conditions. Every other parameter is the same as in the reference model (Table 1, results in Fig. 5). Fig. 6A shows that  $t_p$  and  $\Delta P_f$  both contribute to increasing the width of

the eclogitisation zone. Since eclogitisation occurs when  $P$  reaches the reaction pressure  $P_r$ , any model with a pressure pulse lower than  $\Delta P_r = 4.4$  kbar yields an eclogite width of 0.

Using the data displayed in Fig. 6A, we derived a formula for the width of an eclogitisation zone  $w$  as a function of  $t_p$ ,  $\Delta P_f$ , the width of the initial crack  $w_0$  and the pressure increase required to eclogitise the granulite  $\Delta P_r$ :

$$w \approx \alpha \sqrt{t_p(\Delta P_f - \Delta P_r)} + w_0, \quad (15)$$

where  $\alpha$  is a constant determined empirically (with unit  $m \cdot Pa^{-0.5} \cdot s^{-0.5}$ ), and with  $t_p$  in seconds,  $\Delta P_f$  and  $\Delta P_r$  in Pascals,  $w$  and  $w_0$  in metres. For a simulation time that is twice the duration of the open system,  $\alpha = 4.76 \times 10^{-9} m \cdot Pa^{-0.5} \cdot s^{-0.5}$ . This formula predicts  $w$  with little deviations from the expected value (Fig. 6B,  $r^2 = 0.997$ ), and is shown with the dotted line on Fig. 6C. For a simulation that only lasts until the system closes,  $w$  is predicted by equation (15) with a constant  $\alpha = 4.47 \times 10^{-9} m \cdot Pa^{-0.5} \cdot s^{-0.5}$ , and is shown with the dashed line on Fig. 6C. For a given  $\Delta P_f$ , the time evolution of a model follows closely the widths predicted by equation (15).

Equation (15) shows that  $w$  has a square root dependency to the duration of the pulse  $t_p$  and to the pulse pressure overstep, relative to the reaction pressure,  $\Delta P_f - \Delta P_r$ . For our reference model, with parameters  $t_p = 4.3 \times 10^6$  s (50 days),  $\Delta P_f = 10^9$  Pa,  $\Delta P_r = 4.4 \times 10^8$  Pa, and  $w_0 = 0.01$  m, equation (15) yields  $w = 0.24$  m, very close to the modelled value (Fig. 5). With parameters  $t_p = 1.58 \times 10^8$  s (5 years),  $\Delta P_f = 5 \times 10^8$  Pa,  $\Delta P_r = 4.4 \times 10^8$  Pa, and  $w_0 = 0.01$  m, equation (15) yields  $w = 0.47$  m.

## 4. Discussion

### 4.1. General features of the HC model

#### 4.1.1. Time evolution of the system

Our results show that a very sharp pressure/porosity reaction front can propagate into a rock that has zero porosity, and hence, zero permeability. When the system is open and is driven by a high pressure gradient, eclogite width increases as a function of  $\sqrt{t}$ , which is typical of a diffusion process (e.g. Turcotte and Schubert, 2002), although the model does not explicitly solve a diffusion equation.  $\Delta P_f$  is as important as  $t_p$  in the widening of eclogitisation zones: the pressure gradient determines how fast fluid can flow into the dry granulite.

When the system closes, the impermeability of granulite causes the fluid flow to be extremely slow, preventing fluid pressure diffusion. As a result, the high pressure plateau persists long after the end of the short-lived fluid pressure pulse (Figs. 4b, 5a), preserving the eclogitisation zone without any sustained pressure perturbation.

In our reference model (Fig. 5), a 25 cm wide eclogitisation zone can form in 100 days. This result is in agreement with that of Beinlich et al. (2020), who show that a reaction front can advance as fast as 10 cm per year, and with that of Taetz et al. (2018), who show that the duration of fluid-rock interaction in an eclogite mélange is 1 to 4 months. Our time estimate is also close to that of the hydro-mechanical-chemical model of Malvoisin et al. (2020), who conclude that eclogitisation of granulite can occur on the order of weeks.

#### 4.1.2. Contribution of compressibility and eclogitisation to front propagation

Two processes contribute to an increase in solid density, and thus an increase in porosity: compressibility (increase in density of a given phase with increasing pressure) and eclogitisation (replacement of low density minerals by high density minerals). We compared the importance of these two processes by switching them on and off in different simulations (Fig. 7). The results show that both effects contribute to the widening of the hydration zone. Eclogitisation generates most of the porosity by a significant increase in solid density, creating a stronger fluid flow and therefore a faster hydration front. Compressibility creates only little porosity, and therefore limited hydration.

#### 4.1.3. Simplifications of the 1D HC model

**Permeability.** We consider a homogeneous, isotropic-permeable rock, whereas metamorphic rocks can have anisotropic permeabilities that are 1 to 2 orders of magnitude higher along the metamorphic fabric than in the normal direction (e.g. Acosta and Violay, 2020). This anisotropy cannot be included in our 1D model, but a 2D model would allow to model preferential growth of eclogite fingers in the direction of the metamorphic fabric of the granulite (Putnis et al., 2021).

**Deformation.** The aim of the present paper is to show, with a simple hydro-chemical model, that a high pressure perturbation, here caused by a fluid pulse, can propagate and drive a reactive

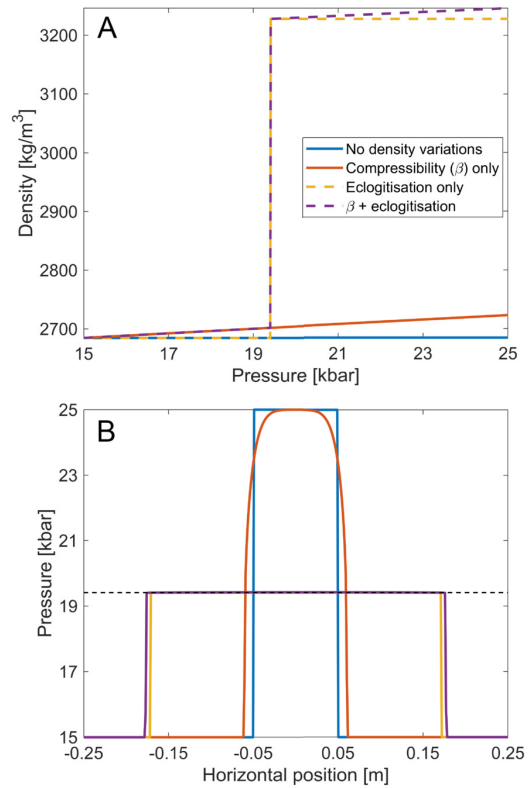


**Fig. 7.** Effect of density changes on the widening of an eclogitisation zone. (A) Solid density as a function of pressure for 4 different scenarios. Blue: the solid is incompressible and non-reactive; its density never increases. Orange: the solid is non-reactive; its density only increases due to compressibility. Yellow: the solid is incompressible, its density only increases due to transformation of granulite into eclogite. Purple: the solid density increases due to compressibility and transformation of granulite into eclogite, as used throughout this study. (B) Pressure profiles after 100 days. The blue profile is identical to the initial pressure profile. Thickness of the initial perturbation (compared to Figs. 3, 5) was increased for clearer visualisation.

porous fluid flow into an impermeable rock. Coupling shear deformation with hydro-chemical processes is out of the scope of this study, and an extension of our work would include viscous deformation in order to simulate the growth of shear zones. During deformation, the weak shear zones could exhibit larger pressures than the strong, dry host-rock, if they have a suitable orientation relative to the background stress field (Moulas et al., 2014; Jamtveit et al., 2018b). Stress caused by shear deformation could self sustain the high pressure anomaly in the shear zone and promote hydration front propagation and shear zone widening.

## 4.2. Applications to Holsnøy case study

### 4.2.1. High pressure sustainability in eclogite

In Holsnøy, eclogitisation occurs in (1) eclogite shear zones, that undergo deformation during eclogitisation (e.g. Austrheim, 1987; Bras et al., 2021), and (2) eclogite fingers that undergo static eclogitisation without associated macroscopic deformation (e.g. Jamtveit et al., 2000; Zertani et al., 2019; Baïsset et al., 2023). In our model we attribute overpressure only to a short-lived fluid pressure pulse, but additional causes of overpressure may be at play, in both eclogite fingers and shear zones.

**Eclogite fingers.** Consistent with our work, Putnis (2021) inferred a pressure gradient from the host-rock granulite to an eclogite finger, deducing that the eclogite finger experienced a higher

pressure. It was also shown (Jamtveit et al., 2000; Baïsset et al., 2023) that static eclogitisation of granulite causes perturbation in the local stress field, and could accelerate the propagation of fluids. Yamato et al. (2022) recently proposed that eclogitisation-induced densification of reacting granulite can generate sufficient shear stress to fail the rocks, and self-propagates eclogitisation in a finger-like structure. Reaction-induced densification therefore appears to be a likely mechanism that can sustain high pressures where eclogitisation takes place.

**Shear zones.** Sustained high pressure in eclogite shear zones can be achieved by weakening-induced overpressure (Jamtveit et al., 2018b), and numerous studies showed that eclogitisation mechanically weakens the granulite (Jolivet et al., 2005; Bras et al., 2021; Baïsset et al., 2023; Kaatz et al., 2023). This weakening can have crucial effects: Mancktelow (1993) showed that in deforming rocks, weak and strong layers can experience pressure differences of several kbar. Numerical simulations and analytical solutions show that the presence of a weak shear zone within a strong stressed lower crust can significantly increase the pressure inside the shear zone, potentially more than 10 kbar (Schmalholz and Podladchikov, 2013; Moulas et al., 2014; Jamtveit et al., 2018b; Moulas et al., 2022). The relevance of weakening induced pressure variations has also been suggested based on field observations (e.g. Luisier et al., 2019). Weakening-induced pressure increase in eclogite shear zones is therefore probably significant (Jamtveit et al., 2018b) and could self-sustain overpressure in the eclogite, efficiently promoting fluid flow and further eclogitisation of the dry lower crust.

#### 4.2.2. Metastability

As stated in the introduction, there is currently a debate on the pressure state of granulite in Holsnøy: the juxtaposition of eclogite and granulite regions can be either interpreted as (1) metastability of granulite at eclogite-facies conditions at 21 kbar (Bhowany et al., 2018) or (2) local pressure variations between granulite and eclogite (see discussion in Putnis et al., 2021). Here, we show that the local pressure hypothesis is consistent with widening of eclogitisation zones. However, we can also test the metastable hypothesis with two modifications to our numerical code:

1. Set the background pressure to 21 kbar, and
2. Change the reaction pressure from the value predicted by thermodynamic modelling (19.4 kbar) to 21.01 kbar, just above the background pressure.

By doing so, granulite is stable up to 21 kbar, at eclogite pressure conditions. Any little increase in pressure caused by fluid flow triggers the transition from granulite to eclogite, satisfyingly reproducing the metastable behaviour where the reaction is triggered by a fluid influx. We here use a pressure of 21 kbar, close to the peak pressure estimated by Bhowany et al. (2018), but any pressure greater than  $P_r$  could be used. The general behaviour of the system is the same as in the stable scenario (see supplementary figure S3), the only difference being a wider eclogitisation zone in the metastable case (32 cm) compared to the stable case (24 cm). Although metastable granulite does not thermodynamically require a large pressure increase to transform into eclogite, a pressure gradient is still necessary to drive the fluid into the dry granulite by Darcy flow.

#### 4.3. Reaction front propagation controlled by density of solid components

##### 4.3.1. Theoretical considerations

We showed that the widening of high pressure hydrated zones is possible in the case of the granulite to eclogite transformation.

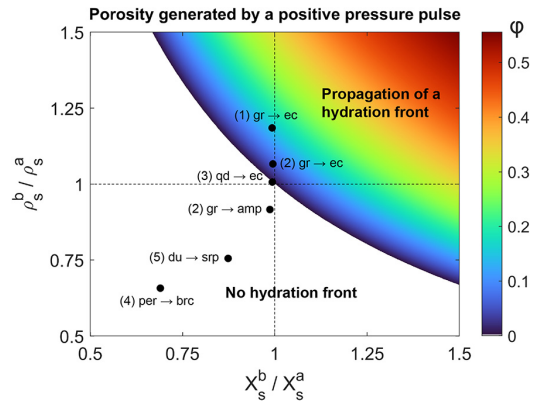


**Fig. 8.** Porosity generated by the transformation of a low pressure rock a (with solid density  $\rho_s^a$  and proportion of non volatile component  $X_s^a$ ) into a high pressure rock b (with  $\rho_s^b$  and  $X_s^b$ ). Porosity is created only when the reaction increases the solid mass stored in the solid, i.e.  $X_s^b \rho_s^b > X_s^a \rho_s^a$ . Reactions in the white field do not generate porosity. Abbreviations: gr = granulite; ec = eclogite; amp = amphibolite; qd = quartz-diorite; per = periclase; brc = brucite; du = dunite; srp = serpentinite; atg = antigorite. Source of  $\rho_s$  and  $X_s$  data: (1) This work, (2) Centrella (2019); (3) Früh-Green (1994); (4) Schmalholz et al. (2020); (5) Malvoisin et al. (2021).

In a general case, propagation of a hydration front in a dry rock is only possible if the metamorphic reaction induces porosity, otherwise the fluid could not flow and no hydration would occur. In our hydro-chemical model without solid deformation, porosity is constrained by rock properties, which implies that changes in thermodynamic properties caused by a metamorphic reaction are enough to predict whether it generates porosity. Since we consider that solid mass is only stored in the solid phase and not in the fluid phase, equation (9) can be used to describe the transformation of a protolith (rock a) with solid density  $\rho_s^a$ , mass fraction of volatile components in the solid  $X_{\text{H}_2\text{O}}^a$  and no porosity, into a transformed rock b with  $\rho_s^b$ ,  $X_{\text{H}_2\text{O}}^b$  and reaction-induced porosity  $\phi_r$ :

$$\rho_T^s = \rho_s^a (1 - X_{\text{H}_2\text{O}}^a) = \rho_s^b (1 - X_{\text{H}_2\text{O}}^b)(1 - \phi_r). \quad (16)$$

Introducing the notation for the mass fraction of solid components in the solid  $X_s = 1 - X_{\text{H}_2\text{O}}$ , equation (16) is used to compute the porosity generated by the reaction from rock a to rock b:

$$\phi_r = 1 - \frac{\rho_s^a X_s^a}{\rho_s^b X_s^b}. \quad (17)$$

The reaction generates porosity when  $\phi_r$  is greater than 0, which is true only if:

$$\rho_s^b X_s^b > \rho_s^a X_s^a, \quad (18)$$

i.e. if the metamorphic reaction increases  $\rho_s X_s$ . Equation (18) can be rearranged as:

$$\frac{X_s^b}{X_s^a} > \frac{1}{\rho_s^b / \rho_s^a}. \quad (19)$$

Fig. 8 shows the porosity created by the metamorphic reaction that transforms rock a into rock b with increasing pressure, excluding any solid deformation. No porosity is created in the white field because reactions in this field decrease the amount of solid mass stored in the solid ( $\rho_s^b X_s^b < \rho_s^a X_s^a$ ). As expected from equation (19), the boundary between the two regions follows an inverse relationship. On Fig. 8, reactions are displayed on a prograde path: rock a is stable at low pressure and rock b at high pressure. Only the prograde reactions in the top right field of the diagram can propagate

into a rock with no porosity, through a positive pressure pulse. If reactions in the white field (e.g. periclase  $\rightarrow$  brucite) were instead displayed on a retrograde path (brucite  $\rightarrow$  periclase), they would appear in the colour field, meaning that these reverse reactions can propagate a low pressure perturbation into a no porosity, high pressure region. This is for instance the case in the study of Schmalholz et al. (2020), who show with numerical model similar to ours that a front of low pressure, dense periclase can propagate into a high pressure, low density brucite region.

Two situations are hence capable of generating a reaction/pres-  
sure front that propagates into a zero-porosity region. If the high  
pressure rock has a higher  $\rho_s X_s$  than the low pressure rock (colour  
field in Fig. 8), a sharp high pressure, high density front can prop-  
agate into a low pressure, low-density rock. Conversely, if the high  
pressure rock has a lower  $\rho_s X_s$  than the low pressure rock (white  
field), a sharp low pressure, high density front can propagate into  
a high pressure, low-density rock. Such situations were also dis-  
cussed by Malvoisin et al. (2015), although they described these  
systems in terms of negative and positive Clapeyron slopes instead  
of, respectively, increase and decrease of  $\rho_s X_s$ . They showed that a  
sharp pressure/porosity front propagates only for negative Clapey-  
ron slope and positive pressure pulses, and for positive Clapeyron  
slopes and negative pressure pulses.

#### 4.3.2. Applications

Even if  $X_s$  and  $\rho_s$  changes contribute in exactly the same manner to reaction-induced porosity, in natural metamorphic reaction changes in density are generally much greater than changes in  $X_s$ . For instance the data of Centrella (2019) shows that eclogitisation of granulite increases density by 7%, but decreases  $X_s$  by only 0.5%. Therefore, even if in a general case an increase in  $\rho_s X_s$  is required, in most natural cases an increase in  $\rho_s$  (a decrease in solid volume) should be sufficient to explain reaction-induced porosity in a high pressure front.

Consistent with our work, Putnis and John (2010) showed that increased porosity enhances fluid transport, mineral replacement and propagation of a reaction front. Our results suggest that in purely rigid, non-deforming rocks, only reactions which decrease the solid volume (i.e. increase solid density) would be able to efficiently propagate through generation of porosity. Hövelmann et al. (2012) experimentally showed that carbonation reaction of peridotite fills the pre-existing porosity because the reaction increases the rock volume, which ultimately self-limits the reaction.

However there is evidence that other mechanisms can generate porosity at the reactive interface, even when the reaction lowers the solid density. Jamtveit et al. (2008) showed that stress induced by volume increase can generate extensive (micro-)fracturing, which creates a connected network that allows fluid transport. In a locality nearby Holsnøy, Moore et al. (2020) described sharp amphibolitisation fronts into granulite, with enhanced permeability/porosity in the less dense amphibolite. They showed evidence of abundant mass redistribution, which our model does not account for, resulting in an overall mass loss during fluid rock interaction. This can explain generation of porosity even though amphibolitisation increases the rock volume.

Shear zones in Monte Mucrone (Italian Alps) studied by Früh-  
Green (1994) do not show evidence of widening. Their chemical  
analysis shows that in the meta-diorite protolith and the eclogite  
shear zone,  $X_s$  and  $\rho_s$  are almost identical ( $X_s^2/X_s^1 = 0.994$ ,  
 $\rho_s^2/\rho_s^1 = 1.007$ ). This indicates that the reaction, close to [1, 1]  
coordinates on Fig. 8, generate neither porosity nor fracturing in-  
duced by volume increase, and thus no hydration front that prop-  
agates into the protolith.

In general, retrogression of high grade rocks replaces dense and  
anhydrous minerals (garnet, pyroxene) by low density and/or hy-  
drous minerals (amphiboles, mica, chlorite, plagioclase). Low grade

rocks therefore generally have a lower rock density and a higher water content, i.e. a lower  $\rho_s X_s$  than higher grade rocks (e.g. Hacker et al., 2003). Our work implies that retrogression must be supported by some other porosity-generating mechanisms, such as mass transport or brittle deformation caused by volume increase. We suggest that in absence of such mechanisms, retrogression may be limited and high grade rocks may be preserved during their exhumation.

#### 4.4. Hydraulic diffusion

##### 4.4.1. Hydraulic diffusion during eclogitisation

Kaatz et al. (2022) showed that  $H_2O$  content variations across eclogite shear zones are affected by solid state diffusion of hydro-  
gen, but their work does not show if solid state diffusion plays a significant role in the widening of the eclogitisation zones. Putnis and John (2010) showed that mineral replacement during metomorphic reactions occurs by fluid transport associated with reaction-induced porosity, rather than solid state diffusion. For this reason, our model includes Darcy flow instead of solid state fluid diffusion of hydrogen and oxygen atoms into the crystalline lattice, like some papers have done in the past to model eclogitisation (Bras et al., 2021; Kaatz et al., 2023).

Nevertheless, Fig. 6 shows that the front propagation distance is proportional to the square root of time, implying that fluid transport by reactive Darcy flow is a diffusive transport, termed hydraulic diffusion (e.g. Connolly, 1997). By analogy with a general diffusion law, a hydraulic diffusivity constant  $D_H$  can be used to relate the characteristic length of diffusion  $L$  and the characteristic time of diffusion  $\tau$ :

$$L = \sqrt{D_H \tau}. \quad (20)$$

Using this relationship, a hydraulic diffusivity can be determined for the granulite-eclogite case when a fluid pulse is active, us-  
ing our empirically derived equation (15) with  $\alpha = 4.47 \times 10^{-9}$   
 $m \cdot Pa^{-0.5} \cdot s^{-0.5}$ . The characteristic length of diffusion is the dis-  
tance travelled by the hydration front, in our case  $L = \frac{w-w_0}{2}$ . The characteristic time is the duration of the fluid pressure pulse  
( $\tau = t_p$ ). Reformulating equation (15) with these parameters yields

$$L = \sqrt{\left(\frac{4.47 \times 10^{-9}}{2}\right)^2 (\Delta P_f - \Delta P_r) \tau}. \quad (21)$$

The ratio of permeability coefficient to fluid viscosity  $k_0/\eta_f$  has a first order control on the timing of the hydration process. Tests for varying simulation times  $t$  and  $k_0/\eta_f$  indeed show that the results of our model are not only a function of  $t$ , but rather  $t \times k_0/\eta_f$  (supplementary figure S4). As an example, in a simulation where  $k_0/\eta_f$  is 10 times greater than our reference model, the results displayed on Fig. 5 appear after 10 days instead of 100. We can therefore introduce the  $k_0/\eta_f$  ratio in equation (21):

$$L = \sqrt{0.05 \frac{k_0}{\eta_f} (\Delta P_f - \Delta P_r) \tau}. \quad (22)$$

Substituting equation (22) into equation (20) yields an equation for  $D_H$ :

$$D_H \approx 0.05 \frac{k_0}{\eta_f} (\Delta P_f - \Delta P_r). \quad (23)$$

In our reference model where  $k_0/\eta_f = 10^{-16} m^3 \cdot s \cdot kg^{-1}$  and  $\Delta P_f - \Delta P_r = 5.6 \times 10^8$  Pa, equation (23) yields a hydraulic dif-  
fusivity in the order of  $10^{-9} m^2 \cdot s^{-1}$ . This is orders of magnitude

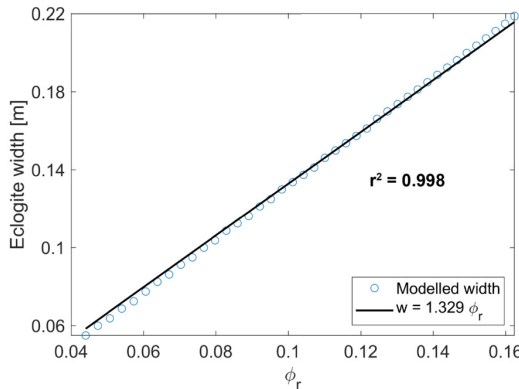


**Fig. 9.** Linear fit of hydration zone width as a function of reaction-induced porosity  $\phi_r$ . The width of the hydration zone increases linearly with  $\phi_r$ . The parameters of the simulations are the same as in the reference model, except  $w_0 = 0$  m. The simulation ends when the system closes, after 50 days.  $\phi_r$  is set by modifying the densities of granulite and eclogite in the look-up table.

higher than solid state diffusivity of hydrogen or oxygen atoms in rock forming minerals, that range from  $10^{-11}$  to  $10^{-18}$  m $^2$  · s $^{-1}$ , in most cases  $10^{-13}$  to  $10^{-15}$  m $^2$  · s $^{-1}$ , at temperatures relevant for this study (Ingrin and Blanchard, 2006; Farver, 2010). Our work therefore shows that the propagation of a reacting hydration front by porous flow is a diffusive process that is potentially orders of magnitudes faster than solid-state diffusion.

#### 4.4.2. General hydraulic diffusivity

Equation (23) applies to our granulite to eclogite model. In a general case, the width of the hydration zone must also be controlled by the reaction-induced porosity  $\phi_r$ . Tests with varying  $\phi_r$  (Fig. 9) reveal that the width of the hydration zone is proportional to  $\phi_r$ , therefore:

$$L = \frac{\phi_r}{\phi_r^e} \sqrt{0.05 \frac{k_0}{\eta_f} (\Delta P_f - \Delta P_r) \tau}, \quad (24)$$

where  $\phi_r^e = 0.1625$  is the porosity induced by eclogitisation of granulite (Fig. 2C). Additionally, since  $\phi_r$  is thermodynamically constrained by equation (17), we can substitute  $\phi_r$  for properties of the protolith ( $\rho_s^a, X_s^a$ ) and of the transformed rock ( $\rho_s^b, X_s^b$ ):

$$L = \left(1 - \frac{\rho_s^a X_s^a}{\rho_s^b X_s^b}\right) \sqrt{1.9 \frac{k_0}{\eta_f} (\Delta P_f - \Delta P_r) \tau}. \quad (25)$$

Substituting equation (25) into equation (20) yields a general equation for the hydraulic diffusivity  $D_H$  that can be estimated for any reaction:

$$D_H = 1.9 \left(1 - \frac{\rho_s^a X_s^a}{\rho_s^b X_s^b}\right)^2 \frac{k}{\eta_f} (\Delta P_f - \Delta P_r). \quad (26)$$

## 5. Conclusion

We present a physically consistent hydro-chemical model of eclogitisation of impermeable granulite, that can explain the widening of eclogite shear zones and eclogite fingers in Holsnøy. Our work shows that hydration of a zero-porosity rock is possible only if density changes controlled by pressure changes are taken into account: solid compressibility or metamorphic reactions. Fluid overpressure will drive a reactive, porous fluid flow into an impermeable rock, as long as the high-pressure rock is denser than its impermeable protolith. Our model can simulate any reaction inducing density changes, as well as metastable scenarios.

In our model without mechanics, overpressure is only caused by a fluid pressure pulse, and future work should take solid deformation into account. Deformation could enhance the overpressure and subsequent reactive fluid flow, as long as the high pressure rock is mechanically weaker than its protolith.

Local pressure perturbations of several kbars, caused by fluid pulses or weakening-induced overpressure, can induce reaction front propagation at a rate of tens of centimetres per year, as long as the pressure perturbation is present. The rate at which the reaction front propagates is typical of a diffusive process. This complex and coupled hydro-chemical process can hence be approximated by a diffusion law, where the diffusivity can be calculated for any reaction from the pressure gradients and rock properties.

## CRediT authorship contribution statement

**Erwan Bras:** Conceptualization, Methodology, Software, Writing – original draft. **Philippe Yamato:** Conceptualization, Writing – review & editing. **Stefan M. Schmalholz:** Conceptualization, Writing – review & editing. **Thibault Duretz:** Software, Writing – review & editing. **Yury Y. Podladchikov:** Methodology, Software.

## Declaration of competing interest

The authors declare that they have no known competing financial interests or personal relationships that could have appeared to influence the work reported in this paper.

## Data availability

All numerical results have been generated with a self-developed MATLAB code, which is available on the platform Zenodo under: <https://doi.org/10.5281/zenodo.7966767>.

## Acknowledgements

We thank Marie Bässet for her help in the field and for providing photograph 1B, and Loïc Labrousse for multiple discussions about eclogitisation processes. This work has been partially financially supported by the INSU SYSTER program (AO Tellus), and by the University of Lausanne. P.Y. thanks the Institut Universitaire de France for financial support. We thank 2 anonymous reviewers for their very insightful comments that have improved and clarified the paper, and Alex Webb for editorial handling.

## Appendix A. Supplementary material

Supplementary material related to this article can be found online at <https://doi.org/10.1016/j.epsl.2023.118256>.

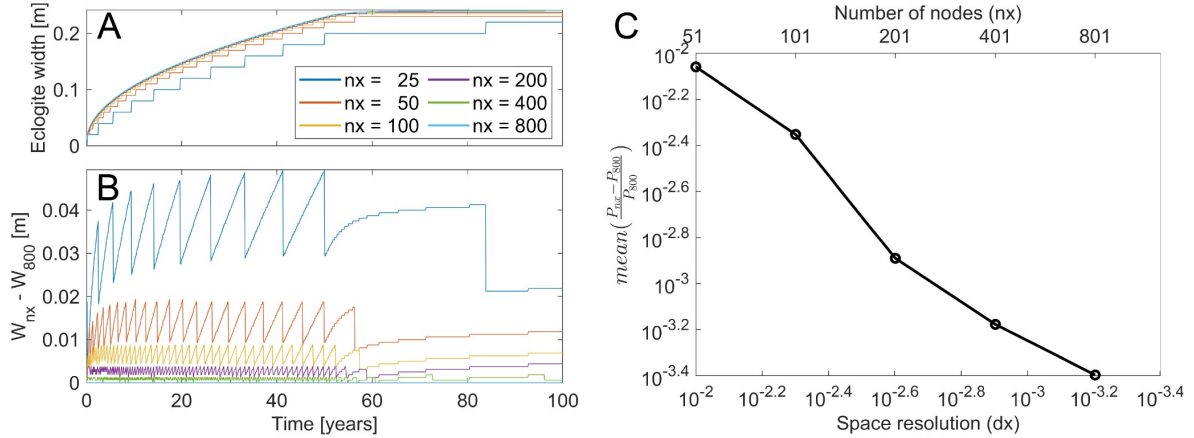
## References

- Acosta, M., Violay, M., 2020. Mechanical and hydraulic transport properties of transverse-isotropic gneiss deformed under deep reservoir stress and pressure conditions. *Int. J. Rock Mech. Min. Sci.* 130, 104235. <https://doi.org/10.1016/j.ijrmms.2020.104235>.
- Andersen, T.B., Jamtveit, B., Dewey, J.F., Swensson, E., 1991. Subduction and education of continental crust: major mechanisms during continent-continent collision and orogenic extensional collapse, a model based on the south Norwegian Caledonides. *Terra Nova* 3, 303–310. <https://doi.org/10.1111/j.1365-3121.1991.tb00148.x>.
- Arbogast, T., Hesse, M.A., Taicher, A.L., 2017. Mixed methods for two-phase Darcy-Stokes mixtures of partially melted materials with regions of zero porosity. *SIAM J. Sci. Comput.* 39, B375–B402. <https://doi.org/10.1137/16M1091095>.
- Audet, P., Bostock, M.G., Christensen, N.I., Peacock, S.M., 2009. Seismic evidence for overpressured subducted oceanic crust and megathrust fault sealing. *Nature* 457, 76–78. <https://doi.org/10.1038/nature07650>.
- Audet, A., Keppler, H., 2004. Viscosity of fluids in subduction zones. *Science* 303, 513–516. <https://doi.org/10.1126/science.1092282>.

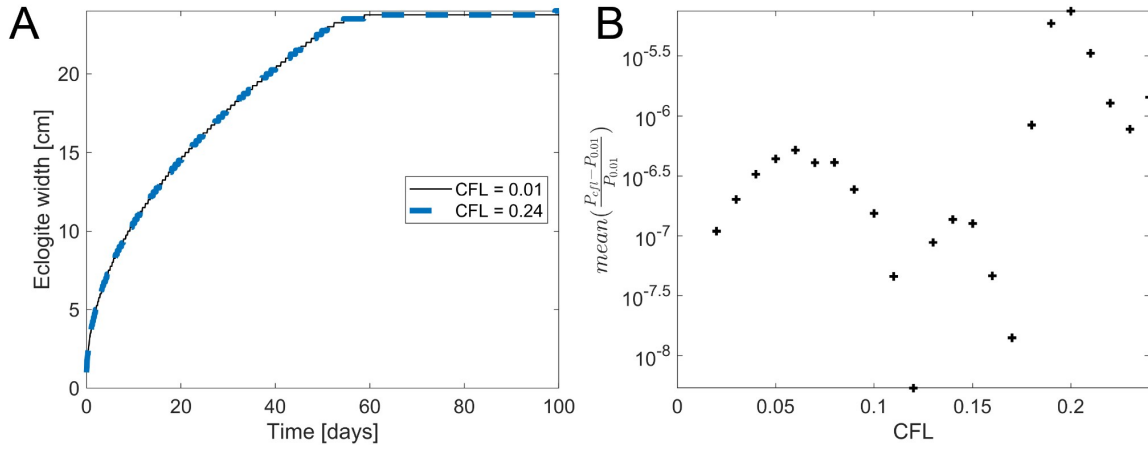
- Austrheim, H., 1987. Eclogitization of lower crustal granulites by fluid migration through shear zones. *Earth Planet. Sci. Lett.* 81, 221–232. [https://doi.org/10.1016/0012-821X\(87\)90158-0](https://doi.org/10.1016/0012-821X(87)90158-0).
- Austrheim, H., 1998. Influence of fluid and deformation on metamorphism of the deep crust and consequences for the geodynamics of collision zones. In: Hacker, B.R., Liou, J.G. (Eds.), *When Continents Collide: Geodynamics and Geochemistry of Ultrahigh-Pressure Rocks*. Springer Netherlands, Dordrecht, pp. 297–323.
- Austrheim, H., 2013. Fluid and deformation induced metamorphic processes around moho beneath continental collision zones: examples from the exposed root zone of the Caledonian mountain belt, W-Norway. *Tectonophysics* 609, 620–635. <https://doi.org/10.1016/j.tecto.2013.08.030>.
- Baïsset, M., Labrousse, L., Yamato, P., Schubnel, A., 2023. Twinning and partial melting as early weakening processes in plagioclase at high pressure: insights from Holsnøy (Scandinavian Caledonides, Norway). *Contrib. Mineral. Petrol.* 178, 19. <https://doi.org/10.1007/s00410-023-01998-x>.
- Beinlich, A., John, T., Vrijmoed, J.C., Tominaga, M., Magna, T., Podladchikov, Y.Y., 2020. Instantaneous rock transformations in the deep crust driven by reactive fluid flow. *Nat. Geosci.* 13, 307–311. <https://doi.org/10.1038/s41561-020-0554-9>.
- Bhowany, K., Hand, M., Clark, C., Kelsey, D.E., Reddy, S.M., Pearce, M.A., Tucker, N.M., Morrissey, L.J., 2018. Phase equilibrium modelling constraints on p-t conditions during fluid catalysed conversion of granulite to eclogite in the Bergen arcs, Norway. *J. Metamorph. Geol.* 36, 315–342. <https://doi.org/10.1111/jmg.12294>.
- Bingen, B., Davis, W.J., Austrheim, H., 2001. Zircon U-Pb geochronology in the Bergen arc eclogites and their Proterozoic protoliths, and implications for the pre-Scandian evolution of the Caledonides in western Norway. *Geol. Soc. Am. Bull.* 113, 640–649. [https://doi.org/10.1130/0016-7606\(2001\)113<0640:ZUPGIT>2.0.CO;2](https://doi.org/10.1130/0016-7606(2001)113<0640:ZUPGIT>2.0.CO;2).
- Bras, E., Baïsset, M., Yamato, P., Labrousse, L., 2021. Transient weakening during the granulite to eclogite transformation within hydrous shear zones (Holsnøy, Norway). *Tectonophysics* 819, 229026. <https://doi.org/10.1016/j.tecto.2021.229026>.
- Broadwell, K.S., Locatelli, M., Verlaguet, A., Agard, P., Caddick, M.J., 2019. Transient and periodic brittle deformation of eclogites during intermediate-depth subduction. *Earth Planet. Sci. Lett.* 521, 91–102. <https://doi.org/10.1016/j.epsl.2019.06.008>.
- Centrella, S., 2019. *The Granulite- to Eclogite- and Amphibolite-Facies Transition: a Volume and Mass Transfer Study in the Lindås Nappe, Bergen Arcs, West Norway. Special Publications*, vol. 478. Geological Society, London, pp. 241–264.
- Connolly, J., 1997. Devolatilization-generated fluid pressure and deformation-propagated fluid flow during prograde regional metamorphism. *J. Geophys. Res., Solid Earth* 102, 18149–18173. <https://doi.org/10.1029/97JB00731>.
- Connolly, J.A., 2005. Computation of phase equilibria by linear programming: a tool for geodynamic modeling and its application to subduction zone decarbonation. *Earth Planet. Sci. Lett.* 236, 524–541. <https://doi.org/10.1016/j.epsl.2005.04.033>.
- Costa, A., 2006. Permeability-porosity relationship: a reexamination of the Kozeny-Carman equation based on a fractal pore-space geometry assumption. *Geophys. Res. Lett.* 33. <https://doi.org/10.1029/2005GL025134>.
- Dahlen, F., 1992. Metamorphism of nonhydrostatically stressed rocks. *Am. J. Sci.* 292, 184–198. <https://doi.org/10.2475/ajs.292.3.184>.
- Farver, J.R., 2010. Oxygen and hydrogen diffusion in minerals. *Rev. Mineral. Geochem.* 72, 447–507. <https://doi.org/10.2138/rmg.2010.72.10>.
- Fruh-Green, G.L., 1994. Interdependence of deformation, fluid infiltration and reaction progress recorded in eclogitic metagranitoids (Sesia Zone, Western Alps). *J. Metamorph. Geol.* 12, 327–343. <https://doi.org/10.1111/j.1525-1314.1994.tb00026.x>.
- Gerya, T., 2019. *Introduction to Numerical Geodynamic Modelling*. Cambridge University Press.
- Hack, A.C., Thompson, A.B., 2011. Density and viscosity of hydrous magmas and related fluids and their role in subduction zone processes. *J. Petrol.* 52, 1333–1362. <https://doi.org/10.1093/petrology/egq048>.
- Hacker, B.R., Abers, G.A., Peacock, S.M., 2003. Subduction factory 1. Theoretical mineralogy, densities, seismic wave speeds, and H<sub>2</sub>O contents. *J. Geophys. Res., Solid Earth* 108. <https://doi.org/10.1029/2001JB001127>.
- Hetényi, G., Cattin, R., Brunet, F., Bollinger, L., Vergne, J., Nábělek, J.L., Diament, M., 2007. Density distribution of the India plate beneath the Tibetan Plateau: geophysical and petrological constraints on the kinetics of lower-crustal eclogitization. *Earth Planet. Sci. Lett.* 264, 226–244. <https://doi.org/10.1016/j.epsl.2007.09.036>.
- Holland, T., Powell, R., 1998. An internally consistent thermodynamic data set for phases of petrological interest. *J. Metamorph. Geol.* 16, 309–343. <https://doi.org/10.1111/j.1525-1314.1998.00140.x>.
- Hoover, W.F., Penniston-Dorland, S., Baumgartner, L., Bouvier, A.S., Dragovic, B., Locatelli, M., Angiboust, S., Agard, P., 2022. Episodic fluid flow in an eclogite-facies shear zone: insights from Li isotope zoning in garnet. *Geology* 50, 746–750. <https://doi.org/10.1130/G49737.1>.
- Hövelmann, J., Austrheim, H., Jamtveit, B., 2012. Microstructure and porosity evolution during experimental carbonation of a natural peridotite. *Chem. Geol.* 334, 254–265. <https://doi.org/10.1016/j.chemgeo.2012.10.025>.
- Incel, S., Hilairat, N., Labrousse, L., John, T., Deldicque, D., Ferrand, T., Wang, Y., Renner, J., Morales, L., Schubnel, A., 2017. Laboratory earthquakes triggered during eclogitization of lawsonite-bearing blueschist. *Earth Planet. Sci. Lett.* 459, 320–331. <https://doi.org/10.1016/j.epsl.2016.11.047>.
- Ingrin, J., Blanchard, M., 2006. Diffusion of hydrogen in minerals. *Rev. Mineral. Geochem.* 62, 291–320. <https://doi.org/10.2138/rmg.2006.62.13>.
- Jackson, J.A., Austrheim, H., McKenzie, D., Priestley, K., 2004. Metastability, mechanical strength, and the support of mountain belts. *Geology* 32, 625–628. <https://doi.org/10.1130/G20397.1>.
- Jamtveit, B., Austrheim, H., Malthe-Sørensen, A., 2000. Accelerated hydration of the Earth's deep crust induced by stress perturbations. *Nature* 408, 75–78. <https://doi.org/10.1038/35040537>.
- Jamtveit, B., Malthe-Sørensen, A., Kostenko, O., 2008. Reaction enhanced permeability during retrogressive metamorphism. *Earth Planet. Sci. Lett.* 267, 620–627. <https://doi.org/10.1016/j.epsl.2007.12.016>.
- Jamtveit, B., Ben-Zion, Y., Renard, F., Austrheim, H., 2018a. Earthquake-induced transformation of the lower crust. *Nature* 556, 487–491. <https://doi.org/10.1038/s41586-018-0045-y>.
- Jamtveit, B., Moula, E., Andersen, T.B., Austrheim, H., Corfu, F., Petley-Ragan, A., Schmalholz, S.M., 2018b. High pressure metamorphism caused by fluid induced weakening of deep continental crust. *Sci. Rep.* 8, 17011. <https://doi.org/10.1038/s41598-018-35200-1>.
- Jamtveit, B., Petley-Ragan, A., Incel, S., Dunkel, K.G., Aupart, C., Austrheim, H., Corfu, F., Menegon, L., Renard, F., 2019. The effects of earthquakes and fluids on the metamorphism of the lower continental crust. *J. Geophys. Res., Solid Earth* 124, 7725–7755. <https://doi.org/10.1029/2018JB016461>.
- John, T., Schenck, V., 2006. Interrelations between intermediate-depth earthquakes and fluid flow within subducting oceanic plates: constraints from eclogite facies pseudotachylites. *Geology* 34, 557–560. <https://doi.org/10.1130/G22411.1>.
- Jolivet, L., Raimbourg, H., Labrousse, L., Avigad, D., Leroy, Y., Austrheim, H., Andersen, T.B., 2005. Softening triggered by eclogitization, the first step toward exhumation during continental subduction. *Earth Planet. Sci. Lett.* 237, 532–547. <https://doi.org/10.1016/j.epsl.2005.06.047>.
- Kaatz, L., Zertani, S., Moula, E., John, T., Labrousse, L., Schmalholz, S.M., Andersen, T.B., 2021. Widening of hydrous shear zones during incipient eclogitization of metastable dry and rigid lower crust—Holsnøy, western Norway. *Tectonics* 40, e2020TC006572. <https://doi.org/10.1029/2020TC006572>.
- Kaatz, L., Reynes, J., Hermann, J., John, T., 2022. How fluid infiltrates dry crustal rocks during progressive eclogitization and shear zone formation: insights from H<sub>2</sub>O contents in nominally anhydrous minerals. *Contrib. Mineral. Petrol.* 177, 72. <https://doi.org/10.1007/s00410-022-01938-1>.
- Kaatz, L., Schmalholz, S.M., John, T., 2023. Numerical simulations reproduce field observations showing transient weakening during shear zone formation by diffusional hydrogen influx and H<sub>2</sub>O inflow. *Geochem. Geophys. Geosyst.* 24 (5), e2022GC010830. <https://doi.org/10.1029/2022GC010830>.
- Katz, R., Knepley, M.G., Smith, B., Spiegelman, M., Coon, E.T., 2007. Numerical simulation of geodynamic processes with the portable extensible toolkit for scientific computation. *Phys. Earth Planet. Inter.* 163, 52–68. <https://doi.org/10.1016/j.pepi.2007.04.016>.
- Labrousse, L., Hetényi, G., Raimbourg, H., Jolivet, L., Andersen, T.B., 2010. Initiation of crustal-scale thrusts triggered by metamorphic reactions at depth: insights from a comparison between the Himalayas and Scandinavian Caledonides. *Tectonics* 29, TC5002. <https://doi.org/10.1029/2009TC002602>.
- Landau, L.D., Lifshitz, E.M., 1980. *Statistical Physics, Part 1, Course of Theoretical Physics*, vol. 5. Pergamon Press, Oxford.
- Llana-Fúnez, S., Wheeler, J., Faulkner, D.R., 2012. Metamorphic reaction rate controlled by fluid pressure not confining pressure: implications of dehydration experiments with gypsum. *Contrib. Mineral. Petrol.* 164, 69–79. <https://doi.org/10.1007/s00410-012-0726-8>.
- Luisier, C., Baumgartner, L., Schmalholz, S.M., Siron, G., Vennemann, T., 2019. Metamorphic pressure variation in a coherent Alpine nappe challenges lithostatic pressure paradigm. *Nat. Commun.* 10, 4734. <https://doi.org/10.1038/s41467-019-12727-z>.
- Malvoisin, B., Podladchikov, Y.Y., Vrijmoed, J.C., 2015. Coupling changes in densities and porosity to fluid pressure variations in reactive porous fluid flow: local thermodynamic equilibrium. *Geochem. Geophys. Geosyst.* 16, 4362–4387. <https://doi.org/10.1002/2015GC006019>.
- Malvoisin, B., Austrheim, H., Hetényi, G., Reynes, J., Hermann, J., Baumgartner, L.P., Podladchikov, Y.Y., 2020. Sustainable densification of the deep crust. *Geology* 48, 673–677. <https://doi.org/10.1130/G47201.1>.
- Malvoisin, B., Podladchikov, Y.Y., Myasnikov, A.V., 2021. Achieving complete reaction while the solid volume increases: a numerical model applied to serpentinitization. *Earth Planet. Sci. Lett.* 563, 116859. <https://doi.org/10.1016/j.epsl.2021.116859>.
- Mancktelow, N.S., 1993. Tectonic overpressure in competent mafic layers and the development of isolated eclogites. *J. Metamorph. Geol.* 11, 801–812. <https://doi.org/10.1111/j.1525-1314.1993.tb00190.x>.
- Menegon, L., Campbell, L., Mancktelow, N., Camacho, A., Wex, S., Papa, S., Toffol, G., Pennacchioni, G., 2021. The earthquake cycle in the dry lower continental crust: insights from two deeply exhumed terranes (Musgrave Ranges, Australia and Lofoten, Norway). *Philos. Trans. R. Soc. A* 379, 20190416. <https://doi.org/10.1098/rsta.2019.0416>.

- Miller, S.A., 2013. The role of fluids in tectonic and earthquake processes. *Adv. Geophys.* 54, 1–46. <https://doi.org/10.1016/B978-0-12-380940-7.00001-9>.
- Mindaleva, D., Uno, M., Higashino, F., Nagaya, T., Okamoto, A., Tsuchiya, N., 2020. Rapid fluid infiltration and permeability enhancement during middle-lower crustal fracturing: evidence from amphibolite-granulite-facies fluid-rock reaction zones, Sør Rondane Mountains, East Antarctica. *Lithos* 372, 105521. <https://doi.org/10.1016/j.lithos.2020.105521>.
- Moore, J., Beinlich, A., Piazolo, S., Austrheim, H., Putnis, A., 2020. Metamorphic differentiation via enhanced dissolution along high permeability zones. *J. Petrol.* 61, egaa096. <https://doi.org/10.1093/petrology/egaa096>.
- Moulas, E., Burg, J.P., Podladchikov, Y., 2014. Stress field associated with elliptical inclusions in a deforming matrix: mathematical model and implications for tectonic overpressure in the lithosphere. *Tectonophysics* 631, 37–49. <https://doi.org/10.1016/j.tecto.2014.05.004>.
- Moulas, E., Kaus, B., Jamtveit, B., 2022. Dynamic pressure variations in the lower crust caused by localized fluid-induced weakening. *Commun. Earth Environ.* 3, 157. <https://doi.org/10.1038/s43247-022-00478-7>.
- Newton, R., Charlu, T., Kleppa, O., 1980. Thermochemistry of the high structural state plagioclases. *Geochim. Cosmochim. Acta* 44, 933–941. [https://doi.org/10.1016/0016-7037\(80\)90283-5](https://doi.org/10.1016/0016-7037(80)90283-5).
- Plümper, O., John, T., Podladchikov, Y.Y., Vrijmoed, J.C., Scambelluri, M., 2017. Fluid escape from subduction zones controlled by channel-forming reactive porosity. *Nat. Geosci.* 10, 150–156. <https://doi.org/10.1038/ngeo2865>.
- Putnis, A., 2021. Fluid–mineral interactions: controlling coupled mechanisms of reaction, mass transfer and deformation. *J. Petrol.* 62, egab092. <https://doi.org/10.1093/petrology/egab092>.
- Putnis, A., John, T., 2010. Replacement processes in the Earth's crust. *Elements* 6, 159–164. <https://doi.org/10.2113/gselements.6.3.159>.
- Putnis, A., Jamtveit, B., Austrheim, H., 2017. Metamorphic processes and seismicity: the Bergen arcs as a natural laboratory. *J. Petrol.* 58, 1871–1898. <https://doi.org/10.1093/petrology/egx076>.
- Putnis, A., Moore, J., Prent, A.M., Beinlich, A., Austrheim, H., 2021. Preservation of granulite in a partially eclogitized terrane: metastable phenomena or local pressure variations? *Lithos* 400, 106413. <https://doi.org/10.1016/j.lithos.2021.106413>.
- Räss, L., Duretz, T., Podladchikov, Y., 2019. Resolving hydromechanical coupling in two and three dimensions: spontaneous channelling of porous fluids owing to decompression weakening. *Geophys. J. Int.* 218, 1591–1616. <https://doi.org/10.1093/gji/ggz239>.
- Räss, L., Utkin, I., Duretz, T., Omelin, S., Podladchikov, Y.Y., 2022. Assessing the robustness and scalability of the accelerated pseudo-transient method. *Geosci. Model Dev.* 15, 5757–5786. <https://doi.org/10.5194/gmd-15-5757-2022>.
- Schmalholz, S.M., Podladchikov, Y.Y., 2013. Tectonic overpressure in weak crustal-scale shear zones and implications for the exhumation of high-pressure rocks. *Geophys. Res. Lett.* 40, 1984–1988. <https://doi.org/10.1002/grl.50417>.
- Schmalholz, S.M., Moulas, E., Plümper, O., Myasnikov, A.V., Podladchikov, Y.Y., 2020. 2d hydro-mechanical-chemical modeling of (de)hydration reactions in deforming heterogeneous rock: the periclaste-brucite model reaction. *Geochem. Geophys. Geosyst.* 21, e2020GC009351. <https://doi.org/10.1029/2020GC009351>.
- Scott, D.R., Stevenson, D.J., 1986. Magma ascent by porous flow. *J. Geophys. Res., Solid Earth* 91, 9283–9296. <https://doi.org/10.1029/JB091iB09p09283>.
- Shi, F., Wang, Y., Yu, T., Zhu, L., Zhang, J., Wen, J., Gasc, J., Incel, S., Schubnel, A., Li, Z., Chen, T., Liu, W., Prakapenka, V., Jin, Z., 2018. Lower-crustal earthquakes in southern Tibet are linked to eclogitization of dry metastable granulite. *Nat. Commun.* 9, 1–13. <https://doi.org/10.1038/s41467-018-05964-1>.
- Shmonov, V., Vitiovova, V., Zharikov, A., Grafchikov, A., 2003. Permeability of the continental crust: implications of experimental data. *J. Geochem. Explor.* 78, 697–699. [https://doi.org/10.1016/S0375-6742\(03\)00129-8](https://doi.org/10.1016/S0375-6742(03)00129-8).
- Taetz, S., John, T., Bröcker, M., Spandler, C., Stracke, A., 2018. Fast intraslab fluid-flow events linked to pulses of high pore fluid pressure at the subducted plate interface. *Earth Planet. Sci. Lett.* 482, 33–43. <https://doi.org/10.1016/j.epsl.2017.10.044>.
- Turcotte, D.L., Schubert, G., 2002. *Geodynamics*. Cambridge University Press.
- Viette, D.R., Hacker, B.R., Allen, M.B., Seward, G.G., Tobin, M.J., Kelley, C.S., Cinque, G., Duckworth, A.R., 2018. Metamorphic records of multiple seismic cycles during subduction. *Sci. Adv.* 4, eaao0234. <https://doi.org/10.1126/sciadv.aao0234>.
- Vrijmoed, J.C., Podladchikov, Y.Y., Andersen, T.B., Hartz, E.H., 2009. An alternative model for ultra-high pressure in the Svarthverget Fe-Ti garnet-peridotite, Western Gneiss Region, Norway. *Eur. J. Mineral.* 21, 1119–1133. <https://doi.org/10.1127/0935-1221/2009/0021-1985>.
- Yamato, P., Duretz, T., Angiboust, S., 2019. Brittle/ductile deformation of eclogites: insights from numerical models. *Geochim. Geophys. Geosyst.* 20, 3116–3133. <https://doi.org/10.1029/2019GC008249>.
- Yamato, P., Duretz, T., Baïsset, M., Luisier, C., 2022. Reaction-induced volume change triggers brittle failure at eclogite facies conditions. *Earth Planet. Sci. Lett.* 584, 117520. <https://doi.org/10.1016/j.epsl.2022.117520>.
- Zertani, S., Labrousse, L., John, T., Andersen, T.B., Tilmann, F., 2019. The interplay of eclogitization and deformation during deep burial of the lower continental crust—a case study from the Bergen arcs (western Norway). *Tectonics* 38, 898–915. <https://doi.org/10.1029/2018TC005297>.
- Zertani, S., John, T., Brachmann, C., Vrijmoed, J.C., Plümper, O., 2022. Reactive fluid flow guided by grain-scale equilibrium reactions during eclogitization of dry crustal rocks. *Contrib. Mineral. Petrol.* 177, 61. <https://doi.org/10.1007/s00410-022-01928-3>.

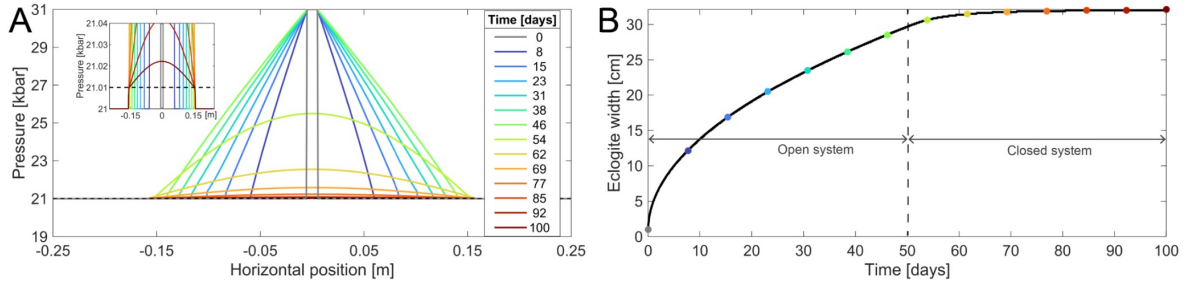
Supplementary figures for the paper “Eclogitisation of dry and impermeable granulite by fluid flow with reaction-induced porosity: insights from hydro-chemical modelling”, by Bras et al., submitted to EPSL.



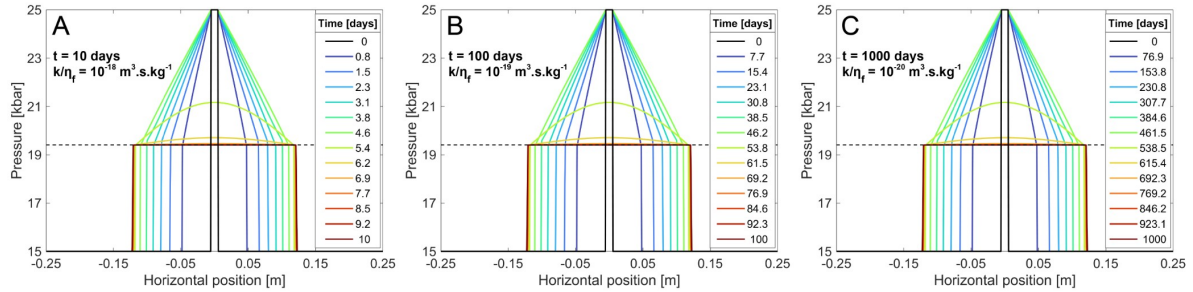
SUPPLEMENTARY FIGURE S1: Space resolution test. Each simulation has a model time of 100 days. (A) Width of the eclogitisation zone after a simulation of 100 days, for various spatial resolutions, for a model length of 1 m. (B) Difference in eclogite width between the spatial resolutions shown in (A) and  $nx = 800$ . (C) Convergence of the mean error in modelled pressure after 100 days, relative to the pressure in the  $nx = 800$  model.



SUPPLEMENTARY FIGURE S2: Time resolution test. Each simulation has a model time of 100 days. (A) Identical eclogite width over time for 2 extreme time resolutions. The time step  $dt$  varies during the simulation depending on the variables of the model, but the same Courant–Friedrichs–Lewy condition (CFL) is applied for all time steps. (B) Mean error in modelled pressure after 100 days, relative to the pressure in the  $CFL = 0.01$  model. Notice that the magnitude of the error is  $1e-5$  to  $1e-8$ , compared to  $1e-3$  for space resolution.



SUPPLEMENTARY FIGURE S3: Result of a simulation in a metastable scenario after 100 days. All parameters are the same as in figure 5, except  $P_r = 21.01$  kbar and  $P_{bg} = 21$  kbar. (A) Evolution of pressure with time. The reaction line (dotted black line) overlaps with the background pressure, and with the pressure profile of the last 4 time steps. The inset shows details around 21 kbar. (B) Evolution of the width of the eclogitisation zone over time. The colour dots correspond to profiles in A.



SUPPLEMENTARY FIGURE S4: Comparison of 3 simulations with varying  $t$  and  $k_0/\eta_f$ , but identical  $t \times k_0/\eta_f$ . At the end of the simulations each pressure profile is identical.



# 4

## Local pressure variations in two-phase flow models : implications for eclogitisation of granulite in the Bergen Arcs of Norway

### Sommaire du présent chapitre

---

<b>Points clés</b>	<b>98</b>
<b>4.1 Résumé</b>	<b>99</b>
<b>4.2 Abstract</b>	<b>100</b>
<b>4.3 Introduction</b>	<b>100</b>
<b>4.4 Methods</b>	<b>104</b>
4.4.1 Hydro-chemical model . . . . .	104
4.4.1.1 Conservation of total mass . . . . .	104
4.4.1.2 Conservation of solid mass . . . . .	105
4.4.1.3 Rock properties . . . . .	106
4.4.1.4 Fluid pressure . . . . .	107
4.4.2 Mechanical model . . . . .	108
4.4.2.1 Continuity equation . . . . .	108
4.4.2.2 Conservation of momentum . . . . .	108
4.4.2.3 Deviatoric stress . . . . .	109
4.4.2.4 Shear viscosity . . . . .	109
4.4.2.5 Frictional rheology . . . . .	110
4.4.3 Solving procedure . . . . .	111
4.4.4 Model configuration . . . . .	113
4.4.4.1 Initial set up . . . . .	113
4.4.4.2 Choice of physical properties . . . . .	113

4.4.5 Resolution test . . . . .	115
<b>4.5 Results</b>	<b>115</b>
4.5.1 Reference model . . . . .	116
4.5.2 Parametric study . . . . .	118
<b>4.6 Discussion</b>	<b>120</b>
4.6.1 Deformation-induced eclogitisation . . . . .	120
4.6.2 Competition between strain rate and Darcy flow . . . . .	121
4.6.3 Implications for eclogitisation in Holsnøy . . . . .	122
4.6.4 Comparison with single phase models . . . . .	123
4.6.5 Transient weakening . . . . .	124
4.6.6 Choice of a thermodynamic pressure . . . . .	125
4.6.7 Limitations and perspectives . . . . .	126
<b>4.7 Summary and conclusion</b>	<b>127</b>
<b>Appendix</b>	<b>129</b>
<b>Supplementary figures</b>	<b>130</b>
<b>References</b>	<b>131</b>

---

## Points clés

- La déformation engendre des surpressions qui peuvent expliquer la coexistence de la granulite et de l'éclogite.
- Lorsqu'une déformation est appliquée, un front de réaction peut se propager à une vitesse de l'ordre de 10 centimètres par millier d'années dans la granulite.
- Les modèles mécaniques qui ne considèrent ni réaction ni flux de fluides peuvent surrestimer les surpressions induites par la déformation.

## 4.1 Résumé

Le chapitre précédent démontre qu'en présence d'une perturbation de haute pression, un front d'éclogitisation peut se propager dans la granulite. L'article utilise l'exemple d'un pulse de fluides comme cause plausible d'une perturbation de pression, mais afin de simplifier le propos la déformation n'est pas prise en compte. Le présent chapitre vient donc compléter le modèle précédent en considérant maintenant la déformation ainsi que, à l'instar du chapitre 2, les effets de la réaction métamorphique sur la rhéologie.

Nous présentons un modèle numérique réactif hydro-mécanique en 2 dimensions, qui étudie l'interaction entre l'éclogitisation des roches de la croûte inférieure (granulite), la circulation des fluides et la déformation. Comme dans le précédent chapitre, une augmentation de pression fluide peut déclencher la réaction métamorphique, ce qui augmente la densité de la roche et diminue sa viscosité. La déformation et la densification entraînent des variations de porosité, induisant donc un flux de fluides en présence de gradients de pression fluide. La déformation et la circulation de fluides contrôlent les variations de pression fluide.

Nous montrons qu'une inclusion mécaniquement faible située dans une matrice de granulite résistante soumise à une déformation génère des variations de pression à l'intérieur et autour de l'inclusion. La surpression peut localement déclencher l'éclogitisation et l'affaiblissement rhéologique transitoire qui s'ensuit, propageant la réaction à l'extérieur de l'inclusion. Cependant, il existe une compétition entre la déformation visqueuse qui tend à générer des variations de pression, et la diffusion de la pression du fluide par flux de Darcy qui tend à réduire les gradients de pression. Les variations de pression qui en résultent sont systématiquement inférieures à celles prévues par les modèles qui ne considèrent pas de phase fluide. Ces derniers modèles peuvent donc surestimer les surpressions induites par la déformation.

Nous appliquons notre modèle aux granulites et éclogites de Holsnøy et montrons que des surpressions de 4 kbar peuvent être atteintes si la perméabilité de la croûte inférieure est  $\leq 10^{-24} \text{ m}^2$ . Nous estimons qu'un front d'éclogitisation induit par la déformation peut se propager dans la granulite à une vitesse de l'ordre de la dizaine de centimètres par millier d'années.

L'article est en préparation pour être publié dans : Bras, E., Yamato, P., Duretz, T., Schmalholz, S. M., & Podladchikov, Y. Y. Local pressure variations in two-phase flow models : implications for eclogitisation of granulite in the Bergen Arcs of Norway.

## 4.2 Abstract

Eclogitisation is an emblematic process of continental subduction zones, where conversion of lower crustal rocks into eclogite facies rocks involves fluid-rock interactions, rheological weakening, and an increase in rock density. Field observations indicate that deformation and fluid flow are driving factors of lower crust eclogitisation. Here we present a two-phase, two-dimensional fully coupled hydro-mechanical reactive numerical model that investigates the interplay between eclogitisation of lower crustal rocks (granulite), fluid flow and deformation.

A mechanically weak inclusion embedded in a strong granulite matrix under deformation generates pressure variations in and around the inclusion. Overpressure can locally trigger eclogitisation and subsequent rheological weakening, propagating the reaction away from the inclusion. However, there is a competition between viscous deformation that tends to generate pressure variations, and fluid pressure diffusion by Darcy flow that tends to reduce pressure gradients, effectively limiting the overpressures that can be achieved. We suggest that the effect of porous flow and density variations on local pressure variations can be significant and should be taken into account when modelling metamorphic processes in the lower crust.

We apply our model to the granulites and eclogites of Holsnøy, part of the Scandinavian Caledonides in Norway, and show that overpressures of 4 kbar can be achieved if the lower crust permeability is  $\leq 10^{-24} \text{ m}^2$ . We estimate that an eclogitisation front could propagate into granulite at a rate of tens of centimetres per thousand years.

## 4.3 Introduction

The lower continental crust is the place of complex retroactions between metamorphism, rock deformation and fluid transport, which govern seismicity and long-term lithosphere dynamics (Labrousse et al., 2010; Jamtveit et al., 2019; Moulas et al., 2022). Eclogitisation of lower crustal rocks during subduction is an emblematic example of retroactions between metamorphism, deformation and fluids (Engvik et al., 2001; Austrheim, 2013). Conversion of dry and mechanically strong crustal rocks (granulite) into denser eclogite results in drastic rheological weakening (Bras et al., 2021; Kaatz et al., 2021; Baïsset et al., 2023), and enhanced fluid flow by generation of porosity (Putnis et al., 2021; Bras et al., 2023; Hoover et al., 2023). Deformation can generate local overpressures that trigger metamorphic reactions (Moulas et al., 2022), and can promote fluid-rock interaction by creating pathways that facilitate fluid migration (Mancktelow and Pennacchioni, 2005; Fusseis et al., 2009). Fluids can promote metamorphic reactions by providing efficient mineral replacement mechanisms (Putnis, 2009) or by triggering

kinetically delayed reactions (Austrheim, 1987; Wain et al., 2001), and can facilitate deformation by hydrofracturing (Audet et al., 2009). The list of mechanisms cited here is far from exhaustive, and there is a substantial body of literature on the interplay between fluids, deformation and reaction in metamorphic contexts.

The island of Holsnøy, in southwestern Norway, constitutes an ideal natural laboratory for investigating these couplings (Austrheim, 1987, 2013; Putnis et al., 2017). The relation between eclogite and granulite is exceptionally well preserved there, making it an ideal analogue for the metamorphic state of the lower crust being deeply buried during orogenic events (Jackson et al., 2004; Labrousse et al., 2010). A large part of the island consists of anorthositic granulites, which were formed at ca. 930 Ma during the Grenvillian orogeny (Bingen et al., 2001). The anhydrous Grenvillian granulites were subducted during convergence and collision between Baltica and Laurentia during the Caledonian orogeny, at 400–440 Ma (Andersen et al., 1991; Glodny et al., 2008). The high-pressure event occurring during the collision stage caused the partial eclogitisation of the granulitic lower crust, associated with fluid infiltration and shear deformation, and was presumably initiated by fracturing associated with earthquakes (Austrheim, 1987; Jamtveit et al., 2016, 2018b). The Caledonian overprint is characterised by seemingly contemporaneous eclogite and amphibolite facies reworking of the granulite (Jamtveit et al., 2018b, 2019; Moore et al., 2020b) that can coexist on the same outcrop (Centrella, 2019). Peak pressure ( $P$ ) and temperature ( $T$ ) conditions in Holsnøy have been estimated at 670–690 °C and 21–22 kbar (Bhowany et al., 2018). Eclogitisation is spatially heterogeneous at the outcrop scale and occurs as eclogite shear zones that crosscut the granulite protolith, and as static eclogite (a.k.a. eclogite fingers) that overprint the granulite foliation (figure 4.1, Zertani et al., 2019; Kaatz et al., 2021; Putnis et al., 2021).

Several authors (e.g. Austrheim, 1987; Kaatz et al., 2022; Zertani et al., 2022) argued that eclogite and granulite coexist in close spatial proximity because granulite is metastable: granulite experienced eclogite facies  $P$ - $T$  conditions, but remained largely untransformed because it lacked fluids to trigger eclogitisation. Only regions infiltrated by fluids therefore transformed into eclogite. However, recent studies suggested that the coexistence of granulite, eclogite, and amphibolite due to tectonically induced local pressure variations may be a more consistent interpretation of the field data (Jamtveit et al., 2018b; Putnis et al., 2021; Moulas et al., 2022). Alternatively, we recently (Bras et al., 2023) suggested that in the presence of a high fluid pressure gradients caused by a fluid pulse, a high pressure reaction front could propagate into the granulite, satisfactorily explaining the widening of eclogite shear zones that is observed in the field.

Considering potential local pressure variations is of crucial importance, because the pressure registered by metamorphic minerals may not easily be converted to depth using a hydrostatic assumption (Moulas et al., 2013; Schmalholz and Podladchikov,

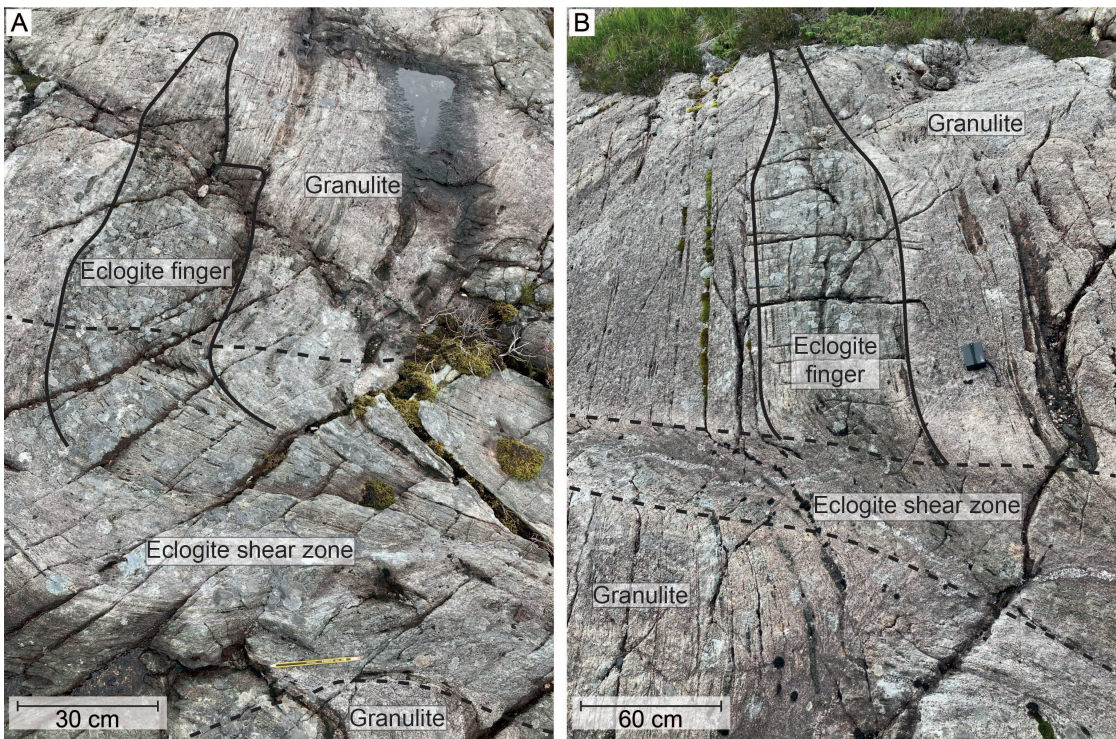


Figure 4.1 – Photographs from Holsnøy (western Norway), showing eclogite fingers that protrude from eclogite shear zones into the granulite, along its foliation. A: 60°35'38"N, 5°01'52"E. B: 60°35'24"N, 5°01'41"E.

2014; Bauville and Yamato, 2021; Tajčmanová et al., 2021). Field observations (Pleuger and Podladchikov, 2014; Luisier et al., 2019; Hoiland et al., 2022; Simon et al., 2023), experiments (Hirth and Tullis, 1994; Cionoiu et al., 2019; Cionoiu et al., 2022) and numerical modelling (Schmalholz and Podladchikov, 2013; Schmalholz et al., 2014a; Luisier et al., 2023) have indeed demonstrated that tectonic stresses can be significant and should be considered when relating pressure to depth. Local pressure variations could be in the order of 10 kbar for crustal conditions and can be expected from any metamorphic context (Gerya, 2015). The importance of tectonic stress has been further demonstrated at the grain scale with implications for thermodynamic equilibrium calculations (Tajčmanová et al., 2014, 2015; Luisier et al., 2023), for inferring metamorphic P-T paths and decyphering subduction dynamics (Yamato and Brun, 2017; Bauville and Yamato, 2021).

In a rheologically heterogeneous system, weak and strong materials can experience and record pressure deviations (underpressures and overpressures) of several kbar from their lithostatic pressure (Mancktelow, 1993, 2008). Force balance between pressure and deviatoric stress requires an increase of the pressure if the deviatoric stresses decrease due to the presence of a weak material (Schmalholz and Podladchikov, 2013), and

vice-versa. A well-studied example is the case of an elliptical inclusion embedded in a viscous matrix of different strength (Schmid and Podladchikov, 2003; Moulas et al., 2014). The magnitude and spatial distribution of pressure variations is controlled by the relative strength between the matrix and the inclusion, the aspect ratio and the orientation of the inclusion relative to the bulk compression direction (Moulas et al., 2014).

Models that compute stress and pressure variations caused by mechanical heterogeneities in deforming rocks have been successfully applied to eclogitisation in the Bergen Arcs of Norway (Jamtveit et al., 2018b; Moulas et al., 2022). They showed that tectonic overpressures could reach 5 kbar, consistent with the difference measured by Bhowany et al. (2018) between the pressure of pseudotachylite formation (15-16 kbar) and the peak eclogite facies pressure (21-22 kbar) (Jamtveit et al., 2018b). Local pressure variations could hence explain the juxtaposition of granulite and eclogite at the same depth (Moulas et al., 2022). Alternatively, other models have highlighted the role of fluids as a driving mechanism of eclogitisation: Bras et al. (2021) and Kaatz et al. (2021, 2023) modelled the widening of eclogite shear zones with a diffusion equation that mimics the effects of porous fluid flow and/or solid state diffusion of hydrogen and oxygen. Finally, recent models showed that densification is a crucial aspect of the eclogitisation reaction. Bras et al. (2023) used a coupled hydro-chemical model to study the propagation of the eclogitisation reaction through reaction-induced porosity, in response to a fluid pulse. Yamato et al. (2022) showed that reaction-induced volume changes can trigger brittle failure at eclogite facies conditions, and can enhance the propagation of the eclogitisation process by a runaway mechanism, even without considering rheological modifications induced by mineral reactions.

Although fluid flow and deformation have been recognised as driving factors of eclogitisation in Holsnøy for almost 40 years (Austrheim and Griffin, 1985), none of these models simultaneously considers solid deformation due to tectonics, material transport due to fluid flow and changes of physical properties due to metamorphic reactions. In order to couple deformation, fluid flow and reaction during metamorphism, Malvoisin et al. (2015) developed a mass conservative, two-phase reactive model that relies on local thermodynamic equilibrium. Two-phase models consider that the medium consists of a mixture of two phases of independent properties (e.g. McKenzie, 1984; Keller et al., 2013), here a solid phase and a fluid phase stored in the porous space. Malvoisin et al. (2020) applied this model to granulite eclogitisation in Holsnøy, but they do not consider shear deformation, and focus on the influence of the reaction on the generation of seismicity rather than on the propagation of a reaction front. Schmalholz et al. (2020) extended the model of Malvoisin et al. (2015) to include shear deformation and termed the approach hydro-mechanical-chemical (HMC) modelling. HMC models are suitable

to quantify the interplay between metamorphic reactions and fluid flow in a deforming, heterogeneous medium (Schmalholz et al., 2020).

This HMC modelling approach is therefore particularly well suited to investigate the processes at play during eclogitisation of granulite in the Bergen Arcs, that involve coupling between fluid flow, deformation and metamorphic reaction. In this work, we apply a HMC model to the Holsnøy case study, in order to determine how shear deformation can trigger eclogitisation of lower-pressure granulite, and drive propagation of eclogitisation zones. Our numerical algorithm is similar to that of Schmalholz et al. (2020), building upon our previously published hydro-chemical model (Bras et al., 2023), with the addition of shear deformation.

## 4.4 Methods

We consider a 2D HMC model, similar to that of Schmalholz et al. (2020), where a deforming porous rock undergoes metamorphic reactions in response to fluid pressure variations. The model is based on local thermodynamic equilibrium and mass conservation. Metamorphic reactions lead to changes in rock density and exchange of  $\text{H}_2\text{O}$  between the fluid and the solid, hence modifying the porosity of the system, and thus the porosity-dependant permeability. Reaction-induced permeability leads to fluid flow controlled by fluid pressure gradients. Metamorphic reactions also lead to changes in viscosity, hence modifying the stress and solid velocity fields. Solid and fluid flow induce changes in fluid pressure. In the following we first present the equations governing the hydro-chemical aspect of our model, and then the equations governing the mechanical aspect of our model.

### 4.4.1 Hydro-chemical model

In our model, the volatile species, assumed here to be pure  $\text{H}_2\text{O}$ , are either structurally bound to the solid, or constitute the fluid filling the porosity. We assume that dissolution in the fluid of solid species, such as Si, Al, Na and Ca, is negligible. Following Malvoisin et al. (2015) and Schmalholz et al. (2020), solving this system requires (1) conservation of total mass per unit volume of the system ( $\rho_T$ , the sum of fluid mass and solid mass) and (2) conservation of the mass per unit volume of solid species ( $\rho_T^s$ ). All variables used in this study are listed in table 4.1.

#### 4.4.1.1 Conservation of total mass

We consider a porous medium, with porosity  $\phi$ , which consists of a solid phase with density  $\rho_s$  and a fluid phase with density  $\rho_f$  stored in the pores. Per unit volume, the

total mass  $\rho_T$  of the porous medium is:

$$\rho_T = \rho_f \phi + \rho_s (1 - \phi). \quad (4.1)$$

In absence of a diffusive flux, the conservation equation of  $\rho_T$ , expressing the variation of  $\rho_T$  per unit volume over time, is:

$$\frac{\partial}{\partial t} \rho_T = -\nabla \cdot [\rho_f \phi \vec{v}_f + \rho_s (1 - \phi) \vec{v}_s]. \quad (4.2)$$

Unlike Bras et al. (2023), our model here includes solid deformation, so we do not assume that  $\vec{v}_s = 0$ . The force balance for the fluid can be expressed using Darcy's law in the absence of gravity:

$$\phi (\vec{v}_f - \vec{v}_s) = -\frac{k_0 \phi^3}{\eta_f} \nabla P_f, \quad (4.3)$$

where  $k_0$  is the permeability coefficient in a porosity-dependant Carman-Kozeny type permeability expression (e.g. Costa, 2006),  $\eta_f$  is the fluid viscosity, and  $P_f$  is the fluid pressure. Rearranging equation (4.2) and substituting in equation (4.3) yields our total mass conservation equation (see details in Schmalholz et al., 2020):

$$\frac{\partial}{\partial t} \rho_T = \nabla \cdot \left[ \rho_f \frac{k_0 \phi^3}{\eta_f} \nabla P_f \right] - \nabla \cdot (\rho_T \vec{v}_s). \quad (4.4)$$

#### 4.4.1.2 Conservation of solid mass

We assume that non-volatile components, such as Si, Al, Na or Mg, never enter the fluid phase, whereas the volatile component H<sub>2</sub>O can be part of the solid phase in the form of hydrous minerals.  $X_s$  is the mass fraction of non-volatile components structurally bound in the solid. The total solid mass (i.e. excluding structurally bound H<sub>2</sub>O) of the system per unit volume,  $\rho_T^s$ , is:

$$\rho_T^s = (1 - \phi) \rho_s X_s. \quad (4.5)$$

The conservation equation of solid mass is:

$$\frac{\partial}{\partial t} \rho_T^s = -\nabla \cdot (\rho_T^s \vec{v}_s). \quad (4.6)$$

Since non-volatile components remain in the solid there is no contribution of the fluid velocity to the conservation of solid mass. Unlike Bras et al. (2023), we do not assume that the solid mass is always constant since solid velocity leads to changes in solid mass. After some algebraic operations, detailed in the appendix, equation (4.6) can be

expressed as:

$$\frac{d}{dt}(\log \phi) = \frac{1-\phi}{\phi} \left( \frac{d}{dt}(\log(\rho_s X_s)) + \nabla \cdot \vec{v}_s \right), \quad (4.7)$$

and can be used to compute changes in porosity. Rearranging conservation equation (4.6) in terms of  $\log \phi$ , rather than  $\phi$ , ensures that  $\phi$  always stays positive, since the logarithmic function is only defined for positive inputs.

#### 4.4.1.3 Rock properties

Solving the previous conservation equations requires prior knowledge of the densities of the fluid  $\rho_f$  and of the solid  $\rho_s$  at any pressure, as well as the amount of non-volatile elements structurally bound to the solid  $X_s$ . For simplicity, we consider that granulite is stable at low pressure, until it reaches a reaction pressure  $P_r$ , at which it transforms into eclogite. When solid-fluid interactions are considered, it is the fluid pressure that determines which phases are stable in a local equilibrium domain, rather than the mean stress (e.g Dahlen, 1992). Indeed, field data (Holdaway and Goodge, 1990) and experiments (Llana-Fúnez et al., 2012) indicate that metamorphic reactions are controlled by fluid pressure rather than by confining pressure. Fluid pressure is therefore an appropriate macroscopic proxy of the pressure rocks are in equilibrium with.

Granulite has a density  $\rho_g$  at background pressure, and eclogite has a density  $\rho_e$  at reaction pressure. Rocks densities vary as a function of pressure according to a solid compressibility  $\beta_s$ . The solid density at equilibrium can therefore be computed at any pressure:

$$\rho_s^{EQ} = \begin{cases} \rho_g \times e^{\beta_s(P_f - P_{bg})} & \text{if } P_f < P_r, \\ \rho_e \times e^{\beta_s(P_f - P_r)} & \text{if } P_f > P_r. \end{cases} \quad (4.8)$$

Granulite and eclogite respectively have a fraction  $X_s^g$  and  $X_s^e$  of non-volatile components structurally bound to the solid. Assuming that these fractions do not depend on pressure, the equation determining  $X_s$  at equilibrium as a function of pressure is:

$$X_s^{EQ} = \begin{cases} X_s^g & \text{if } P_f < P_r, \\ X_s^e & \text{if } P_f > P_r. \end{cases} \quad (4.9)$$

We derived the fluid density  $\rho_f$  as a function of pressure with the Gibbs energy minimisation software perplex (Connolly, 2005) at a constant temperature of 700 °C, assuming a pure H<sub>2</sub>O fluid and using the CORK equation of state for H<sub>2</sub>O (Holland and Powell, 1991):

$$\rho_f^{EQ} = \rho_f(P_f). \quad (4.10)$$

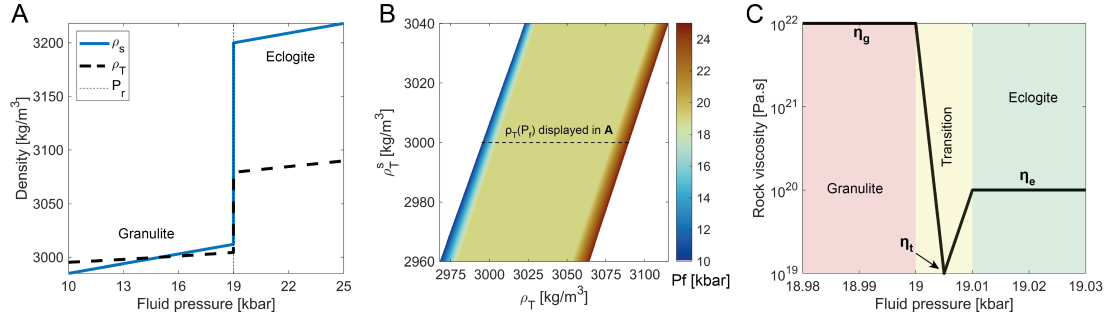


Figure 4.2 – Look-up tables used in the numerical model, relating density (A), mass (B) and viscosity (C) to fluid pressure at 700 °C. (A) Equilibrium solid density (blue line) as a function of fluid pressure. The density jump at the reaction pressure  $P_r$  is 1 MPa wide: the transition from granulite density (left) to eclogite density (right) occurs between 19 and 19.01 kbar. Additionally, the dashed line indicates a profile of total mass  $\rho_T$  as a function of fluid pressure, for a fixed  $\rho_T^s = 3000 \text{ kg m}^{-3}$ . There exist one such line for every possible  $\rho_T^s$ , which yields the 2D relation illustrated on B. (B) 2D inverse look-up table used to compute fluid pressure  $P_f$  as a function of total mass  $\rho_T$  and total solid mass  $\rho_T^s$ . The dashed line corresponds to the one in (A). The wide yellow region corresponds to pressures between 19 and 19.01 kbar. See the text for details. (C) Shear viscosity  $\eta$  as a function of fluid pressure. Below 19 kbar and above 19.01 kbar,  $\eta$  has constant values of respectively  $\eta_g = 10^{22}$  and  $\eta_g = 10^{20} \text{ Pa s}$ . Between 19 and 19.01 kbar,  $\eta$  transitions from  $\eta_g$  to  $\eta_e$  by going through a transient weak viscosity  $\eta_t = 10^{19} \text{ Pa s}$ .

For numerical efficiency,  $\rho_s^{EQ}(P_f)$ ,  $X_s^{EQ}(P_f)$  and  $\rho_f^{EQ}(P_f)$  are precomputed as look-up tables. The evolution of solid density with fluid pressure is illustrated in figure 4.2A. We assume that  $\rho_f$  always corresponds to  $\rho_f^{EQ}$  as a result of its equation of state. Due to the step-like variation of  $\rho_s$  and  $X_s$  with varying  $P_f$  during the eclogitisation reaction (figure 4.2A), we assume that the reaction is controlled by a kinetic reaction timescale, so that values of  $\rho_s$  and  $X_s$  do not change instantaneously in response to fluid pressure variations. We use a first-order reaction kinetics, as already implemented in a number of studies (e.g. Omlin et al., 2017; Yamato et al., 2022):

$$\frac{\partial \rho_s}{\partial t} = \frac{\rho_s^{EQ} - \rho_s}{t_k}, \quad (4.11)$$

$$\frac{\partial X_s}{\partial t} = \frac{X_s^{EQ} - X_s}{t_k}, \quad (4.12)$$

where  $t_k$  is the kinetics time scale.

#### 4.4.1.4 Fluid pressure

For a given  $\rho_T^s$ ,  $\phi$  can be computed from  $\rho_s$  and  $X_s$  using equation (4.5). Since  $\rho_s$  and  $X_s$  are functions of fluid pressure (equations 4.8, 4.9),  $\phi$  is a function of both  $P_f$  and  $\rho_T^s$ . Hence, the total mass of the system  $\rho_T$  can be computed as a function of  $P_f$  and  $\rho_T^s$ . For a

given  $\rho_T^s$ ,  $\rho_T$  monotonously increases with pressure, as a consequence of thermodynamic stability (e.g. Landau and Lifshitz, 1980), which means that for every given pressure there is a uniquely corresponding  $\rho_T$  (figure 4.2A). This uniqueness makes the inverse statement true: at a fixed  $\rho_T^s$ , for every given  $\rho_T$  there is one uniquely corresponding pressure. Therefore, for every given pair  $(\rho_T^s, \rho_T)$  there is one uniquely corresponding pressure. We can therefore build an inverse look-up table that is used to compute  $P_f$  as a function of  $\rho_T^s$  and  $\rho_T$ :

$$P_f = P_f(\rho_T, \rho_T^s). \quad (4.13)$$

The inverse look-up table is shown in figure 4.2B. This approach allows for faster numerical convergence than directly using equation 4.4 to update  $P_f$  (e.g. as in Schmalholz et al., 2020), and better highlights the underlying relation between mass and pressure.

#### 4.4.2 Mechanical model

##### 4.4.2.1 Continuity equation

We consider a visco-elastic volumetric deformation for which the divergence of solid velocity  $\nabla v_s$  is related to the difference between total pressure  $P_t$  and fluid pressure  $P_f$  (Yarushina and Podladchikov, 2015):

$$\nabla \cdot \vec{v}_s = -\beta_d \frac{dP_t}{dt} + (\beta_d - \beta_s) \frac{dP_f}{dt} - \frac{P_t - P_f}{(1-\phi)\eta_b}, \quad (4.14)$$

where  $\eta_b$  is the bulk (or pore) viscosity,  $\beta_d$  is the drained compressibility. For the range of porosities considered here,  $\eta_b$  is the same magnitude as the shear viscosity  $\eta$  (Katz et al., 2022). Therefore, for simplicity we consider:

$$\eta_b = \eta. \quad (4.15)$$

##### 4.4.2.2 Conservation of momentum

Conservation of fluid momentum is given by the Darcy's law (section 4.4.1). Conservation of total momentum is given by Stokes' equation, assuming no inertial forces and no gravity:

$$\nabla \sigma_{ij} = 0, \quad (4.16)$$

where  $\sigma_{ij}$  is the total stress tensor, which is related to the deviatoric stress tensor  $\tau_{ij}$  by:

$$\sigma_{ij} = \tau_{ij} - \delta_{ij} P_t, \quad (4.17)$$

with  $P_t$  the total pressure and  $\delta$  the Kronecker delta. In 2D Cartesian coordinates, equation (4.17) becomes

$$\frac{\partial \tau_{xx}}{\partial x} + \frac{\partial \tau_{xy}}{\partial y} - \frac{\partial P_t}{\partial x} = 0, \quad (4.18)$$

$$\frac{\partial \tau_{xy}}{\partial x} + \frac{\partial \tau_{yy}}{\partial y} - \frac{\partial P_t}{\partial y} = 0. \quad (4.19)$$

#### 4.4.2.3 Deviatoric stress

Shear viscosity  $\eta$  relates the deviatoric stress  $\tau_{ij}$  to the deviatoric strain rate  $D_{ij}$ . For a linear viscous rheology,  $\tau_{ij}$  is proportional to  $D_{ij}$ :

$$\tau_{ij} = (1 - \phi)2\eta D_{ij}. \quad (4.20)$$

We introduce the factor  $1 - \phi$  to take into account that the solid deformation only contributes a part to the total deviatoric stress of the two-phase medium (e.g. Keller et al., 2013).  $D_{ij}$  is related to the total strain rate tensor  $\dot{\epsilon}_{xy}$  and the divergence of solid velocity  $\nabla v_s$  by:

$$D_{ij} = \dot{\epsilon}_{ij} - \frac{1}{3}\nabla \cdot \vec{v}_s, \quad (4.21)$$

$$D_{ij} = \frac{1}{2}\left(\frac{\partial v_i}{\partial x_j} + \frac{\partial v_j}{\partial x_i}\right) - \frac{1}{3}\delta_{ij}\frac{\partial v_i}{\partial x_i}. \quad (4.22)$$

In absence of internal sources of angular momentum, all tensors are symmetric, i.e.  $\tau_{ij} = \tau_{ji}$  (e.g. Gerya, 2019).

#### 4.4.2.4 Shear viscosity

Here we assume that viscosity only depends of the metamorphic state (granulite, eclogite or granulite undergoing eclogitisation). Granulite has a fixed viscosity  $\eta_g$  and eclogite has a fixed viscosity  $\eta_e$ . When the fluid pressure reaches  $P_r$ , viscosity transitions from  $\eta_g$  to  $\eta_e$  over a small pressure range with a transient weakening behaviour, first weakening to a transient viscosity  $\eta_t$  before strengthening to the eclogite viscosity  $\eta_e$  (Bras et al., 2021; Kaatz et al., 2023):

$$\log_{10}(\eta^{EQ}) = \begin{cases} \log_{10}(\eta_g) & \text{if } P_f < P_r, \\ \frac{P_f - P_r}{\epsilon} \log_{10}(\eta_t) + \frac{P_r + \epsilon - P_f}{\epsilon} \log_{10}(\eta_g) & \text{if } P_r < P_f < P_r + \epsilon, \\ \frac{P_f - P_r - \epsilon}{\epsilon} \log_{10}(\eta_e) + \frac{P_r + 2\epsilon - P_f}{\epsilon} \log_{10}(\eta_t) & \text{if } P_r + \epsilon < P_f < P_r + 2\epsilon, \\ \log_{10}(\eta_e) & \text{if } P_f > P_r + 2\epsilon, \end{cases} \quad (4.23)$$

where  $\epsilon$  is a small pressure step, here set at  $\epsilon = 0.5$  MPa. The evolution of rock viscosity with fluid pressure is illustrated on figure 4.2C. The logarithmic mixing law between the end-member viscosities  $\eta_g$ ,  $\eta_t$  and  $\eta_e$  lies between the Reuss (harmonic mean) and Voigt (arithmetic mean) bounds (Supplementary figure S1), and is comparable to the Minimized Power Geometric model of Huet et al. (2014).

Since viscosity depends on the metamorphic state, we assume that  $\eta$  does not change instantaneously in response to fluid pressure variations, but varies according to the same reaction kinetics as  $\rho_s$  and  $X_s$ :

$$\frac{\partial \eta}{\partial t} = \frac{\eta^{EQ} - \eta}{t_k}. \quad (4.24)$$

#### 4.4.2.5 Frictional rheology

To account for frictional rheology, we consider a viscoplastic Drucker-Prager rheology, which adds a viscous element to the plastic yield function (Duretz et al., 2020). We consider a non-dilatant viscoplastic model, where the yield function  $F$  is:

$$F = \tau_{II} - C \cos(\alpha) - P_e \sin(\alpha) - \eta^{vp} \dot{\varepsilon}^{vp}, \quad (4.25)$$

where  $\tau_{II} = \sqrt{0.5(\tau_{xx}^2 + \tau_{yy}^2 + \tau_{zz}^2) + \tau_{xy}^2}$  is the square root of the second invariant of the deviatoric stress tensor,  $C$  is the cohesion,  $\alpha$  is the friction angle,  $P_e$  is an effective pressure,  $\eta^{vp}$  is a viscoplastic regularisation viscosity,  $\dot{\varepsilon}^{vp}$  is the viscoplastic strainrate. Here we consider the case of plane total strain, hence we account for out-of-plane deviatoric strain rate and stress components ( $\tau_{zz}$ ). Following Li et al. (2023), in order to properly capture the behaviour of porous and non-porous regions,  $P_e$  is defined as:

$$P_e = P_s - e^{-\phi_p/\phi} P_f, \quad (4.26)$$

where  $\phi_p$  is a porosity threshold, and  $P_s$  is the solid pressure. Since the total pressure  $P_t$  can be defined as  $P_t = \phi P_f + (1 - \phi) P_s$  (e.g. Keller et al., 2013),  $P_s$  can be computed from  $P_f$ ,  $P_t$  and  $\phi$ .

Plastic failure is reached when  $F > 0$ , and the effective viscosity drops until  $\tau_{II}$  is small enough to satisfy  $F = 0$ . Here, viscoplasticity is only used for its regularisation effect and we do not aim to relate the parameters of the viscoplastic model to experimental rock deformation data. Following Duretz et al. (2020), we assume that the viscoplastic element causes an additional stress  $\hat{\sigma}$ , so the resulting regularisation viscosity is  $\eta^{vp} = \hat{\sigma}/\dot{\varepsilon}_{bg}$ . This overstress is typically in the order of 1 MPa or less.

### 4.4.3 Solving procedure

Our HMC model consists of a closed system of 18 equations and 18 unknowns ( $\rho_s^{EQ}$ ,  $X_s^{EQ}$ ,  $\eta^{EQ}$ ,  $\rho_s$ ,  $\rho_f$ ,  $X_s$ ,  $\eta$ ,  $\eta_b$ ,  $\rho_T^s$ ,  $\rho_T$ ,  $\phi$ ,  $P_f$ ,  $P_t$ ,  $v_x$ ,  $v_y$ ,  $\tau_{xx}$ ,  $\tau_{yy}$ ,  $\tau_{xy}$ ) summarised in table 4.1. We discretise this governing system of equation with a finite-difference method on a regular Cartesian staggered grid (e.g. Gerya, 2019).

$\rho_T$ ,  $\rho_T^s$ ,  $v_x$  and  $v_y$  are solved iteratively with a pseudo-transient (PT) method (e.g. Räss et al., 2022), using, respectively, equations (4.4), (4.6), (4.18) and (4.19). To apply this method, we transform these 4 equations into PT equations by moving every term to right hand side, and adding a pseudo time derivative of the unknown variables  $\rho_T$ ,  $\rho_T^s$ ,  $v_x$  and  $v_y$  to the left hand side. The PT equations are:

$$\frac{\Delta^{PT} \rho_T}{\Delta t_{\rho_T}} = -\frac{\partial \rho_T}{\partial t} + \left( \nabla \cdot \left[ \rho_f \frac{k_0 \phi^3}{\eta_f} \nabla P_f \right] - \nabla \cdot (\rho_T \vec{v}_s) \right), \quad (4.27)$$

$$\frac{\Delta^{PT} \log \phi}{\Delta t_{\log \phi}} = -\frac{d}{dt}(\log \phi) - \frac{1-\phi}{\phi} \left( \frac{d}{dt}(\log(\rho_s X_s)) + \nabla \cdot \vec{v}_s \right). \quad (4.28)$$

$$\frac{\Delta^{PT} v_x}{\Delta t_v} = \frac{\partial \tau_{xx}}{\partial x} + \frac{\partial \tau_{xy}}{\partial y} - \frac{\partial P_t}{\partial x}, \quad (4.29)$$

$$\frac{\Delta^{PT} v_y}{\Delta t_v} = \frac{\partial \tau_{xy}}{\partial x} + \frac{\partial \tau_{yy}}{\partial y} - \frac{\partial P_t}{\partial y}. \quad (4.30)$$

At a given physical time-step, the values of the unknown variables are iteratively updated within a PT iteration loop. The value of the PT derivatives on the left-hand side, also called residuals, converge towards zero during the interations. When the residuals are zero, then the corresponding steady-state equations are solved. In practice, the iterations continue until the residuals are all smaller than a chosen convergence tolerance. We use an accelerated PT method (also called damping, dynamic relaxation or second order Richardson method) to speed up the convergence of the PT iterations (e.g. Frankel, 1950; Räss et al., 2022). The pseudo time steps  $\Delta t_{\rho_T}$ ,  $\Delta t_{\log \phi}$ ,  $\Delta t_v$  are chosen to minimise the number of PT iterations loops required to reach convergence.

The other unknowns ( $\rho_s$ ,  $\rho_f$ ,  $X_s$ ,  $\phi$ ,  $P_f$ ,  $P_t$ ,  $\tau_{xx}$ ,  $\tau_{yy}$ ,  $\tau_{xy}$ ,  $\eta$ ,  $\eta_b$ ) can be determined without PT iterations and are solved explicitly. To summarise, at each time step the following equations are solved until the residuals of the PT equations are smaller than the chosen tolerance:

1. Compute equilibrium  $\rho_s^{EQ}$ ,  $X_s^{EQ}$ ,  $\rho_f$  and  $\eta^{EQ}$  as a function of  $P_f$  with equations (4.8), (4.9), (4.10), (4.23).
2. Compute  $\rho_s$ ,  $X_s$ ,  $\eta$  and  $\eta_b$  as a function of  $\rho_s^{EQ}$ ,  $X_s^{EQ}$  and  $\eta^{EQ}$  with kinetics equations (4.11), (4.12), (4.24) and (4.15).

3. Use the PT equation (4.27) (total mass conservation) to compute  $\rho_T$  as a function of  $\phi, \rho_f, \rho_s, v_x, v_y$ .
4. Use the PT equation (4.28) (solid mass conservation) to compute  $\log \phi$  as a function of  $\phi, \rho_s X_s, v_x, v_y$ .  $\phi$  can be recovered as  $\phi = \exp(\log \phi)$ .
5. Compute  $\rho_T^s$  using equation (4.5) as a function of  $\phi, \rho_s$  and  $X_s$ .
6. Use the inverse look-up table (equation 4.13) to compute  $P_f$  as a function of  $\rho_T$  and  $\rho_T^s$ .
7. Compute deviatoric shear stresses  $\tau_{ij}$  as a function of  $v_x, v_y, \eta, \phi$  with equation (4.20) (linear viscosity equation), and correct the deviatoric shear stresses  $\tau_{ij}$  if the plastic yield is reached (equation 4.25).
8. Use the PT equations (4.29), (4.30) to compute  $v_x$  and  $v_y$  as a function of  $\tau_{xx}, \tau_{yy}, \tau_{xy}$  and  $P_t$ .
9. Rearrange equation (4.14) to explicitly solve for  $P_t$  as a function of  $P_f, \phi, v_s$  and  $\eta_b$ :

$$\frac{dP_t}{dt} = \left( -\nabla \cdot \vec{v}_s + (\beta_d - \beta_s) \frac{dP_f}{dt} - \frac{P_t - P_f}{(1-\phi)\eta_b} \right) / \beta_d. \quad (4.31)$$

Table 4.1 – Model variables. The equations used to determine the value of the model unknowns are indicated.

Symbol	Meaning	Unit	Value
$P_f$	Fluid Pressure	Pa	Eq. 4.13
$P_t$	Total Pressure	Pa	Eq. 4.31
$\tau_{ij}$	Deviatoric stress tensor	Pa	Eq. 4.20
$\phi$	Porosity	-	Eq. 4.28
$\rho_T$	Total mass per unit volume	$\text{kg m}^{-3}$	Eq. 4.27
$\rho_T^s$	Total solid mass per unit volume	$\text{kg m}^{-3}$	Eq. 4.5
$\rho_s^{EQ}$	Solid density at equilibrium	$\text{kg m}^{-3}$	Eq. 4.8
$\rho_s$	Solid density	$\text{kg m}^{-3}$	Eq. 4.11
$\rho_f$	Fluid density	$\text{kg m}^{-3}$	Eq. 4.10
$X_s^{EQ}$	Non-volatile mass fraction at equilibrium	-	Eq. 4.9
$X_s$	Non-volatile mass fraction	-	Eq. 4.12
$\vec{v}_s$	Solid velocity with components $v_x, v_y$	$\text{m s}^{-1}$	Eq. 4.29, 4.30
$\eta^{EQ}$	Shear viscosity at equilibrium	Pa s	Eq. 4.23
$\eta$	Shear viscosity	Pa s	Eq. 4.24
$\eta_b$	Bulk viscosity	Pa s	Eq. 4.15

#### 4.4.4 Model configuration

##### 4.4.4.1 Initial set up

The initial physical set-up of our model is illustrated on figure 4.3. At the start, the total, solid and fluid pressures are uniform and equal to the same background pressure  $P_{bg}$ . A weak and porous inclusion is placed in the centre of the 1x1 m domain. It can represent an inclusion of wet granulite, weaker than dry granulite (Rybacki and Dresen, 2000), or an eclogite shear zone undergoing eclogitisation (figure 4.1). The viscosity perturbation is smoothed to decrease the viscosity contrast and thereby increase numerical efficiency. A pure shear deformation is applied to the domain, with compression in the horizontal (x) direction and extension in the vertical (y) direction.

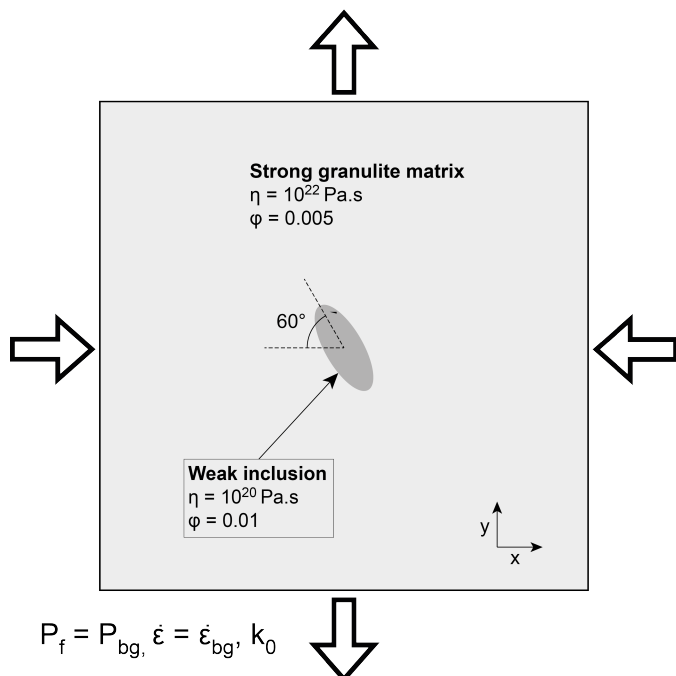


Figure 4.3 – Model configuration. The domain size is 1x1 metre. Initially, fluid pressure  $P_f$  is equal to the background pressure  $P_{bg}$ , and is uniform across the domain.

##### 4.4.4.2 Choice of physical properties

We set the model parameters close to natural values reported in the litterature. Unless stated otherwise, all simulations displayed in this study use the parameters described below and listed in table 4.2. The background pressure  $P_{bg}$ , background strainrate  $\dot{\epsilon}_{bg}$  and the permeability coefficient  $k_0$  are not set because their values are badly constrained and are tested in a parametric study.

The reaction pressure at which granulite transforms into eclogite is set to  $P_r = 19$  kbar (Jamtveit et al., 1990; Zhong et al., 2019). Granulite density is set to  $\rho_g = 3000 \text{ kg m}^{-3}$  at background pressure, and eclogite density to  $\rho_e = 3200 \text{ kg m}^{-3}$  at reaction

Table 4.2 – Model parameters. The values of  $P_{bg}$ ,  $\dot{\varepsilon}_{bg}$  and  $k_0$  are not fixed since they are tested in the parametric study section.

Symbol	Meaning	Unit	Value
$P_r$	Reaction pressure	Pa	$19 \times 10^8$
$\eta_f$	Fluid viscosity	Pa s	$10^{-3}$
$\eta_g$	Granulite viscosity	Pa s	$10^{22}$
$\eta_e$	Eclogite and inclusion viscosity	Pa s	$10^{20}$
$\eta_t$	Transient viscosity	Pa s	$10^{19}$
$\beta_s$	Solid compressibility	Pa <sup>-1</sup>	$10^{-11}$
$\beta_d$	Drained compressibility	Pa <sup>-1</sup>	$2 \times 10^{-11}$
$\hat{\sigma}$	Viscoplastic overstress	Pa	$10^6$
$C$	Cohesion	Pa	$50 \times 10^6$
$\alpha$	Friction angle	°	30
$\phi_0$	Background porosity	-	0.005
$\phi_i$	Inclusion porosity	-	0.01
$\phi_p$	Threshold porosity	-	0.05
$X_s^g$	Mass fraction of solid component in granulite	-	1
$X_s^e$	Mass fraction of solid component in eclogite	-	0.995
$\rho_g$	Granulite density at $P_{bg}$	kg m <sup>-3</sup>	3000
$\rho_e$	Eclogite density at $P_r$	kg m <sup>-3</sup>	3200
$t_k$	Kinetics time scale	years	100
$P_{bg}$	Background pressure	Pa	$15 - 18 \times 10^8$
$\dot{\varepsilon}_{bg}$	Background strain rate	s <sup>-1</sup>	$1 - 4 \times 10^{-14}$
$k_0$	Permeability coefficient	m <sup>2</sup>	$10^{-18} - 10^{-21}$

pressure (Austrheim, 1987; Austrheim and Mørk, 1988; Centrella, 2019). The fraction of non-volatile elements structurally bound to the solid is set to  $X_s = 1$  in the granulite and  $X_s = 0.995$  in the eclogite (Rockow et al., 1997; Centrella, 2019).

$\rho_s$  varies as a function of pressure according to a solid compressibility  $\beta_s$ . For simplicity, we use a constant solid compressibility  $\beta_s = 10^{-11}$  Pa<sup>-1</sup>, consistent with computations with the software Perple\_X (Connolly, 2005) on Holsnøy granulite and eclogite (Bras et al., 2023), and also consistent with the Abers and Hacker (2016) database (granulite:  $\beta_s = 1.2 \times 10^{-11}$  Pa<sup>-1</sup>, eclogite:  $\beta_s = 0.9 \times 10^{-11}$  Pa<sup>-1</sup>). The drained compressibility is  $\beta_d = 2 \times 10^{-11}$  Pa<sup>-1</sup>, twice the value of the solid compressibility  $\beta_s$ . This corresponds to a typical Biot-Willis coefficient of 0.5 in crustal rocks (e.g. Selvadurai, 2021; Zhou and Ghassemi, 2022).

Granulite viscosity is  $\eta_g = 10^{22}$  Pa.s, consistent with strength measurements of Rybacki and Dresen (2000) in dry plagioclase at  $\dot{\varepsilon}_{bg} = 10^{-14}$  s<sup>-1</sup>. Eclogite and transient viscosities are respectively  $\eta_e = 10^{20}$  Pa.s and  $\eta_t = 10^{19}$  Pa.s., i.e. 100 and 1000 times weaker than granulite (Bras et al., 2021; Kaatz et al., 2023). The initial inclusion is also

100 times weaker than granulite. Fluid viscosity is  $\eta_f = 10^{-3}$  Pa s (Audéitat and Keppler, 2004; Hack and Thompson, 2011).

Cohesion and friction angle are  $C = 50$  MPa and  $\alpha = 30^\circ$ , as they correspond to an extrapolation of Byerlee (1978) data at high pressure (Yamato et al., 2022). Following Duretz et al. (2020), we consider that the additional stress caused by the viscoplastic element is  $\hat{\sigma} = 1$  MPa. The resulting regularisation viscosity is then  $\eta^{vp} = 10^6/\dot{\varepsilon}_{bg}$ .

The initial porosity is 0.005 in granulite and 0.01 in the weak inclusion, consistent with porosity measurements by Kaatz et al. (2023) in Holsnøy granulite.

The kinetic time scale  $t_k$  been set to 100 years as there are arguments that granulite to eclogite transformation is rather a fast process (Malvoisin et al., 2020).

#### 4.4.5 Resolution test

Spacial resolution tests were performed and are presented in figure 4.4. The results of tests for spatial resolution show convergence with increasing resolution, indicating that the employed finite differences discretisation is appropriate for HMC modelling. We use 200 numerical grid points for the discretisation in space. With this resolution the simulation presented in figure 4.5 can be computed in a matter of days on a standard laptop. Due to the high number of simulations required, our parametric study uses only 100 numerical grid points.

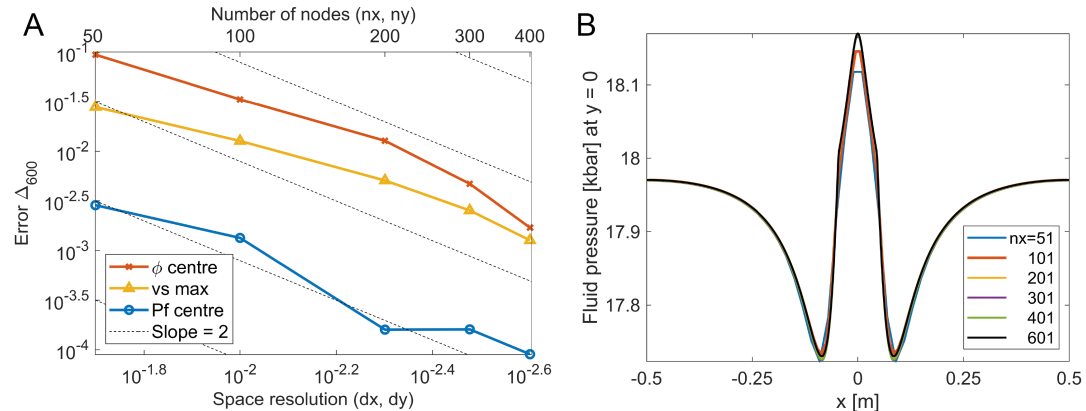


Figure 4.4 – Spatial resolution test. (A) Error relative to a simulation with 600 nodes in the x and y dimensions. (B) Fluid pressure along a horizontal profile at  $y = 0$  (middle of the y dimension), after a simulation time of 100 years.

## 4.5 Results

Our results are presented in two distinct parts. We first show some general results of our model, and study in detail a reference model with specific parameters, in order

to show that tectonic induced propagation of the eclogitisation reaction is possible. Secondly, we conduct a parametric study to determine for which  $P_{bg}$ ,  $\dot{\epsilon}_{bg}$  and  $k_0$  the propagation of eclogitisation is possible. In all figures, perceptually uniform colour maps are used to prevent visual distortion of the data (Crameri, 2018).

#### 4.5.1 Reference model

We start the description of our model with the figure 4.5, which shows the evolution of a reference model, starting from the configuration described in figure 4.3 and ending after 7000 years. Our reference model uses the parameters of table 4.2, and  $P_{bg} = 18$  kbar,  $\dot{\epsilon}_{bg} = 4 \times 10^{-14} \text{ s}^{-1}$ ,  $k_0 = 10^{-20} \text{ m}^2$ . We display the time evolution of 2 model properties, fluid pressure and solid viscosity.

In the starting state, fluid pressure is uniform. The inclusion is weaker and more porous than the surrounding granulite. Due to the viscosity contrast between the strong granulite constituting the matrix and the weak inclusion, high pressure gradients gradually develop due to the imposed tectonic deformation. Fluid pressure increases in a direction perpendicular to the compression direction (above and below the weak inclusion), and decreases parallel to the compression direction (left and right of the weak inclusion). When  $P_f$  reaches the reaction pressure, granulite starts transforming into eclogite and the rock viscosity gradually drops. This weakening drives the tectonic overpressure to areas further away from the inclusion, which eventually reach the reaction pressure and convert to weak eclogite, efficiently propagating the eclogitisation reaction. Underpressures develop left and right of the weak region inclusion, preventing

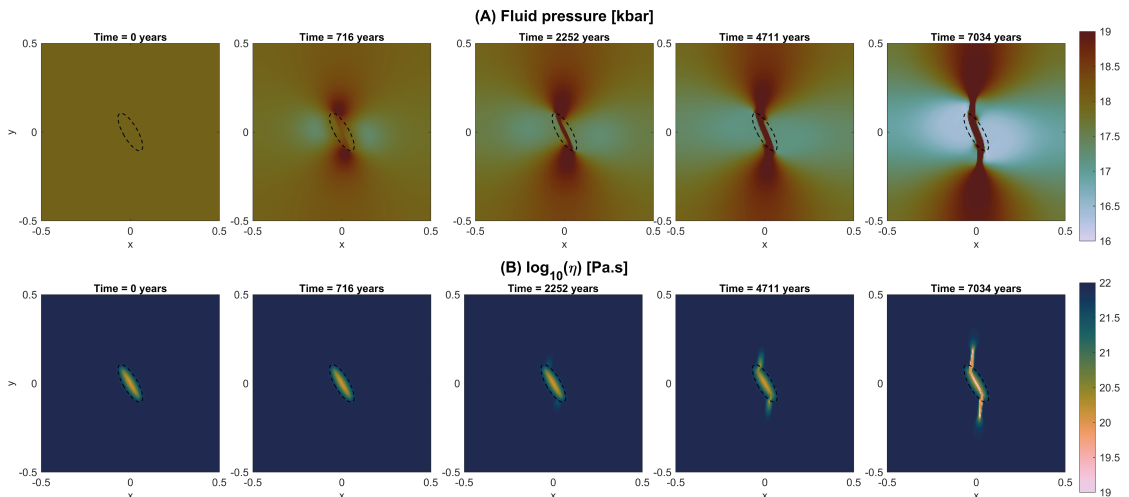


Figure 4.5 – Time evolution of the fluid pressure (A) and viscosity (B) in our reference model:  $P_{bg} = 18$  kbar,  $\dot{\epsilon}_{bg} = 4 \times 10^{-14} \text{ s}^{-1}$ ,  $k_0 = 10^{-20} \text{ m}^2$ . The dotted ellipses show the initial extend of the weak inclusion.

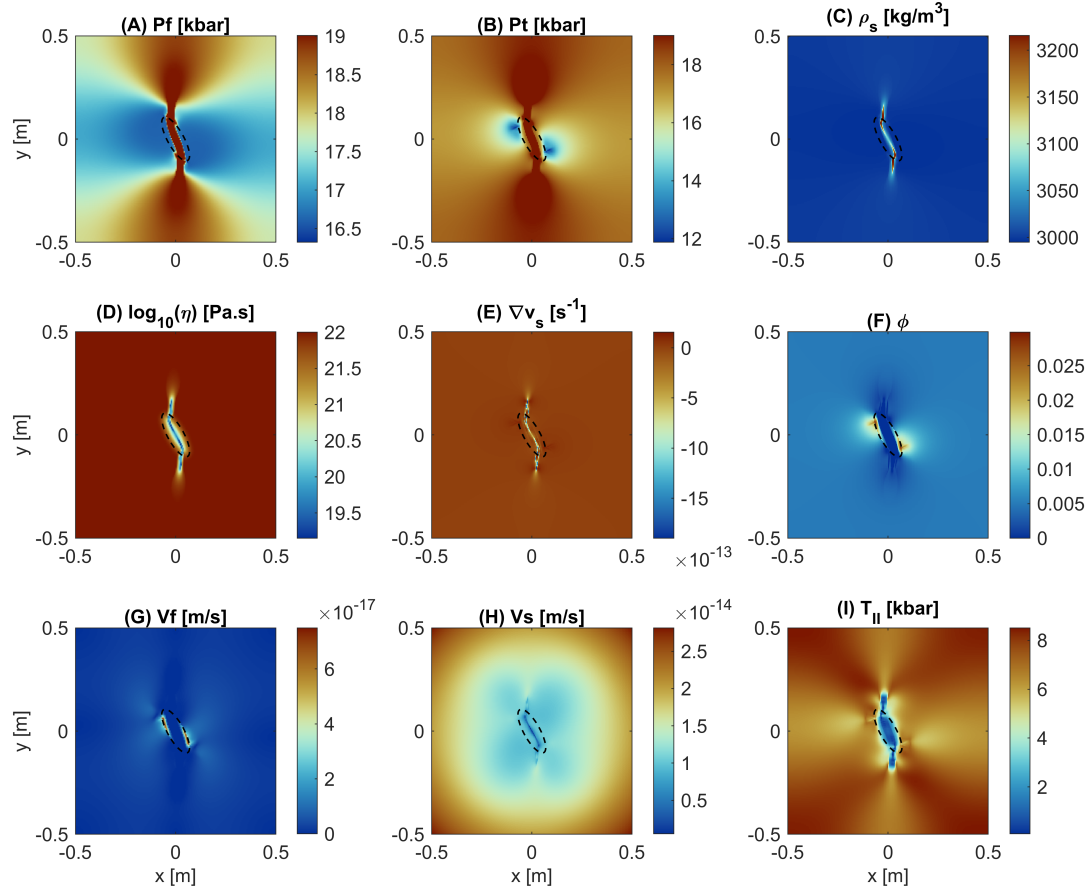


Figure 4.6 – Physical properties of the reference model after 7000 years: (A) fluid pressure, (B) total pressure, (C) Solid density, (D) Shear viscosity, (E) Divergence of solid velocity, (F) Porosity, (G) Fluid velocity, (H) Solid velocity, (I) Second invariant of the stress tensor.

conversion of these areas into eclogite.

To illustrate all features of our HMC model, colour maps of physical properties of the end state (7000 years) of the reference model are displayed on figure 4.6. The high pressure region has an homogeneous  $P_f$  of around 19 kbar, just above the reaction pressure (figure 4.6A).  $P_t$  is close to  $P_f$  due to the poro-visco-elastic volumetric deformation (figure 4.6B), and is sometimes higher than  $P_f$ , resulting in fluid overpressure. The areas where  $P_f$  reached  $P_r$  transformed into eclogite, showing as a result an increased density (figure 4.6C) and a decreased viscosity (figure 4.6D). Divergence of solid velocity is negative in the inclusion and above/below the inclusion, showing volumetric compaction in these areas, and expansion in the rest of the model (figure 4.6E). Consequently, the areas showing volumetric compaction exhibit a reduction in volume and therefore in porosity (figure 4.6F), whereas expanding regions exhibit an increase in volume and in porosity. Significant fluid flow occurs in the inclusion (figure 4.6G), where the fluid pressure gradients are highest between the high  $P_f$  and the low  $P_f$  areas. The magnitude

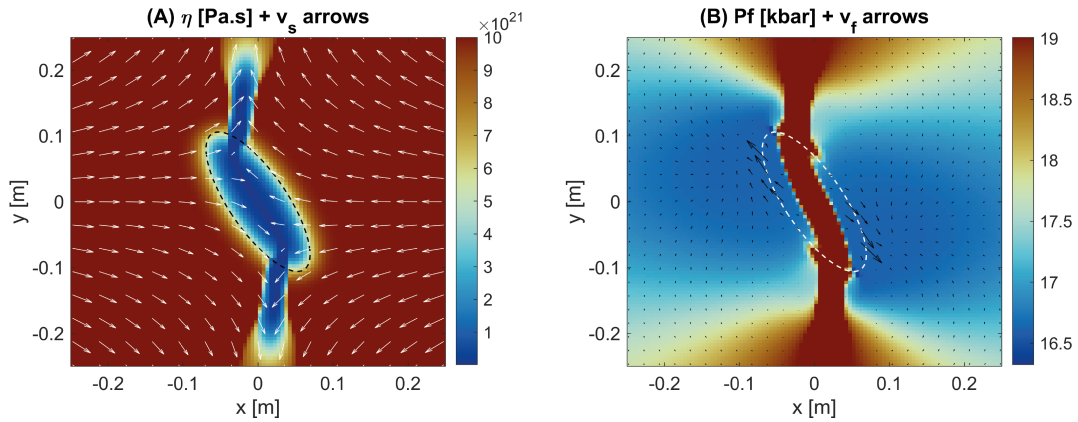


Figure 4.7 – Visualisation of the directions of solid and fluid flow. (A) Enlargement of  $\eta$  colormap with vector field  $v_s$  (arrows) and (B) enlargement of  $P_f$  colormap with vector field  $v_f$  (arrows). The scaling of the arrows is different between A and B (ie the same arrow does not represent the same velocity in A and in B).

of solid velocity is 2 orders of magnitude higher than fluid velocity (figure 4.6H). The  $\text{str}\tau_{II}$  is higher outside the inclusion (figure 4.6I), where shear viscosity is the highest.

In order to visualise the directions of the solid and fluid velocities, figure 4.7 shows an enlargement of figures 4.6A and 4.6D, with arrows indicating  $v_s$  on figure 4.7A and  $v_f$  on figure 4.7B. Due to force balance in response to the applied far-field pure shear, solid material flows from strong regions facing towards the deformation direction, to weak regions and to regions above and below the weak inclusion (figure 4.7A). Due to Darcy law, fluids flow in opposite directions, from the high pressure region in the inclusion towards nearby low pressure regions (4.7B).

#### 4.5.2 Parametric study

Figure 4.7 illustrates that in a two-phase model that takes into account both fluid and solid flow, both processes can counterbalance themselves. For this reason, we conducted a parametric study (figure 4.8) to investigate the role of strain rate and permeability, as well as background pressure, on the modelled fluid pressure. To check if one particular model configuration (with parameters  $k_0/\dot{\varepsilon}_{bg}/P_{bg}$ ) allows for propagation of the eclogitisation reaction, we measured for each  $k_0/\dot{\varepsilon}_{bg}/P_{bg}$  triplet what is the maximum pressure reached at a distance  $d = 10$  cm above the weak inclusion (figure 4.8). For short we note this pressure  $P_f^{10}$ . Simulations were stopped when  $P_f^{10}$  reaches  $P_r$ , or when  $P_f^{10}$  reaches a plateau and stops increasing. Therefore, a triplet  $k_0/\dot{\varepsilon}_{bg}/P_{bg}$  allows for propagation of the reaction front only if  $P_f^{10} = P_r$ .

Higher  $P_{bg}$  and  $\dot{\varepsilon}_{bg}$  tend to increase  $P_f^{10}$ , whereas higher  $k_0$  tend to decrease  $P_f^{10}$ . High overpressures are thus favored by low permeability and high background strainrate.

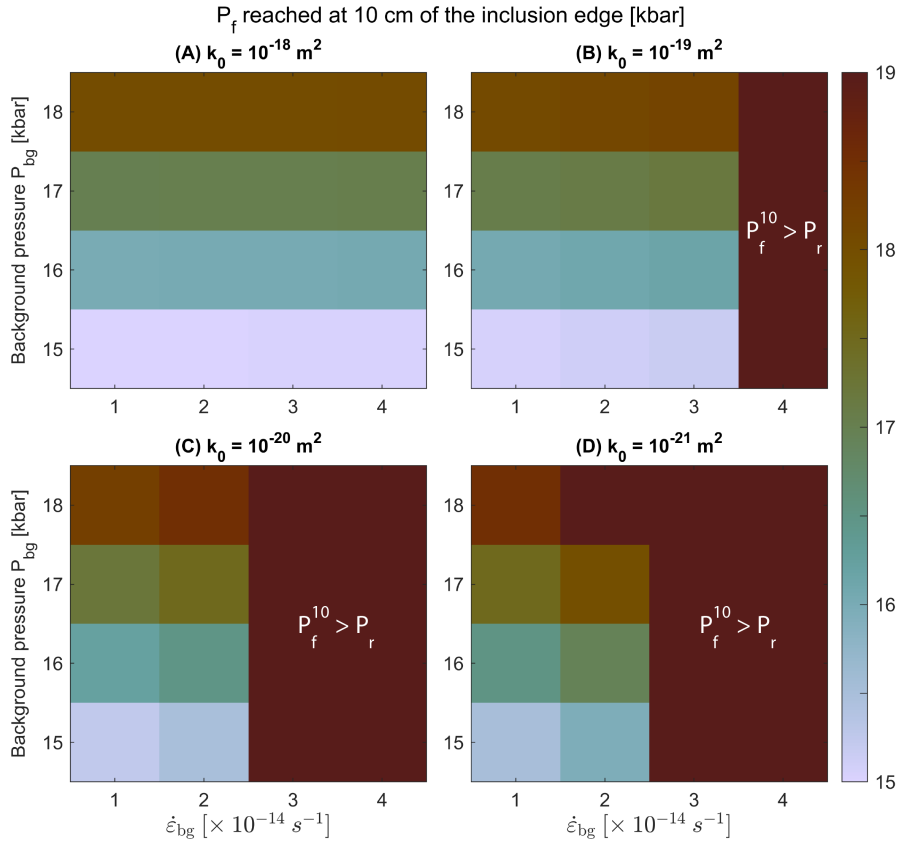


Figure 4.8 – Parametric study on the role of  $k_0$ ,  $\dot{\varepsilon}_{bg}$  and  $P_{bg}$  on modelled fluid pressure, measured at 10 cm of the weak inclusion edge. In simulations that did not reach  $P_r$ , the maximal pressure is displayed; otherwise  $P_r$  is displayed.

Propagation of eclogitisation (i.e.  $P_f^{10} > P_r$ ) is not possible if  $k_0 = 10^{-18} \text{ m}^2$ . It is possible for  $k_0 = 10^{-19} \text{ m}^2$  only if  $P_{bg} = 18 \text{ kbar}$ . It is possible for  $k_0 < 10^{-19} \text{ m}^2$  at any  $P_{bg} > 15 \text{ kbar}$ , as long as  $\dot{\varepsilon}_{bg}$  is sufficiently high.

The results of our parametric study are illustrated in figure 4.9 with some example  $P_f$  colormaps of models with various  $\dot{\varepsilon}_{bg}$  and  $k_0$ . The comparison of models A/C/E to respectively B/D/F shows the importance of solid deformation: a higher  $\dot{\varepsilon}_{bg}$  results in greater and faster pressure variations. Indeed, figure 4.9G shows that  $P_f^{10}$  increases with a steeper slope in models with higher  $\dot{\varepsilon}_{bg}$ . The comparison of models A/B to C/D to E/F shows the importance of fluid flow: a lower  $k_0$  results in greater pressure variations. In the higher  $k_0$  models (A and B), fluid pressure diffuses faster into the granulite, preventing a fast pressure build-up by solid deformation. Indeed, figure 4.9G shows that the curve  $P_f^{10}(t)$  flattens faster in models with higher  $k_0$ . In model A and in the magenta model, fluid pressure rapidly stops increasing and the reaction pressure is never reached. Overall, propagation of a high pressure front is faster in low permeability and high background strainrate conditions.

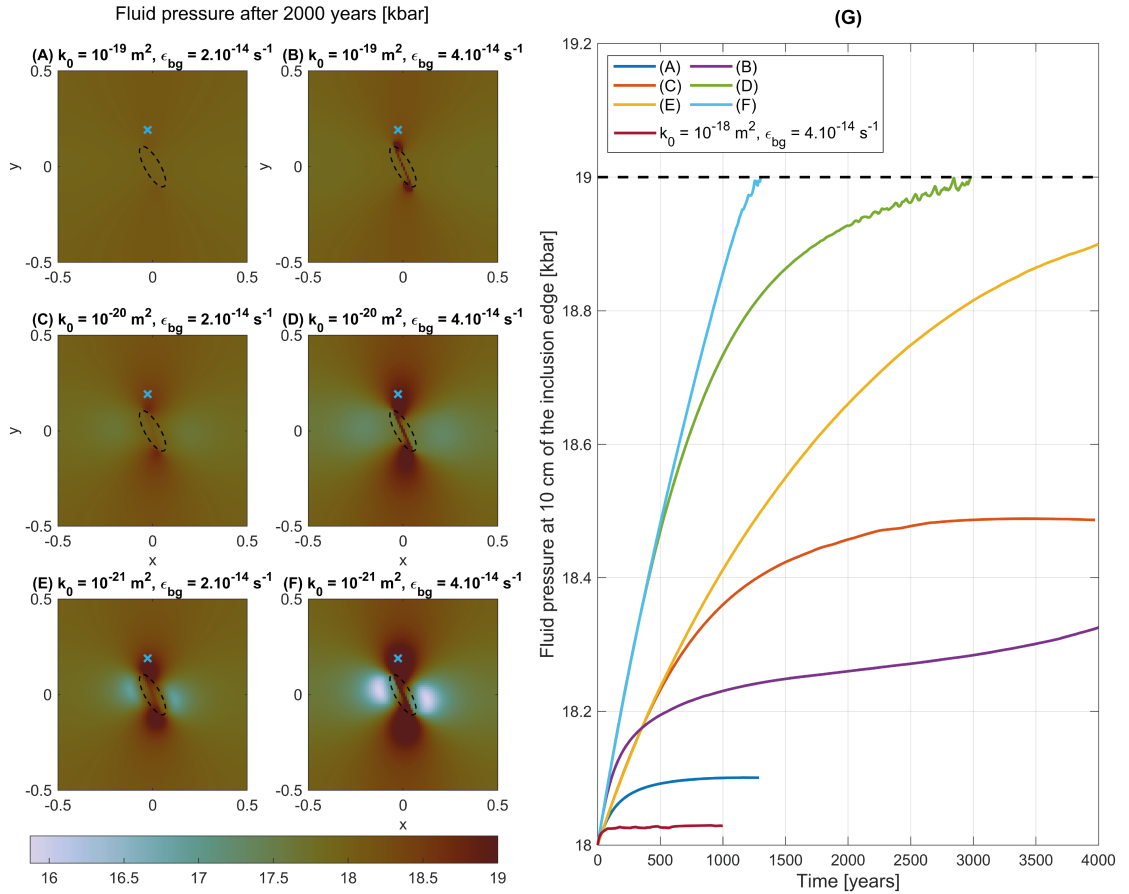


Figure 4.9 – (A) to (F) Fluid pressure for different simulations with  $P_{bg} = 18$  kbar after 2000 years. The position where  $P_f^{10}$  is saved is marked by the blue cross. (G) Time evolution of  $P_f^{10}$  for simulations (A) to (F). The additional simulation (magenta line) has no associated  $P_f$  colour map because no significant pressure variations would appear. Simulations were stopped when  $P_f^{10}$  reached  $P_r$  or when  $P_f^{10}$  reached a maximum and started decreasing.

## 4.6 Discussion

### 4.6.1 Deformation-induced eclogitisation

Figure 4.5 shows that far-field deformation can induce propagation of the eclogitisation reaction outside the initial viscosity perturbation. The viscosity contrasts give rise to solid velocity gradients that translate to progressive changes in fluid pressure through the conservation equations. If  $P_f$  reaches the reaction pressure, the rock transiently weakens as granulite transforms into eclogite. This extends the low viscosity area, hence pushing solid velocity gradients outwards, and promoting the reaction-front propagation.

Our inverse look-up table approach clearly highlights the relation between total

mass and fluid pressure: for a given  $\rho_T^s$ , if the total mass increases then the fluid pressure increases in response (equation 4.13, figure 4.2B). Eclogitisation thus occurs to accommodate an increase in mass through a densification reaction, consistent with the conceptual model of Centrella (2019).

A striking characteristic of HMC models is that once fluid pressure reaches the reaction it seems to stop increasing. This stabilisation of  $P_f$  at the reaction pressure is also apparent in other published HC and HMC models: Schmalholz et al. (2020) (their figure 7); Bras et al. (2023) (their figure 5). Actually  $P_f$  continues to increase, but very slowly because of the coupling between masses and fluid pressure (figure 4.2B). For simplicity, let us consider that solid mass has a constant value of  $\rho_t^s = 3000 \text{ kg m}^{-3}$ , so that the relation between total mass and pressure is that shown on figure 4.2A. The coupling between  $\rho_T$  and  $P_f$  dictates that  $\rho_T$  must heavily increase, from around 3000 to  $3100 \text{ kg m}^{-3}$ , in order to have  $P_f > P_r$ . This means that any  $\rho_T$  between 3000 and  $3100 \text{ kg m}^{-3}$  corresponds to a fluid pressure of about 19 kbar. This stays true for all  $\rho_t^s$ , which is the reason why most  $\rho_T$  in the inverse look-up table (figure 4.2B) return a value of about 19 kbar.

#### 4.6.2 Competition between strain rate and Darcy flow

In our HMC model 2 competing processes contribute to changes in pressure:

(1) Solid deformation caused by the imposed strain rate tend to create pressure variations around viscosity anomalies, whose patterns and magnitude depend on the orientation, shape and viscosity contrasts of the anomaly (Schmalholz and Podladchikov, 2013; Moulas et al., 2014; Jamtveit et al., 2018b). In our reference model, deformation makes solid mass flow from the left/right of the inclusion, towards the top/bottom of the inclusion (figure 4.7A). Therefore fluid pressure increases above/below the inclusion, and decreases left/right of the inclusion. Higher background strain rates result in a higher solid mass flow and therefore higher pressure variations.

(2) Darcy flow is a diffusive process (e.g. Connolly, 1997; Malvoisin et al., 2015; Bras et al., 2023) that makes fluid mass flow from high pressure to low pressure regions (figure 4.7B). In our model it tends to counterbalance the fluid pressure gradients created by solid deformation. Higher permeability coefficients  $k_0$  result in a higher fluid flow and therefore faster smoothing of the pressure variations.

The competitions between solid deformation and Darcy flow therefore dictates the behaviour of the model. Our parametric study (figure 4.8 and 4.9) suggests that propagation of eclogitisation is only possible for high back ground strain rate, low permeability and high background pressure. If  $\dot{\varepsilon}_{bg}$  is low and  $k_0$  is high, for example in figure 4.9A, then  $P_f$  is controlled by Darcy flow: The pressure gradients generated by deformation are rapidly smoothed by fluid pressure diffusion, so that the pressure

variations are negligible. If  $\dot{\varepsilon}_{bg}$  is high and  $k_0$  is low, for example in figures 4.9F, then  $P_f$  is controlled by deformation: The decrease in  $P_f$  caused by Darcy flow is slower than the increase caused by solid deformation. Despite  $P_f$  diffusion, significant overpressures develop in the extension direction.

#### 4.6.3 Implications for eclogitisation in Holsnøy

For the range of  $\dot{\varepsilon}_{bg}$  tested in figure 4.8, only simulations that have a permeability coefficient  $k_0 \leq 10^{-19} \text{ m}^2$  can generate overpressures of several kbar. Considering a porosity  $\phi = 0.03$ , the maximum observed in the reference simulation, this leads to a Carman-Kozeny permeability  $k_0\phi^3$  in the order of  $10^{-24} \text{ m}^2$ . This is consistent with low estimates of crust permeability (e.g. Shmonov et al., 2003; Ingebritsen and Manning, 2010; Mindaleva et al., 2020; Angiboust and Raimondo, 2022). The permeability of the lower crustal rocks must be low to allow the generation of overpressures of several kbar, that can transform granulite into eclogite. A pulse or a series of pulses of high fluid pressure related to seismic aftershocks can however provide an additional source of high pressure, enhancing the propagation of the reaction front (Malvoisin et al., 2020; Putnis et al., 2021; Bras et al., 2023). The development of large underpressured areas where granulite is preserved is consistent with the heterogeneity of eclogitisation in Holsnøy, where fingers of eclogite penetrate into the untransformed granulite.

In our reference simulation (figure 4.5), the reaction front propagated around 30 cm from the border of the inclusion into the granulite in about 7000 years. This rate is much smaller than if the pressure gradient is generated by a sustained fluid pulse (Bras et al., 2023), because there is no external supply of mass / fluid pressure, but rather a redistribution of mass / fluid pressure induced by the fluid and solid velocities. This propagation rate is consistent with the large extend of eclogite facies overprint in Holsnøy (Zertani et al., 2019) that occurred within ca 5 Ma (Jamtveit et al., 2019).

Our parametric study focuses on relatively low strain rates ( $\dot{\varepsilon} \leq 4 \times 10^{-14} \text{ s}^{-1}$ ) because we aim at simulating the evolution of eclogite fingers, which occurs without intense deformation (Zertani et al., 2019). Figure 4.10 shows that for higher strain rates, frictional deformation, rather than viscous, becomes predominant in the model. This results in the development of shear bands (e.g. Duretz et al., 2021), where effective viscosity decreases due to plastic failure (equation 4.25). Here,  $P_f$  rapidly increases along a weak shear band instead of slowly propagating as a result of viscous deformation only, like in figure 4.5. This mode of propagation that associates intense deformation and fluid flow along a shear band (figure 4.10A) resembles that of Holsnøy eclogite shear zones, and could be subject of a future work.

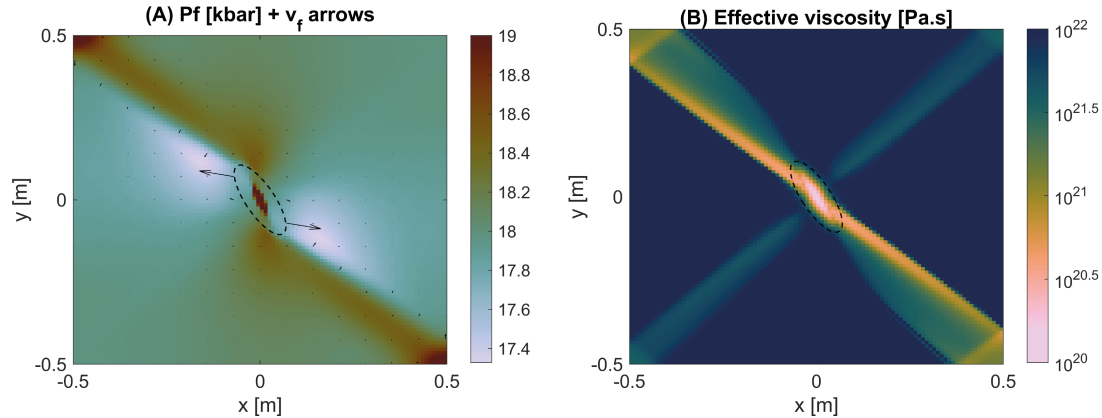


Figure 4.10 – Effect of intense shear deformation, in a simulation with  $P_{bg} = 18$  kbar,  $k_0 = 10^{-20}$  m $^2$ ,  $\dot{\epsilon}_{bg} = 10^{-13}$  s $^{-1}$ , after 1000 years. (A): Fluid pressure and vector field of fluid velocity (arrows). Small black arrows show fluids flowing from the high pressure shear band towards the low pressure granulite. (B) Effective viscosity showing the extend of frictional plastic deformation. Effective viscosity decreases due to plastic failure when the yield criterion is met.

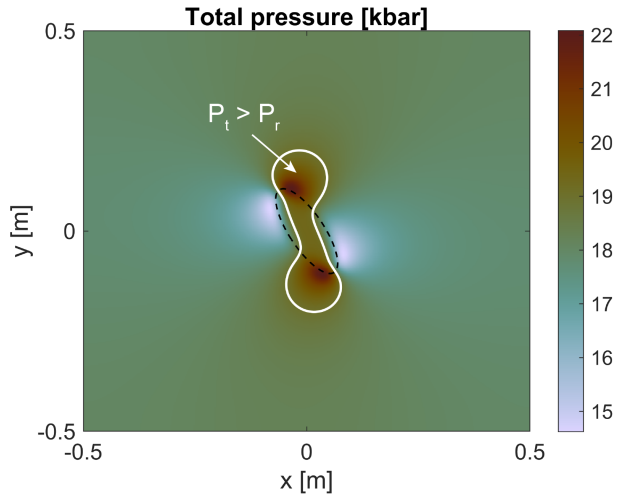
#### 4.6.4 Comparison with single phase models

We can compare our two-phase model to incompressible, single phase mechanical (SPM) models, such as that of Jamtveit et al. (2018b), that are commonly used to explain that overpressures can induce eclogitisation (e.g. Putnis et al., 2021). Figure 4.11 shows the distribution of pressure in an SPM model, with the configuration of figure 4.3. Since single-phase models do not consider fluids, fluid pressure cannot be defined. To facilitate the comparison, we assume that in the SPM model fluid pressure is equal to the solid pressure computed from the force balance equations, and that fluid pressure is the thermodynamic equilibrium pressure. Figure 4.11 showcases major differences between SPM to HMC models:

(1) Figure 4.11 shows how pressure is distributed as an immediate response to applied deformation, without any time-sensitive mechanism. This is fundamentally different to HMC models, where pressure varies over time as a consequence of changes in mass ( $\rho_T$  and  $\rho_T^s$ ) governed by conservation equations (4.4 and 4.6) that have a time dependence.

(2) In the HMC model,  $\rho_T$  needs to massively increase in order to complete the eclogitisation reaction. Given that  $\rho_T$  increases as a consequence of solid and fluid flow, it takes a long time to complete this reaction, independently of reaction kinetics. In our reference simulation  $P_f$  rarely exceeds 19.01 kbar, the pressure at which the reaction is complete, because of the time needed for this small pressure increase. Contrary to the HMC model, pressure in the SPM model does not need to cross this reaction barrier and instantaneously increases above  $P_r$ .

Figure 4.11 – Solid pressure in a SPM model with spatial resolution  $nx = 400$  and for the same configuration as our reference model, except  $\dot{\epsilon}_{bg} = 2 \times 10^{-14} \text{ s}^{-1}$ . Rocks are assumed incompressible, and fluid and mass conservation are not considered. The only equations that are solved are the Stokes equation 4.18, 4.19 and the continuity equation for incompressible fluids:  $\nabla \cdot v_s = 0$ . In the area inside the solid white line the fluid pressure is higher than the reaction pressure.



(3) Since fluids are not considered in the SPM model, the tectonically-induced increase in pressure is not balanced by Darcy flow, resulting in higher pressure variations.

Overall, pressure variations estimated by SPM models are similar to those predicted by HMC models. However they cannot estimate the time required for the completion of the reaction, because they do not involve any time-sensitive mechanism, and they tend to overestimate pressure gradients because they do not consider fluid pressure diffusion via porous flow.

#### 4.6.5 Transient weakening

During transformation of mechanically strong granulite into weaker eclogite, the rock goes through a transient weak stage during which the rock viscosity is lowest than both granulite and eclogite viscosity (Bras et al., 2021; Rogowitz and Huet, 2021; Baïsset et al., 2023; Kaatz et al., 2023). Our model reproduces these observations by including transient weakening (figure 4.2C). We tested the contribution of transient weakening to the propagation of the eclogitisation reaction, by comparing our reference configuration (figure 4.5) with the same configuration but without transient weakening (figure 4.12). Instead the viscosity decreases steadily during granulite to eclogite transformation:

$$\log_{10}(\eta^{EQ}) = \frac{P_f - P_r}{2\epsilon} \log_{10}(\eta_e) + \frac{P_r + 2\epsilon - P_f}{2\epsilon} \log_{10}(\eta_g) \text{ if } P_r < P_f < P_r + 2\epsilon. \quad (4.32)$$

After the same simulation time (7000 years), the reaction has propagated significantly further in the transient weakening simulation (figure 4.12): approximately 30 cm away from the inclusion in the transient weakening case, and only 15 cm away without transient weakening. This confirms the observation of Bras et al. (2021) who suggested that transient weakening contributes to the propagation of eclogitisation zones.

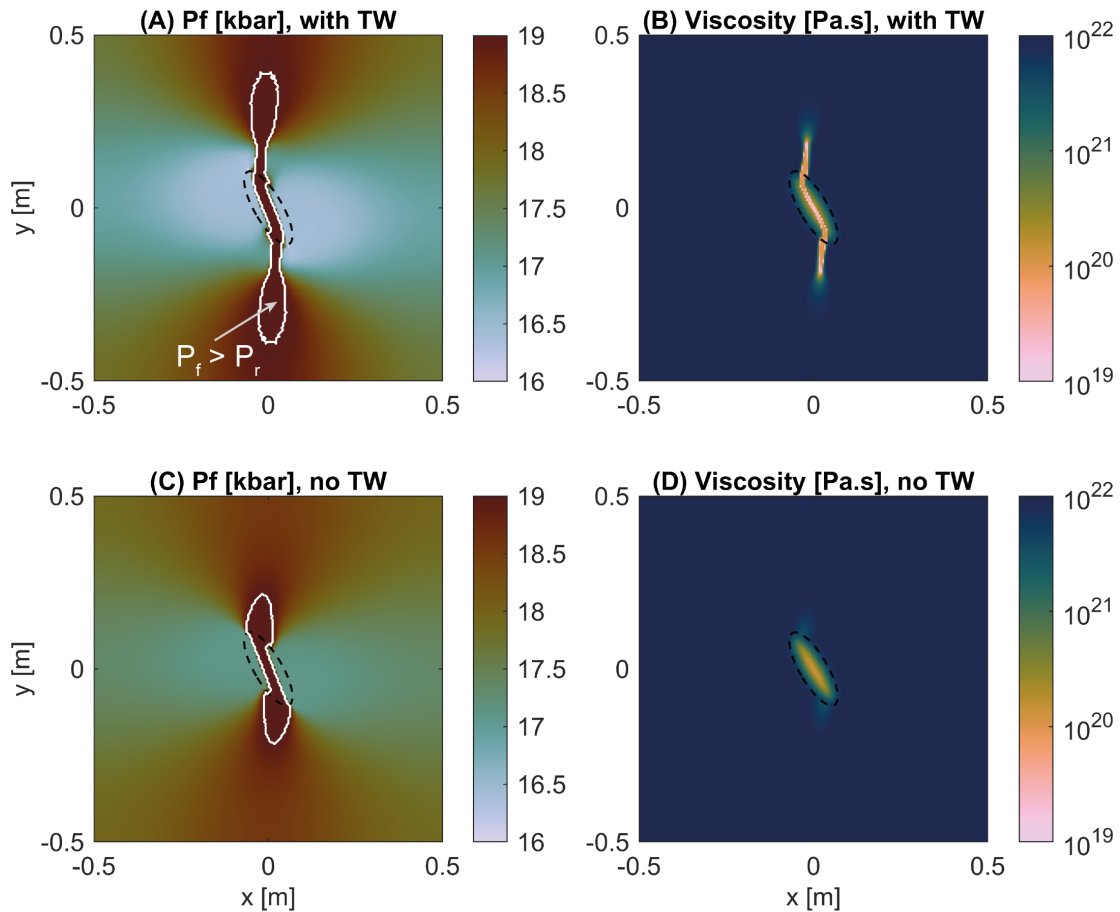


Figure 4.12 – Effect of transient weakening (TW) on the propagation of eclogitisation, after 7000 years. Fluid pressure (A, C) and viscosity (B, D) in our reference model (A, B), and in a simulation with the same parameters as our reference model ( $P_{bg} = 18$  kbar,  $\dot{\varepsilon}_{bg} = 4 \times 10^{-14}$  s $^{-1}$ ,  $k_0 = 10^{-20}$  m $^2$ ), but without transient weakening (C, D). Panels A and B are the same as the final panels of figure 4.5A/B. The pressure is higher than the reaction pressure in the area inside the solid white line.

#### 4.6.6 Choice of a thermodynamic pressure

When a solid phase, a fluid phase, deformation and thermodynamic equilibrium are considered together, the question of which pressure dictates the stable mineralogic assemblages becomes crucial. Indeed, stress and fluids can have significant effects of metamorphic reactions (Wheeler, 2014; Hobbs and Ord, 2016; Moulas et al., 2019). In metamorphic systems, the pressure at which a particular mineral assemblage is in equilibrium with, often termed thermodynamic pressure, is classically estimated by minimisation of the Gibbs free energy of a chemical system (e.g. Connolly, 2005). Traditionnally, petrologists have considered that the thermodynamic pressure registered by metamorphic rocks only reflects a burial depth (e.g. Thompson and England, 1984),

i.e. is equivalent to a lithostatic pressure. This has led to the assumption that the presence of ultra-high pressure minerals was a proof of rock burial to depths >90 km (Chopin, 1984). Relating thermodynamic pressure to depth assumes that the stress state is isotropic, i.e. that all normal stress components are equal to a mean-stress value, and that shear stresses are zero (Moulas et al., 2019). However, geodynamics models based on continuum mechanics show that in metamorphic settings mean stress can significantly deviate from lithostatic pressure (e.g. Schmalholz and Podladchikov, 2013). Indeed, some experiments show that the stability of mineral assemblages is controlled by the mean stress ( $\bar{\sigma} = (\sigma_{xx} + \sigma_{yy} + \sigma_{zz})/3$ , Cionoiu et al., 2019; Cionoiu et al., 2022). Other experiments (Hirth and Tullis, 1994; Richter et al., 2016) indicate that it is the maximum principal stress  $\sigma_1$ , rather than the mean stress, that controls the metamorphic reaction.

However, these experiments that support the use of either the mean stress or  $\sigma_1$  as the thermodynamic pressure rely on simple polymorphic reactions (aragonite - calcite and quartz - coesite) that do not involve fluids. When fluids are present, then a fluid pressure is defined and can deviate from the mean stress (e.g. Sibson, 1994). When solid-fluid interactions are considered, theoretical considerations (Dahlen, 1992), field data (Holdaway and Goodge, 1990) and experiments (Llana-Fúnez et al., 2012) indicate that it is the fluid pressure that determines which phases are stable in a local equilibrium domain, rather than the mean stress. Therefore, it appears that fluid pressure is the most accurate proxy for the pressure that rocks are in equilibrium with (Malvoisin et al., 2015), hence why we use it as the thermodynamic pressure in our model. However, the question of which pressure controls the metamorphic reactions pressure is far from trivial (Wheeler, 2014), and future work should aim at reproducing experiments by Richter et al. (2016) or Cionoiu et al. (2019) with reactions that involve fluids.

#### 4.6.7 Limitations and perspectives

Here we only consider a linear viscous rheology, because it leads to faster numerical convergence of the set of pseudo-transient equations, and because it is representative of deformation by diffusion-creep processes, such as dissolution-precipitation creep (e.g. Ranalli, 1995). These deformation processes are at play during metamorphic processes such as eclogitisation of granulite (e.g. Pollok et al., 2008; Putnis and John, 2010; Stünitz et al., 2020; Putnis, 2021; Rogowitz and Huet, 2021). Moreover, simulations with a non-linear or a linear viscosity yield similar results (Supplementary figure S2). A refinement of our model could consider both deformation by dislocation-creep in granulite (Rybacki and Dresen, 2000) and by diffusion-creep in the reacting rock and eclogite.

Eclogitisation of granulite is a densification reaction that increases the solid density  $\rho_s$  (eq. 4.8, figure 4.2A) but decreases  $X_s$  (eq. 4.9). Since the change in  $X_s$  induced by the reaction is small (from  $X_s^g = 1$  to  $X_s^e = 0.995$ ), overall the reaction increases the density

of solid components  $\rho_s X_s$ . Porosity can be computed as  $\phi = 1 - \rho_T^s / (\rho_s X_s)$  (eq. 4.5). In the absence of solid deformation,  $\rho_T^s$  is constant and an increase in  $\rho_s X_s$  generates reaction-induced porosity (Bras et al., 2023). However, in the presence of solid deformation, conservation equation 4.6 dictates that the total solid mass increases in the reacting regions where the solid velocity divergence is negative (figure 4.6A). If the increase in  $\rho_T^s$  is higher than the increase in  $\rho_s X_s$ , this results in an overall porosity decrease. In our reference model, porosity drops to near zero in the eclogite regions (figure 4.6F), which is not consistent with microstructural observations (Putnis et al., 2021) and porosity measurements (Kaatz et al., 2023). This situation is similar to non-deforming models where the reaction decreases the solid density, thereby increasing the solid volume and decreasing the porosity. Malvoisin et al. (2021) show that in this type of models, the increase in solid volume during reaction is more likely accommodated through deformation rather than through a decrease in porosity. A similar solution could be applied to our HMC model, by having the increase in  $\rho_T^s$  contribute to a pressure increase rather than an unrealistic porosity decrease. This could have the effect of amplifying the pressure variations and reducing the porosity decrease.

Finally, our model could be refined by considering the dissolution of non-volatile elements (Si, Na, Mg...) in the fluid phase. Non-negligible solubility of solid species could result in an abundant solid mass redistribution driven by fluid flow (Moore et al., 2020a) that could enhance the generation of porosity at the reaction front.

## 4.7 Summary and conclusion

- Deformation can induce local pressure variations of up to 4 kbar, that can explain the juxtaposition of different metamorphic facies rocks at the same crustal level.
- We estimate that a high pressure eclogitisation front can propagate into the granulite at a rate of tens of centimetres per thousand years.
- Our study supports field observations (Putnis et al., 2021) and models (Jamtveit et al., 2018b; Moulas et al., 2022) that describe heterogeneous eclogitisation caused by pressure variations. However, single phase models probably overestimate pressure variations and cannot estimate the time scale of eclogitisation.
- Pressure variations greater than 4 kbar can be induced by deformation alone only if lower crustal permeability is very low. The likely presence of pulses of high fluid pressure related to brittle deformation (Malvoisin et al., 2020; Putnis et al., 2021) can provide an external source of high pressure, enhancing the propagation of the reaction front (Bras et al., 2023).
- Transient weakening significantly contributes to propagation of the eclogitisation front.

In conclusion, deformation likely generates local pressure variations that contributes to heterogeneous eclogitisation, even if they are counterbalanced by fluid pressure diffusion caused by porous flow. Our study highlights the complex couplings between fluid flow, deformation, and metamorphic reactions. The effect of porous flow and density variations can be significant and should be taken into account when modelling metamorphic processes in the lower crust.

### Acknowledgments

We thank Diwan Desnos for his work on a early version of this project. This work has been partially financially supported by the INSU SYSTER program (AO Tellus), and by the University of Lausanne. P.Y. thanks the Institut Universitaire de France for financial support.

### Data Availability

All numerical results have been generated with a self-developed MATLAB code, which is available on the platform Zenodo under: <https://doi.org/10.5281/zenodo.8389250>.

## Appendix

Here, we show the steps to transform equation (4.6) into (4.7). We start from the conservation equation of solid mass (4.6):

$$\frac{\partial}{\partial t} \rho_T^s = -\nabla \cdot (\rho_T^s \vec{v}_s). \quad (4.33)$$

Introducing the shorthand notation  $\rho_X = \rho_s X_s$ , and substituting in equation (4.5) yields

$$\frac{\partial}{\partial t} [(1-\phi)\rho_X] = -\nabla \cdot [(1-\phi)\rho_X \vec{v}_s]. \quad (4.34)$$

Applying the product rule of differentiation to both sides of the equation yields:

$$\rho_X \frac{\partial}{\partial t} (1-\phi) + (1-\phi) \frac{\partial}{\partial t} \rho_X = -(1-\phi) \rho_X \nabla \cdot \vec{v}_s - \vec{v}_s \rho_X \nabla (1-\phi) - (1-\phi) \vec{v}_s \nabla \rho_X. \quad (4.35)$$

Replacing derivatives of  $(1-\phi)$  by derivatives of  $\phi$  and rearranging yields:

$$-\rho_X \frac{\partial \phi}{\partial t} - \vec{v}_s \rho_X \nabla \phi = -(1-\phi) \rho_X \nabla \cdot \vec{v}_s - (1-\phi) \vec{v}_s \nabla \rho_X - (1-\phi) \frac{\partial}{\partial t} \rho_X. \quad (4.36)$$

The term  $\vec{v}_s \nabla \phi$  on the left-hand side represents an advection term for  $\phi$ , and the term  $\vec{v}_s \nabla \rho_X$  on the right-hand side represents an advection term for  $\rho_X$ . Both side can hence be combined to their total time derivative,  $d/dt$ :

$$-\rho_X \frac{d\phi}{dt} = -(1-\phi) \rho_X \nabla \cdot \vec{v}_s - (1-\phi) \frac{d}{dt} \rho_X. \quad (4.37)$$

Dividing both sides by  $-\rho_X \phi$  yields

$$\frac{1}{\phi} \frac{d\phi}{dt} = \frac{1-\phi}{\phi} \nabla \cdot \vec{v}_s + \frac{1-\phi}{\rho_X \phi} \frac{d}{dt} \rho_X. \quad (4.38)$$

The left and right-hand side can now be replaced by the time derivative of the natural logarithm of, respectively,  $\phi$  and  $\rho_X$ , to yield our final equation (4.7):

$$\frac{d}{dt} (\log \phi) = \frac{1-\phi}{\phi} \left( \nabla \cdot \vec{v}_s + \frac{d}{dt} (\log \rho_X) \right). \quad (4.39)$$

## Supplementary figures

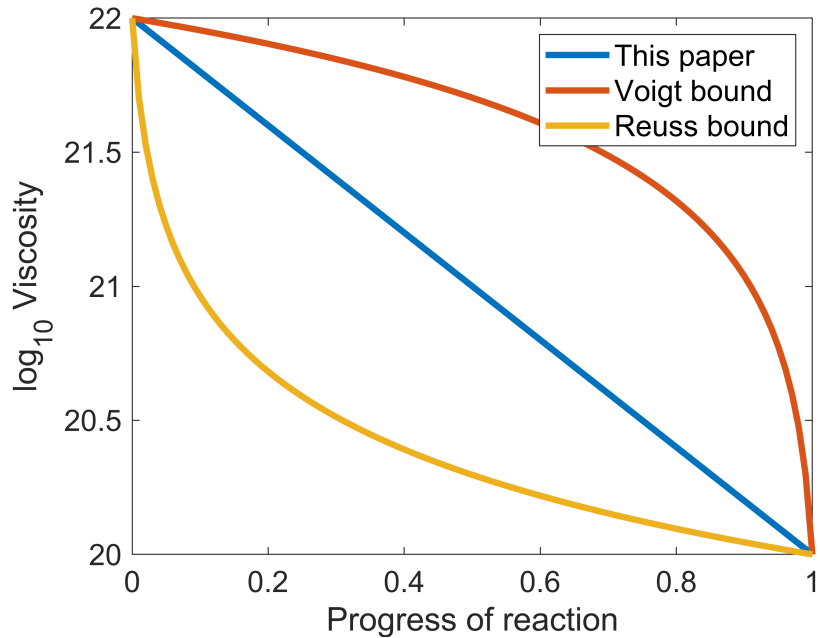


Figure S1 – Comparison of our logarithmic viscosity mixing law with the reuss (harmonic mean) and voigt (arithmetic mean) bounds.

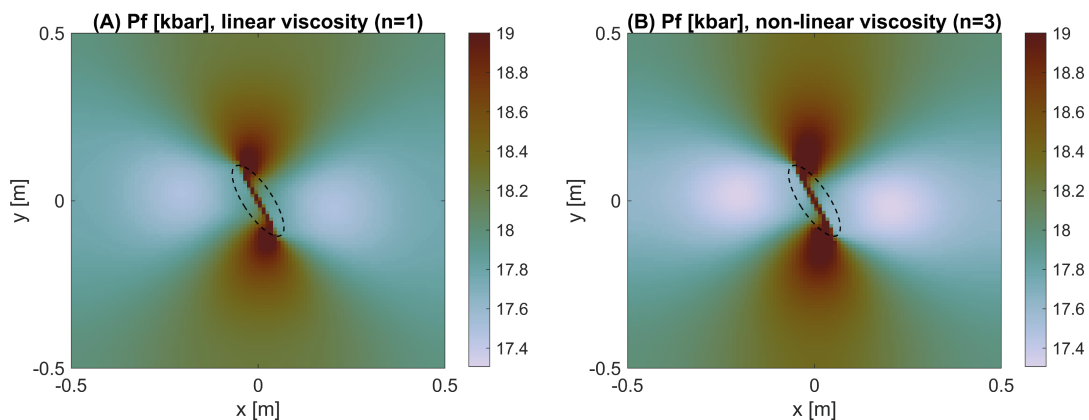


Figure S2 – Comparison of our reference model (A), with linear viscosity typical of deformation by diffusion creep, and the same model (B) with non-linear viscosity typical of deformation by dislocation creep (stress exponent  $n = 3$ ).

## Bibliographie du présent chapitre

- Abers, G. A. & Hacker, B. R. (2016). A MATLAB toolbox and Excel workbook for calculating the densities, seismic wave speeds, and major element composition of minerals and rocks at pressure and temperature. *Geochemistry, Geophysics, Geosystems*, 17(2), 616-624. <https://doi.org/10.1002/2015GC006171>
- Andersen, T. B., Jamtveit, B., Dewey, J. F. & Swensson, E. (1991). Subduction and education of continental crust : Major mechanisms during continent-continent collision and orogenic extensional collapse, a model based on the south Norwegian Caledonides. *Terra Nova*, 3(3), 303-310. <https://doi.org/10.1111/j.1365-3121.1991.tb00148.x>
- Angiboust, S. & Raimondo, T. (2022). Permeability of subducted oceanic crust revealed by eclogite-facies vugs. *Geology*, 50(8), 964-968. <https://doi.org/10.1130/G50066.1>
- Audet, P., Bostock, M. G., Christensen, N. I. & Peacock, S. M. (2009). Seismic evidence for overpressured subducted oceanic crust and megathrust fault sealing. *Nature*, 457(7225), 76-78. <https://doi.org/10.1038/nature07650>
- Audétat, A. & Keppler, H. (2004). Viscosity of fluids in subduction zones. *Science*, 303(5657), 513-516. <https://doi.org/10.1126/science.1092282>
- Austrheim, H. (1987). Eclogitization of lower crustal granulites by fluid migration through shear zones. *Earth and Planetary Science Letters*, 81(2-3), 221-232. [https://doi.org/10.1016/0012-821X\(87\)90158-0](https://doi.org/10.1016/0012-821X(87)90158-0)
- Austrheim, H. (2013). Fluid and deformation induced metamorphic processes around Moho beneath continent collision zones : Examples from the exposed root zone of the Caledonian mountain belt, W-Norway. *Tectonophysics*, 609, 620-635. <https://doi.org/10.1016/j.tecto.2013.08.030>
- Austrheim, H. & Griffin, W. L. (1985). Shear deformation and eclogite formation within granulite-facies anorthosites of the Bergen Arcs, western Norway. *Chemical Geology*, 50(1-3), 267-281. [https://doi.org/10.1016/0009-2541\(85\)90124-X](https://doi.org/10.1016/0009-2541(85)90124-X)
- Austrheim, H. & Mørk, M. (1988). The lower continental crust of the Caledonides mountain chain : Evidence from former deep crustal sections in western Norway.
- Baïsset, M., Labrousse, L., Yamato, P. & Schubnel, A. (2023). Twinning and partial melting as early weakening processes in plagioclase at high pressure : insights from Holsnøy (Scandinavian Caledonides, Norway). *Contributions to Mineralogy and Petrology*, 178, 19. <https://doi.org/10.1007/s00410-023-01998-x>
- Bauville, A. & Yamato, P. (2021). Pressure-to-depth conversion models for metamorphic rocks : derivation and applications. *Geochemistry, Geophysics, Geosystems*, 22(1), e2020GC009280. <https://doi.org/10.1029/2020GC009280>
- Bhowany, K., Hand, M., Clark, C., Kelsey, D. E., Reddy, S. M., Pearce, M. A., Tucker, N. M. & Morrissey, L. J. (2018). Phase equilibria modelling constraints on P-T conditions during fluid catalysed conversion of granulite to eclogite in the Bergen Arcs, Norway. *Journal of Metamorphic Geology*, 36(3), 315-342. <https://doi.org/10.1111/jmg.12294>
- Bingen, B., Davis, W. J. & Austrheim, H. (2001). Zircon U-Pb geochronology in the Bergen arc eclogites and their Proterozoic protoliths, and implications for the pre-Scandian evolution of the Caledonides in western Norway. *Geological Society*

- of America Bulletin*, 113(5), 640-649. [https://doi.org/10.1130/0016-7606\(2001\)113<0640:ZUPGIT>2.0.CO;2](https://doi.org/10.1130/0016-7606(2001)113<0640:ZUPGIT>2.0.CO;2)
- Bras, E., Yamato, P., Schmalholz, S. M., Duretz, T. & Podladchikov, Y. Y. (2023). Eclogitisation of dry and impermeable granulite by fluid flow with reaction-induced porosity : Insights from hydro-chemical modelling. *Earth and Planetary Science Letters*, 617, 118256. <https://doi.org/10.1016/j.epsl.2023.118256>
- Bras, E., Baïsset, M., Yamato, P. & Labrousse, L. (2021). Transient weakening during the granulite to eclogite transformation within hydrous shear zones (Holsnøy, Norway). *Tectonophysics*, 819, 229026. <https://doi.org/10.1016/j.tecto.2021.229026>
- Byerlee, J. (1978). Friction of rocks. *Rock friction and earthquake prediction*, 615-626.
- Centrella, S. (2019). The granulite-to eclogite-and amphibolite-facies transition : a volume and mass transfer study in the Lindås Nappe, Bergen Arcs, west Norway. *Geological Society, London, Special Publications*, 478(1), 241-264. <https://doi.org/10.1144/SP478.9>
- Chopin, C. (1984). Coesite and pure pyrope in high-grade blueschists of the Western Alps : a first record and some consequences. *Contributions to Mineralogy and Petrology*, 86, 107-118. <https://doi.org/10.1007/BF00381838>
- Cionoiu, S., Moulas, E., Stünitz, H. & Tajčmanová, L. (2022). Locally Resolved Stress-State in Samples During Experimental Deformation : Insights Into the Effect of Stress on Mineral Reactions. *Journal of Geophysical Research : Solid Earth*, 127(8), e2022JB024814. <https://doi.org/10.1029/2022JB024814>
- Cionoiu, S., Moulas, E. & Tajčmanová, L. (2019). Impact of interseismic deformation on phase transformations and rock properties in subduction zones. *Scientific Reports*, 9(1), 19561. <https://doi.org/10.1038/s41598-019-56130-6>
- Connolly, J. (1997). Devolatilization-generated fluid pressure and deformation-propagated fluid flow during prograde regional metamorphism. *Journal of Geophysical Research : Solid Earth*, 102(B8), 18149-18173. <https://doi.org/10.1029/97JB00731>
- Connolly, J. A. (2005). Computation of phase equilibria by linear programming : a tool for geodynamic modeling and its application to subduction zone decarbonation. *Earth and Planetary Science Letters*, 236(1-2), 524-541. <https://doi.org/10.1016/j.epsl.2005.04.033>
- Costa, A. (2006). Permeability-porosity relationship : A reexamination of the Kozeny-Carman equation based on a fractal pore-space geometry assumption. *Geophysical research letters*, 33(2). <https://doi.org/10.1029/2005GL025134>
- Crameri, F. (2018). Scientific colour maps. *Zenodo*, 10. <https://doi.org/10.5281/zenodo.1243862>
- Dahlen, F. (1992). Metamorphism of nonhydrostatically stressed rocks. *American Journal of Science*, 292(3), 184-198. <https://doi.org/10.2475/ajs.292.3.184>
- Duretz, T., de Borst, R. & Yamato, P. (2021). Modeling lithospheric deformation using a compressible visco-elasto-viscoplastic rheology and the effective viscosity approach. *Geochemistry, Geophysics, Geosystems*, 22(8), e2021GC009675. <https://doi.org/10.1029/2021GC009675>
- Duretz, T., de Borst, R., Yamato, P. & Le Pourhiet, L. (2020). Toward robust and predictive geodynamic modeling : The way forward in frictional plasticity. *Geophysical Research Letters*, 47(5), e2019GL086027. <https://doi.org/10.1029/2019GL086027>

- Engvik, A., Austrheim, H. & Erambert, M. (2001). Interaction between fluid flow, fracturing and mineral growth during eclogitization, an example from the Sunnfjord area, Western Gneiss Region, Norway. *Lithos*, 57(2-3), 111-141. [https://doi.org/10.1016/S0024-4937\(01\)00037-8](https://doi.org/10.1016/S0024-4937(01)00037-8)
- Frankel, S. P. (1950). Convergence rates of iterative treatments of partial differential equations. *Mathematics of Computation*, 4(30), 65-75.
- Fusseis, F., Regenauer-Lieb, K., Liu, J., Hough, R. M. & De Carlo, F. (2009). Creep cavitation can establish a dynamic granular fluid pump in ductile shear zones. *Nature*, 459(7249), 974-977. <https://doi.org/10.1038/nature08051>
- Gerya, T. (2019). *Introduction to numerical geodynamic modelling*. Cambridge University Press. <https://doi.org/10.1017/9781316534243>
- Gerya, T. (2015). Tectonic overpressure and underpressure in lithospheric tectonics and metamorphism. *Journal of Metamorphic Geology*, 33(8), 785-800. <https://doi.org/10.1111/jmg.12144>
- Glodny, J., Kühn, A. & Austrheim, H. (2008). Geochronology of fluid-induced eclogite and amphibolite facies metamorphic reactions in a subduction–collision system, Bergen Arcs, Norway. *Contributions to Mineralogy and Petrology*, 156, 27-48. <https://doi.org/10.1007/s00410-007-0272-y>
- Hack, A. C. & Thompson, A. B. (2011). Density and viscosity of hydrous magmas and related fluids and their role in subduction zone processes. *Journal of Petrology*, 52(7-8), 1333-1362. <https://doi.org/10.1093/petrology/egq048>
- Hirth, G. & Tullis, J. (1994). The brittle-plastic transition in experimentally deformed quartz aggregates. *Journal of Geophysical Research : Solid Earth*, 99(B6), 11731-11747. <https://doi.org/10.1029/93JB02873>
- Hobbs, B. E. & Ord, A. (2016). Does non-hydrostatic stress influence the equilibrium of metamorphic reactions? *Earth-Science Reviews*, 163, 190-233. <https://doi.org/10.1016/j.earscirev.2016.08.013>
- Hoiland, C., Hourigan, J. & Miller, E. (2022). Evidence for large departures from lithostatic pressure during Late Cretaceous metamorphism in the northern Snake Range metamorphic core complex, Nevada. *Tectonic Evolution of the Sevier-Laramide Hinterland, Thrust Belt, and Foreland, and Postorogenic Slab Rollback (180–20 Ma)*. Geological Society of America. [https://doi.org/10.1130/2021.2555\(07\)](https://doi.org/10.1130/2021.2555(07))
- Holdaway, M. & Goodge, J. (1990). Rock pressures vs. fluid pressure as a controlling influence on mineral stability; an example from New Mexico. *American Mineralogist*, 75(9-10), 1043-1058.
- Holland, T. & Powell, R. (1991). A Compensated-Redlich-Kwong (CORK) equation for volumes and fugacities of CO<sub>2</sub> and H<sub>2</sub>O in the range 1 bar to 50 kbar and 100–1600 °C. *Contributions to Mineralogy and Petrology*, 109, 265-273. <https://doi.org/10.1007/BF00306484>
- Hoover, W. F., Penniston-Dorland, S., Piccoli, P. & Kylander-Clark, A. (2023). Reaction-Induced Porosity in an Eclogite-Facies Vein Selvage (Monviso Ophiolite, W. Alps) : Textural Evidence and In Situ Trace Elements and Sr Isotopes in Apatite. *Journal of Petrology*, 64(1), egac128. <https://doi.org/10.1093/petrology/egac128>
- Huet, B., Yamato, P. & Grasemann, B. (2014). The Minimized Power Geometric model : An analytical mixing model for calculating polyphase rock viscosities consistent

- with experimental data. *Journal of Geophysical Research : Solid Earth*, 119(4), 3897-3924. <https://doi.org/10.1002/2013JB010453>
- Ingebritsen, S. E. & Manning, C. (2010). Permeability of the continental crust : dynamic variations inferred from seismicity and metamorphism. *Geofluids*, 10(1-2), 193-205. <https://doi.org/10.1111/j.1468-8123.2010.00278.x>
- Jackson, J. A., Austrheim, H., McKenzie, D. & Priestley, K. (2004). Metastability, mechanical strength, and the support of mountain belts. *Geology*, 32(7), 625-628. <https://doi.org/10.1130/G20397.1>
- Jamtveit, B., Austrheim, H. & Putnis, A. (2016). Disequilibrium metamorphism of stressed lithosphere. *Earth-Science Reviews*, 154, 1-13. <https://doi.org/10.1016/j.earscirev.2015.12.002>
- Jamtveit, B., Petley-Ragan, A., Incel, S., Dunkel, K. G., Aupart, C., Austrheim, H., Corfu, F., Menegon, L. & Renard, F. (2019). The effects of earthquakes and fluids on the metamorphism of the lower continental crust. *Journal of Geophysical Research : Solid Earth*, 124(8), 7725-7755. <https://doi.org/10.1029/2018JB016461>
- Jamtveit, B., Bucher-Nurminen, K. & Austrheim, H. (1990). Fluid controlled eclogitization of granulites in deep crustal shear zones, Bergen arcs, Western Norway. *Contributions to Mineralogy and Petrology*, 104, 184-193. <https://doi.org/10.1007/BF00306442>
- Jamtveit, B., Moulas, E., Andersen, T. B., Austrheim, H., Corfu, F., Petley-Ragan, A. & Schmalholz, S. M. (2018b). High pressure metamorphism caused by fluid induced weakening of deep continental crust. *Scientific Reports*, 8(1), 17011. <https://doi.org/10.1038/s41598-018-35200-1>
- Kaatz, L., Reynes, J., Hermann, J. & John, T. (2022). How fluid infiltrates dry crustal rocks during progressive eclogitization and shear zone formation : insights from H<sub>2</sub>O contents in nominally anhydrous minerals. *Contributions to Mineralogy and Petrology*, 177(7), 72. <https://doi.org/10.1007/s00410-022-01938-1>
- Kaatz, L., Schmalholz, S. & John, T. (2023). Numerical simulations reproduce field observations showing transient weakening during shear zone formation by diffusional hydrogen influx and H<sub>2</sub>O inflow. *Geochemistry, Geophysics, Geosystems*, 24(5), e2022GC010830. <https://doi.org/10.1029/2022GC010830>
- Kaatz, L., Zertani, S., Moulas, E., John, T., Labrousse, L., Schmalholz, S. M. & Andersen, T. B. (2021). Widening of hydrous shear zones during incipient eclogitization of metastable dry and rigid lower crust—Holsnøy, western Norway. *Tectonics*, 40(3), e2020TC006572. <https://doi.org/10.1029/2020TC006572>
- Katz, R. F., Jones, D. W. R., Rudge, J. F. & Keller, T. (2022). Physics of melt extraction from the mantle : Speed and style. *Annual Review of Earth and Planetary Sciences*, 50, 507-540. <https://doi.org/10.1146/annurev-earth-032320-083704>
- Keller, T., May, D. A. & Kaus, B. J. (2013). Numerical modelling of magma dynamics coupled to tectonic deformation of lithosphere and crust. *Geophysical Journal International*, 195(3), 1406-1442. <https://doi.org/10.1093/gji/ggt306>
- Labrousse, L., Hetényi, G., Raimbourg, H., Jolivet, L. & Andersen, T. B. (2010). Initiation of crustal-scale thrusts triggered by metamorphic reactions at depth : Insights from a comparison between the Himalayas and Scandinavian Caledonides. *Tectonics*, 29(5), TC5002. <https://doi.org/10.1029/2009TC002602>

- Landau, L. D. & Lifshitz, E. M. (1980). *Statistical Physics, Part 1, Course of Theoretical Physics* (T. 5). Pergamon press, Oxford.
- Li, Y., Pusok, A. E., Davis, T., May, D. A. & Katz, R. F. (2023). Continuum approximation of dyking with a theory for poro-viscoelastic–viscoplastic deformation. *Geophysical Journal International*, 234(3), 2007-2031. <https://doi.org/10.1093/gji/ggad173>
- Llana-Fúnez, S., Wheeler, J. & Faulkner, D. R. (2012). Metamorphic reaction rate controlled by fluid pressure not confining pressure : implications of dehydration experiments with gypsum. *Contributions to Mineralogy and Petrology*, 164, 69-79. <https://doi.org/10.1007/s00410-012-0726-8>
- Luisier, C., Tajčmanová, L., Yamato, P. & Duretz, T. (2023). Garnet microstructures suggest ultra-fast decompression of ultrahigh-pressure rocks. *Nature Communications*, 14(1), 6012. <https://doi.org/10.1038/s41467-023-41310-w>
- Luisier, C., Baumgartner, L., Schmalholz, S. M., Siron, G. & Vennemann, T. (2019). Metamorphic pressure variation in a coherent Alpine nappe challenges lithostatic pressure paradigm. *Nature communications*, 10(1), 4734. <https://doi.org/10.1038/s41467-019-12727-z>
- Malvoisin, B., Podladchikov, Y. Y. & Myasnikov, A. V. (2021). Achieving complete reaction while the solid volume increases : A numerical model applied to serpentisation. *Earth and Planetary Science Letters*, 563, 116859. <https://doi.org/10.1016/j.epsl.2021.116859>
- Malvoisin, B., Podladchikov, Y. Y. & Vrijmoed, J. C. (2015). Coupling changes in densities and porosity to fluid pressure variations in reactive porous fluid flow : Local thermodynamic equilibrium. *Geochemistry, Geophysics, Geosystems*, 16(12), 4362-4387. <https://doi.org/10.1002/2015GC006019>
- Malvoisin, B., Austrheim, H., Hetényi, G., Reynes, J., Hermann, J., Baumgartner, L. P. & Podladchikov, Y. Y. (2020). Sustainable densification of the deep crust. *Geology*, 48(7), 673-677. <https://doi.org/10.1130/G47201.1>
- Mancktelow, N. S. (1993). Tectonic overpressure in competent mafic layers and the development of isolated eclogites. *Journal of metamorphic Geology*, 11(6), 801-812. <https://doi.org/10.1111/j.1525-1314.1993.tb00190.x>
- Mancktelow, N. S. (2008). Tectonic pressure : Theoretical concepts and modelled examples. *Lithos*, 103(1-2), 149-177. <https://doi.org/10.1016/j.lithos.2007.09.013>
- Mancktelow, N. S. & Pennacchioni, G. (2005). The control of precursor brittle fracture and fluid–rock interaction on the development of single and paired ductile shear zones. *Journal of structural Geology*, 27(4), 645-661. <https://doi.org/10.1016/j.jsg.2004.12.001>
- McKenzie, D. (1984). The generation and compaction of partially molten rock. *Journal of petrology*, 25(3), 713-765. <https://doi.org/10.1093/petrology/25.3.713>
- Mindaleva, D., Uno, M., Higashino, F., Nagaya, T., Okamoto, A. & Tsuchiya, N. (2020). Rapid fluid infiltration and permeability enhancement during middle–lower crustal fracturing : Evidence from amphibolite–granulite-facies fluid–rock reaction zones, Sør Rondane Mountains, East Antarctica. *Lithos*, 372, 105521. <https://doi.org/10.1016/j.lithos.2020.105521>

- Moore, J., Beinlich, A., Piazolo, S., Austrheim, H. & Putnis, A. (2020a). Metamorphic differentiation via enhanced dissolution along high permeability zones. *Journal of Petrology*, 61(10), egaa096. <https://doi.org/10.1093/petrology/egaa096>
- Moore, J., Beinlich, A., Porter, J. K., Talavera, C., Berndt, J., Piazolo, S., Austrheim, H. & Putnis, A. (2020b). Microstructurally controlled trace element (Zr, U-Pb) concentrations in metamorphic rutile : an example from the amphibolites of the Bergen Arcs. *Journal of Metamorphic Geology*, 38(1), 103-127. <https://doi.org/10.1111/jmg.12514>
- Moulas, E., Podladchikov, Y. Y., Aranovich, L. Y. & Kostopoulos, D. (2013). The problem of depth in geology : When pressure does not translate into depth. *Petrology*, 21, 527-538. <https://doi.org/10.1134/S0869591113060052>
- Moulas, E., Kaus, B. & Jamtveit, B. (2022). Dynamic pressure variations in the lower crust caused by localized fluid-induced weakening. *Communications Earth & Environment*, 3(1), 157. <https://doi.org/10.1038/s43247-022-00478-7>
- Moulas, E., Schmalholz, S. M., Podladchikov, Y., Tajčmanová, L., Kostopoulos, D. & Baumgartner, L. (2019). Relation between mean stress, thermodynamic, and lithostatic pressure. *Journal of metamorphic geology*, 37(1), 1-14. <https://doi.org/10.1111/jmg.12446>
- Moulas, E., Burg, J.-P. & Podladchikov, Y. (2014). Stress field associated with elliptical inclusions in a deforming matrix : Mathematical model and implications for tectonic overpressure in the lithosphere. *Tectonophysics*, 631, 37-49. <https://doi.org/10.1016/j.tecto.2014.05.004>
- Omlin, S., Malvoisin, B. & Podladchikov, Y. Y. (2017). Pore fluid extraction by reactive solitary waves in 3-D. *Geophysical Research Letters*, 44(18), 9267-9275. <https://doi.org/10.1002/2017GL074293>
- Pleuger, J. & Podladchikov, Y. Y. (2014). A purely structural restoration of the NFP20-East cross section and potential tectonic overpressure in the Adula nappe (central Alps). *Tectonics*, 33(5), 656-685. <https://doi.org/10.1002/2013TC003409>
- Pollok, K., Lloyd, G. E., Austrheim, H. & Putnis, A. (2008). Complex replacement patterns in garnets from Bergen Arcs eclogites : a combined EBSD and analytical TEM study. *Geochemistry*, 68(2), 177-191. <https://doi.org/10.1016/j.chemer.2007.12.002>
- Putnis, A. (2021). Fluid–mineral interactions : controlling coupled mechanisms of reaction, mass transfer and deformation. *Journal of Petrology*, 62(12), egab092. <https://doi.org/10.1093/petrology/egab092>
- Putnis, A. (2009). Mineral replacement reactions. *Reviews in mineralogy and geochemistry*, 70(1), 87-124. <https://doi.org/10.2138/rmg.2009.70.3>
- Putnis, A. & John, T. (2010). Replacement processes in the Earth's crust. *Elements*, 6(3), 159-164. <https://doi.org/10.2113/gselements.6.3.159>
- Putnis, A., Jamtveit, B. & Austrheim, H. (2017). Metamorphic processes and seismicity : the Bergen Arcs as a natural laboratory. *Journal of Petrology*, 58(10), 1871-1898. <https://doi.org/10.1093/petrology/egx076>
- Putnis, A., Moore, J., Prent, A. M., Beinlich, A. & Austrheim, H. (2021). Preservation of granulite in a partially eclogitized terrane : Metastable phenomena or local pressure variations? *Lithos*, 400, 106413. <https://doi.org/10.1016/j.lithos.2021.106413>

- Ranalli, G. (1995). *Rheology of the Earth*. Springer Science & Business Media.
- Räss, L., Utkin, I., Duretz, T., Omlin, S. & Podladchikov, Y. Y. (2022). Assessing the robustness and scalability of the accelerated pseudo-transient method. *Geoscientific Model Development*, 15(14), 5757-5786. <https://doi.org/10.5194/gmd-15-5757-2022>
- Richter, B., Stünitz, H. & Heilbronner, R. (2016). Stresses and pressures at the quartz-to-coesite phase transformation in shear deformation experiments. *Journal of Geophysical Research : Solid Earth*, 121(11), 8015-8033. <https://doi.org/10.1002/2016JB013084>
- Rockow, K. M., Haskin, L. A., Jolliff, B. & Fountain, D. M. (1997). Constraints on element mobility associated with the conversion of granulite to eclogite along fractures in an anorthositic complex on Holsnøy, Norway. *Journal of Metamorphic Geology*, 15(3), 401-418. <https://doi.org/10.1111/j.1525-1314.1997.00028.x>
- Rogowitz, A. & Huet, B. (2021). Evolution of fluid pathways during eclogitization and their impact on formation and deformation of eclogite : A microstructural and petrological investigation at the type locality (Koralpe, Eastern Alps, Austria). *Tectonophysics*, 819, 229079. <https://doi.org/10.1016/j.tecto.2021.229079>
- Rybacki, E. & Dresen, G. (2000). Dislocation and diffusion creep of synthetic anorthite aggregates. *Journal of Geophysical Research : Solid Earth*, 105(B11), 26017-26036. <https://doi.org/10.1029/2000JB900223>
- Schmalholz, S. M. & Podladchikov, Y. (2014). Metamorphism under stress : The problem of relating minerals to depth. *Geology*, 42(8), 733-734. <https://doi.org/10.1130/focus0822014.1>
- Schmalholz, S. M. & Podladchikov, Y. Y. (2013). Tectonic overpressure in weak crustal-scale shear zones and implications for the exhumation of high-pressure rocks. *Geophysical Research Letters*, 40(10), 1984-1988. <https://doi.org/10.1002/grl.50417>
- Schmalholz, S. M., Moulas, E., Plümper, O., Myasnikov, A. V. & Podladchikov, Y. Y. (2020). 2D Hydro-Mechanical-Chemical Modeling of (De)hydration Reactions in Deforming Heterogeneous Rock : The Periclase-Brucite Model Reaction. *Geochemistry, Geophysics, Geosystems*, 21(11), e2020GC009351. <https://doi.org/10.1029/2020GC009351>
- Schmalholz, S. M., Duretz, T., Schenker, F. L. & Podladchikov, Y. Y. (2014a). Kinematics and dynamics of tectonic nappes : 2-D numerical modelling and implications for high and ultra-high pressure tectonism in the Western Alps. *Tectonophysics*, 631, 160-175. <https://doi.org/10.1016/j.tecto.2014.05.018>
- Schmid, D. W. & Podladchikov, Y. Y. (2003). Analytical solutions for deformable elliptical inclusions in general shear. *Geophysical Journal International*, 155(1), 269-288. <https://doi.org/10.1046/j.1365-246X.2003.02042.x>
- Selvadurai, A. (2021). On the poroelastic Biot coefficient for a granitic rock. *Geosciences*, 11(5), 219. <https://doi.org/10.3390/geosciences11050219>
- Shmonov, V., Vitiovtova, V., Zharikov, A. & Grafchikov, A. (2003). Permeability of the continental crust : implications of experimental data. *Journal of Geochemical Exploration*, 78, 697-699. [https://doi.org/10.1016/S0375-6742\(03\)00129-8](https://doi.org/10.1016/S0375-6742(03)00129-8)

- Sibson, R. H. (1994). Crustal stress, faulting and fluid flow. *Geological Society, London, Special Publications*, 78(1), 69-84. <https://doi.org/10.1144/GSL.SP.1994.078.01.07>
- Simon, M., Pitra, P., Yamato, P. & Poujol, M. (2023). Isothermal compression of an eclogite from the Western Gneiss Region (Norway). *Journal of Metamorphic Geology*, 41(1), 181-203. <https://doi.org/10.1111/jmg.12692>
- Stünitz, H., Neufeld, K., Heilbronner, R., Finstad, A. K., Konopásek, J. & Mackenzie, J. R. (2020). Transformation weakening : Diffusion creep in eclogites as a result of interaction of mineral reactions and deformation. *Journal of Structural Geology*, 139, 104129. <https://doi.org/10.1016/j.jsg.2020.104129>
- Tajčmanová, L., Podladchikov, Y., Powell, R., Moulas, E., Vrijmoed, J. & Connolly, J. (2014). Grain-scale pressure variations and chemical equilibrium in high-grade metamorphic rocks. *Journal of Metamorphic Geology*, 32(2), 195-207. <https://doi.org/10.1111/jmg.12066>
- Tajčmanová, L., Vrijmoed, J. & Moulas, E. (2015). Grain-scale pressure variations in metamorphic rocks : implications for the interpretation of petrographic observations. *Lithos*, 216, 338-351. <https://doi.org/10.1016/j.lithos.2015.01.006>
- Tajčmanová, L., Manzotti, P. & Alvaro, M. (2021). Under pressure : high-pressure metamorphism in the Alps. *Elements : An International Magazine of Mineralogy, Geochemistry, and Petrology*, 17(1), 17-22. <https://doi.org/10.2138/gselements.17.1.17>
- Thompson, A. B. & England, P. C. (1984). Pressure—temperature—time paths of regional metamorphism II. Their inference and interpretation using mineral assemblages in metamorphic rocks. *Journal of Petrology*, 25(4), 929-955. <https://doi.org/10.1093/petrology/25.4.929>
- Wain, A., Waters, D. & Austrheim, H. (2001). Metastability of granulites and processes of eclogitisation in the UHP region of western Norway. *Journal of Metamorphic Geology*, 19(5), 609-625. <https://doi.org/10.1046/j.0263-4929.2001.00333.x>
- Wheeler, J. (2014). Dramatic effects of stress on metamorphic reactions. *Geology*, 42(8), 647-650. <https://doi.org/10.1130/G35718.1>
- Yamato, P. & Brun, J.-P. (2017). Metamorphic record of catastrophic pressure drops in subduction zones. *Nature Geoscience*, 10(1), 46-50. <https://doi.org/10.1038/ngeo2852>
- Yamato, P., Duretz, T., Baïsset, M. & Luisier, C. (2022). Reaction-induced volume change triggers brittle failure at eclogite facies conditions. *Earth and Planetary Science Letters*, 584, 117520. <https://doi.org/10.1016/j.epsl.2022.117520>
- Yarushina, V. M. & Podladchikov, Y. Y. (2015). (De) compaction of porous viscoelastic-plastic media : Model formulation. *Journal of Geophysical Research : Solid Earth*, 120(6), 4146-4170. <https://doi.org/10.1002/2014JB011258>
- Zertani, S., Labrousse, L., John, T., Andersen, T. B. & Tilmann, F. (2019). The interplay of Eclogitization and deformation during deep burial of the lower continental crust—A case study from the Bergen Arcs (Western Norway). *Tectonics*, 38(3), 898-915. <https://doi.org/10.1029/2018TC005297>
- Zertani, S., John, T., Brachmann, C., Vrijmoed, J. C. & Plümper, O. (2022). Reactive fluid flow guided by grain-scale equilibrium reactions during eclogitization of dry crustal rocks. *Contributions to Mineralogy and Petrology*, 177(6), 61. <https://doi.org/10.1007/s00410-022-01928-3>

- Zhong, X., Andersen, N. H., Dabrowski, M. & Jamtveit, B. (2019). Zircon and quartz inclusions in garnet used for complementary Raman thermobarometry : application to the Holsnøy eclogite, Bergen Arcs, Western Norway. *Contributions to Mineralogy and Petrology*, 174, 1-17. <https://doi.org/10.1007/s00410-019-1584-4>
- Zhou, X. & Ghassemi, A. (2022). Experimental Determination of Poroelastic Properties of Utah FORGE Rocks. *ARMA US Rock Mechanics/Geomechanics Symposium*, ARMA-2022. <https://doi.org/10.56952/ARMA-2022-2137>



# 5

## Synthèse, discussions et perspectives

### Sommaire du présent chapitre

---

<b>5.1 Synthèse des résultats</b>	<b>142</b>
5.1.1 Synthèse de l'article 1 . . . . .	142
5.1.2 Synthèse de l'article 2 . . . . .	143
5.1.3 Synthèse de l'article 3 . . . . .	144
<b>5.2 Discussions</b>	<b>145</b>
5.2.1 Variations locales de pression . . . . .	145
5.2.2 Vitesse de propagation de l'éclogitisation . . . . .	146
5.2.3 Perméabilité et porosité dans la croûte inférieure . . . . .	147
<b>5.3 L'éclogitisation de la croûte inférieure vue d'Holsnøy</b>	<b>149</b>
<b>5.4 Perspectives et travaux futurs</b>	<b>149</b>
5.4.1 Amphibolitisation . . . . .	149
5.4.2 Pression d'équilibre métamorphique . . . . .	151
<b>Bibliographie</b>	<b>152</b>

---

Ce manuscrit fait progresser notre compréhension des processus et des couplages métamorphiques dans les zones de convergence, à travers l'étude de l'éclogitisation de la croûte inférieure subduite en profondeur sous les chaînes de montagnes. Dans le chapitre 2, l'accent a été mis sur le processus de transformation métamorphique et son influence sur la rhéologie, mettant en évidence l'affaiblissement transitoire au cours de l'éclogitisation. Dans le chapitre 3, je me suis concentré sur la rétroaction positive entre éclogitisation et transport de fluides, en montrant que la propagation d'un front hydro-réactif est possible dans un milieu imperméable. Enfin dans le chapitre 4, j'ai étudié le couplage entre déformation, transport de fluides et éclogitisation, où j'ai montré qu'un enfouissement à des profondeurs de 70 km n'est pas nécessaire pour éclogitiser localement la granulite.

Dans ce chapitre, je propose tout d'abord une synthèse des principaux résultats de cette thèse, article par article (section 5.1). Si ces résultats concernent principalement l'éclogitisation, ils peuvent être applicables à d'autres contextes géologiques. Ensuite, je replace dans un contexte plus global certains éléments abordés par cette thèse, qui sont toujours sujets à discussion (section 5.2). Il s'agit de la pression à laquelle la granulite s'est transformée, de la vitesse de propagation de l'éclogitisation, et de la génération de porosité lors des réactions métamorphiques. Troisièmement, je propose un scénario de l'éclogitisation de la croûte inférieure observée à Holsnøy, inféré à partir d'une synthèse de la littérature, de mes observations pétrologiques, de mes observations de terrains, et de mes modèles numériques (section 5.3). Pour finir, je présente deux perspectives de recherche envisagées à l'issue de ce travail de thèse. La première est l'étude de l'association entre amphibolitisation et éclogitisation de la croûte inférieure ; la deuxième est la caractérisation de la pression d'équilibre thermodynamique.

## 5.1 Synthèse des résultats

### 5.1.1 Synthèse de l'article 1

1. La bordure des bandes de cisaillement est une zone de résistance minimale, mécaniquement plus faible que la granulite à l'extérieur et que l'éclogite au coeur de la bande de cisaillement. Elle enregistre donc l'essentiel de la déformation.
2. Une étude pétrologique détaillée révèle une séquence de réactions minérales responsables de la transformation de granulite en éclogite. Les premières réactions affaiblissent la roche en cours de transformation, et les dernières restaurent en partie la résistance de l'éclogite.
3. Dans un premier temps, l'affaiblissement de la granulite est engendré par la déstabilisation du plagioclase, qui s'opère en 2 étapes, celle du pôle calcique (anorthite)

et celle du pôle sodique (albite) du plagioclase. L'affaiblissement est causé par une diminution de la taille de grains, la cristallisation de phases peu résistantes, la diminution du volume solide, l'augmentation de la quantité de fluide. La persistance d'hétérogénéités chimiques de la granulite crée une interconnexion de bandes peu résistantes qui contrôlent la rhéologie de l'ensemble.

4. Le durcissement est causé par une homogénéisation de la composition chimique, assistée par la circulation de fluides, qui cause une augmentation de la taille des grains, la diminution de la quantité de phases peu résistantes, un changement de volume limité, et une disparition des hétérogénéités texturales.
5. L'élargissement des bandes de cisaillement éclogitiques est dû aussi bien à la circulation de fluides qui affaiblissent la roche, qu'au re-durcissement de l'éclogite en fin de réaction, qui repousse la localisation de la déformation vers l'extérieur de la bande de cisaillement et favorise ainsi son élargissement.

Cet article a soulevé la question du mécanisme de circulation des fluides, et de l'impact de la réaction métamorphique sur cette circulation. Comment la diminution de volume causée par l'éclogitisation peut-elle accélérer le transport des fluides ? Une granulite sans porosité peut-elle être sujette à une hydratation autre que la diffusion intracristalline d'atomes d'hydrogène et d'oxygène ?

### 5.1.2 Synthèse de l'article 2

1. En présence d'un pulse de fluides, ou d'une succession de pulses, l'éclogitisation peut se propager à une vitesse de l'ordre de 10 cm par an dans une granulite imperméable. L'éclogite est préservée après la fin du pulse de fluides.
2. La propagation d'un front d'hydratation / de réaction de haute pression dans une roche sans porosité est possible si sa densité augmente avec la pression, par compressibilité ou par une réaction métamorphique de densification. Inversement, un front de réaction de basse pression peut se propager dans une roche imperméable si la réaction métamorphique induit une diminution de densité.
3. La vitesse du front de réaction peut être approximée par une loi de diffusion pour n'importe quelle réaction, où la diffusivité peut être estimée pour toute réaction à partir du gradient de pression imposé, et des propriétés du protolith et de la roche transformée.
4. Il existe une rétroaction positive entre éclogitisation et fluides : un pulse de fluides provoque l'éclogitisation, et cette réaction génère de la porosité qui favorise la circulation de fluides. Cette boucle de rétroaction positive est entretenue tant que le système est ouvert et qu'un fluide est apporté au système. Dans le cas

d'une réaction qui diminue la densité, l'augmentation de volume vient remplir la porosité existante et potentiellement freiner la circulation de fluides.

Cet article a soulevé la question du rôle de la déformation dans le maintien d'un gradient de pression qui permet la propagation d'un front de réaction. La déformation seule permet-elle d'entretenir des variations de pression capables d'éclogitiser la granulite ? Quel est alors l'effet du transport de fluides ?

### 5.1.3 Synthèse de l'article 3

1. A Holsnøy, la déformation d'un milieu rhéologiquement hétérogène peut induire des variations locales de pression de l'ordre de 4 kbar. Les surpressions peuvent localement déclencher l'éclogitisation et l'affaiblissement rhéologique transitoire qui s'ensuit, propageant la réaction et les surpressions vers l'extérieur de la région en cours d'éclogitisation. Ce processus peut expliquer la juxtaposition de roches de faciès métamorphiques différents au même niveau crustal.
2. Il existe néanmoins une compétition entre la déformation visqueuse qui tend à générer des variations de pression, et la diffusion de la pression du fluide par flux de Darcy qui tend à réduire les gradients de pression. Les modèles qui ne considèrent pas de phase fluide peuvent donc surestimer les surpressions induites par la déformation.
3. Des surpressions de 4 kbar peuvent être induites par la seule déformation si la perméabilité des roches est très basse, de l'ordre de  $10^{-24} \text{ m}^2$  ou inférieure. La présence probable de pulses de haute pression fluide associés à la déformation cassante peut fournir une source externe de haute pression, favorisant la propagation du front de réaction.
4. Un front d'éclogitisation induit seulement par la déformation peut se propager dans la granulite à une vitesse de quelques dizaines de centimètres par millier d'années. L'affaiblissement transitoire contribue de manière significative à cette propagation.

Cet article illustre bien la rétroaction entre fluides, déformation et réaction métamorphique, mais laisse en suspens certaines questions auxquelles je n'ai pu donner de réponse définitive au cours de cette thèse, et qui pourront faire l'objet de futurs travaux : à quelle pression la granulite est-elle métastable ? A quelle vitesse se propage le front d'éclogitisation ? Comment évolue la porosité au cours de l'éclogitisation ?

## 5.2 Discussions

Dans cette section je replace dans un contexte plus global certains éléments abordés par cette thèse qui sont toujours sujets à discussion : les variations locales de pression, la vitesse de propagation de l'éclogitisation, et la perméabilité de la croûte inférieure.

### 5.2.1 Variations locales de pression

Une question restée en suspens tout au long de cette thèse est la pression jusqu'à laquelle une granulite peut rester métastable. Estimer cette pression permettrait de donner une estimation de la profondeur à laquelle se produit l'éclogitisation, ce qui a une conséquence majeure sur la rhéologie de la croûte inférieure et par là même l'évolution tectonique de l'unité étudiée.

L'hypothèse établie de longue date par Austrheim et ses coauteurs (e.g. Austrheim et Griffin, 1985 ; Austrheim, 1987 ; Bjørnerud et al., 2002 ; Jackson et al., 2004) est que la subduction calédonienne a porté la granulite à des conditions de pression-température du faciès éclogitique, mais en l'absence de perturbation apportée au système sous forme de fluides ou de déformation, l'assemblage minéralogique de la granulite a été préservé. Durant la subduction, la déformation cassante et l'infiltration de fluides ont localement sorti la granulite de son état de déséquilibre thermodynamique et provoqué l'éclogitisation. Cette hypothèse suppose que la pression enregistrée par l'éclogite est purement lithostatique, et qu'elle a été enfouie à des profondeurs d'environ 70 km pour expérimenter des pressions de 21-22 kbar (Bhowany et al., 2018 ; Jamtveit et al., 2018b). Trois arguments principaux supportent la deuxième hypothèse, celle des variations locales de pression (Jamtveit et al., 2018b ; Bhowany, 2020 ; Putnis et al., 2021 ; Moulas et al., 2022), selon laquelle la granulite n'a pas été portée à des pressions du faciès éclogite, mais est éclogitisée grâce aux variations de pressions locales. Les arguments sont les suivants :

Premièrement, le chapitre 2 montre qu'à l'extérieur des bandes de cisaillement, le pôle anorthite du plagioclase granulitique a commencé à se transformer en zoisite, alors que le pôle albite ne se transforme pas en omphacite. Putnis et al. (2021) font la même observation à l'extérieur d'une digitation éclogitique. Or, la déstabilisation de l'anorthite s'opère à bien plus basse pression (10-11 kbar) que celle de l'albite (16-17 kbar), ce qui suggère que la pression dans la granulite est inférieure à celle de la déstabilisation de l'albite.

Deuxièmement, des bandes de cisaillement éclogitiques et amphibolitiques peuvent coexister sur le même affleurement, où la foliation granulitique peut être suivie à travers l'éclogite et l'amphibolite. Centrella (2019) montre que la proximité spatiale de ces faciès métamorphiques n'est pas compatible avec des réactions qui se produisent sur un

chemin prograde (amphibolite puis éclogite) ou rétrograde (éclogite puis amphibolite). La juxtaposition des deux faciès métamorphiques nécessite alors des variations de pression locales entre les domaines amphibolitisés et éclogitisés (Centrella, 2019).

Troisièmement, une synthèse des datations de la littérature (Jamtveit et al., 2019) suggère que le métamorphisme amphibolitique, qui s'observe sur toute l'île d'Holsnøy, est quasiment contemporains du métamorphisme éclogitiques. Bhowany (2020) montre que l'hypothèse d'une pression lithostatique nécessite des vitesses d'exhumation extrêmement rapides, comprises entre 100 et 6000 mm/an, pour accommoder une différence de pression d'environ 9 kbar entre éclogite et granulite. Or les vitesses d'exhumation de roches subduites sont généralement 5 à 10 mm/an, au maximum 40 mm/an dans certains contextes (Agard et al., 2009 ; Guillot et al., 2009), bien moindres que les vitesses estimées pour Holsnøy.

La présence de variations locales de pressions donne donc une explication cohérente aux observations de terrain. J'ai montré dans cette thèse que ces variations de pression peuvent être causées par l'apport épisodique (pulses) de pression fluide, étudié dans le chapitre 3, et par les surpressions tectoniques, étudiées dans le chapitre 4. Ainsi, la granulite n'est vraisemblablement pas métastable à des conditions de pressions de 21-22 kbar, correspondant à une profondeur de 70 km (Bhowany et al., 2018). L'interprétation la plus cohérente avec les arguments précédents est que la granulite est métastable aux conditions maximales à laquelle l'activité sismique a été relevée dans les pseudotachylytes d'Holsnøy (Jamtveit et al., 2018b) : 15 à 17 kbar et 650 à 750 °C (Bhowany et al., 2018 ; Petley-Ragan et al., 2018 ; Zhong et al., 2021), soit une profondeur d'environ 55-60 km.

### 5.2.2 Vitesse de propagation de l'éclogitisation

Estimer la vitesse de propagation des bandes de cisaillements et digitations éclogitiques permet d'estimer la vitesse à laquelle les propriétés physiques de la croûte inférieure (densité, viscosité, vitesse des ondes sismiques...) changent durant la subduction. Chacun des chapitres de cette thèse donne une estimation de cette vitesse, à chaque fois avec une méthode différente.

Le modèle numérique du chapitre 2 (Bras et al., 2021) donne une estimation de la vitesse d'élargissement des bandes de cisaillement de l'ordre de 1 mètre par million d'années, soit  $10^{-6}$  m/an. Cependant cette estimation n'est pas quantitative car le modèle approxime le transport des fluides par la diffusion d'atomes d'oxygène et d'hydrogène, et ne prend pas en compte de couplages entre déformation, réaction et flux de Darcy.

Le chapitre 3 (Bras et al., 2023), de manière similaire au chapitre 2, explique l'éclogitisation par un pulse de fluides qui se propage latéralement dans la granulite. Le pulse de fluides est ici modélisé par une haute pression fluide, et l'éclogitisation se propage

dans la granulite grâce au couplage entre le flux de Darcy et la réaction de densification. En présence d'un pulse de pression fluide, j'ai estimé que les bandes de cisaillement et digitation éclogitiques peuvent s'élargir à une vitesse de l'ordre de 10 centimètres par an, soit  $10^{-1}$  m/an. Toutefois l'éclogitisation ne se propage que lorsque le système est ouvert à des pulses de fluides épisodiques qui sont généralement de courte durée.

Le chapitre 4 explique la formation et l'extension de zones éclogitiques par les variations de pression induites par la déformation, sans apport de fluide par un pulse. Dans ce modèle, l'éclogitisation se propage à une vitesse de l'ordre de 10 centimètres par millier d'années, soit  $10^{-4}$  m/an. Ce chapitre montre que la propagation d'un front de réaction est relativement lent si le système reste fermé. Il s'agit d'une limite basse de la vitesse car l'éclogitisation se fait en général à la suite d'un apport de fluides au système (Austrheim, 1987 ; Putnis et al., 2021).

La vitesse de propagation de l'éclogitisation à long terme est donc vraisemblablement comprise entre la limite basse de  $10^{-4}$  m/an lorsque aucun fluide n'est apporté au système, et la limite haute de  $10^{-1}$  m/an du chapitre 3 lorsque qu'un pulse de haute pression fluide est actif. Si les pulses de fluides sont fréquents alors la vitesse de propagation peut être de l'ordre de quelques centimètres par an. Cette estimation est cohérente avec les estimations de John et al. (2012), Taetz et al. (2018) et Beinlich et al. (2020), qui ont estimé des vitesses de propagation de front de réaction qui varient entre quelques centimètres et quelques décimètres par an. Dans les systèmes qu'il ont étudiés, la durée de l'interaction entre les fluides et les roches métamorphiques étaient respectivement de 800 ans, 20 ans et quelques mois. La diffusion rapide d'atomes d'hydrogènes dans les minéraux nominalement anhydres de la granulite pourrait également contribuer à la propagation du front d'éclogitisation, à une vitesse de l'ordre de  $10^{-3}$  m/an (Kaatz et al., 2022, 2023).

La propagation de l'éclogitisation n'apparaît donc pas comme un processus continu, mais plutôt comme une alternance entre des périodes de rapide propagation due à des pulses de fluides potentiellement liés à des répliques sismiques (Malvoisin et al., 2020), et des périodes de propagation plus lente due à la déformation et à la diffusion d'éléments à l'état solide.

### 5.2.3 Perméabilité et porosité dans la croûte inférieure

Dans la croûte inférieure, la porosité est de manière générale trop basse pour être connectée et permettre une circulation permanente de fluides comme dans la croûte supérieure (Yardley, 1997 ; Yardley et Valley, 1997). La croûte est donc essentiellement imperméable, sauf de manière localisée et épisodique lorsque la déformation fragile crée des chemins qui permettent aux fluides d'être transportés à travers la croûte (Jamtveit et al., 2016, 2019).

Il est donc intéressant de déterminer si l'éclogitisation associée à ce transport de fluides permet d'augmenter de manière permanente la perméabilité de la croûte. L'éclogitisation de la granulite est une réaction de densification (Bras et al., 2021), à cause de laquelle un front de réaction de haute pression fluide peut se propager dans la croûte imperméable (Bras et al., 2023). Cela semble suggérer que l'éclogitisation cause une augmentation durable de la porosité et de la perméabilité de la croûte inférieure. De la même manière, Plümper et al. (2017) proposent que les réactions de densification et déshydratation dans la lithosphère océanique causent l'apparition de réseaux poreux. Le transport de fluides à grande échelle dans ces réseaux est dominé par les phénomènes de compaction-décompaction comme les ondes de porosité (Connolly, 1997; Connolly et Podladchikov, 1998).

Toutefois, le chapitre 4 suggère que si on prend en compte l'affaiblissement mécanique causé par l'éclogitisation, alors la déformation tend au contraire à diminuer la porosité dans l'éclogite déformée ductilement. Cette observation est cohérente avec des expériences de déformation sur des granites qui montrent que, contrairement à la déformation fragile, la déformation ductile peut causer une diminution de la porosité (Violay et al., 2017). Il existe donc une compétition entre génération de porosité par densification et destruction de cette porosité par déformation visqueuse.

A Holsnøy, des observations pétrologiques montrent que l'éclogitisation génère de la porosité (Putnis et al., 2021), mais celle-ci peut n'être que temporaire (Zertani et al., 2022). En effet, la dissolution des produits de réaction peut temporairement générer de la porosité qui est ensuite remplie par les produits de réaction qui précipitent à partir du fluide sur-saturé (Putnis, 2015). Invoquant un processus similaire, Michalchuk et al. (2023) ont récemment décrit des mylonites de la croûte inférieure calédonienne dans lesquelles la précipitation d'amphibole, biotite et feldspath dans l'espace poreux réduit la porosité d'environ 85 % durant la mylonitisation. Durant la déformation accommodée par fluage diffusion, les pores s'ouvrent et se ferment à mesure que les grains glissent les uns le long de autres (Michalchuk et al., 2023). Le fluide riche en éléments dissous est redistribué et précipite dans ces pores temporaires, comblant progressivement la porosité.

Il est donc plausible que l'éclogitisation augmente la porosité et la perméabilité de la croûte inférieure de manière transitoire plutôt que permanente. Dans un premier temps, la dissolution du protolith (Rogowitz et Huet, 2021) et la précipitation de minéraux éclogitiques plus denses (Zertani et al., 2022) créent de la porosité et facilitent la circulation de fluides. Cependant la déformation ductile tend à fermer les pores nouvellement créés (Rogowitz et Huet, 2021) et permet la cristallisation rapide de nouveaux minéraux qui comblient les pores (Michalchuk et al., 2023).

### 5.3 L'éclogitisation de la croûte inférieure vue d'Holsnøy

En m'appuyant sur les principaux résultats de ma thèse (section 5.1), de la discussion de mes résultats (section 5.2), et d'une synthèse de la littérature, je propose ici un scénario de l'éclogitisation de la croûte inférieure à partir de l'exemple d'Holsnøy. Ce scénario est illustré sous forme d'un schéma présenté sur la figure 5.1.

Durant la subduction calédonienne, la croûte inférieure granulitique de Baltica est enfouie en profondeur. Elle est préservée des réactions métamorphiques car quasiment anhydre et imperméable. La forte déformation dans la croûte inférieure rigide provoque des déformations fragiles et des séismes, dont la trace fossile est visible à Holsnøy (**étape 1**, Petley-Ragan et al., 2018). L'activité sismique se produit d'abord à des conditions de 10 kbar, 600 °C (Jamtveit et al., 2018b; Petley-Ragan et al., 2019), puis à des conditions maximales de 15-17 kbar, 650-750 °C (Bhowany et al., 2018; Petley-Ragan et al., 2018; Zhong et al., 2021), correspondant à une profondeur d'environ 55-60 km.

Les répliques sismiques dans une croûte peu perméable peuvent être à l'origine de pulses de fluides pressurisés qui éclogitissent localement la granulite (Malvoisin et al., 2020; Putnis et al., 2021; Bras et al., 2023). Les zones ainsi métamorphisées sont affaiblies et forment des bandes de cisaillement qui se déforment ductilement lorsqu'elles sont bien orientées dans le champ de contraintes (**étape 2**). Les contrastes rhéologiques entre granulite et éclogite induisent des surpressions locales qui favorisent la conversion de granulite en éclogite (chapitre 4).

Le déplacement d'un front d'éclogitisation vers des zones de plus basse pression est possible dans la granulite même si elle est imperméable (Bras et al., 2023). Ce processus, assisté par le re-durcissement de l'éclogite à la fin de la séquence de réactions (Bras et al., 2021; Kaatz et al., 2023, chapitre 4), et éventuellement par la diffusion intracristalline, contribuent à l'élargissement des bandes de cisaillement éclogitiques (**étape 3**).

La génération de sous-pressions et de surpressions (Moulas et al., 2022, chapitre 4) est cohérente avec la coexistence entre amphibolite et éclogite sur les mêmes affleurements (Centrella, 2019) et plus largement à l'échelle d'Holsnøy.

### 5.4 Perspectives et travaux futurs

Pour clôturer ce manuscrit, je propose ici deux pistes de recherche qui permettront de comprendre plus finement la croûte continentale inférieure dans de futures études.

#### 5.4.1 Amphibolitisation

Métamorphismes éclogitique et amphibolitique sont concomitants à Holsnøy. Si l'on veut étudier le devenir de la croûte inférieure dans les zones de subduction, il faut

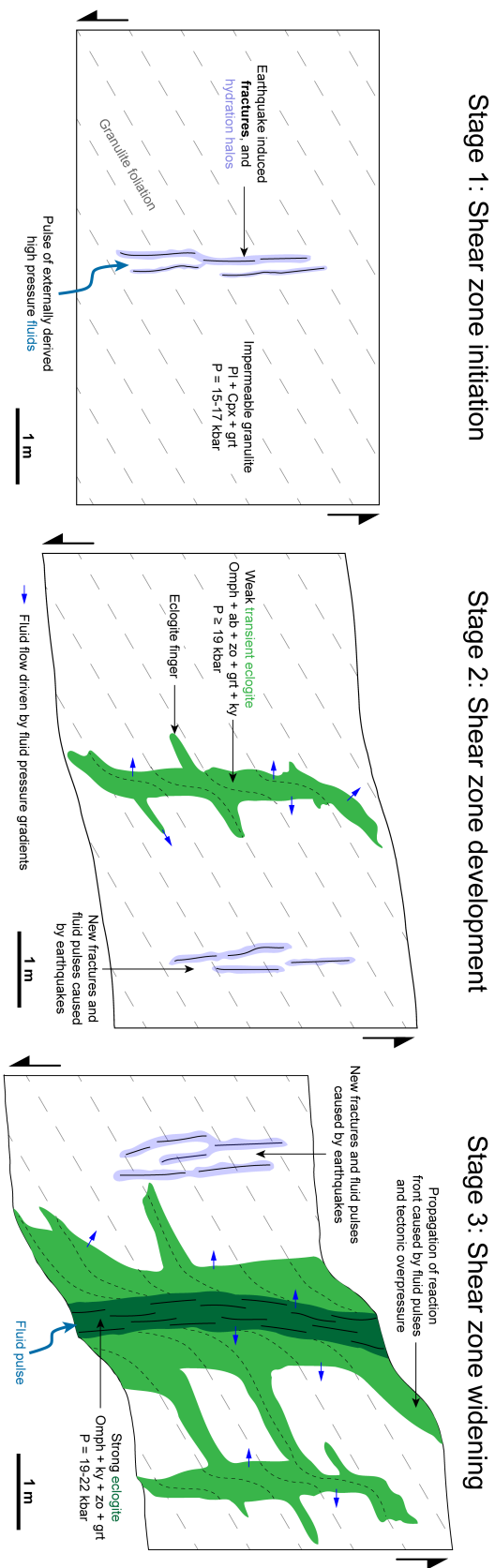


FIGURE 5.1 – Schéma conceptuel de l'évolution des bandes de cisaillement éclogitiques à Holsnøy, Norvège.

**Étape 1 :** des séismes et répliques fracturent la granulite, ce qui augmente localement sa perméabilité. Des fluides s'infiltrent dans ces zones de faiblesse sous formes de pulses de haute pression fluide. La granulite est mécaniquement résistante, essentiellement composée de plagioclase, clinopyroxène et grenat.

**Étape 2 :** les hautes pressions fluides éclogitissent et affaiblissent la granulite, formant ainsi des bandes de cisaillement éclogitiques. Dans un premier temps l'éclogitisation n'est pas complète et résulte en un assemblage transitoire peu résistant d'omphacite, albite, zoisite, grenat, disthène. La déformation génère des surpressions tectoniques qui entretiennent des gradients de pression entre éclogite et granulite. Le transport de fluides le long de la foliation granulitique crée des digitations éclogitiques.

**Étape 3 :** De nouveaux pulses de fluides et les surpressions tectoniques permettent l'élargissement des bandes de cisaillement qui se connectent entre elles. L'éclogitisation est complète dans le cœur des bandes de cisaillement, avec un assemblage à omphacite, disthène, zoisite et grenat, ce qui restaure en partie la résistance de la roche. L'essentiel de la déformation se concentre alors sur la bordure des bandes de cisaillement.

donc s'intéresser aussi bien à l'amphibolitisation qu'à l'éclogitisation. Cette étude doit passer par des datations précises des zones d'éclogitisation et d'amphibolitisation qui coexistent à l'échelle de l'affleurement comme à l'échelle de Holsnøy (Kühn et al., 2002; Glodny et al., 2008; Centrella, 2019).

Du point de vue mécanique, l'amphibolitisation de la granulite génère une augmentation de volume, susceptible de générer des contraintes capables d'amplifier les variations de pressions à l'origine de l'éclogitisation (Centrella, 2019). Les modèles numériques futurs devraient donc prendre en compte l'effet de l'amphibolitisation, qui pourra être étudiée par un modèle proche de celui que j'ai développé.

#### 5.4.2 Pression d'équilibre métamorphique

Pour finir, il me paraît essentiel de comprendre quelle est la pression d'équilibre qui contrôle la stabilité des assemblages métamorphiques. En effet, le chapitre 4 a montré que dans un système métamorphique qui inclut de la déformation et des fluides, il existe plusieurs pressions qui peuvent prendre des valeurs différentes. Il est alors difficile de déterminer laquelle de ces pressions contrôle les assemblages métamorphiques (Dahlen, 1992; Wheeler, 2014; Hobbs et Ord, 2018; Moulas et al., 2019) : pression lithostatique, pression solide, contrainte principale maximale  $\sigma_1$ , pression fluide, ou pression totale ?

Il est déjà bien établi que la pression lithostatique ( $P_{litho} = \rho g z$ ) n'est en général pas une bonne approximation de cette pression d'équilibre (Petrini et Podladchikov, 2000; Schmalholz et al., 2014b; Tajčmanová et al., 2015; Moulas et al., 2019). Certaines expériences de laboratoire suggèrent la pression solide (ou contrainte moyenne,  $\bar{\sigma} = (\sigma_{xx} + \sigma_{yy} + \sigma_{zz})/3$ ) comme pression d'équilibre thermodynamique (Cionoiu et al., 2019; Cionoiu et al., 2022), d'autres la contrainte principale maximale  $\sigma_1$  (Hirth et Tullis, 1994; Richter et al., 2016).

Cependant, ces expériences utilisent des réactions polymorphiques (aragonite - calcite et quartz - coésite) qui n'impliquent pas de fluides. En présence de fluides, la pression fluide ( $P_f$ ) semble contrôler les assemblages métamorphiques (Holdaway et Goodge, 1990, Llana-Fúnez et al., 2012). Une pression totale, moyenne de  $\bar{\sigma}$  et de  $P_f$  pondérée par la porosité ( $P_t = (1 - \phi)\bar{\sigma} + \phi P_f$ ) peut aussi être employée (Dahlen, 1992; Keller et al., 2013).

La question de savoir quelle est la pression d'équilibre thermodynamique est donc loin d'être triviale (Wheeler, 2014), et il semble difficile à l'heure actuelle de la déterminer dans un cas général. Les travaux expérimentaux futurs devraient viser à comprendre quelle pression contrôle les réactions métamorphiques lorsque les fluides et la déformation sont impliqués.

## Bibliographie du présent chapitre

- Agard, P., Yamato, P., Jolivet, L. & Burov, E. (2009). Exhumation of oceanic blueschists and eclogites in subduction zones : timing and mechanisms. *Earth-Science Reviews*, 92(1-2), 53-79. <https://doi.org/10.1016/j.earscirev.2008.11.002>
- Austrheim, H. (1987). Eclogitization of lower crustal granulites by fluid migration through shear zones. *Earth and Planetary Science Letters*, 81(2-3), 221-232. [https://doi.org/10.1016/0012-821X\(87\)90158-0](https://doi.org/10.1016/0012-821X(87)90158-0)
- Austrheim, H. & Griffin, W. L. (1985). Shear deformation and eclogite formation within granulite-facies anorthosites of the Bergen Arcs, western Norway. *Chemical Geology*, 50(1-3), 267-281. [https://doi.org/10.1016/0009-2541\(85\)90124-X](https://doi.org/10.1016/0009-2541(85)90124-X)
- Beinlich, A., John, T., Vrijmoed, J. C., Tominaga, M., Magna, T. & Podladchikov, Y. Y. (2020). Instantaneous rock transformations in the deep crust driven by reactive fluid flow. *Nature Geoscience*, 13(4), 307-311. <https://doi.org/10.1038/s41561-020-0554-9>
- Bhowany, K. (2020). *Constraints on the fluid enhanced eclogitisation of granulite domains in the Bergen Arcs, Norway* (thèse de doct.).
- Bhowany, K., Hand, M., Clark, C., Kelsey, D. E., Reddy, S. M., Pearce, M. A., Tucker, N. M. & Morrissey, L. J. (2018). Phase equilibria modelling constraints on P-T conditions during fluid catalysed conversion of granulite to eclogite in the Bergen Arcs, Norway. *Journal of Metamorphic Geology*, 36(3), 315-342. <https://doi.org/10.1111/jmg.12294>
- Bjørnerud, M., Austrheim, H. & Lund, M. (2002). Processes leading to eclogitization (densification) of subducted and tectonically buried crust. *Journal of Geophysical Research : Solid Earth*, 107(B10), ETG-14. <https://doi.org/10.1029/2001JB000527>
- Bras, E., Yamato, P., Schmalholz, S. M., Duretz, T. & Podladchikov, Y. Y. (2023). Eclogitisation of dry and impermeable granulite by fluid flow with reaction-induced porosity : Insights from hydro-chemical modelling. *Earth and Planetary Science Letters*, 617, 118256. <https://doi.org/10.1016/j.epsl.2023.118256>
- Bras, E., Baïsset, M., Yamato, P. & Labrousse, L. (2021). Transient weakening during the granulite to eclogite transformation within hydrous shear zones (Holsnøy, Norway). *Tectonophysics*, 819, 229026. <https://doi.org/10.1016/j.tecto.2021.229026>
- Centrella, S. (2019). The granulite-to eclogite-and amphibolite-facies transition : a volume and mass transfer study in the Lindås Nappe, Bergen Arcs, west Norway. *Geological Society, London, Special Publications*, 478(1), 241-264. <https://doi.org/10.1144/SP478.9>
- Cionoiu, S., Moulas, E., Stünitz, H. & Tajčmanová, L. (2022). Locally Resolved Stress-State in Samples During Experimental Deformation : Insights Into the Effect of Stress on Mineral Reactions. *Journal of Geophysical Research : Solid Earth*, 127(8), e2022JB024814. <https://doi.org/10.1029/2022JB024814>
- Cionoiu, S., Moulas, E. & Tajčmanová, L. (2019). Impact of interseismic deformation on phase transformations and rock properties in subduction zones. *Scientific Reports*, 9(1), 19561. <https://doi.org/10.1038/s41598-019-56130-6>

- Connolly, J. (1997). Devolatilization-generated fluid pressure and deformation-propagated fluid flow during prograde regional metamorphism. *Journal of Geophysical Research : Solid Earth*, 102(B8), 18149-18173. <https://doi.org/10.1029/97JB00731>
- Connolly, J. & Podladchikov, Y. Y. (1998). Compaction-driven fluid flow in viscoelastic rock. *Geodinamica Acta*, 11(2-3), 55-84. <https://doi.org/10.1080/09853111.1998.11105311>
- Dahlen, F. (1992). Metamorphism of nonhydrostatically stressed rocks. *American Journal of Science*, 292(3), 184-198. <https://doi.org/10.2475/ajs.292.3.184>
- Glodny, J., Kühn, A. & Austrheim, H. (2008). Geochronology of fluid-induced eclogite and amphibolite facies metamorphic reactions in a subduction–collision system, Bergen Arcs, Norway. *Contributions to Mineralogy and Petrology*, 156, 27-48. <https://doi.org/10.1007/s00410-007-0272-y>
- Guillot, S., Hattori, K., Agard, P., Schwartz, S. & Vidal, O. (2009). Exhumation processes in oceanic and continental subduction contexts : a review. *Subduction zone geodynamics*, 175-205. [https://doi.org/10.1007/978-3-540-87974-9\\_10](https://doi.org/10.1007/978-3-540-87974-9_10)
- Hirth, G. & Tullis, J. (1994). The brittle-plastic transition in experimentally deformed quartz aggregates. *Journal of Geophysical Research : Solid Earth*, 99(B6), 11731-11747. <https://doi.org/10.1029/93JB02873>
- Hobbs, B. E. & Ord, A. (2018). Coupling of fluid flow to permeability development in mid-to upper crustal environments : a tale of three pressures. *Geological Society, London, Special Publications*, 453(1), 81-120. <https://doi.org/10.1144/SP453.9>
- Holdaway, M. & Goode, J. (1990). Rock pressures vs. fluid pressure as a controlling influence on mineral stability ; an example from New Mexico. *American Mineralogist*, 75(9-10), 1043-1058.
- Jackson, J. A., Austrheim, H., McKenzie, D. & Priestley, K. (2004). Metastability, mechanical strength, and the support of mountain belts. *Geology*, 32(7), 625-628. <https://doi.org/10.1130/G20397.1>
- Jamtveit, B., Austrheim, H. & Putnis, A. (2016). Disequilibrium metamorphism of stressed lithosphere. *Earth-Science Reviews*, 154, 1-13. <https://doi.org/10.1016/j.earscirev.2015.12.002>
- Jamtveit, B., Petley-Ragan, A., Incel, S., Dunkel, K. G., Aupart, C., Austrheim, H., Corfu, F., Menegon, L. & Renard, F. (2019). The effects of earthquakes and fluids on the metamorphism of the lower continental crust. *Journal of Geophysical Research : Solid Earth*, 124(8), 7725-7755. <https://doi.org/10.1029/2018JB016461>
- Jamtveit, B., Moulas, E., Andersen, T. B., Austrheim, H., Corfu, F., Petley-Ragan, A. & Schmalholz, S. M. (2018b). High pressure metamorphism caused by fluid induced weakening of deep continental crust. *Scientific Reports*, 8(1), 17011. <https://doi.org/10.1038/s41598-018-35200-1>
- John, T., Gussone, N., Podladchikov, Y. Y., Bebout, G. E., Dohmen, R., Halama, R., Klemd, R., Magna, T. & Seitz, H.-M. (2012). Volcanic arcs fed by rapid pulsed fluid flow through subducting slabs. *Nature Geoscience*, 5(7), 489-492. <https://doi.org/10.1038/ngeo1482>
- Kaatz, L., Reynes, J., Hermann, J. & John, T. (2022). How fluid infiltrates dry crustal rocks during progressive eclogitization and shear zone formation : insights from H<sub>2</sub>O contents in nominally anhydrous minerals. *Contributions to Mineralogy and Petrology*, 177(7), 72. <https://doi.org/10.1007/s00410-022-01938-1>

- Kaatz, L., Schmalholz, S. & John, T. (2023). Numerical simulations reproduce field observations showing transient weakening during shear zone formation by diffusional hydrogen influx and H<sub>2</sub>O inflow. *Geochemistry, Geophysics, Geosystems*, 24(5), e2022GC010830. <https://doi.org/10.1029/2022GC010830>
- Keller, T., May, D. A. & Kaus, B. J. (2013). Numerical modelling of magma dynamics coupled to tectonic deformation of lithosphere and crust. *Geophysical Journal International*, 195(3), 1406-1442. <https://doi.org/10.1093/gji/ggt306>
- Kühn, A., Glodny, J., Austrheim, H. & Råheim, A. (2002). The Caledonian tectono-metamorphic evolution of the Lindås Nappe : Constraints from U-Pb, Sm-Nd and Rb-Sr ages of granitoid dykes. *Norwegian Journal of Geology/Norsk Geologisk Forening*, 82(1).
- Llana-Fúnez, S., Wheeler, J. & Faulkner, D. R. (2012). Metamorphic reaction rate controlled by fluid pressure not confining pressure : implications of dehydration experiments with gypsum. *Contributions to Mineralogy and Petrology*, 164, 69-79. <https://doi.org/10.1007/s00410-012-0726-8>
- Malvoisin, B., Austrheim, H., Hetényi, G., Reynes, J., Hermann, J., Baumgartner, L. P. & Podladchikov, Y. Y. (2020). Sustainable densification of the deep crust. *Geology*, 48(7), 673-677. <https://doi.org/10.1130/G47201.1>
- Michalchuk, S. P., Zertani, S., Renard, F., Fusseis, F., Chogani, A., Plümper, O. & Menegon, L. (2023). Dynamic Evolution of Porosity in Lower-Crustal Faults During the Earthquake Cycle. *J. Geophys. Res. Solid Earth*, 128(8), e2023JB026809. <https://doi.org/10.1029/2023JB026809>
- Moulas, E., Kaus, B. & Jamtveit, B. (2022). Dynamic pressure variations in the lower crust caused by localized fluid-induced weakening. *Communications Earth & Environment*, 3(1), 157. <https://doi.org/10.1038/s43247-022-00478-7>
- Moulas, E., Schmalholz, S. M., Podladchikov, Y., Tajčmanová, L., Kostopoulos, D. & Baumgartner, L. (2019). Relation between mean stress, thermodynamic, and lithostatic pressure. *Journal of metamorphic geology*, 37(1), 1-14. <https://doi.org/10.1111/jmg.12446>
- Petley-Ragan, A., Ben-Zion, Y., Austrheim, H., Ildefonse, B., Renard, F. & Jamtveit, B. (2019). Dynamic earthquake rupture in the lower crust. *Science Advances*, 5(7), eaaw0913. <https://doi.org/DOI:10.1126/sciadv.aaw0913>
- Petley-Ragan, A., Dunkel, K. G., Austrheim, H., Ildefonse, B. & Jamtveit, B. (2018). Microstructural records of earthquakes in the lower crust and associated fluid-driven metamorphism in plagioclase-rich granulites. *Journal of Geophysical Research : Solid Earth*, 123(5), 3729-3746. <https://doi.org/10.1029/2017JB015348>
- Petrini & Podladchikov. (2000). Lithospheric pressure-depth relationship in compressive regions of thickened crust. *Journal of metamorphic Geology*, 18(1), 67-77. <https://doi.org/10.1046/j.1525-1314.2000.00240.x>
- Plümper, O., John, T., Podladchikov, Y. Y., Vrijmoed, J. C. & Scambelluri, M. (2017). Fluid escape from subduction zones controlled by channel-forming reactive porosity. *Nature Geoscience*, 10(2), 150-156. <https://doi.org/10.1038/ngeo2865>
- Putnis, A. (2015). Transient porosity resulting from fluid–mineral interaction and its consequences. *Reviews in Mineralogy and Geochemistry*, 80(1), 1-23. <https://doi.org/10.2138/rmg.2015.80.01>

- Putnis, A., Moore, J., Prent, A. M., Beinlich, A. & Austrheim, H. (2021). Preservation of granulite in a partially eclogitized terrane : Metastable phenomena or local pressure variations? *Lithos*, 400, 106413. <https://doi.org/10.1016/j.lithos.2021.106413>
- Richter, B., Stünitz, H. & Heilbronner, R. (2016). Stresses and pressures at the quartz-to-coesite phase transformation in shear deformation experiments. *Journal of Geophysical Research : Solid Earth*, 121(11), 8015-8033. <https://doi.org/10.1002/2016JB013084>
- Rogowitz, A. & Huet, B. (2021). Evolution of fluid pathways during eclogitization and their impact on formation and deformation of eclogite : A microstructural and petrological investigation at the type locality (Koralpe, Eastern Alps, Austria). *Tectonophysics*, 819, 229079. <https://doi.org/10.1016/j.tecto.2021.229079>
- Schmalholz, S. M., Medvedev, S., Lechmann, S. M. & Podladchikov, Y. (2014b). Relationship between tectonic overpressure, deviatoric stress, driving force, isostasy and gravitational potential energy. *Geophysical Journal International*, 197(2), 680-696. <https://doi.org/10.1093/gji/ggu040>
- Taetz, S., John, T., Bröcker, M., Spandler, C. & Stracke, A. (2018). Fast intraslab fluid-flow events linked to pulses of high pore fluid pressure at the subducted plate interface. *Earth and Planetary Science Letters*, 482, 33-43. <https://doi.org/10.1016/j.epsl.2017.10.044>
- Tajčmanová, L., Vrijmoed, J. & Moulas, E. (2015). Grain-scale pressure variations in metamorphic rocks : implications for the interpretation of petrographic observations. *Lithos*, 216, 338-351. <https://doi.org/10.1016/j.lithos.2015.01.006>
- Violay, M., Heap, M. J., Acosta, M. & Madonna, C. (2017). Porosity evolution at the brittle-ductile transition in the continental crust : Implications for deep hydrogeothermal circulation. *Scientific reports*, 7(1), 7705. <https://doi.org/10.1038/s41598-017-08108-5>
- Wheeler, J. (2014). Dramatic effects of stress on metamorphic reactions. *Geology*, 42(8), 647-650. <https://doi.org/10.1130/G35718.1>
- Yardley, B. W. (1997). The evolution of fluids through the metamorphic cycle. *Fluid flow and transport in rocks : Mechanisms and effects* (p. 99-121). Springer.
- Yardley, B. W. & Valley, J. W. (1997). The petrologic case for a dry lower crust. *Journal of Geophysical Research : Solid Earth*, 102(B6), 12173-12185. <https://doi.org/10.1029/97JB00508>
- Zertani, S., John, T., Brachmann, C., Vrijmoed, J. C. & Plümper, O. (2022). Reactive fluid flow guided by grain-scale equilibrium reactions during eclogitization of dry crustal rocks. *Contributions to Mineralogy and Petrology*, 177(6), 61. <https://doi.org/10.1007/s00410-022-01928-3>
- Zhong, X., Petley-Ragan, A. J., Incel, S. H., Dabrowski, M., Andersen, N. H. & Jamtveit, B. (2021). Lower crustal earthquake associated with highly pressurized frictional melts. *Nature Geoscience*, 14(7), 519-525. <https://doi.org/10.1038/s41561-021-00760-x>





**Titre :** Couplages entre métamorphisme, fluides et déformation : étude de cas de l'éclogitisation dans les Arcs de Bergen

**Mots-clés :** Éclogitisation, bande de cisaillement, interaction fluides-roche, modélisation numérique

**Résumé :** L'éclogitisation est un processus emblématique des zones de subduction continentales. Elle fait intervenir aussi bien la transformation de l'assemblage minéralogique, une modification de rhéologie et de perméabilité, une interaction entre fluides et roche, et une déformation visqueuse et cassante. Cette thèse a pour objet l'étude de ces couplages, à travers un cas de terrain précis : l'éclogitisation de la granulite de l'île d'Holsnøy, dans les Arcs de Bergen à l'ouest de la Norvège. Les observations de terrain révèlent que la déformation et la circulation de fluides sont les moteurs de l'éclogitisation de la croûte inférieure, mais l'évolution temporelle et les conditions de pression des zones éclogitiques sont toujours énigmatiques.

Dans un premier temps, j'ai réalisé une étude pétrologique détaillée d'une bande de cisaillement

éclogitique, mettant en évidence un affaiblissement transitoire de la granulite, qui passe par une étape de résistance mécanique minimale durant son éclogitisation.

Dans une deuxième étude, j'ai développé un modèle numérique qui montre qu'un front hydro-reactif de haute pression peut se propager rapidement dans la granulite imperméable pour entraîner son éclogitisation.

Troisièmement, j'ai montré avec un autre modèle que dans la croûte inférieure, la déformation d'un milieu rhéologiquement hétérogène peut générer des variations locales de pression de plusieurs kbar, capables d'éclogitisier la granulite. Ces variations de pression peuvent expliquer la juxtaposition de roches de faciès métamorphiques différents au même niveau crustal. La circulations de fluides peut toutefois affecter ces variations de pression.

**Title:** Couplings between metamorphism, fluids and deformation: a case study of eclogitisation in the Bergen Arcs

**Keywords:** Eclogitisation, shear zone, fluid-rock interaction, numerical modeling

**Abstract:** Eclogitisation is an emblematic process of continental subduction zones. It involves transformation of the mineralogical assemblage, changes in rheology and permeability, fluid-rock interactions, and both viscous and brittle deformation. The aim of this thesis is to study these couplings, focusing on a specific field case: the eclogitisation of granulite on Holsnøy Island, in the Bergen Arcs in western Norway. Field observations show that deformation and fluid circulation are the forces that drive eclogitisation of the lower crust, but the temporal evolution and pressure conditions of eclogitic zones are still enigmatic.

In a first study, I carried out a detailed petrological study of an eclogite shear zone, highlighting a transient weakening of the granulite, which goes

through a stage of minimal mechanical strength during its eclogitization.

In a second study, I developed a numerical model showing that a high-pressure hydro-reactive front can propagate rapidly into impermeable granulite, leading to its eclogitisation.

Thirdly, I showed with another numerical model that in the lower crust, deformation of a rheologically heterogeneous medium can generate local pressure variations of several kbar, capable of eclogitising granulite. These pressure variations can explain the juxtaposition of rocks with different metamorphic facies at the same crustal level. Fluid circulation, however, may affect these pressure variations.